HIGHWAY RESEARCH RECORD

Number 131

Design, Performance and Surface Properties of Pavements

12 Reports

Subject Classification

25 Pavement Design
26 Pavement Performance
62 Foundations (Soils)
63 Mechanics (Earth Mass)

HIGHWAY RESEARCH BOARD
DIVISION OF ENGINEERING NATIONAL RESEARCH COUNCIL
NATIONAL ACADEMY OF SCIENCES—NATIONAL ACADEMY OF ENGINEERING

Washington, D. C., 1966 Publication 1375

Department of Design

W. B. Drake, Chairman
Assistant State Highway Engineer for Planning, Research and Materials
Kentucky Department of Highways, Lexington

HIGHWAY RESEARCH BOARD STAFF

F. N. Wray, Engineer of Design

R. C. Edgerton, Assistant Engineer of Design

PAVEMENT DIVISION

Milton E. Harr, Chairman
Professor of Soil Mechanics, School of Civil Engineering
Purdue University, Lafayette, Indiana

COMMITTEE ON RIGID PAVEMENT DESIGN
(As of December 31, 1965)

F. H. Scrivner, Chairman
Pavement Research Engineer, Texas Transportation Institute
Texas A & M University, College Station

W. Ronald Hudson, Secretary
Research Engineer, Department of Civil Engineering
The University of Texas, Austin

Henry Aaron, Chief Engineer, Reinforced Concrete Pavement Division, Wire Reinforcement Institute, Washington, D. C.
Phillip P. Brown, Consultant, Soils, Mechanics and Paving, Bureau of Yards and Docks, Department of the Navy, Washington, D. C.
Harry D. Cashell, Deputy Chief, Structural Research Division, U. S. Bureau of Public Roads, Washington, D. C.
B. E. Colley, Manager, Paving Development Section, Portland Cement Association, Skokie, Illinois
E. A. Finney, Director, Research Laboratory Division, Michigan State Highway Department, Lansing
Phil Fordyce, Supervising Engineer, Pavement Engineering, Portland Cement Association, Chicago, Illinois
W. S. Housel, University of Michigan, Ann Arbor
F. N. Hveem, Sacramento, California
W. H. Jacobs, Executive Secretary, Rail Steel Bar Association, Chicago, Illinois
C. D. Jensen, Director of Research and Testing, Pennsylvania Department of Highways, Harrisburg
Wallace J. Liddle, Engineer of Materials and Research, Utah State Department of Highways, Salt Lake City
Phillip L. Melville, Civil Engineering Branch, Engineering Division, Military Construction, Office, Chief of Engineers, Department of the Army, Washington, D. C.
Ernest T. Perkins, Executive Director, East Hudson Parkway Authority, Pleasantville, N. Y.
Thomas B. Pringle, Chief, Civil Engineering Branch, Engineering Division, Military Construction, Office, Chief of Engineers, Department of the Army, Washington, D.C.
M. D. Shelby, Research Engineer, Texas Transportation Institute, Texas A & M University, College Station
W. T. Spencer, Assistant Chief, Division of Materials and Tests, Indiana State Highway Commission, Indianapolis
Otto A. Strassenmeyer, Associate Highway Engineer - Research and Development, Connecticut State Highway Department, Wethersfield

William Van Breemen, Consultant, Trenton, N. J.
K. B. Woods, Goss Professor of Engineering, School of Civil Engineering, Purdue University, Lafayette, Indiana

COMMITTEE ON FLEXIBLE PAVEMENT DESIGN
(As of December 31, 1965)

R. E. Livingston, Chairman
Consultant, Denver, Colorado

Stuart Williams, Secretary
Highway Research Engineer, U. S. Bureau of Public Roads
Washington, D. C.

A. C. Benkelman, Altamonte Springs, Florida
John A. Bishop, Director, Soils and Pavement Division, U. S. Naval Civil Engineering Laboratory, Port Hueneme, California
Thomas L. Bransford, Professor of Civil Engineering, Auburn University, Auburn, Alabama
W. H. Campen, Manager, Omaha Testing Laboratories, Omaha, Nebraska
Bonner S. Coffman, Associate Professor of Civil Engineering, Ohio State University, Columbus
Robert A. Crawford, Assistant Research Engineer, South Dakota Department of Highways, Pierre
George H. Dent, Benjamin E. Beavin Company, Baltimore, Maryland
James M. Desmond, State Materials Engineer, Wyoming State Highway Department, Cheyenne
Charles R. Foster, Coordinator of Research, National Asphalt Pavement Association, Texas A & M University, College Station
J. E. Gray, Engineering Director, National Crushed Stone Association, Washington, D. C.
John M. Griffith, Director of Research and Development, The Asphalt Institute, University of Maryland, College Park
Frank B. Hennion, Assistant Chief, Civil Engineering Branch, Engineering Division, Military Construction, Office, Chief of Engineers, Department of the Army, Washington, D. C.
Raymond C. Herner, Consulting Engineer, Indianapolis, Indiana
W. S. Housel, University of Michigan, Ann Arbor
Charles W. Johnson, Engineering Director, New Mexico State Highway Department, Santa Fe
Henry J. Lichtefeld, Chief, Construction and Maintenance Standards Branch, Federal Aviation Agency, Washington, D. C.
Wallace J. Liddle, Engineer of Materials and Research, Utah State Department of Highways, Salt Lake City
Alfred W. Maner, Staff Engineer, The Asphalt Institute, University of Maryland, College Park
Chester McDowell, Supervising Soils Engineer, Texas Highway Department, Austin
C. E. Minor, Materials and Research Engineer, Washington State Department of Highways, Olympia
Carl L. Monismith, University of California, Berkeley
A. O. Neiser, Assistant State Highway Engineer, Kentucky Department of Highways, Frankfort
Frank P. Nichols, Jr., Associate Engineering Director, National Crushed Stone Association, Washington, D. C.
R. L. Peyton, Assistant State Highway Engineer, State Highway Commission of Kansas, Topeka

E. G. Robbins, Portland Cement Association, Chicago, Illinois
George B. Sherman, Supervising Highway Engineer, California Division of Highways, Sacramento
Rollin J. Smith, Shawnee Mission, Kansas
Fred Sternberg, Senior Highway Engineer - Research, Connecticut State Highway Department, Hartford
John H. Swanberg, Chief Engineer, Minnesota Department of Highways, St. Paul
B. A. Vallerga, Director of Engineering, Materials Research & Development, Woodward-Clyde-Sherard & Associates, Oakland, California

COMMITTEE ON SURFACE PROPERTIES—VEHICLE INTERACTION

(As of December 31, 1965)

David C. Mahone, Chairman
Highway Research Engineer
Virginia Council of Highway Investigation and Research
Charlottesville

M. D. Armstrong, Director of Research, Ontario Department of Highways, Toronto, Canada
Joseph E. Bell, Division of Materials Development and Research, D. C. Department of Highways and Traffic, Washington, D. C.
Thomas H. Boone, Technologist, National Bureau of Standards, Washington, D. C.
A. D. Brickman, Department of Mechanical Engineering, Pennsylvania State University, University Park
W. F. R. Briscoe, Manager, Tire Reliability, Product Development, United States Rubber Company, Detroit, Michigan
John E. Burke, Engineer of Research and Development, Illinois Division of Highways, Springfield
William C. Burnett, Associate Civil Engineer, Bureau of Physical Research, New York State Department of Public Works, Albany
A. Y. Casanova, III, Highway Research Engineer, Structures and Applied Mechanics Division, U. S. Bureau of Public Roads, Washington, D. C.
John H. Cox, Manager, Fleet and Commercial Testing, Firestone Tire and Rubber Company, Akron, Ohio
Louis F. DiNicola, III, Division of Research, New Jersey State Highway Department, Trenton
Blaine R. Englund, Assistant Plant Engineer, General Motors Proving Ground, Milford, Michigan
William Gartner, Jr., Engineer of Research, Florida State Road Department, Gainesville
B. G. Hutchinson, Department of Civil Engineering, University of Waterloo, Waterloo, Ontario, Canada
Robert N. Janeway, President, Janeway Engineering Company, Detroit, Michigan
Upshur T. Joyner, Landing and Impact Branch, Dynamic Loads Division, NASA, Langley Research Center, Hampton, Virginia
H. W. Kummer, Research Assistant, Department of Mechanical Engineering, Pennsylvania State University, University Park
Henry J. Lichtefeld, Chief, Construction and Maintenance Standards Branch, Federal Aviation Agency, Washington, D. C.
Samuel I. Lipka, Highway Engineer, Office of Planning, Advance Planning Division, U. S. Bureau of Public Roads, Washington, D. C.
B. Franklin McCullough, Supervising Design Research Engineer, Texas Highway Department, Austin
Robert B. McGough, Consultant, Department of the Air Force, Headquarters, United States Air Force, Washington, D. C.

W. E. Meyer, Professor of Mechanical Engineering, Department of Mechanical Engineering, Pennsylvania State University, University Park
Desmond F. Moore, Dublin, Eire
Ralph A. Moyer, Research Engineer, Institute of Transportation and Traffic Engineering, University of California, Berkeley
F. William Petring, Manager, Road Safety and Traffic Controls Engineering Department, Ford Motor Company, Dearborn, Michigan
Rolands L. Rizenbergs, Research Engineer, Kentucky Department of Highways, Lexington
Richard K. Shaffer, Research Coordinator, Pennsylvania Department of Highways, Harrisburg
W. E. Teske, Paving Engineer, Portland Cement Association, Chicago, Illinois
E. A. Whitehurst, Director, Tennessee Highway Research Program, University of Tennessee, Knoxville
Ross G. Wilcox, Executive Secretary, Safe Winter Driving League, Chicago, Illinois
Dillard D. Woodson, The Asphalt Institute, University of Maryland, College Park

COMMITTEE ON PAVEMENT CONDITION EVALUATION

(As of December 31, 1965)

Malcolm D. Graham, Chairman
Director, Bureau of Physical Research
New York State Department of Public Works, Albany

Robert F. Baker, Director, Office of Research & Development, U. S. Bureau of Public Roads, Washington, D. C.
Frederick E. Behn, Assistant Engineer of Specifications and Development, Ohio Department of Highways, Columbus
A. Y. Casanova, III, Highway Research Engineer, Structures and Applied Mechanics Division, U. S. Bureau of Public Roads, Washington, D. C.
W. B. Drake, Assistant State Highway Engineer for Planning, Research and Materials, Kentucky Department of Highways, Lexington
Karl H. Dunn, Materials Research Engineer, State Highway Commission of Wisconsin, Madison
Leroy D. Graves, Associate Professor of Civil Engineering, Notre Dame University, Notre Dame, Indiana
W. S. Housel, University of Michigan, Ann Arbor
W. Ronald Hudson, Research Engineer, Department of Civil Engineering, The University of Texas, Austin
Louis C. Lundstrom, Director of Automotive Safety Engineering, General Motors Technical Center, General Motors Corporation, Warren, Michigan
Alfred W. Maner, Staff Engineer, The Asphalt Institute, University of Maryland, College Park
Phillip L. Melville, Civil Engineering Branch, Engineering Division, Military Construction, Office, Chief of Engineers, Department of the Army, Washington, D.C.
A. B. Moe, Manager, Maintenance Branch, Bureau of Yards and Docks, U. S. Navy, Washington, D. C.
Frank P. Nichols, Jr., Associate Engineering Director, National Crushed Stone Association, Washington, D. C.
Bayard E. Quinn, Mechanical Engineering School, Purdue University, Lafayette, Indiana
Foster A. Smiley, Maintenance Engineer, Iowa State Highway Commission, Ames
Elson B. Spangler, Research Laboratories, General Motors Corporation, General Motors Technical Center, Warren, Michigan

Bertram D. Tallamy, Consulting Engineer, Washington, D. C.
W. E. Teske, Paving Engineer, Portland Cement Association, Chicago, Illinois
Frank Y. Wilkinson, Federal Aviation Agency, Washington, D. C.
Eldon J. Yoder, Joint Highway Research Project, Purdue University, Lafayette, Indiana

COMMITTEE ON THEORY OF PAVEMENT DESIGN

(As of December 31, 1965)

Aleksandar S. Vesić, Chairman
Professor of Civil Engineering, Duke University
Durham, North Carolina

W. F. Abercrombie, State Highway Materials Engineer, State Highway Department of Georgia, Altanta
Richard G. Ahlvin, Chief, Flexible Pavement Branch, U. S. Army Engineer Waterways Experiment Station, Vicksburg, Mississippi
Robert F. Baker, Director, Office of Research & Development, U. S. Bureau of Public Roads, Washington, D. C.
E. S. Barber, Consulting Engineer, Soil Mechanics and Foundations, Arlington, Virginia
William P. Hofmann, Director, Bureau of Soil Mechanics, New York State Department of Public Works, Albany
Eugene Y. Huang, Department of Civil Engineering, Michigan Technological University, Houghton
W. Ronald Hudson, Research Engineer, Department of Civil Engineering, The University of Texas, Austin
Carl L. Monismith, University of California, Berkeley
John P. Nielsen, Senior Task Engineer, U. S. Naval Civil Engineering Laboratory, Port Hueneme, California
Gordon K. Ray, Manager, Paving Bureau, Portland Cement Association, Chicago, Illinois
Robert L. Schiffman, Professor of Soil Mechanics, The Winslow Laboratories, Rensselaer Polytechnic Institute, Troy, N. Y.
James F. Shook, The Asphalt Institute, University of Maryland, College Park

Department of Soils, Geology and Foundations

Eldon J. Yoder, Chairman
Joint Highway Research Project
Purdue University, Lafayette, Indiana

Chester McDowell, Vice Chairman
Supervising Soils Engineer
Texas Highway Department, Austin

HIGHWAY RESEARCH BOARD STAFF

A. W. Johnson, Engineer of Soils and Foundations

J. W. Guinnee, Assistant Engineer of Soils and Foundations

DIVISION B

H. Bolton Seed, Chairman
Department of Civil Engineering
University of California, Berkeley

Carl L. Monismith, Vice Chairman
University of California, Berkeley

COMMITTEE ON STRENGTH AND DEFORMATION CHARACTERISTICS OF PAVEMENT SECTIONS
(As of December 31, 1965)

Carl L. Monismith, Chairman
University of California, Berkeley

E. S. Barber, Consulting Engineer, Soil Mechanics and Foundations, Arlington, Virginia
Bonner S. Coffman, Department of Civil Engineering, Ohio State University, Columbus
B. E. Colley, Manager, Paving Development Section, Portland Cement Association, Skokie, Illinois
F. N. Finn, Chief Engineer, Materials Research & Development, Oakland, California
Raymond A. Forsyth, Senior Materials and Research Engineer, Materials and Research Department, California Division of Highways, Sacramento
W. S. Housel, University of Michigan, Ann Arbor
W. Ronald Hudson, Department of Civil Engineering, University of Texas, Austin
R. L. Kondner, Associate Professor of Civil Engineering, Department of Civil Engineering, Northwestern University, Evanston, Illinois
H. G. Larew, Department of Civil Engineering, University of Virginia, Charlottesville
T. F. McMahon, U. S. Bureau of Public Roads, Washington, D. C.
B. P. Shields, Research Council of Alberta, Edmonton, Alberta, Canada
Eugene L. Skok, Jr., Department of Civil Engineering, University of Minnesota, Minneapolis
J. E. Stephens, Professor of Civil Engineering, University of Connecticut, Storrs
Aleksandar S. Vesić, Duke University, Durham, North Carolina

Foreword

The first three papers present the results of three different kinds of investigations into the theories and practices used in the design and construction of concrete pavements. The first paper explains a theoretical solution for the design of rigid slabs. Some new concepts are offered in an attempt to avoid certain limitations of conventional mathematics and hand solutions. Sample problems given illustrate the generality of the method and the use of a computer program. Moving load tests on an eight-year-old prestressed concrete slab at the University of Pittsburgh, reported in the second paper, demonstrated the continuation of adequate bond between concrete and the grouted prestressed tendons. Some longitudinal cracking in the pavement slab suggested the need for transverse reinforcement. The other paper, which relates only to concrete pavement, reports on deflection testing of a continuously-reinforced concrete pavement in Texas.

Investigations by the Highway Department and the University of South Carolina have provided a very practical method for determining the modulus of deformation of subgrade materials, useful in the design of flexible pavements. The paper "Application of AASHO Road Test Findings to the Design of Flexible Pavements" describes how the new soil support test method can be applied locally and used in conjunction with the AASHO "Interim Guide" on flexible pavements.

The fifth paper examines and discusses the basic theories involved in the analyses of "Structural Behavior of Road Test Flexible Pavement." It is an abridgment of an NCHRP project report.

A report on observed deflections of flexible pavements in Maryland provides a study of relative pavement deflection and pavement performance as they vary with subgrade moisture content and the effect of traffic. A contribution toward the development of nondestructive testing for flexible pavements is described in the following paper. The pulse velocity measurement technique used in Texas, where the effects of moisture content, density, voids, pressure and temperature on the wave velocities in various materials were studied, is presented.

An abridgment of a report on Research in Oregon gives a summary of data on "Fatigue and Deflection of Asphaltic Concrete Pavements." Pavement performance was found to be affected by time of year, location, type of base rock, age of pavement and layer thickness. Another abridgment presents a correlation developed between flexible pavement performance and local factors.

A Canadian paper from the University of Waterloo represents a continuation in the study of ideas and methods relating to the measurement of pavement serviceability. Included are the results of an added test program and the re-examination of the inter-relationships between subjective and objective measurements.

The last two papers relate to safety, inasmuch as they discuss the results of research aimed at controlling the skid resistance of pavements. The work at Cornell Aeronautics Laboratory included a study of hydroplaning of tires as affected by the texture and drainage characteristics of pavement surfaces.

In Texas, as described in the last paper, skid test values were correlated with accident data to aid in a determination of safe limits for pavement surface maintenance and traffic speeds.

Contents

Analysis of Discontinuous Orthotropic Pavement Slabs Subjected to Combined Loads

W. RONALD HUDSON and HUDSON MATLOCK
Center for Highway Research, The University of Texas, Austin

A method of solving for the deflected shape of freely discontinuous orthotropic plates and pavement slabs subjected to a variety of loads including transverse loads, in-plane forces and externally applied couples is presented. The method is applicable for plates and pavement slabs with freely variable foundation support including holes in the subgrade.

Anisotropic elasticity governs the behavior of orthotropic plates and pavement slabs and is used to develop the necessary equations. The method is not limited by discontinuities and uses an efficient alternating-direction iteration means of solving the resulting equations. The method allows considerable freedom in configuration, loading, flexural stiffness and boundary conditions. It solves the problem rapidly and should provide a tool for use in later studies of repetitive stochastic loading. Three principal features are incorporated into the method: (a) the plate is defined by a finite-element model consisting of bars, springs, elastic blocks and torsion bars; these are further grouped for analysis into orthogonal systems of beam-column elements; (b) each individual line-element of the two dimensional system is solved rapidly and directly by recursive techniques; and (c) an alternating-direction iterative method is utilized for coordinating the solution of the individual line-elements into the slab solution.

The computer program utilizes the equations and techniques developed and can be used by the reader. Several sample problems illustrate the generality of the method and the use of the computer program. The results compare well with closed-form solutions.

•THE analysis of pavement slabs is a difficult task. To date neither a theoretical approach nor experimental work has solved the problem. In 1926 H. M. Westergaard completed an analysis of stresses in pavement slabs (32) and his equations have become the definitive design equations for pavement slabs in the United States. Many other engineers and mathematicians have attempted to solve this design problem. Unfortunnately, limitations of conventional mathematics and of hand solutions have restricted developments. Thus the Westergaard solutions, as well as all others, are subjected to limiting severely assumptions which often are not realistic.

Several large-scale road tests have been conducted in attempts to bridge the gap between theory and reality. These include the Bates Test in 1922, the Maryland Road Test in 1950, and the AASHO Road Test in 1958. All three of these full-scale experiments have added to the knowledge of pavement design. However, only the AASHO Road Test was large enough to provide significant information. Work with the AASHO Road Test data has shown that a mechanistic model of structural behavior is essential in the study of load, environment and performance.

The problem, then, is to develop a mechanistic model for describing slab behavior and to develop better methods for solving these equations. The method should allow

Paper sponsored by Committee on Rigid Pavement Design and presented at the 45th Annual Meeting.

for freely discontinuous variation of input parameters including bending stiffness and load. Combination loading should be provided for and should include lateral loads, in-plane forces, and applied couples or moments. Freely variable foundation conditions are needed. Such a technique should apply not only to the general slab-on-foundation case, but also for orthotropic plates with various configurations of structural support.

This paper describes such a method of solving for the deflected shape of orthotropic plates and pavement slabs. (Throughout this paper, the term slab is often used as an abbreviation for pavement slab and slab-on-foundation.) From this deflected shape the stresses, deflections, loads, and bending moments can easily be determined. The method developed takes advantage of groundwork laid by others. The finite-element method was developed by Matlock (18, 19, 29), and variations and extensions of his methods have been made by Tucker, Haliburton, Ingram, and Salani (29, 18, 12, 24).

The principal features incorporated into the finite-element method are (a) representation of structural members by a physical model of bars and springs which are grouped for analysis into systems of orthogonal beams, (b) a rapid method for solution of individual beams that serve as line elements of a two-dimensional slab, and (c) an alternating-direction iteration technique for coordinating the solutions of individual beams which ties the system together.

NOTATION

Symbol	Dimensions	Definition
a, b		Temporary bar numbering used in derivations.
a_x, b_x		Coefficient in the matrix equation.
$c_{i,j}$	lb/in.^{2}	Constants used to relate stress to strain in general anisotropic elasticity (i refers to stress component, j refers to strain component).
$C^x_{i,j}$	$\frac{\text{in.-lb}}{\text{rad}}$	Torsional stiffness of slab element i, j about the x-axis.
$C^{x'}_{i,j}$	in.-lb	Torque exerted on the x-beam due to the relative rotation in torsion bar i, j.
$D_{i,j}$	in.-lb	Bending stiffness of an isotropic plate.
$D^x_{i,j}$, D_x	in.-lb	Bending stiffness of an orthotropic plate in the x-direction.
$D^y_{i,j}$, D_y	in.-lb	Bending stiffness of an orthotropic plate in the y-direction.
D_{xy}	in.-lb	$\frac{G_o t^3}{12}$
D_1	in.-lb	$\frac{E'' t^3}{12}$
E_x	lb/in.^{2}	Modulus of elasticity in x-direction.
E_y	lb/in.^{2}	Modulus of elasticity in y-direction.
E'_x	lb/in.^{2}	$\frac{E_x}{1 - \nu_{xy}\nu_{yx}}$
E'_y	lb/in.^{2}	$\frac{E_y}{1 - \nu_{yx}\nu_{xy}}$
E''	lb/in.^{2}	$\nu_{yx}E'_x = \nu_{xy}E'_y$

ϵ_x	in./in.	Total strain in x-direction.
ϵ_y	in./in.	Total strain in y-direction.
ϵ_z	in./in.	Total strain in z-direction.
$F_{V_{i,j}}$	lb	Vertical forces at joint i, j.
φ		Angular rotation across a plate element.
G	lb/in.^{2}	Shear modulus = $\frac{E}{12(1+\nu)}$.
G_o	lb/in.^{2}	Approximate orthotropic shear modulus $\left(\frac{E_x E_y}{E_y(1+\nu_{xy}) + E_x(1+\nu_{xy})}\right)$
γ	in./in.	Shear strain.
H	in.-lb	$D_1 + 2D_{xy}$.
h_x	in.	The increment length along the x-beams.
h_y	in.	The increment length along the y-beams.
i		An integer used to number mesh points, stations, and bars in the x-direction.
j		An integer used to number mesh points, stations, and bars in the y-direction.
k	lb/in.^{2}/in.	Support modulus of the foundation.
M_a	lb/in.	Moment acting on Bar a about the center of the bar.
M_x	in.-lb	Bending moment acting on an element of the plate in the x-direction.
M_y	in.-lb	Bending moment acting on an element of the plate in the y-direction.
M_{xy}	in.-lb	Twisting moment tending to rotate the element about the x-axis (clockwise-positive).
M_{yx}	in.-lb	Twisting moment tending to rotate the element about the y-axis (clockwise-positive).
$M^{x'}_{i,j}$	in.-lb	The bending moment in the x-beam at Station i, j (equals $h_y M^x_{i,j}$).
$M^{y'}_{i,j}$	in.-lb	The bending moment in the y-beam at Station i, j (equals $h_x M^y_{i,j}$).
ν_{xy}		Poisson's ratio which results in strain in the y-direction if stress is applied in the x-direction.
ν_{yx}		Poisson's ratio which results in strain in the x-direction if stress is applied in the y-direction.
$P^x_{i,j}$	lb	Axial load in the x-beam in Bar i, j (equals $h_y p^x_{i,j}$).

$p^x_{i,j}$	lb/in.	Unit axial load in the slab x-direction at Station i, j.
q	lb/in.^{2}	Distributed lateral load.
Q	lb	Concentrated lateral load.
$Q_{i,j}$	lb	Externally applied load at point i, j.
$Q^x_{i,j}$	lb	Load absorbed internally by the x-beam system at Station i, j.
$Q^y_{i,j}$	lb	Load absorbed internally by the y-beam system at Station i, j.
$\overline{QBMY}_{i,j}$	lb	Load absorbed by the y-beam in bending.
$\overline{QPY}_{i,j}$	lb	Load absorbed by the y-beam due to axial load.
$\overline{QTMY}_{i,j}$	lb	Load absorbed by the y-beam in twisting.
S_f	lb/in.	Fictitious spring stiffness or closure parameter.
S_{fx}	lb/in.	Fictitious spring representing the x-beams.
S_{fy}	lb/in.	Fictitious spring representing the y-beams.
$S_{i,j}$	lb/in.	Elastic restraint used to represent the foundation in the finite-element model.
σ_x	lb/in.^{2}	Stress applied in the x-direction.
σ_y	lb/in.^{2}	Stress applied in the y-direction.
σ_z	lb/in.^{2}	Stress applied in the z-direction.
t	in.	Slab thickness.
$T^x_{i,j}$	in./lb	External torque applied to Bar i on the j^{th} x-beam.
$T^y_{i,j}$	in./lb	External torque applied to Bar j on the i^{th} y-beam.
τ	lb/in.^{2}	Shear stress.
$V^x_{a,j}$	lb	Shear in Bar a of the j^{th} x-beam.
$w_{i,j}$	in.	Lateral deflection.
$w^x_{i,j}$	in.	Deflection of the j^{th} x-beam at Station i.
$w^y_{i,j}$	in.	Deflection of the i^{th} y-beam at Station j.
x, y, z		Standard Cartesian coordinate directions.

THEORY OF ELASTIC PLATES AND SLABS

A review of the various theories involved in the analysis of plate and slab bending will be helpful in understanding the problem at hand. A brief discussion of the bihar-

monic equation is presented in this section. A discussion of generalized Hooke's Law which leads into the derivation of the equation of bending for orthotropic plates follows. The effect of in-plane forces applied to the plate in combined loadings is presented next. Finally, elastic foundations are discussed as related to pavement support.

General Plate Theory

The bending of a plate depends greatly on its thickness as compared with its other dimensions. Timoshenko (28) distinguishes three kinds of plate bending: (a) thin plates with small deflections, (b) thin plates with large deflections, and (c) thick plates.

For thin plates with small deflections (i.e., the deflection is small in comparison with thickness), a satisfactory approximate theory of bending of a plate by lateral loads can be developed by making the following assumptions:

1. There is no deformation in the middle plane of the plate. This plane remains neutral during bending.
2. Planes of the plate lying initially normal to the middle surface of the plate remain normal to the middle surface of the plate after bending.
3. The normal stresses in the direction transverse to the plate can be disregarded. (This assumption is necessary in the analysis of bending of the plate as will be seen later; approximate corrections can be made to account for pressures directly under the transverse load.)

With these assumptions, all components of stress can be expressed in terms of the deflected shape of the plate. This function has to satisfy a linear partial differential equation which, together with the boundary conditions, completely defines the deflection w. The solution of this differential equation gives all necessary information for calculating the stresses at any point in the plate.

Timoshenko (28) develops the theory of bending of plates very thoroughly from the simplest problem of bending in a long rectangular plate subjected to transverse load to the very complex problems of thick plates with various boundary conditions.

The Isotropic Plate Equation

Structural plates and pavement slabs are normally subjected to loads applied perpendicular to their surface, i.e., lateral loads. Timoshenko and others have derived a differential equation which describes the deflection surface of such plates, the biharmonic equation. With one minor change, Timoshenko's equation is given below. This change is to reverse the sense of the z-axis and make "up" positive. This new coordinate system is consistent with recent beam-column developments (18). The equation becomes

$$\frac{\partial^2 M_x}{\partial x^2} + \frac{\partial^2 M_{yx}}{\partial x \partial y} + \frac{\partial^2 M_y}{\partial y^2} - \frac{\partial^2 M_{xy}}{\partial x \partial y} = q \qquad (1)$$

in which M_x is the bending moment acting on an element of the plate in the x-direction, M_y is the bending moment acting on an element of the plate in the y-direction, M_{xy} is a twisting moment tending to rotate the element about the x-axis (clockwise positive), and M_{yx} is a twisting moment tending to rotate the element about the y-axis. Observing that $M_{xy} = -M_{yx}$ for equilibrium ($\tau_{xy} = \tau_{yx}$), the equation can be condensed into the following form.

$$\frac{\partial^2 M_x}{\partial x^2} + \frac{\partial^2 M_y}{\partial y^2} - 2\frac{\partial^2 M_{xy}}{\partial x \partial y} = q \qquad (2)$$

To evaluate this equation, it is safe to assume that expressions for moment derived for pure bending can also be used for laterally loaded plates. This assumption is equivalent to neglecting the effect on bending of the shearing forces and the compressive stress in

the z-direction produced by the lateral load. Errors introduced into these solutions by such assumptions are negligible provided the thickness of the plate is small in comparison with the other dimensions of the plate.

The equations for moment are derived in Ref. 11 for the general case. For the special case of isotropy, they can be stated

$$M_x = D\left(\frac{\partial^2 w}{\partial x^2} + \nu \frac{\partial^2 w}{\partial y^2}\right) \tag{3}$$

$$M_y = D\left(\frac{\partial^2 w}{\partial y^2} + \nu \frac{\partial^2 w}{\partial x^2}\right) \tag{4}$$

$$M_{xy} = -M_{yx} = -D\,(1 - \nu)\,\frac{\partial^2 w}{\partial x \partial y} \tag{5}$$

where D is the bending stiffness of the plate, ν is the Poisson's ratio, and other terms have been previously defined.

Substituting these expressions into Eq. 2 obtains

$$D\left[\frac{\partial^4 w}{\partial x^4} + 2\frac{\partial^4 w}{\partial x^2 \partial y^2} + \frac{\partial^4 w}{\partial y^4}\right] = q \tag{6}$$

The Generalized Hooke's Law

To obtain the relations between the components of stress and the components of deformation in an elastic body, it is necessary to choose some mathematical model which reflects the elastic properties of the body. In these derivations it is always assumed that the components of strain are linear functions of the components of stress. In other words, it is assumed that a continuous body satisfies the generalized Hooke's Law.

For the most general case of a homogeneous anisotropic body, the equations which express Hooke's Law in Cartesian coordinates x, y, z have the form

$$\begin{aligned}
\epsilon_x &= S_{11}\sigma_x + S_{12}\sigma_y + S_{13}\sigma_z + S_{14}\tau_{yz} + S_{15}\tau_{xz} + S_{16}\tau_{xy} \\
\epsilon_y &= S_{21}\sigma_x + S_{22}\sigma_y + S_{23}\sigma_z + S_{24}\tau_{yz} + S_{25}\tau_{xz} + S_{26}\tau_{xy} \\
\epsilon_z &= S_{31}\sigma_x + S_{32}\sigma_y \quad . \quad . \quad . \quad . \\
\gamma_{yz} &= S_{41}\sigma_x \quad . \quad . \quad . \quad . \quad . \quad . \\
\gamma_{xz} &= S_{51}\sigma_x \quad . \quad . \quad . \quad . \quad . \quad . \\
\gamma_{xy} &= S_{61}\sigma_x + S_{62}\sigma_y + \ldots + S_{66}\tau_{xy}
\end{aligned} \tag{7}$$

These equations contain 36 coefficients $S_{i,j}$, the so-called elastic constants. Solving these equations for stress components obtains an equivalent form for the equations in terms of stress:

$$\begin{aligned}
\sigma_x &= c_{11}\epsilon_x + c_{12}\epsilon_y + c_{13}\epsilon_z + c_{14}\gamma_{yz} + c_{15}\gamma_{xz} + c_{16}\gamma_{xy} \\
\sigma_y &= c_{21}\epsilon_x + c_{22}\epsilon_y + \ldots + c_{26}\gamma_{xy}
\end{aligned}$$

$$\sigma_z = c_{31}\epsilon_x + c_{32}\epsilon_y \quad . \; . \; . \; .$$

$$\tau_{yz} = c_{41}\epsilon_x \quad . \; . \; . \; . \; . \; . \; . \; . \; .$$

$$\tau_{xz} = c_{51}\epsilon_x \quad . \; . \; . \; . \; . \; . \; . \; . \; .$$

$$\tau_{xy} = c_{61}\epsilon_x + c_{62}\epsilon_y + \; . \; . \; . \; + c_{66}\gamma_{xy} \tag{8}$$

Several authors (8) have called the constants $S_{i,j}$ the coefficients of deformation, and the constants $c_{i,j}$ the moduli of elasticity. The moduli of elasticity can be uniquely expressed in terms of the coefficients of deformation when the value of their determinants are different from zero. It has been shown by others that the number of elastic constants in the most general case of anisotropy is reduced to 21 if the deformations of the elastic body can be considered to occur isothermally, that is, the temperature of each element remains constant during the deformation process.

Since

$$S_{12} = S_{21}$$

$$. \; . \; .$$

$$S_{56} = S_{65} \tag{9}$$

and likewise,

$$c_{12} = c_{21}$$

$$. \; . \; .$$

$$c_{56} = c_{65} \tag{10}$$

Eq. 1 can be written in terms of 21 coefficients as follows:

$$\epsilon_x = S_{11}\sigma_x + S_{12}\sigma_y + S_{13}\sigma_z + S_{14}\tau_{yz} + S_{15}\tau_{xz} + S_{16}\tau_{xy}$$

$$\epsilon_y = S_{12}\sigma_x + S_{22}\sigma_y + \; . \; . \; . \; + S_{26}\tau_{xy}$$

$$\epsilon_z = S_{13} \; . \; . \; .$$

$$. \; . \; .$$

$$\gamma_{xy} = S_{16}\sigma_x + S_{26}\sigma_y + \; . \; . \; . \; + S_{66}\tau_{xy} \tag{11}$$

and, likewise Eq. 2 can be written in terms of 21 moduli.

$$\sigma_x = c_{11}\epsilon_x + c_{12}\epsilon_y + c_{13}\epsilon_z + c_{14}\gamma_{yz} + c_{15}\gamma_{xz} + c_{16}\gamma_{xy}$$

$$\sigma_y = c_{12}\epsilon_x + c_{22}\epsilon_y + \; . \; . \; . \; + c_{26}\gamma_{xy}$$

$$\sigma_z = c_{13}\epsilon_x + \; . \; . \; .$$

. . .

$$\tau_{xy} = c_{16}\epsilon_x + c_{26}\epsilon_y + \ldots + c_{66}\gamma_{xy} \tag{12}$$

The problem of determining 21 coefficients to describe the behavior of an elastic body is still formidable. Fortunately, conditions of elastic symmetry permit still further reduction of this number. If the internal structure of a material possesses symmetry of any kind, the same symmetry can be observed in its elastic properties. F. Neumann (8) set forth a principle for crystals which establishes a connection between symmetry of construction and elastic symmetry. In general, this principle says that a material has the same kind of symmetry with regard to physical properties as it has in its crystallography. This principle can be expanded to include bodies which are not crystalline but which possess a symmetry of structure such as wood, plywood, and reinforced concrete.

If an anisotropic body possesses elastic symmetry, the equations of the generalized Hooke's Law are simplified. The simplifications can be thought of as follows: When viewed from the center of the symmetric coordinate system of the body, equal elastic properties are seen in both the positive and negative directions of any axis of symmetry. As a result, elastic bodies possessing symmetry have a smaller number of independent elastic constants than 21. The final number depends on the number of axes or planes of symmetry present in the body.

Three Planes of Elastic Symmetry

The case of interest involves three planes of elastic symmetry passing through each point of a body orthogonally, that is, the planes occur at right angles to each other. If the axes of the coordinate system are directed perpendicular to these planes, the following equations of the generalized Hooke's Law for an orthotropic body can be derived.

$$\begin{aligned}
\epsilon_x &= S_{11}\sigma_x + S_{12}\sigma_y + S_{13}\sigma_z \\
\epsilon_y &= S_{12}\sigma_x + S_{22}\sigma_y + S_{23}\sigma_z \\
\epsilon_z &= S_{13}\sigma_x + S_{23}\sigma_y + S_{33}\sigma_z \\
\gamma_{yz} &= S_{44}\tau_{yz} \\
\gamma_{xz} &= S_{55}\tau_{xz} \\
\gamma_{xy} &= S_{66}\tau_{xy}
\end{aligned} \tag{13}$$

Since the constants $S_{i,j}$ are redundant with $S_{j,i}$, it can be observed that there are nine independent elastic constants remaining.

Plane Stress Case

For the particular case of thin plates in bending, σ_z is taken to be zero (plane stress), and the following equations are obtained:

$$\begin{aligned}
\epsilon_x &= S_{11}\sigma_x + S_{12}\sigma_y \\
\epsilon_y &= S_{12}\sigma_x + S_{22}\sigma_y \\
\gamma_{xy} &= S_{66}\tau_{xy}
\end{aligned} \tag{14}$$

These equations are derived directly from an orthotropic plane stress element (shown in Ref. 11). The corresponding elements for stress in terms of strain are also developed in Ref. 11, and can be stated

$$\sigma_x = \frac{E_x}{1 - \nu_{xy}\nu_{yx}} (\epsilon_x - \nu_{yx}\epsilon_y) = E'_x\epsilon_x - E''\epsilon_y \tag{15}$$

$$\sigma_y = \frac{E_x}{1 - \nu_{xy}\nu_{yx}} (\epsilon_y - \nu_{xy}\epsilon_x) = E'_y\epsilon_y - E''\epsilon_x \tag{16}$$

$$\tau_{xy} = G\,\gamma_{xy} \tag{17}$$

where

$$E'_x = \frac{E_x}{1 - \nu_{xy}\nu_{yx}} \tag{18}$$

$$E'_y = \frac{E_y}{1 - \nu_{xy}\nu_{yx}} \tag{19}$$

$$E'' = \nu_{yx}E'_x = \nu_{xy}E'_y \tag{20}$$

Isotropic Elasticity

Hooke's Law for standard isotropic conditions can be stated

$$\sigma_x = \frac{E}{1 - \nu^2} (\epsilon_x + \nu\epsilon_y) \tag{21}$$

$$\sigma_y = \frac{E}{1 - \nu^2} (\nu\epsilon_x + \epsilon_y) \tag{22}$$

$$\tau_{xy} = G\,\gamma_{xy} \tag{23}$$

where γ_{xy} is the shearing strain, τ_{xy} is the corresponding shearing stress, and the shear modulus is

$$G = \frac{E}{2(1 + \nu)} \tag{24}$$

Other terms have been previously defined. By comparing these equations with Eq. 14, it can be seen that four elastic constants are required to describe the behavior of thin orthotropic plates, whereas two independent elastic constants are required for isotropic plates. The orthotropic constants are E'_x, E'_y, E'', and G_o. The shear modulus, G_o, is an independent constant, and a method for determining it is discussed in Ref. 11. It can be approximated by relating the other three constants as follows:

$$G_o = \frac{E_x E_y}{E_y (1 + \nu_{xy}) + E_x (1 + \nu_{yx})} \tag{25}$$

Orthotropic Elastic Plate Equations

The complete derivation of the differential equation of equilibrium is given in Ref. 11. Utilizing the elastic constants previously described, this equation can be stated

$$D_x \frac{\partial^4 w}{\partial x^4} + 2(D_1 + 2D_{xy}) \frac{\partial^4 w}{\partial x^2 \partial y^2} + D_y \frac{\partial^4 w}{\partial y^4} = q \tag{26}$$

where

$$D_x = \frac{E'_x t^3}{12} \tag{27}$$

$$D_y = \frac{E'_y t^3}{12} \tag{28}$$

$$D_1 = \frac{E'' t^3}{12} \tag{29}$$

$$D_{xy} = \frac{G_o t^3}{12} \tag{30}$$

since

$$H = D_1 + 2D_{xy} \tag{31}$$

Then Eq. 26 reduces to

$$D_x \frac{\partial^4 w}{\partial x^4} + 2H \frac{\partial^4 w}{\partial x^2 \partial y^2} + D_y \frac{\partial^4 w}{\partial y^4} = q \tag{32}$$

For the particular case of isotropy, this equation collapses to the equation

$$D \left[\frac{\partial^4 w}{\partial x^4} + 2 \frac{\partial^4 w}{\partial x^2 \partial y^2} + \frac{\partial^4 w}{\partial y^4} \right] = q \tag{33}$$

where

$$D = \frac{Et^3}{12 (1 - \nu^2)} \tag{34}$$

Since for isotropy

$$E'_x = E'_y = \frac{E}{1 - \nu^2} \tag{35}$$

$$E'' = \frac{\nu E}{1 - \nu^2} \tag{36}$$

$$G = \frac{E}{2(1 + \nu)} \tag{37}$$

Therefore, it can be seen that

$$D_x = D_y = \frac{Et^3}{12(1 - \nu^2)} = D \tag{38}$$

$$H = D_1 + 2D_{xy} = \frac{t^3}{12}(E'' + 2G) = \frac{t^3}{12}\left(\frac{\nu E}{1 - \nu^2} + 2\frac{E}{2(1 + \nu)}\right)$$

$$= \frac{Et^3}{12(1 - \nu^2)} = D \tag{39}$$

These equations were derived for structurally orthotropic materials. A great deal of work today deals with geometrically orthotropic plates. The same equations are used in such cases, but an equivalent thickness t is derived as appropriate to account for the variation in moment of inertia. Hoppmann and Huffington treat this problem in Ref. 10.

Pavement Slabs

Solutions of pavement slabs, or slabs-on-foundation as they are sometimes called, are of particular interest in this paper. For these developments it is satisfactory to assume that the intensity of the reaction of the foundation on the slab is proportional to the deflection w of the slab. This intensity is then given by the expression kw, where the constant k, expressed in pounds per square inch per inch of deflection, is called the "support modulus of the foundation." Determination of numerical values for this modulus depends largely on the properties of the foundation, but a discussion of these properties is beyond the scope of this paper. Such determinations, however, have been made by Terzahgi (27).

Although a great deal of work has been done on the pavement slab problem, probably the most significant accomplishments to date were made by Westergaard (31, 34), particularly with reference to the design problems encountered in concrete pavement. His analysis was done in the early 1920's and relates to three special-case loadings as follows: (a) load applied near the corner of a large rectangular slab (corner load); (b) load applied near the edge of a slab, but at a considerable distance from any corner (edge load); and (c) load applied at the interior of a large slab at considerable distance from any edge (interior load).

Other theoretical work was done by Gerald Pickett, et al. (21) in 1951 in studies of deflections and moments for concrete pavements. This study added additional solutions to those available for use by the practicing engineer. Perhaps more significantly, the results of these solutions were made available for practical use by incorporating them into influence charts similar to those developed by N. M. Newmark (20).

Additional contributions include work by Spangler (25), Teller and Sutherland (26), Kelley (13), and others who have, in the past 25 years, conducted experimental studies on pavement slabs to correlate deflections under static load with those predicted by theory. The evaluation of such work is beyond the scope of this paper, but it is discussed briefly under the heading of needed research.

Nonuniform Conditions

Unfortunately for the designer, most pavement slabs do not meet the stringent assumptions imposed by Westergaard. First, the slabs must in reality be finite (Fig. 1b). Second, uniform support is hard to obtain since local loss of support under the pavement due to pumping or settlement of the foundation is common (Fig. 1c). Richart and Zia (22) have treated this problem by applying a general method developed by Brotchie (4). Their solution relates specifically to a large slab-on-foundation spanning a circular void. They provide the designer with several curves useful in evaluating this specific condition. They do not treat, however, the more general cases of (a) smaller slabs spanning a void of irregular shape, (b) the problem of random placement of a void near a corner or edge, or (c) in the more general case, several voids under a single slab.

Leonards and Harr (16) also treat nonuniform subgrade support. They evaluate the effect of curling on a circular slab. The circular slab is not used in pavement design, but the methods developed may be useful in treating differential temperature effects in the future.

In the methods of this paper, the foundation is represented by the modulus of support k. This approach provides the basis for future consideration of nonlinear elastic foundation support (17). The freely discontinuous inputs allowed by the method provide the capability of varying k anywhere under the slab.

Cracks and Other Discontinuities

The theories described thus far relate to homogeneous materials. No provision has been made for cracks or other discontinuities (Fig. 1d). Other authors have treated this subject in some detail for special cases. These include Ang (1, 2), Williams (36), Reissner (23), and Knowles and Wang (14). Many authors, including those listed, discuss "Reissner bending of plates." This phrase refers to the equations for bending of elastic plates developed by Eric Reissner of MIT. Classical theory, that discussed at the beginning of this chapter, meets the so-called Kirchhoff boundary conditions at free edges, these being a vanishing bending couple and a vanishing sum of transverse force and edgewise rate-of-change of twisting couple at all free plate edges. These two con-

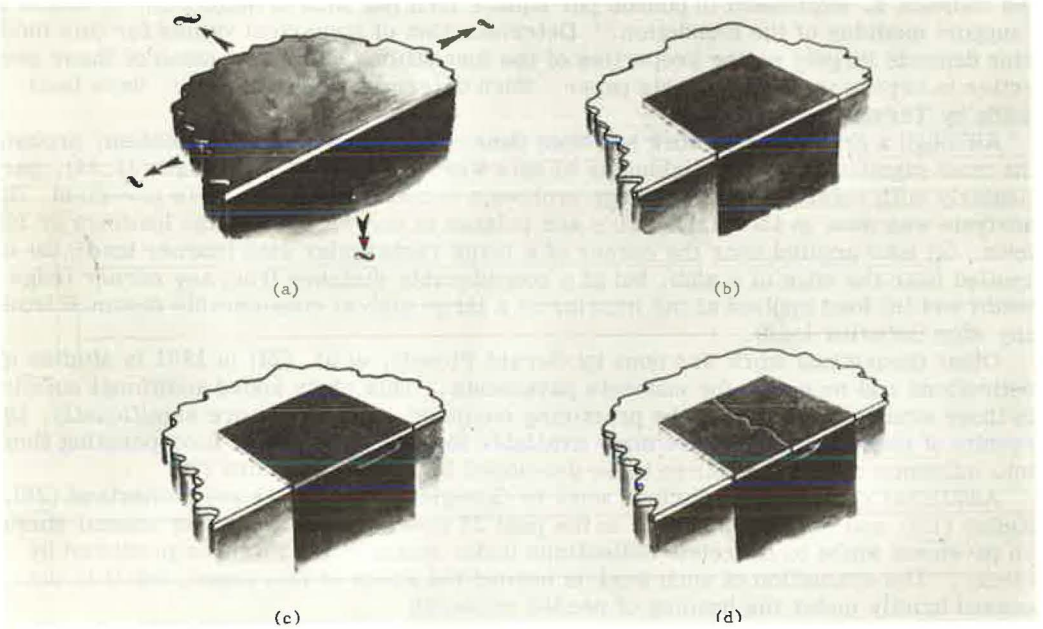

Figure 1. Comparison of real and infinite pavement slabs.

ditions are actually a compression of three independent conditions: (a) vanishing transverse force, (b) vanishing bending couple, and (c) vanishing twisting couple at free edges. "Reissner bending" includes differential equations fulfilling these three boundary conditions.

Reissner's studies further show that stresses near a finite crack in infinite plates are somewhat greater than those calculated by classical theory. This is accentuated near the base of the crack where extremely high stress concentrations might be expected. Such cracks are beyond the scope or application of this work and will not be treated.

The discontinuities of interest are those which occur across the entire slab cross-section at any particular location. Ang, Williams, and Reissner indicate that stress distribution can be predicted reasonably outside a distance half of the plate thickness from the edge of a crack. This is acceptable for the application of the method discussed herein, since this distance also approximates a half increment length in the finite analogy. Furthermore, such accuracy is quite adequate for structural plates and pavement slabs. Corrections to this theory can be obtained from "thick plate" theory and introduced into any solution where needed (33).

Summary of Elastic Theory

The theory described herein is helpful to the development of any method for analyzing plate bending. Closed-form solutions of the problems, however, become more difficult as complexities increase. Hand solutions of isotropic plates are readily accomplished, but for solutions of homogeneous orthotropic plates one must usually resort to computers. The addition of elastic support or finite cracks forces the use of approximate methods and limiting assumptions. Furthermore, each solution represents a special case, and a multitude of special-case solutions are required for the problems of interest. A more general, more rapid method would be of great advantage to the engineer. It would also be helpful if these solutions could be accomplished without resorting to higher order functions such as Bessel and Hankel functions. Such a general theory is the object of the research described herein.

FINITE-ELEMENT THEORY

The theories discussed in the preceding section are based on infinitesimal calculus. There are many rules governing the use of such calculus. In general, the functions must be continuous, and fourth order systems must have two continuous derivatives. Many complex engineering problems do not properly fulfill these conditions and cannot, therefore, be solved by resorting to the calculus. Furthermore, many such classical or analytical methods may not be well adapted for use on high-speed digital computers. As a consequence, approximate, or so-called "numerical," methods have been developed. Hardy Cross (8, p. 1) pioneered the use of such methods in civil engineering with moment distribution methods. Newmark (8, p. 138) and Southwell (8, p. 66) have also been instrumental in these developments. In such numerical methods, the differential equation concerned is replaced by its finite difference equivalent. The problem then reduces to solving a large number of simultaneous algebraic equations instead of one complex differential equation.

The method described herein is slightly different and involves breaking a plate or slab into a system of finite elements, each consisting of rigid bars connected by elastic blocks. The algebraic equations describing the system are derived by free-body anaysis of the finite model.

Assumptions

It is impossible to develop a completely general theory describing the behavior of any structure. It is often difficult to find solutions for the mathematical equations describing even limited theories; therefore, additional conditions and assumptions are often imposed to permit solution. While many of these assumptions are known, it seems worthwhile to restate the assumptions and conditions relative to the finite-element model describing slab behavior.

1. Planes of the plate lying initially normal-to-the-middle surface of the plate remain on the normal-to-the-middle surface of the plate after bending.
2. Normal stresses in the direction perpendicular to the plate surface can be disregarded for the bending solution.
3. There is no axial deformation in the middle plane of the plate and, thus, this plane remains "neutral" during bending.
4. All deformations are small with regard to dimensions of the plate.
5. The bar elements of the model are infinitely stiff and weightless.
6. Each joint in the model is composed of an elastic homogenous and orthotropic material which can be described by four independent elastic constants.
7. Loads, masses, and bending strains occur at the joint.
8. Torsional stiffness of the plate element can be invested in torsion bars.
9. The neutral axis lies in the same plane for all elements even for nonuniform cross-sections. (Violation of this assumption, as stated by Ang and Newmark (2), has been shown to cause little error.)
10. The spacing of the beam elements, designated by h_x and h_y, need not be equal but must be constant for all parallel beams.
11. The number of increments into which each beam is divided is equal to the length of the beam divided by the increment length.

The Physical Model

Numerical methods are most often used as mathematical approximations of a governing differential equation by the substitution of finite-difference forms for derivatives, or by the approximation of a continuum problem with a discrete nodal system. A second and perhaps preferable method is to model the plate or slab physically by a system of finite elements whose behavior can properly be described with algebraic equations. Newmark (8) pioneered such models for articulated beams and plates. He states". . . the use of the model (finite-element model) offers certain advantages; there is no ambiguity concerning the boundary conditions; statical checks on the results have a physical meaning and can be made more accurately; variations in dimensions and physical properties can be more easily treated." For many problems, the finite-difference equations developed by direct substitution for the differential equation and the finite-element model equations developed from a free-body analysis of the model are equivalent. This, however, is not always the case. The physical model seems preferable because it facilitates visualization of the problem and formulation of proper boundary and loading conditions. It is useful, however, to use difference equations to describe the bending moments in the finite-element beams.

Model of a Beam-Column

The basic element in the plate model developed here is the model of a beam subjected to transverse and axial loads (termed a beam-column and developed by Matlock, et al.) (18, 19). Figure 2 shows the development of this model. Figure 2a illustrates a beam element deformed by the action of pure bending and subjected to the assumptions of conventional beam theory. For linearly elastic stress and strain, the stresses acting on the beam element are shown in Figure 2b. If these distributed stresses are to be replaced by concentrated forces as shown in Figure 2c, as they often are for design purposes, it seems reasonable to develop the mechanical model, Figure 2d. Here the deformed beam element is replaced by a pair of hinged plates with linear springs containing the elastic flexural stiffness of the beam restraining movement of the plates, top and bottom. Thus, a beam could be represented by a series of such beam element models (Fig. 2e).

If the thickness of the plates between hinged joints is increased, a cruder representation results (Fig. 2f). It has been shown, however, that representation of real beams by models containing as few as six elements or increments (as they will be called hereafter) give satisfactory approximation of real beams. As a specific example of modeling, Figure 3 indicates a beam-on-foundation subjected to both lateral and axial loads. Supports may be linearly-elastic, non-linear, or fixed. Figure 4 shows these loads and supports depicted in the finite-element model. Many other loads and load com-

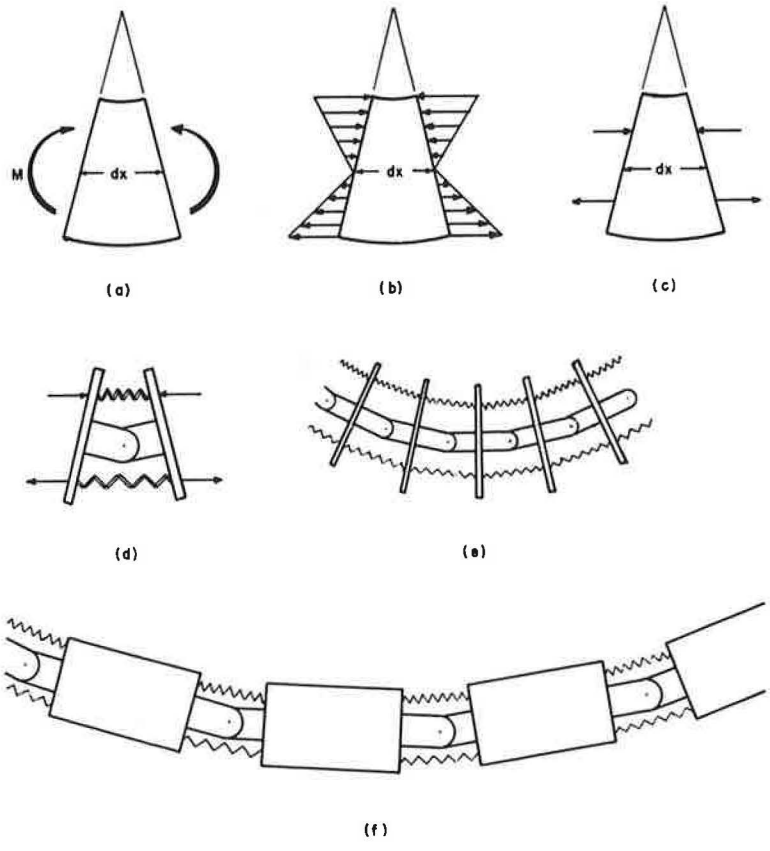

Figure 2. Finite mechanical representation of a conventional beam.

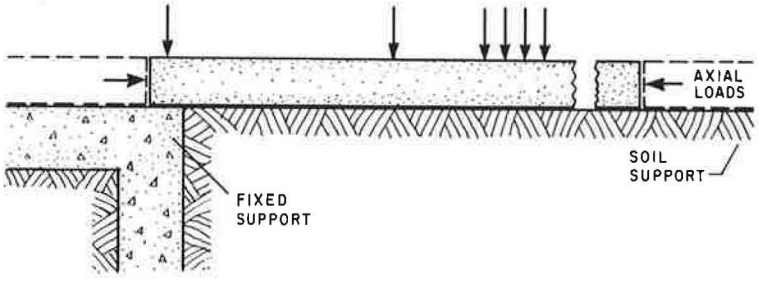

Figure 3. Example beam on foundation subjected to lateral and axial loads.

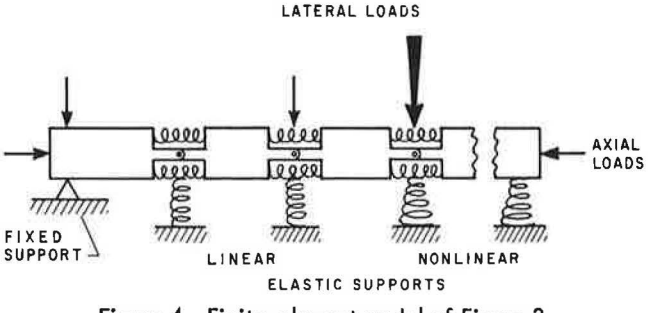

Figure 4. Finite-element model of Figure 3.

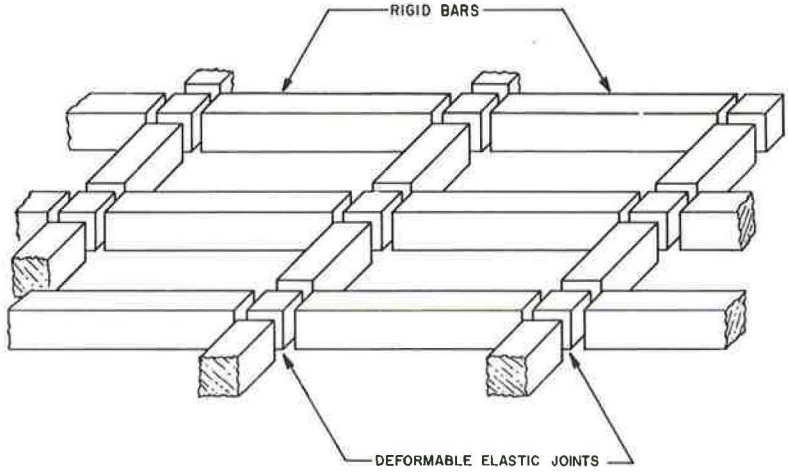

Figure 5. Finite-element model of grid-beam system.

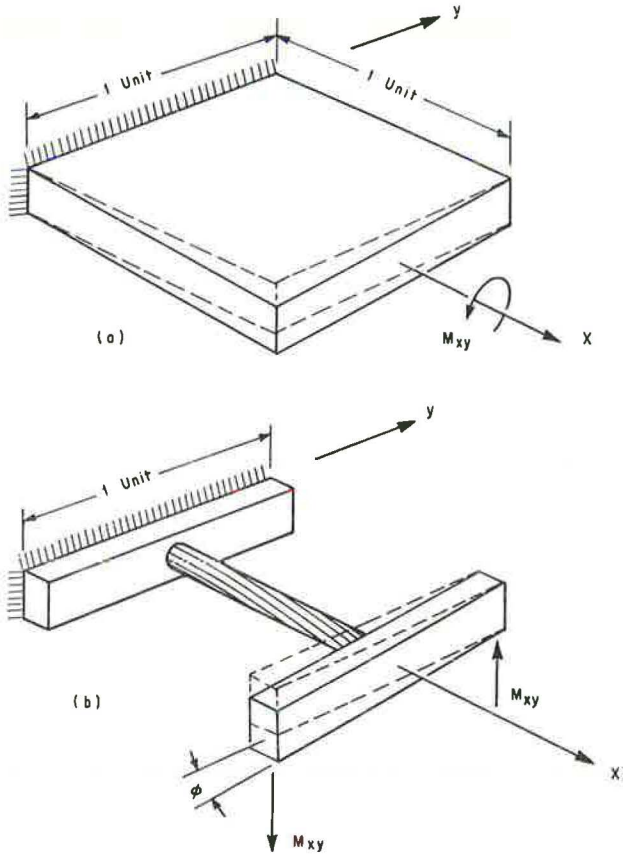

Figure 6. Finite-element representation of torsional stiffness.

binations are possible. These include distributed or concentrated, transverse loads, transverse couples, axial loads, and bending moments. Elastic restraints are included as linear or nonlinear supports, or, as distributed or concentrated rotational restraints. In short, almost any physical combination of loads or restraints can be applied to a beam-column with this method.

Simple Two-Dimensional Systems

If one or more of these beams in each horizontal orthogonal direction are combined, they form a grid-beam system similar to the girder and stiffener system of a bridge deck or similar to the beam system of a waffle floor (Fig. 5). Tucker and Matlock (29) extended the use of the beam-column model to such systems. Each of the beams in this grid-beam system can be solved by the beam-column method as a line member. However, the effect of one beam on the next beam is important if the beams act as a monolithic system.

Such systems account for pure bending only. No torsion or Poisson's ratio effect is considered. In a true grid-beam system, these effects are small and do not affect the solution significantly.

Plates and Slabs

For the plate solution, however, the effects of torsion in particular are of significant importance, and the Poisson's ratio effects are more important than for grid-beam problems. Tucker (30) has worked on this problem as have Ang and Newmark (2). The next step was to determine some method for including these two factors in the model.

First, consider torsion in Figure 6. If a unit element is removed from the slab, a twisting moment M_{xy} can be applied about the x-axis. The torsional stiffness C of the slab is defined as the applied twisting moment divided by the resulting angular rotation, φ, across the element. Then

$$C = \frac{M_{xy}}{\varphi} \tag{40}$$

Considering this element as two beams connected by a torsion bar, the bar modulus can be chosen equal to C so that an applied twisting moment will produce the same rela-

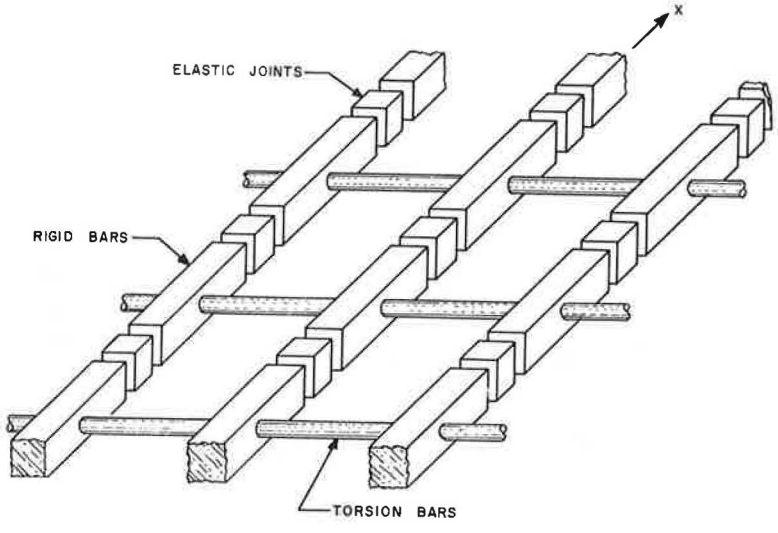

Figure 7. Finite-element x-beam system with torsion bars acting between segments.

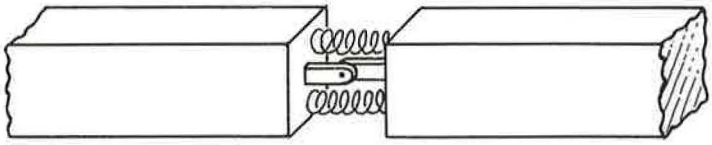

(a) Typical joint from the beam-column model.

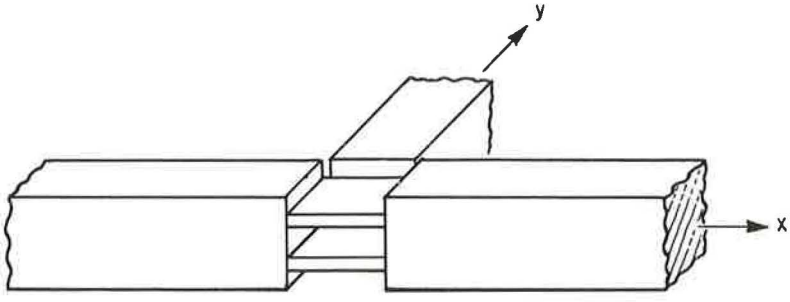

(b) Typical joint from the plate model (partial cutaway).

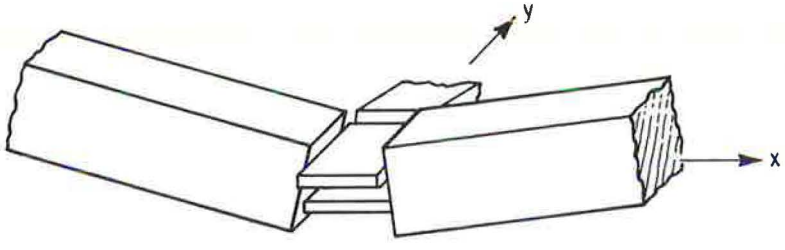

(c) Deformed joint from the plate model.

Figure 8. Action of Poisson's ratio at a finite joint.

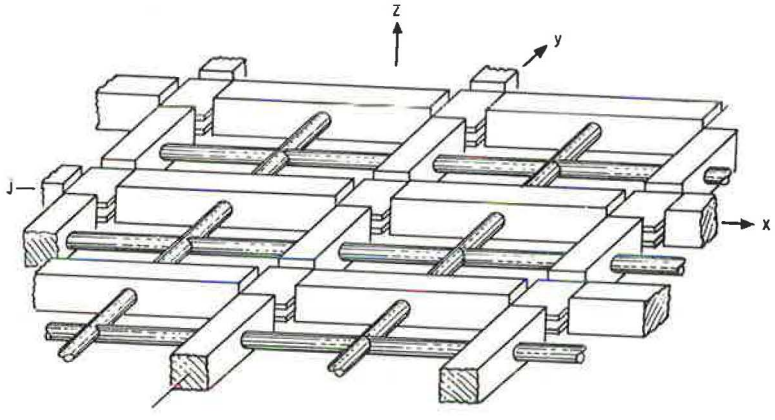

Figure 9. Finite-element model of a plate or slab.

tive angle change φ as in the real unit element of the plate. Using this technique, torsion bars can be inserted between the adjacent bar elements of all the beams in the y-direction of the grid-beam system as shown in Figure 7. These torsion bars are also inserted, of course, between the beams in the orthogonal x direction as shown in Figure 9. It is convenient to think of one set of torsion bars acting with each set of beams since the solution proceeds in this manner. It should be emphasized here that these torsion bars represent the real torsional stiffness of the slab and are always active in the system.

The effect of Poisson's ratio is easier to handle than torsion. Remember that the bending stiffness EI of a beam-column is vested in linear springs restraining the movement of the finite-elements at each joint. The analogous bending stiffness of a plate

$$D = \frac{Et^3}{12\,(1 - \nu^2)} \tag{41}$$

replaces the EI of the beam and must also be concentrated. A pair of linear springs, however, is not satisfactory for this purpose since they can transfer no Poisson's ratio load. These stiffness springs are, therefore, replaced in the plate model by elastic blocks whose stress-strain relationship is equivalent to that of the real plate and which have Poisson's ratio equal that of the plate. Figure 8 illustrates the action of these elastic blocks. The blocks in Figure 8b replace the springs in Figure 8a. If the beams in the x-direction are bent up, the beams in the orthogonal y-direction bend down due to Poisson's ratio (unless they are restrained). The force required to restrain them results in an additional bending moment which equals

$$\Delta M_y = \nu D \left(\frac{\partial^2 w}{\partial x^2}\right) \tag{42}$$

This is likewise true for the action of the y-beams on the x-beams. As a result, the bending moment in an x-beam becomes

$$M_x = D \left(\frac{\partial^2 w}{\partial x^2} + \nu \frac{\partial^2 w}{\partial y^2}\right) \tag{43}$$

Figure 9 shows the assembled slab model. The torsion bars in Figure 9 are considered to resist only torsion.

Input Values for Model

Having developed a model, it is necessary to relate it to a real plate or slab. The plate is divided into increments in the x- and y-directions with increment length h_x and h_y, respectively. These "beam" increments are designated with i in the x-direction and j in the y-direction. The mesh point or joint on the positive end of each increment is arbitrarily numbered the same as that increment. This numbering system then gives the i, j grid indicated in Figure 10. It is also convenient to denote segments of the plate bounded by increments in both the x- and y-directions, because these segments correspond to the torsion bars in Figure 10.

Stiffness and Lateral Load.—To describe the real plate with the model, it is appropriate to look at the j^{th} x-beam. Figure 11 shows a side view of this beam which may be irregular in profile and may be loaded by a varying distributed load q. One increment width of the load, centered on the i^{th} mesh point, is assigned to Station i on the j^{th} x-beam (Station i, j on the model). $Q_{i,j}$ is the lumped load applied at Station i, j. $D_{i,j}$ represents the bending stiffness of the plate segment of which mesh point i, j is the center. The sketch is intended to illustrate that the stiffness may vary. In this case, it decreases from Station i-1 toward Station i+1. The load also varies but increases from Station i-1 toward Station i+1. $Q_{i,j}$ can be expressed by the equation

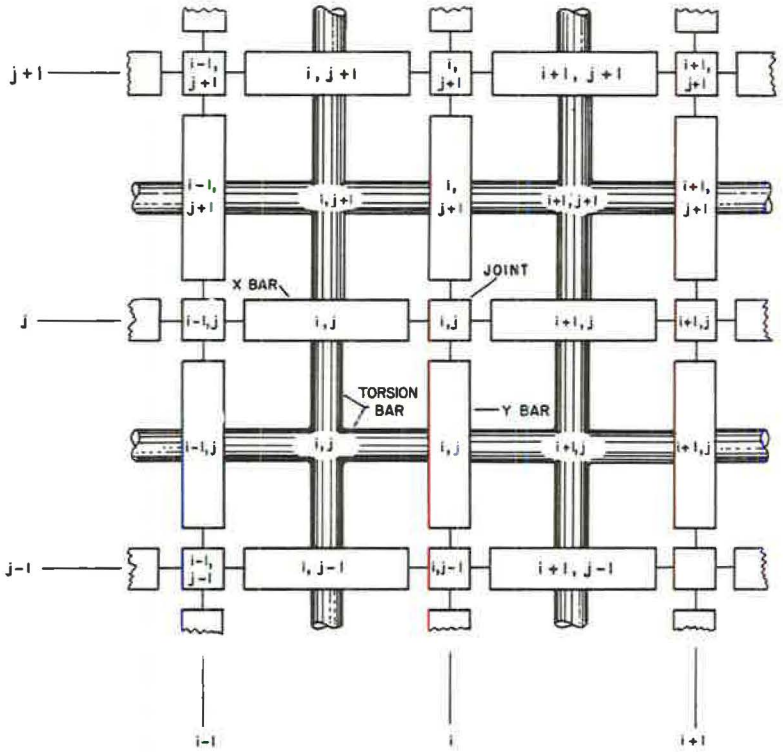

Figure 10. Plan view of the slab model showing all parts with generalized numbering system.

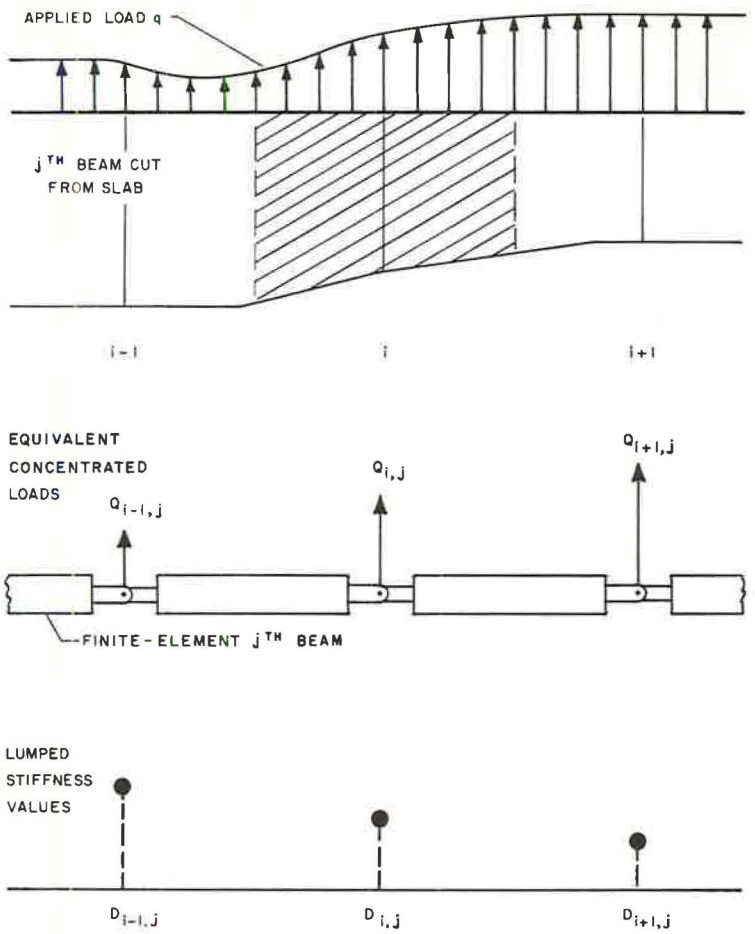

Figure 11. Finite-element representation of a beam cut from slab with finite-element loads and stiffness.

$$Q_{i,j} = \sum_{i-\frac{1}{2}}^{i+\frac{1}{2}} \sum_{j-\frac{1}{2}}^{j+\frac{1}{2}} q + Q_c \tag{44}$$

where Q_c is any concentrated load which may be present at the station in addition to the distributed load.

The stiffness $D_{i,j}$ for a plate is a unit value per inch of width. It is convenient for use in computations to input average values over a full increment width. If $D^x_{i,j}$ represents the average stiffness in the x-direction, it can be calculated

$$D^x_{i,j} = \int_{i-\frac{1}{2}}^{i+\frac{1}{2}} \int_{j-\frac{1}{2}}^{j+\frac{1}{2}} \frac{D^x_{i,j}}{h_x h_y} \tag{45}$$

that is, the average bending stiffness of the plate over an area one increment wide and one increment long, centered at Station i, j. Full development of all input for the model is provided in Ref. 11.

Other Input Values.—It is convenient to represent the torsional stiffness of plate segment i, j as torsion bars i, j acting at the midpoint of the model elements (Fig. 10). It is also helpful for external couples or torques applied to the plate to be input into the stiff beam elements. This is properly shown on the free-body in the next section. Axial loads, P, are also input into the bars with the changes, ΔP, considered to occur at mesh points.

Summary of Finite-Element Theory

A physical model has been chosen to represent the plate or slab for solution by numerical methods in preference to expressing the differential equation governing slab behavior in finite-difference form. The model is straightforward and assists visualization of the problem. Discontinuities and freely discontinuous changes in load, bending stiffness, torsional stiffness, and other parameters are easily understood with the use of a physical model, but limitations on continuity of the differential equation make direct difference approximations suspect.

The greater the number of increments used to model a particular problem, the greater the accuracy of the solution. All exact solutions are based on infinitesimal changes in the real structure. Experience with this model indicates that reasonable results can be obtained with most problems using 8 to 20 increments in each direction, although the number of increments to be used will certainly depend on the dimensions of the problem as well as the accuracy required and the local complexity to be resolved. This is discussed in the section on "Example Problems and Verification of the Method."

FORMULATION OF EQUATIONS

The purpose of this section is to formulate from a free-body analysis the equations necessary to solve for the bending of a slab. It is intended here to give a readable and concise account of these developments rather than a complete mathematical treatment.

Free-Body Analysis

To derive the equations for solution of the bending of a plate or slab, it is helpful to refer to a free-body of the model. Consider first a section of the assembled slab model centered at any mesh point i, j (Fig. 12). For the present, the x-bar to the left of point i, j is called Bar a, and the x-bar to the right of point i, j is called Bar b.

Figure 13 shows these same bars as a free-body with other members of the model fixed and replaced by a system of equivalent forces. $Q^y_{i,j}$ represents the load carried

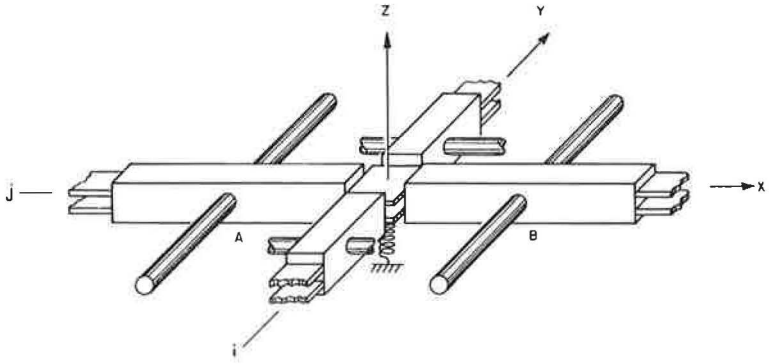

Figure 12. Typical joint i,j taken from finite-element slab model.

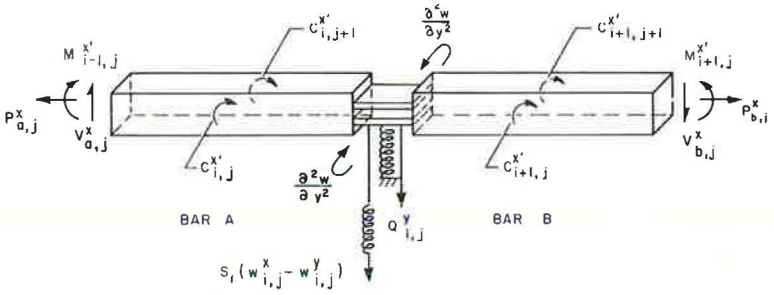

Figure 13. Free-body of joint i,j with other members of the model replaced by an equivalent force system.

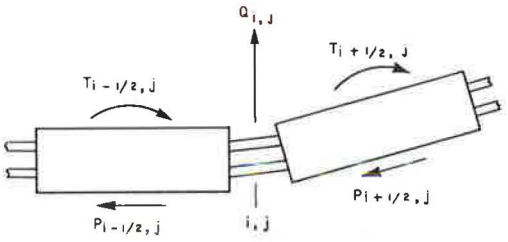

Figure 14. Typical joint i,j with force and restraint inputs shown.

by the y-beam at this intersection and the term $\partial^2 w/\partial y^2$ represents the restraint of the y-beam which provides the Poisson's ratio effect in the x-beam moment. The term $S_f\left(w^x_{i,j} - w^y_{i,j}\right)$ represents the load stored in the fictitious spring closure parameter. These closure springs will be discussed fully in the next two sections. Figure 14 shows the external forces which can be applied to these same two bars. Any of these forces may be zero but are considered to be present for generality. Combining the system of equivalent forces and external loads gives the general free-body of the slab model in Figure 15. This free-body is for a section of an x-beam. A similar free-body can be developed for the y-beam by changing all x's for y's, and all y's for x's.

Summing vertical forces in Figure 15 at joint i, j with up taken as positive gives

$$\Sigma F^x_{v_{i,j}} = Q^y_{i,j} + V^x_{a,j} - V^x_{b,j} - S_{i,j}\left(w^x_{i,j}\right) - Q_{i,j} - S_f\left(w^x_{i,j} - w^y_{i,j}\right) = 0 \quad (46)$$

To evaluate the shear $V^x_{a,j}$, sum moments acting on Bar a about the center of the bar (clockwise rotations are positive). For equilibrium

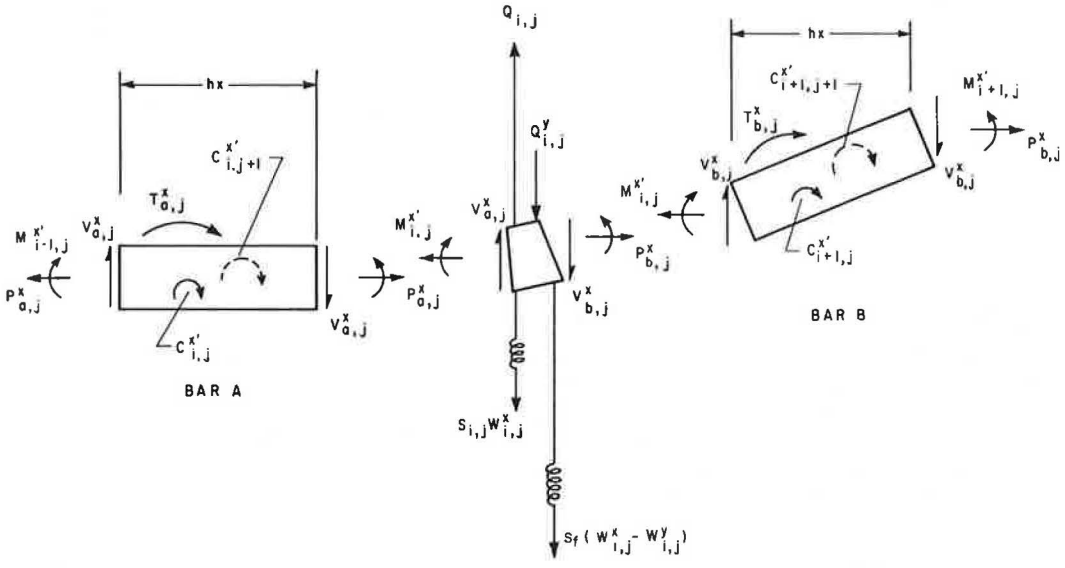

Figure 15. Generalized free-body of joint i,j with all forces and restraints shown.

$$\sum M_a = 0 = M^{x'}_{i-1,j} - M^{x'}_{i,j} + T^{x}_{a,j} + C^{x'}_{i,j} + C^{x'}_{i,j+1} + V_{a,j} h_x + 2P^{x}_{a,j}\left(\frac{-w^{x}_{i-1,j} + w^{x}_{i,j}}{2}\right) = 0 \quad (47)$$

Multiplying through by h_x and clearing obtains

$$-h_x V^{x}_{a,j} = M^{x'}_{i-1,j} - M^{x'}_{i,j} + T^{x}_{a,j} + C^{x'}_{i,j} + C^{x'}_{i,j+1} + P^{x}_{a,j}\left(-w^{x}_{i-1,j} + w^{x}_{i,j}\right) \quad (48)$$

Likewise summing moments about Bar b and multiplying through by h_x obtains an expression for the shear $V^{x}_{b,j}$ as follows:

$$-h_x V^{x}_{b,j} = M^{x'}_{i,j} - M^{x'}_{i+1,j} + T^{x}_{b,j} + C^{x'}_{i+1,j} + C^{x'}_{i+1,j+1} + P^{x}_{b,j}\left(-w^{x}_{i,j} + w^{x}_{i+1,j}\right) \quad (49)$$

Multiplying Eq. 46 through by h_x and substituting Eqs. 48 and 49 for the shears obtains the equation of interest. After convenient grouping of terms and transfer of all known values to the right-hand side of the equation, with a sign change, it becomes

$$\left(M^{x'}_{i-1,j} - 2M^{x'}_{i,j} + M^{x'}_{i+1,j}\right) - \left(- C^{x'}_{i,j} - C^{x'}_{i,j+1} + C^{x'}_{i+1,j} + C^{x'}_{i+1,j+1}\right)$$

$$+ P^{x}_{a,j}\left(- w^{x}_{i-1,j} + w^{x}_{i,j}\right) - P^{x}_{b,j}\left(- w^{x}_{i,j} + w^{x}_{i+1,j}\right) + S_{i,j} h_x w^{x}_{i,j}$$

$$= h_x\left[Q_{i,j} - Q^{y}_{i,j} - S_f\left(w^{x}_{i,j} - w^{y}_{i,j}\right)\right] - T^{x}_{a,j} + T^{x}_{b,j} \qquad (50)$$

This equation relates forces and deflections at point i, j, but all of the prime terms must be evaluated further before the required mathematical manipulations can be performed. It is necessary at this point to substitute the central difference formulations of moment. Accordingly, they are substituted at Stations i-1, j; i, j; and i+1, j.

The term $C'_{i,j}$ represents the force exerted on the x-beam due to the relative rotation between this beam and its neighbors. These expressions must be written for $C^{x'}$ at Stations i, j; i, j+1; and i+1, j+1.

After making these substitutions, Eq. 50 becomes

$$h_y D^{x}_{i-1,j}\left[\left(\frac{w^{x}_{i-2,j} - 2w^{x}_{i-1,j} + w^{x}_{i,j}}{h_x^2}\right) + \nu_{yx}\left(\frac{w^{y}_{i-1,j-1} - 2w^{y}_{i-1,j} + w^{y}_{i-1,j+1}}{h_y^2}\right)\right]$$

$$- 2h_x D^{x}_{i,j}\left[\left(\frac{w^{x}_{i-1,j} - 2w^{x}_{i,j} + w^{x}_{i,j}}{h_x^2}\right) + \nu_{yx}\left(\frac{w^{y}_{i,j-1} - 2w^{y}_{i,j} + w^{y}_{i,j+1}}{h_y^2}\right)\right]$$

$$+ h_y D^{x}_{i+1,j}\left[\left(\frac{w^{x}_{i,j} - 2w^{x}_{i+1,j} + w^{x}_{i+2,j}}{h_x^2}\right) + \nu_{yx}\left(\frac{w^{y}_{i+1,j-1} - 2w^{y}_{i+1,j} + w^{y}_{i+1,j+1}}{h_y^2}\right)\right]$$

$$+ \frac{C^{x}_{i,j}}{h_y}\left(w^{x}_{i-1,j-1} - w^{x}_{i-1,j} - w^{x}_{i,j-1} + w^{x}_{i,j}\right)$$

$$+ \frac{C^{x}_{i,j+1}}{h_y}\left(- w^{x}_{i-1,j} + w^{x}_{i,j} + w^{x}_{i-1,j+1} - w^{x}_{i,j+1}\right)$$

$$- \frac{C^{x}_{i+1,j}}{h_y}\left(- w^{x}_{i,j} + w^{x}_{i+1,j} + w^{x}_{i,j-1} - w^{x}_{i+1,j-1}\right)$$

$$- \frac{C^{x}_{i+1,j+1}}{h_y}\left(- w^{x}_{i,j} + w^{x}_{i+1,j} + w^{x}_{i,j+1} - w^{x}_{i+1,j+1}\right)$$

$$+ P^x_{a,j}\left(-w^x_{i-1,j} + w^x_{i,j}\right) - P^x_{b,j}\left(-w^x_{i,j} + w^x_{i+1,j}\right) + h_x\left(S_{i,j} + S_f\right)w^x_{i,j}$$

$$= h_x\left(Q_{i,j} - Q^y_{i,j} + S_f w^y_{i,j}\right) - T^x_{a,j} + T^x_{b,j} \tag{51}$$

It is convenient in computation to use the same numbering system for bars, torsion bars, and joints. So far in these developments bars have been referred to as a and b. Referring to the numbering system shown in Figure 10, it will be recognized that in reality a becomes i and b becomes i+1. Therefore, for example, $T^x_{a,j}$ becomes $T^x_{i,j}$, $P^x_{b,j}$ becomes $P^x_{i+1,j}$, etc.

This will be an implicit solution for $w^x_{i,j}$, the deflection of the j^{th} x-beam at Station i. It is convenient for solution, however, to utilize the last estimated values for all deflections, w^x, not falling on the j^{th} beam for a particular iteration, and transfer them to the right-hand side of the equation. Furthermore, all of the y-beam deflections $w^y_{i,j}$ will be assumed known from a previous iteration and will also appear on the right-hand side of the equation. After making the notation change of a to i and transferring known values to the right-hand side, it is helpful to clear fractions and rearrange terms. The resulting equation is the equation we seek and is most conveniently written in terms of five unknown deflections, i.e.,

$$a_x w^x_{i-2,j} + b_x w^x_{i-1,j} + c_x w^x_{i,j} + d_x w^x_{i+1,j} + e_x w^x_{i+2,j} = f_x \tag{52}$$

where

$$a_x = \frac{h_y^2}{h_x^2} D^x_{i-1,j} \tag{53}$$

$$b_x = -2.0\,\frac{h_y^2}{h_x^2}\left(D^x_{i-1,j} + D^x_{i,j}\right) - C^x_{i,j} - C^x_{i,j+1} - h_y P^x_{i,j} \tag{54}$$

$$c_x = \frac{h_y^2}{h_x^2}\left(D^x_{i-1,j} + 4D^x_{i,j} + D^x_{i+1,j}\right) + C^x_{i,j} + C^x_{i+1,j} + C^x_{i,j+1} + C^x_{i+1,j+1} + h_x h_y\left(S_{i,j} + S_f\right) + h_y\left(P^x_{i,j} + P^x_{i+1,j}\right) \tag{55}$$

$$d_x = -2.0\,\frac{h_y^2}{h_x^2}\left(D^x_{i,j} + D^x_{i+1,j}\right) - C^x_{i+1,j} - C^x_{i+1,j+1} - h_y P^x_{i+1,j} \tag{56}$$

$$e_x = \frac{h_y^2}{h_x^2} D^x_{i+1,j} \tag{57}$$

$$f_x = h_x h_y \left(Q_{i,j} - Q^y_{i,j} + S_f w^y_{i,j}\right) + h_y \left(T^x_{i,j} + T^x_{i+1,j}\right)$$

$$- \nu_{yx} \left[D^x_{i-1,j} \left(w^y_{i-1,j-1} - 2w^y_{i-1,j} + w^y_{i-1,j+1}\right)\right.$$

$$- 2D^x_{i,j} \left(w^y_{i,j-1} - 2w^y_{i,j} + w^y_{i,j+1}\right) + D^x_{i+1,j} \left(w^y_{i+1,j-1} - 2w^y_{i+1,j}\right.$$

$$\left. + w^y_{i+1,j+1}\right)\Big] - C^x_{i,j} \left(w^x_{i-1,j-1} - w^x_{i,j-1}\right) - C^x_{i,j+1} \left(w^x_{i-1,j+1} - w^x_{i,j+1}\right)$$

$$+ C^x_{i+1,j} \left(w^x_{i,j-1} - w^x_{i+1,j-1}\right) + C^x_{i+1,j+1} \left(w^x_{i,j+1} - w^x_{i+1,j+1}\right) \qquad (58)$$

One term remains to be evaluated, $Q^y_{i,j}$, the load absorbed by the y-beams at any time. This load can be evaluated by numerical differentiation of the deflected pattern of the y-beam system, but it can also be done from the free-body analysis by summing vertical forces in terms of load absorbed by both sets of beams, $Q^x_{i,j}$ and $Q^y_{i,j}$. This summation on the free-body in Figure 15 gives

$$Q_{i,j} - Q^y_{i,j} - Q^x_{i,j} - S_{i,j} w^x_{i,j} + S_f \left(w^x_{i,j} - w^y_{i,j}\right) = 0 \qquad (59)$$

After necessary algebraic manipulations, the appropriate equation for evaluating $Q^y_{i,j}$ is seen to be as follows

$$Q^y_{i,j} = \overline{QBMY}_{i,j} + \overline{QTMY}_{i,j} + \overline{QPY}_{i,j} + \frac{T^y_{i,j} - T^y_{i,j+1}}{h_y} \qquad (60)$$

If this process is repeated for a segment of y-beam, equations comparable to Eqs. 52 through 58 can be developed for the y-beams.

Summary

Eqs. 52 through 58 conveniently describe the model at Station i, j and are statically correct since the summation of forces at any time during the solution will equal zero. There are two such sets of equations, one for the x-system and one for the y-system at each mesh point i, j. The number of stations in each direction is equal to the number of increments plus 4. As an example, a problem divided into eight increments in the x-direction and eight increments in the y-direction would require equations at 12 stations in each direction. Thus the number of equations required to describe the system would be 288; 144 for the y-beams and 144 for the x-beams. This readily explains the need to resort to digital computers to perform the mathematical manipulations.

SOLUTION OF EQUATIONS

The equations derived in the preceding section are formidable. Two sets of such equations are required to describe each mesh point in the system, one for the x-beams and one for the y-beams. To make these equations useful, some general technique for solving them rapidly is necessary. Although some hand methods have been developed for small mesh systems, the high-speed digital computer offers the desirable approach. This section presents several methods available for solution of these equations. A general description of the method chosen for use in this work is included.

Current Methods for Solution of Simultaneous Equations

The methods developed to solve systems of equations like Eq. 52 fall into about five major categories: (a) simple direct-elimination methods, (b) methods involving iterative techniques similar to moment distribution, (c) general relaxation techniques, (d) successive over-relaxation, and (e) alternating-direction-implicit methods. Actually, there are many other methods and many variations of the major methods listed above. The purpose of this writing, however, is not to survey the field of numerical analysis, but to apply a useful method to the solution of plates and slabs.

White and Cottingham (35) found a simple elimination method to be useful in their solution of plate buckling problems. Such elimination methods, however, are time consuming, requiring time in proportion to the cube of the number of equations involved. Another major drawback of this method is storage space since every term in the matrix must be stored even though many are zero.

Newmark (20) discusses several methods for solving simultaneous equations including successive approximation and step-by-step methods, as well as the distribution method. Distribution methods are somewhat more formal than relaxation methods and are organized for hand computations by technicians. Such methods are too cumbersome for efficient use in a digital computer.

The relaxation methods, or more specifically the method of "successive relaxation of constraints," is based on the concept that the structure is maintained in a continuous state, but has acting on it residual loads which are not statically consistent with the correct loading. The "residuals" are reduced by introducing arbitrary changes in displacement until convergence or statical balance is obtained. Southwell (8, p. 66) pioneered such methods. These were also originally developed for hand computation but are flexible enough for use in computers. Liebmann (8, p. 147) coded relaxation techniques for use on digital computers and speeded the process up considerably. Even so, he states, "The disadvantages of this procedure are the slow rate of convergence in many cases and the possible lack of convergence." Other work on this technique includes that by Jacobi, Gauss and Seidel, Richardson, and Frankel.

The SOR method, successive over-relaxation, provides still faster and better trial-and-error solutions by applying a complex relaxation factor which over-relaxes or over-compensates the adjustment of the existing data on any given trial. Otherwise, the method is basically that of relaxation.

The alternating-direction method presented by Conte and Dames (5) appears to offer by far the best techniques for solving the plate equation. Others who have used this method include Griffin and Varga (7) and Tucker (30). Because of its applicability, a more complete discussion of this method is warranted.

Alternating-Direction Implicit Solution

Conte and Dames (5) present an implicit alternating-direction iterative scheme which appears to be more efficient than any of the relaxation methods. Their procedure is an extension of methods developed by Douglas and Rachford. Conte and Dames (5) present a solution of the partial differential equation which governs slab behavior. In simplest terms, the method divides the partial differential equation into two ordinary differential equations and couples their solution by trial and error in a methodical fashion, proceeding first in the x-Cartesian direction, then in the y-direction, thus the name alternating-direction. The most difficult part of using this method is the selection

of proper iteration parameters. Proof of convergence exists for certain parameter selection for regular, well-conditioned systems. For the diverse systems described herein, however, much remains to be done.

Experimentation by Matlock, Tucker, Ingram, Salani, and Haliburton (18, 30, 12, 24) with these methods has led to the use of the alternating-direction iterative method in the solutions in this report. This technique has many favorable characteristics which warrant its use, as follows:

1. The method is rapid and well adapted for computer use.
2. The method fits well with the mechanical model used to describe the system.
3. The process can be easily visualized as a trial-and-error solution of the model.
4. The method is logical and can be understood by practicing engineers.

The concepts developed herein are general in nature. They do not emphasize mathematical rigor and completeness, but are shown to be applicable to many engineering problems. No attempt will be made to prove mathematically absolute convergence, although such proof is available for special-case uniform, homogeneous, isotropic systems. Rather, the advantages and capabilities of the method will be demonstrated by examples later in this report. The validity of these diverse examples and their exhibition of closure or convergence to acceptable tolerance (10^{-6} in. for deflection or 1.0 lb for load) is offered as adequate proof of satisfactory closure.

Use of the alternating-direction iterative method is greatly enhanced by judicious choice of closure parameters. They have been shown to be related to the limiting eigenvalues or characteristic values of the set of equations involved. Many mathematicians maintain that closure parameter values selected for square systems must be used for both halves of any iterative cycle. Ingram (12) has demonstrated a method, however, which is not troubled by this restriction. Furthermore, diverse problems which prove troublesome to solve with the classical single-iteration control methods are readily solved using the Ingram dual-control techniques.

Details of Solutions

For solving the large number of simultaneous equations which result in each half-cycle of the alternating-direction iterative method, Matlock and Haliburton (18) used an efficient two-pass method to solve linearly elastic beam-columns. The method involves the elimination of four unknowns, two each in two passes. The first pass from top to bottom eliminates deflections w^x_{i-2} and w^x_{i-1} from each equation (see Eq. 52). The second pass, in reverse order, eliminates deflections w^x_{i+2} and w^x_{i+1} from each equation, and thus results in the solution for the desired deflection w^x_i. Those readers not familiar with this technique are invited to read Ref. 18.

One of the valuable assets of this method is that boundary conditions as normally discussed are automatically provided with two dummy stations specified at each end of each beam in the system. These dummy stations in reality have no bending stiffness; therefore, a bending stiffness equal zero is input for them. Equation 52 is then formulated for every station in the beam plus two dummy stations on each end.

To solve for $w^x_{i,j}$ then, the plate is considered to be two systems of orthogonal beams interconnected at Station i, j by S_f, the fictitious closure spring constant. Figure 16 shows the slab model with closure springs acting during closure.

With the beam-column as a basic tool, the solution of the system of equations for plates and slabs proceeds as follows:

1. Solve each x-beam successively through the system considering all the y-beams to be held fixed in space. At any particular solution of any x-beam then, the fictitious closure spring acts as restraint on the x-beam of interest.
2. After all x-beams are solved and their new deflection pattern is known, alternate or change directions and fix the x-beams in this new pattern.
3. Solve for the deflected shape of each y-beam in turn. The fictitious springs now act as loads or restraints on the y-beam, serving to transfer the load which has been stored in them from the deflected x-beams.

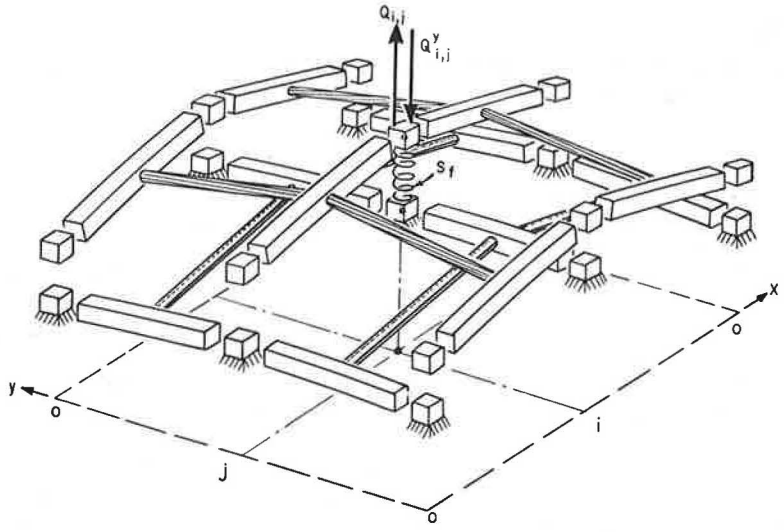

Figure 16. Plate represented in the closure process as two orthogonal systems with closure spring acting between them at Station i,j.

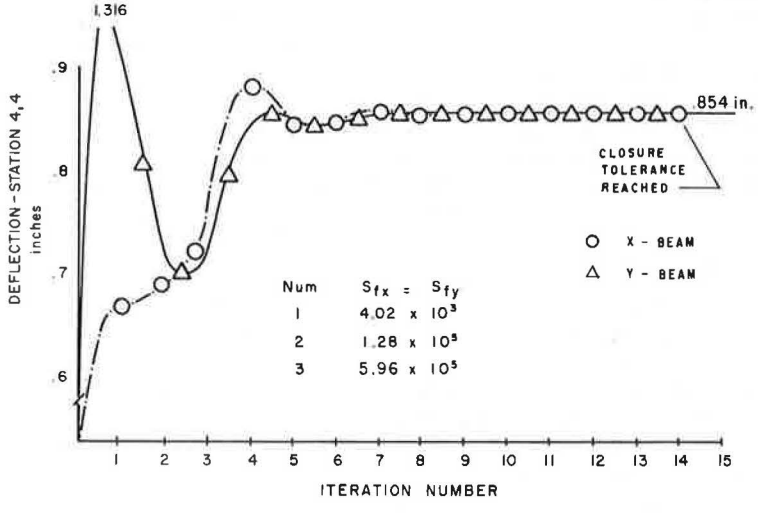

Figure 17. Plot of closure for Example Problem 102.

4. This procedure is repeated alternately until all of the load is properly distributed throughout the system. At this point the summation of static forces at each joint in the system will equal zero within the specified tolerance and the deflection of the x-beam system $w^{x}_{i,j}$, at any point will equal the deflection of the y-beam system, $w^{y}_{i,j}$, at the same point within the specified tolerance so that the term $S_f\left(w^{x}_{i,j} - w^{y}_{i,j}\right)$ vanishes.

The process described is a rapid one requiring from 5 to 25 iterations for most simple problems with closure to six significant digits.

Closure Process

Figure 17 illustrates the closure process for an 8- × 8-increment square plate. The parameters were chosen in accordance with the rules set forth in Ref. 11, p. 59.

THE COMPUTER PROGRAM

The equations derived in the section on "Formulation of Equations" are not useful for hand calculations, but they are extremely well adapted for digital computer methods. During the 18 months of this investigation, 12 programs have been developed which are useful for solving slab and plate problems of various types. The earlier programs are simple in format and application. The most general program is known as SLAB 17. The number 17 signifies that this is the seventeenth version in the chronological sequence of development of SLAB Programs.

These programs are written in FORTRAN computer language for the Control Data Corporation 1604 Digital Computer which has a 48 bit word length and is operated with a FORTRAN-63 monitor system. The compile time for the basic program is less than two minutes; however, normal operating decks may be compiled on binary cards, thus reducing compile time in the computer to about 15 seconds. The exact storage requirements of the program as presently dimensioned are undetermined. In general, however, the dimension statements are such that the program will handle as large a problem as practical with present storage capacity. This program can be modified for use with the IBM 7090 computer by the modification of about 12 input-output cards.

The time required to run problems varies, of course, with the complexity and size of the system, i.e., the number of increments involved, and the number of iterations required to obtain the desired accuracy. To give a general idea of operating time, eight-by-eight problems close to a tolerance of 10^{-6} inches in 10 to 60 iterations, and require 30 to 100 seconds for solution. An increase in size to 16 × 16 with fairly uniform stiffnesses in both directions can be closed to similar tolerances in about 100- to 200-sec computer time. While this may seem high when compared to solution time for simpler problems, the cost of three minutes of computer time ($15 to $30, depending on rental rates) is small compared to three to four days of laborious computation time required to do the problem by hand. More important, perhaps, is the fact that this computer program provides a useful way of making some solutions for the first time.

The FORTRAN Program

A summary flow diagram for the SLAB Programs is given in Figure 18. This flow diagram describes the program tasks briefly. A detailed flow diagram and listing of the program SLAB 17 is provided in Ref. 11.

The format used for inputing data into the program is arranged as conveniently as possible. No effort is made to be frugal with the number of cards required to input one problem. Instead, every effort is made to organize the program input logically and concisely. The problem input deck starts with two cover cards used to identify the program and the particular run being made. After these come necessary data cards.

Output Information

The program output is arranged to be useful to the user. A format which can be trimmed to standard 8½- by 11-in. size is provided. For convenience and help in identifying problems, the program prints out all original input data at the beginning of each problem. These values are tabulated and labeled just as they were input. The first output computed by the program itself is Table 4, "Monitor Deflection." (See Appendix.) This table prints out deflections for both the x-beams and y-beams at the four pre-selected monitor stations specified in Table 1. (See Appendix.) This data can be plotted using other versions of the SLAB Program.

The results desired from the program are printed out in Table 5. (See Appendix.) This table prints in two parts in keeping with the 8½- by 11-in. format. The first half prints external station numbers, x- and y-deflections, bending moments in the x- and y-directions, the external reaction of the slab and the true error in statics as determined

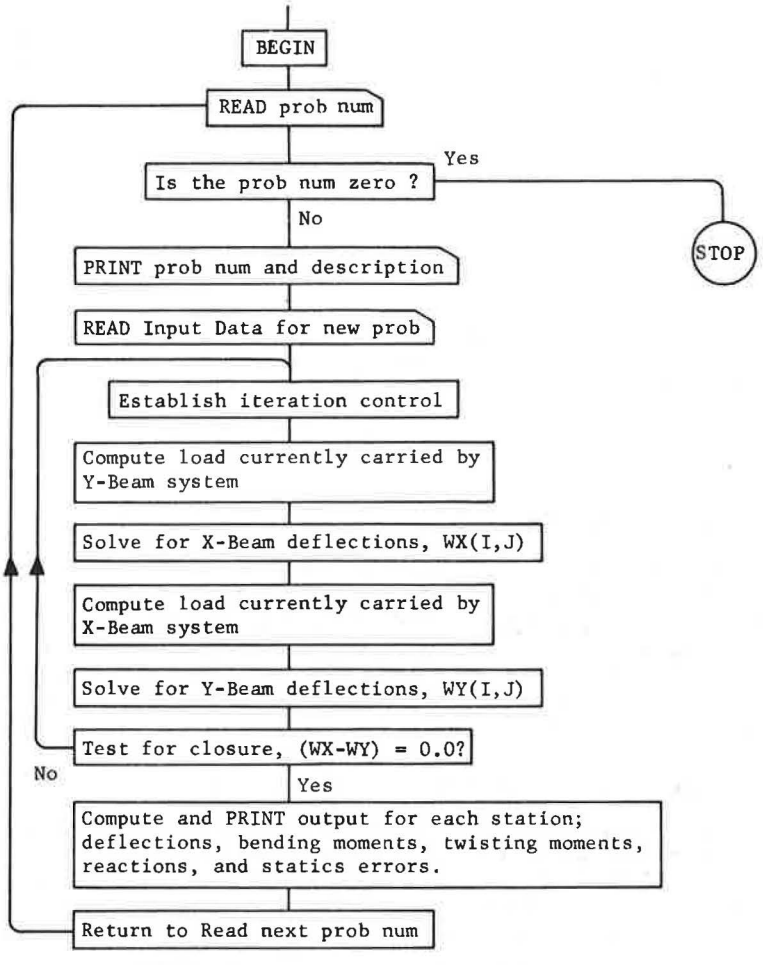

Figure 18. Summary flow chart, slab program.

by summation of vertical forces at each station. Part 2 of Table 5 prints out station numbers and twisting moments in the x- and y-directions at each station. Four additional spaces are provided for printing out stresses and direction of principal stress in later programs to be equipped with stress calculating options.

An automatic plot routine can be coupled with SLAB 17 and used to plot any of the variables available at mesh points in the system, although its major use is normally plotting deflection contours.

The bending and twisting moment outputs are calculated by numerical differentiation of the deflected shape. In both cases central differences are used to provide moments at each mesh point in order that these moments may be available for calculation of principal stresses.

Summary of Program Details

SLAB 17 is the most general and useful program available at the present time for solving the equations developed herein. The program is written in FORTRAN-63 language for the CDC 1604 computer and solves slab and plate problems very rapidly. Ref. 11 contains all information about the program from flow diagrams to output information, and can be extracted as an operating manual for use with the program. Twelve other programs are available for solving various types of problems. Several of these will be developed to provide special-case solutions which solve more rapidly than the general method.

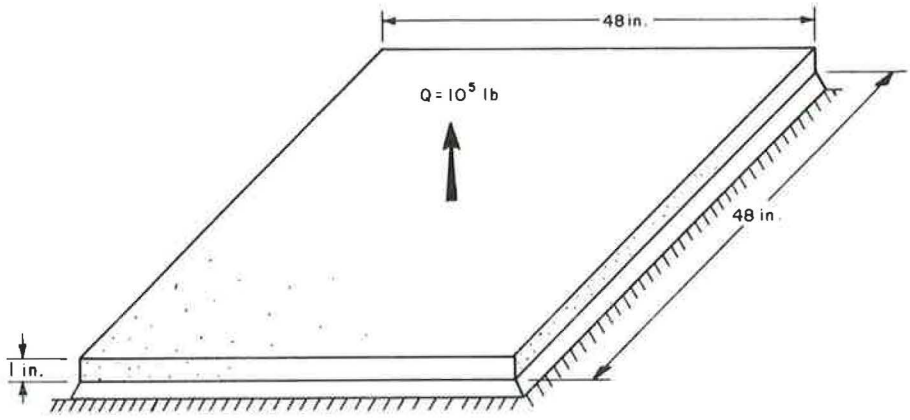

Figure 19. Square steel plate simply supported at all edges (Example Problem 101).

EXAMPLE PROBLEMS AND VERIFICATION OF THE METHOD

Developments of equations and discussions of techniques are important in analytical work of this kind; however, application of the method and demonstration of technique in solving actual problems is equally important. This section provides the solution to several example problems to demonstrate Program SLAB 17 and its use in engineering calculations. Closed-form solutions for some of the problems are provided as a mathematical check to the computed solutions. Sample computer output for example Problem 201 is provided in the Appendix.

Problem Series 100—Simply-Supported Plate With Variations

As a first example, a series of problems illustrating many of the variations possible in the program are applied to a 48-in.-sq simply supported steel plate 1 in. thick (Fig. 19). The modulus of elasticity is 30,000,000 psi. Poisson's ratio is 0.25. Loading variations will be discussed with the individual cases. Once the reader acquaints himself with the physical properties of this plate, it will be possible to evaluate very rapidly five separate cases of load and variations of parameters.

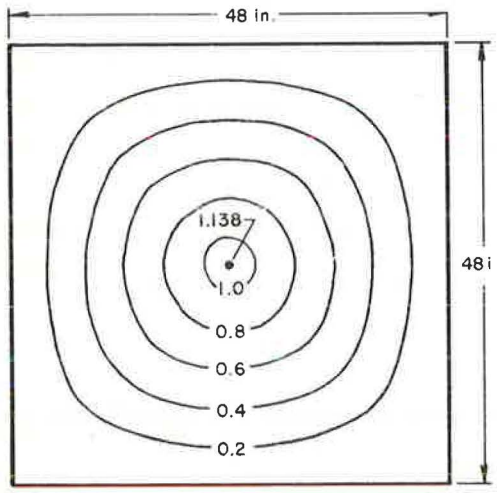

Figure 20. Deflection contours for Example Problem 101 with 100-kip concentrated load at the center.

Problem 101—Concentrated Load.—The problem of a simply supported square or rectangular plate with concentrated load is considered by Timoshenko for various load conditions. Several equations for solving this problem are presented using single and double trigonometric series. A consensus value of solutions for maximum deflection, which occurs under the load, is 1.07 inches. Figure 20 is a plot obtained automatically from SLAB 17 coupled with a plot routine for the complete deflected shape of the plate when it is divided into eight 6-in. increments in each direction. The maximum deflection w_{max} is noted to be 1.138 inches. This differs 0.07 inch, or 6 percent from the closed-form solution. If the number of increments is increased to 16 in each direction, a maximum deflection of 1.08 inches results. Thus, the error is reduced to 1 percent, probably as good as the accuracy

of the closed-form solution using a truncated double trigonometric series. Contours of maximum bending moment or twisting moment could have been plotted, if desired, just as easily as the deflections.

Problem 102—In-Plane Forces.—In addition to the concentrated load at the center, add a uniform in-plane force in the y-direction of 16,667 pounds per inch of plate width. In the closed-form solution this term appears in the denominator of the series solution and does not have as much effect as might be expected. The maximum deflection occurs under the load and is 0.787 inch. The computed solution for an 8 × 8 grid is 0.854 inch. The difference of 0.067 inch is almost identical with that in Problem 101. Increasing the number of increments would reduce the difference accordingly.

Problem 103—Two-Way In-Plane Forces.—Add to Problem 102 an equal in-plane tensile force in the x-direction. The computed solution for maximum deflection reduces to 0.661 inch. If the force in the x-direction is tensile or positive but the force in the y-direction is compressive or negative, the effects on maximum deflection offset each other as would be expected. This solution gives a maximum deflection of 1.14 inches, the same as Problem 101.

Problem 106—End Supports With Line Loads.—Modify the basic problem slightly by removing the simple supports under two edges of the plate. This leaves the plate supported as a wide-beam on simple supports (Fig. 21). Unlike a beam, however, the plate should exhibit Poisson's ratio effects. Poisson's ratio manifests itself in such a structure by anticlastic bending. This may be explained in the following way. If moments are applied to the plate at opposite ends of the x-axis, a simple analysis would indicate that a uniform moment in the x-direction, M_x, would be present throughout the plate. Two conditions are known from physical equations governing plate behavior. First, the bending moment in the y-direction at the free y-edges must be zero. And, second, the bending moment in the y-direction may be stated as follows:

$$M_y = D_y \left(\frac{\partial^2 w}{\partial y^2} + \nu_{xy} \frac{\partial^2 w}{\partial x^2} \right) \tag{61}$$

The first stated condition requires that the second condition, Eq. 61, be identically zero. Note that the bending in the x-direction is not zero, thus the differential $\partial^2 w/\partial x^2$ cannot be equal to zero. Then for Eq. 61 to be identically zero

$$\frac{\partial^2 w}{\partial y^2} = -\nu \frac{\partial^2 w}{\partial x^2} \tag{62}$$

Thus, bending in the y-direction will be present at the two edges with a sense opposite that in the x-direction. This is illustrated in Figure 22. Figure 23 illustrates the same plate when Poisson's ratio equals zero. This can be recognized as bending equivalent to that of a beam in which Poisson's ratio can be neglected. Brief reference to Eq. 61 indicates that if Poisson's ratio equals zero, the bending in the y-direction is unaffected by bending in the x-direction since they are related only through Poisson's ratio.

Two solutions were run, one with Poisson's ratio $\nu = 0.0$, the second with Poisson's ratio $\nu = 0.25$. The hand solution as a beam gives w_{max} at the center of the beam or plate of -0.566 inch. The SLAB 17 solution for eight increments $\nu = 0.0$ gives w_{max} = -0.576 inch, a difference of 2 percent. A 16 × 16 solution reduces this difference to less than one percent. For Poisson's ratio of 0.25 a center deflection of w = -0.575 inch results. This increases to -0.640 inch at the two edges due to anticlastic bending.

Problem 107—End Supports with Applied Torques.—This problem is the equivalent of Problem 106 except the moment due to the applied line loads acting at 6-in. distance from the two simple supports is converted to a uniform moment applied near the ends.

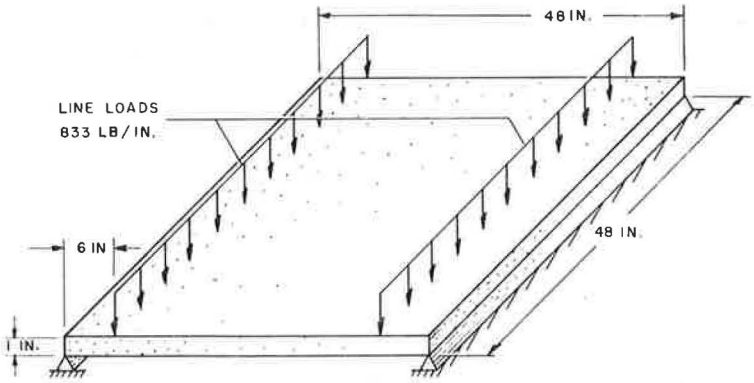

Figure 21. Plate simply supported on two edges with line loads (Example Problem 106).

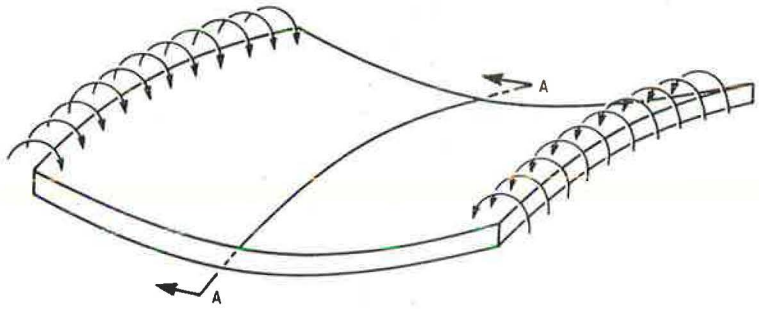

Figure 22. Anticlastic bending of plate subjected to uniform bending moment at opposite edges (Example Problem 107).

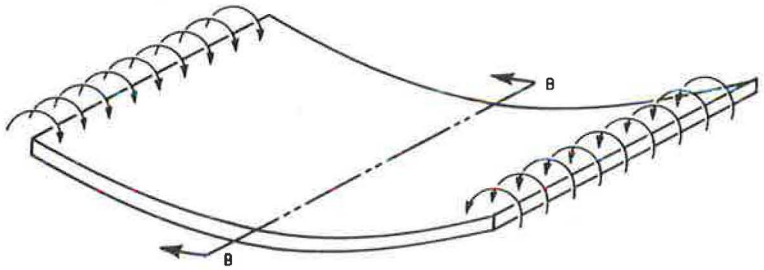

Figure 23. A plate bending as a beam when Poisson's ratio is zero (Example Problem 106).

It is illustrated in Figure 24. The results are exactly comparable to those of Problem 106 as was expected. This indicates that Program SLAB 17 handles applied torques satisfactorily.

Slabs-on-Foundation—Westergaard Cases, Problem Series 200

For slab-on-foundation problems, the matter of checking theory becomes more complicated because of the lack of closed-form solutions. Three example problems related to the three Westergaard cases are presented here since these solutions are well known

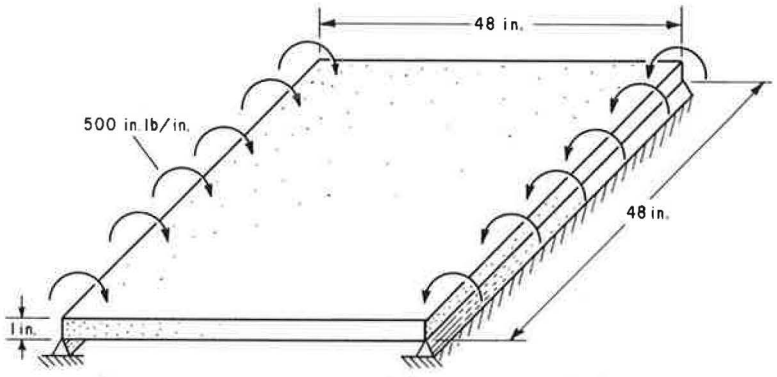

Figure 24. Simply supported plate with a bending moment applied at opposite ends (Example Problem 107).

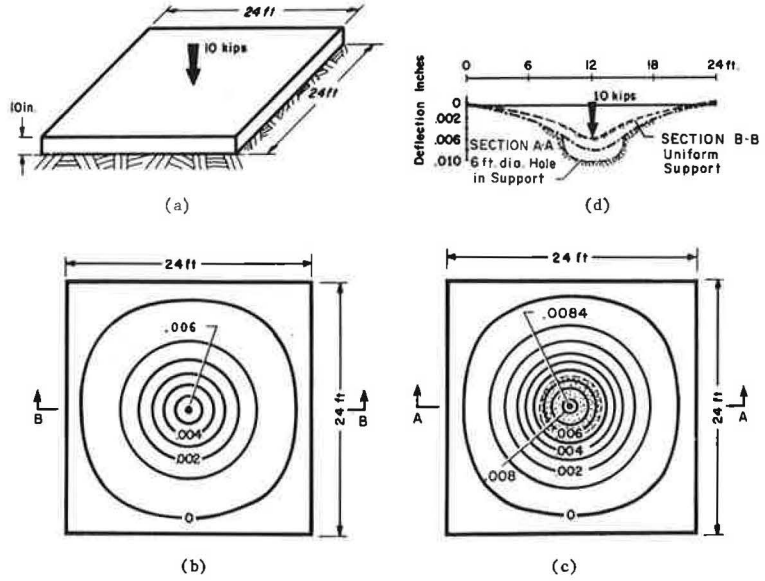

Figure 25. Pavement slab subjected to 10-kip wheel load at the center, with and without uniform subgrade support.

and are currently used as a basis for most rigid pavement design. A single pavement slab was chosen for comparison and examined separately for the three Westergaard cases. The closed-form solutions come from Westergaard, (32, p. 102). A standard slab example is used for the computed deflection as shown in Figure 25a.

The examples all involve a 10-in. slab thickness, 24 ft square in plan dimension with a modulus of elasticity of 3,000,000 psi and $\nu = 0.20$. The subgrade modulus was assumed to be 200 pounds per square inch per inch of deflection and a single concentrated load of 10 kips was applied in each case.

Problem 201—Center Load.—With these physical constants the Westergaard solution gives the deflection under a load applied at the center of an infinite slab to be -0.0057 inch. The computed results are -0.0060 inch. In addition, one can see from Figure 25b that the computed solution gives the complete deflection contours of the slab, whereas the Westergaard equation gives the deflection only under the load. This solution

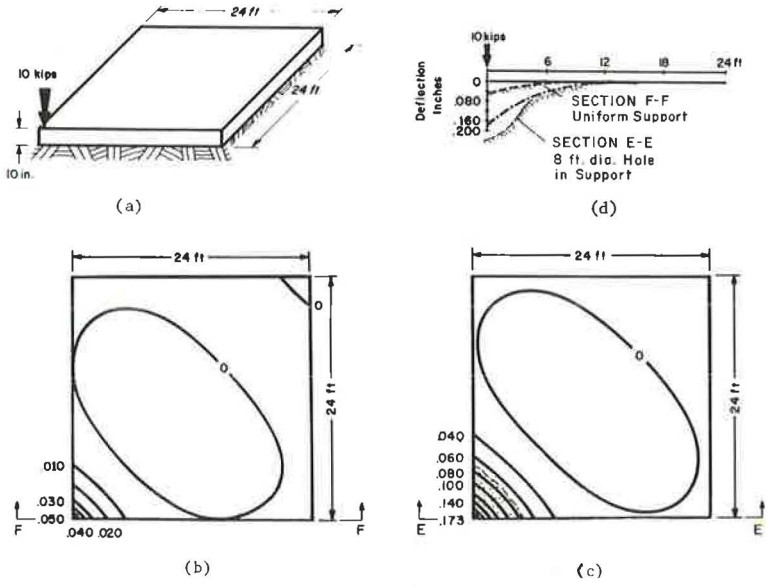

Figure 26. Pavement slab subjected to 10-kip wheel load at the corner, with and without uniform subgrade support.

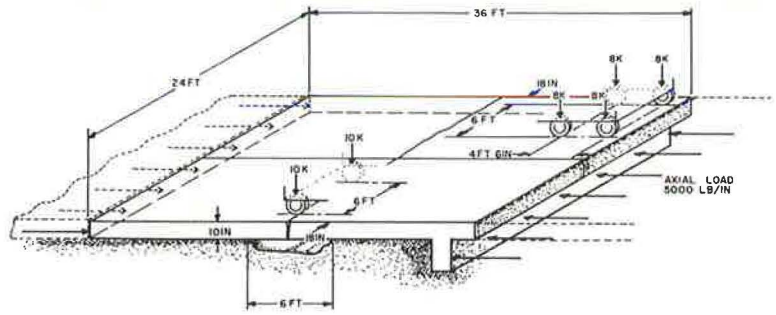

Figure 27. Lug anchor example problem.

involves 8 increments. A solution using 12 or 16 increments gives deflection results closer to that of Westergaard.

Problem 202—Edge Load.—For the case of edge loading, Westergaard gives -0.019-inch deflection for a point under the load at the edge of a slab and infinitely far from any other boundaries. These, of course, are not realistic boundaries since pavements certainly have finite limits. In reality, because of cracking or jointing, the load is nearly always relatively close to some boundary in any direction. The finite-element solution based again on the 24-ft-square slab, but with the load centered along one edge, gives a deflection of -0.018 inch. These results compare within 4 percent. Exact comparison need not be expected since one solution is for a real slab and the other for an infinite slab.

Problem 203—Corner Load.—The third Westergaard case is the load applied at a rectangular corner, infinitely far from any other discontinuity. The comparable real slab is shown in Figure 26a. The Westergaard solution gives -0.049 inch of deflection under the load. The finite-element solution shown in Figure 26b is -0.050 inch. The deflection contours are also of interest and are not easily obtained from the Westergaard solution.

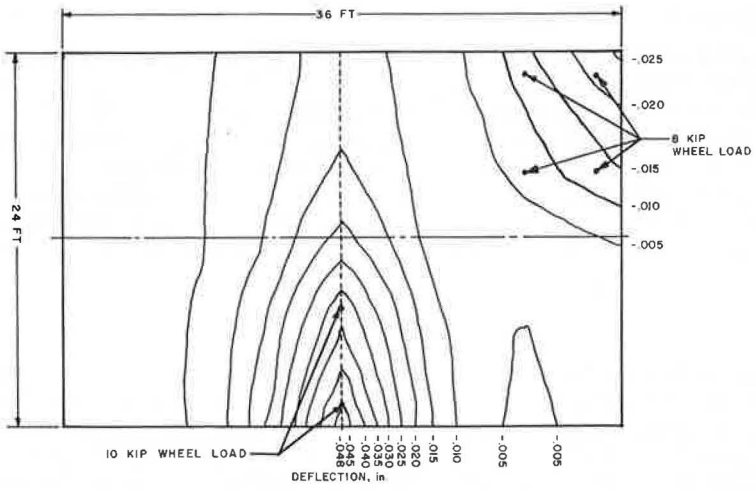

Figure 28. Deflection contours of lug anchor example problem in Figure 27.

To summarize these comparisons it has been shown that the finite-element method described herein agrees within 2 to 5 percent with the Westergaard slab-on-foundation solutions which are currently used for pavement design. In addition, the new method readily provides deflection contours. The same is not true with the Westergaard solution although computer programs do exist to solve those equations explicitly.

Nonuniform Subgrade Support.—To illustrate nonuniform subgrade support, the three cases previously described for center, edge, and corner loadings were rerun with a hole cut in the subgrade centered under the load. For the center load case, the hole 6 feet in diameter cut in the subgrade results in an increased deflection of 40 percent to -0.0084 inch. For the nonuniformly supported edge load, a hole 6 feet in diameter is centered under the load. The resulting deflection under the load is -0.35 inch (Fig. 25c) or nearly double that of the slab with uniform support. Figure 25d compares an edge view with and without uniform support. The corner load case has a hole 8 feet in diameter cut in the subgrade centered at the corner. The resulting deflection increased to -0.173 inch or about $3\frac{1}{2}$ times that of the uniform case as shown in Figures 26c and 26d. It is not intended to draw conclusions at this time concerning these relative increases in deflection nor their effect on pavement performance. It is merely desired to indicate that the method is easily adaptable to solutions for such nonuniform cases which probably represent a majority of pavement actually in service in the United States.

Lug Anchor Example, Problem 602

One of the strengths of the method described herein is its ability to handle complex problems with combination loads and variations in flexure stiffness and support conditions. Figure 27 illustrates such a problem. A 10-in. thick reinforced concrete slab was used. Near one end the slab has a 24-in. deep lug anchor extending into the subgrade. The slab has a centerline joint and a crack which developed from a combination of shrinkage and previous overstress. The joint and crack develop only 20 percent of the stiffness of the surrounding slab. The soil has settled under the crack in the slab and left a section unsupported. For any nonuniformly supported slab such as this, the dead weight of the slab must be considered when evaluating moments and stresses. This weight acts as a uniform load of 300 lb per station. Two 10-kip and four 8-kip wheel loads are considered in this example. An axial load of 5,000 lb/in. is being resisted by the lug anchor. The resulting deflected shape is shown in Figure 28. The maximum deflection of 0.048 inch occurs at the edge of the slab at the transverse crack. It is virtually impossible to obtain this general solution by any other existing methods of analysis.

Summary of Example Problems

The foregoing example problems have been solved to indicate the broad capability of the new method. Two points are worth noting. For those cases having closed-form solutions, the finite-element solution with 8 to 10 increments produced results within 2 to 5 percent of the closed-form solution. If the number of increments was increased to 16, the error comparison reduced to 1 to 3 percent. Perhaps more important are those cases for which no closed-form solution exists. The finite-element method permits, for the first time, the evaluation of such cases. It will be helpful if solutions of these new cases can be compared with experimental data obtained from field or model studies.

SUMMARY

This report examines the analysis of plates and pavement slabs. A study of the technical literature resulted in the selection of some sixty helpful references. Many of these papers contain solutions for special-case plates with simple supports and simple load patterns. These solutions are mathematically complex and are often shrouded in jargon not always relatable to real problems. A particular void is noted in the analysis of pavement slabs. The best work available (Westergaard's) is limited by special-case loads and severe assumptions including infinite or semi-infinite plan dimensions and uniform support conditions.

A method has been presented which is not limited by the simplifying assumptions needed for closed-form solutions. The technique is based on a physical model of the problem which is described mathematically. The principal features of the method are as follows:

1. Representation of the plate or slab by a finite-element model of beam-column elements with freely discontinuous stiffness and load. These line elements are grouped into two systems of orthogonal beams or beam-columns.
2. A rapid, direct solution of individual beams using recursive techniques.
3. An alternating-direction iteration method for combining the solutions of the individual beams into a coordinated slab solution.

The finite-element model is helpful in visualizing the problem and forming the solution. The model consists of:

1. Infinitely stiff and weightless bar elements to connect the joints.
2. Elastic joints where bending occurs, made of an elastic, homogeneous, and orthotropic material which can be described by four independent elastic constants.
3. Torsion bars which represent the torsional stiffness of the plate.
4. Elastic support springs which provide foundation support.

All properties and loads can be freely variable from point to point. Concentrated or distributed loads can be handled including transverse loads, in-plane forces, and external couples. Elastic restraints are provided by vertical support springs.

The alternating-direction iteration method is used to solve the equations describing the behavior of the model because it is well adapted and easy to visualize. The model and method are too complex for hand calculations. A computer program which solves the equations implicitly for the deflection patterns has been developed. The program is written in FORTRAN-63 for the CDC 1604 computer. Minor changes of input formats are required to convert it for use on an IBM 7090. Compile time is 90 to 100 seconds but binary decks are available which compile in about 15 seconds. Automatic plot routines are available for use with the program.

This method has application to a broad variety of complex plate and slab problems which cannot be solved by any other existing method. Applications to complex pavement design problems are of particular interest. The use of the method as a tool in stochastic modeling of pavement life and performance studies is of particular interest. Immediate use of the method in developing new pavement design information is suggested.

NEEDED RESEARCH

The finite-element model described herein is a useful tool. The development of such a method opens the door to studies which heretofore could not be conducted. Such applications of this method are discussed in this section. A look into the method pinpoints several areas of study which could lead to improvement.

Study of Material Properties

It would be helpful if the orthotropic properties of materials used in slabs could be determined for exact input into this program. In particular, information is needed on the relationship of Poisson's ratio and Young's modulus for orthotropic materials, and on torsional rigidity for "torsionally stiff" and "torsionally soft" rib reinforced orthotropic plates.

Comparison With Field Measurements

"The proof of any pudding is in the eating." It is desirable that studies of pavement structures be made in the laboratory and in the field, and that corresponding mathematical analyses be made with the finite-element model. Correlation of these data will help in the evaluation of theory and will lead to improved methods for determining some of the unknowns in the field studies. Deflection measurements will be helpful in this regard as will curvature measurements.

Evaluation of Support Characteristics

Current methods of measuring and specifying pavement support are probably unsatisfactory. It is not adequate to describe a constant k-value for a subgrade or a subbase to be used under a pavement slab. This value is not a linear quantity but is highly dependent on the deflection of the slab lying immediately above. It is also related to overall slab deflections. The true support value is dependent on many things. The first step in such evaluation is the study of nonlinear support conditions for the finite-element model.

ACKNOWLEDGMENTS

This investigation was conducted under the auspices of the Center for Highway Research, The University of Texas. The project of which it is a part was sponsored by the Texas Highway Department and the U. S. Bureau of Public Roads. This support is gratefully acknowledged as is that of the Computation Center, The University of Texas, for the use of its computer.

REFERENCES

1. Ang, D. D., and Williams, M. L. Combined Stresses in an Orthotropic Plate Having a Finite Crack. Jour. of Applied Mechanics, Vol. 28, Series E, No. 3, p. 372, Sept. 1961.
2. Ang. A. H. S., and Newmark, Nathan M. A Numerical Procedure for the Analysis of Continuous Plates. Proc. Second Conf. on Electronic Computation, Structural Division, ASCE, p. 379, Sept. 1960.
3. Badir, Mounir. Bending of Rectangular Plates. Jour. of the Soil Mechanics and Foundations Division, ASCE, Vol. 87, No. ST6, p. 105, Aug. 1961.
4. Brotchie, J. F. General Method for Analysis of Slabs and Plates. Jour. of ACI, Vol. 29, No. 1, p. 31, July 1957.
5. Conte, S. D., and Dames, R. T. An Alternating Direction Method for Solving the Biharmonic Equation. Mathematical Tables and Aids to Computation, Vol. 12, No. 63, p. 198, July 1958.
6. Clough, Ray. The Finite Element Method in Plane Stress Analysis. Proc. of the Second Conf. on Electronic Computation, Vol. 86; Jour. of the Structural Division, ASCE, No. ST4, 1960.

7. Griffin, D. S., and Varga, R. S. Numerical Solution of Plane Elasticity Problems. SIAM Jour., Vol. 11, Dec. 1963.
8. Grinter, et al. Numerical Methods of Analysis in Engineering. The Macmillan Company, p. 138, 1949.
9. Hearmon, R. F. S. Applied Anisotropic Elasticity. Oxford Univ. Press, Amen House, London, England, 1961.
10. Hoppman, W. H., 2nd, Huffington, N. J., Jr., and Magness, L. S. A Study of Orthogonally Stiffened Plates. ASME Trans., Jour. of Applied Mechanics, Sept. 1956.
11. Hudson, W. R., and Matlock, Hudson. Discontinuous Orthotropic Plates and Pavement Slabs. Research Rept. No. 56-6, Center for Highway Research, Univ. of Texas, 1965.
12. Ingram, W. B. A Finite-Element Method for Bending Analysis of Layered Structural Systems. Ph.D. dissertation, Univ. of Texas, 1965.
13. Kelly, E. F. Application of the Results of Research to the Structural Design of Concrete Pavements. Public Roads, Vol. 20, 1939.
14. Knowles, J. K., and Wang, M. M. On the Bending of an Elastic Plate Containing a Crack. Jour. of Mathematics and Physics, 1961.
15. Lekhnitski, S. K. Theory of Elasticity of an Anisotropic Elastic Body. Translated by P. Fern. Holden-Day, Inc., San Francisco, 1963.
16. Leonards, G. A., and Harr, M. E. Analysis of Concrete Slabs on Ground. Jour. of Soils and Foundation Division, ASCE, Vol. 85, SM3, June 1959.
17. Matlock, Hudson. Analysis of Several Beam-on-Foundation Problems. Paper presented at ASCE Houston Convention, Feb. 21, 1962.
18. Matlock, Hudson, and Haliburton, T. A. A Finite-Element Method of Solution for Linearly Elastic Beam-Columns. Research Rept. No. 56-1, Center for Highway Research, Univ. of Texas, 1965.
19. Matlock, Hudson, and Ingram, Wayne B. Bending and Buckling of Soil-Supported Structural Elements. Proc. Second Pan-American Conf. on Soil Mechanics and Foundation Engineering, No. 32, Brazil, June 1963.
20. Newmark, N. M. Numerical Methods of Analysis of Bars, Plates, and Elastic Bodies. Numerical Methods of Analysis in Engineering. L. E. Grinter, ed. pp. 139-168, Macmillan Company, New York, 1949.
21. Pickett, Gerald, Raville, Milton E., James, William C., and McCormick, Frank J. Deflections, Moments and Reactive Pressures for Concrete Pavements. Kansas State College Bull., No. 65, Engineering Experiment Station, Oct. 15, 1951.
22. Richart, F. E., and Zia, P. Effects of Local Loss of Support on Foundation Design. Jour. of Soil Mechanics and Foundations Division, ASCE Paper No. 3056, SM1, Feb. 1962.
23. Reissner, Eric. On the Bending of Elastic Plates. Quarterly of Applied Mathematics, Vol. 5, pp. 55-68, 1947.
24. Salani, H. J. A Finite-Element Method for Vibrating Beams and Plates. Ph.D. dissertation, Univ. of Texas, 1965.
25. Spangler, M. G. Stresses in the Corner Region of Concrete Pavements. Iowa Engineering Experiment Station Bull. 157, 1942.
26. Teller, L. W., and Sutherland, E. C. The Structural Design of Concrete Pavements. Public Roads, Vol. 16, Nos. 8, 9, and 10; Vol. 17, No. 7; Vol. 23, No. 8, Federal Works Agency, Public Roads Administration.
27. Terzaghi, Karl. Evaluation of Coefficients of Subgrade Reaction. Geotechnique, Vol. 5, Dec. 1955.
28. Timoshenko, S., and Woinowsky-Krieger, S. Theory of Plates and Shells. Engineering Society Monographs, 2nd Ed., pp. 143-149, McGraw-Hill, New York, 1959.
29. Tucker, Richard L., and Matlock, Hudson. A General Method for Grid-Beam Solution. Unpublished Paper, Department of Civil Engineering, Univ. of Texas, 1964.

30. Tucker, Richard L. A General Method for Solving Grid-Beam and Plate Problems. Ph.D. dissertation, Univ. of Texas, 1963.
31. Westergaard, H. M. Analytical Tools for Judging Results of Structural Tests of Concrete Pavements. Public Roads, Vol. 14, 1933.
32. Westergaard, H. M. Computation of Stresses in Concrete Roads. Proc. Highway Research Board, Vol. 5, Pt. I, pp. 90-112, 1926.
33. Westergaard, H. M. New Formulas for Stresses in Concrete Pavement of Airfields. Proc. ASCE, Vol. 73, No. 5, May 1947.
34. Westergaard, H. M. Stresses in Concrete Pavements Computed by Theoretical Analysis. Public Roads, Vol. 7, No. 2, April 1926.
35. White, Richard N., Cottingham, Willard S. Stability of Plates Under Partial Edge Loadings. Proc. Engineering Mechanics Division, ASCE, Vol. 88, No. EM5, p. 67, October 1962.
36. Williams, M. L. The Bending Stress Distribution at the Base of a Stationary Crack. Jour. of Applied Mechanics, Vol. 28, Series E, No. 1, p. 78, March 1961.

Appendix

SAMPLE COMPUTER SOLUTIONS OF EXAMPLE PROBLEMS

EXAMPLE DATA INPUT

```
 201      8X8 SOF ,  PR=.20  CENTER LOAD, HWY REPORT 6            WRH      29AP5
   4     6     0    24     8     8 3.600E 01 3.600E 01 1.000E-05 0.200E 00
   4     4     0     0     0     4     4     0
4.920E 03 2.460E 04 1.230E 05 6.160E 05
4.920E 03 2.460E 04 1.230E 05 6.160E 05
   0     0     8     8 0.652E 08 0.652E+08           0.650E 05
   0     1     8     7 0.652E 08 0.652E+08           0.650E 05
   1     0     7     8 0.652E 08 0.652E+08           0.650E 05
   1     1     7     7 0.652E 08 0.652E+08           0.650E 05
   1     1     8     8                                          2.080E+08 2.080E+08
   4     4     4     4                      1.000E 04
```

```
PROGRAM SLAB 17 - MASTER DECK - WR HUDSON, H MATLOCK      REVISION DATE 26 JUL 65
CE051022   HWY SLAB PROJECT        SLAB 17      W R HUDSON
RUN EXAMPLE PROBLEMS FOR FINAL CHECK DECK 3 SLAB 17


PROB
  201      8X8 SOF ,  PR=.20  CENTER LOAD, HWY REPORT-6          WRH      29AP5

TABLE 1.  CONTROL DATA

     NUM VALUES TABLE 2                                                  4
     NUM CARDS TABLE 3A                                                  6
     NUM CARDS TABLE 3B                                                  0
     MAX NUM ITERATIONS                                                 24
     NUM INCREMENTS  MX                                                  8
     NUM INCREMENTS  MY                                                  8
     INCR LENGTH  HX                                          3.600E 01
     INCR LENGTH  HY                                          3.600E 01
     CLOSURE TOLERANCE                                        1.000E-05
     POISSONS RATIO                                           2.000E-01

     MONITOR STAS  I,J              4  4      0  0      0  4      4  0

TABLE 2A.  ITERATION CONTROL DATA

     F. SPRING REPRESENTING X BEAM

      4.920E 03
      2.460E 04
      1.230E 05
      6.160E 05


TABLE 2B.  ITERATION CONTROL DATA

     F. SPRING REPRESENTING Y BEAM

      4.920E 03
      2.460E 04
      1.230E 05
      6.160E 05

TABLE 3A. STIFFNESS AND LOAD DATA, FULL VALUES ADDED AT ALL STAS I,J IN RECT.

   FROM    THRU      DX          DY          Q          S          CX          CY

   0  0    8  8   6.520E 07   6.520E 07          0   6.500E 04          0          0
   0  1    8  7   6.520E 07   6.520E 07          0   6.500E 04          0          0
   1  0    7  8   6.520E 07   6.520E 07          0   6.500E 04          0          0
   1  1    7  7   6.520E 07   6.520E 07          0   6.500E 04          0          0
   1  1    8  8           0           0          0          0   2.080E 08   2.080E 08
   4  4    4  4           0           0  1.000E 04          0          0          0
```

TABLE 3B. STIFFNESS AND LOAD DATA, FULL VALUES ADDED AT ALL STAS I,J IN RECT.

FROM	THRU	TX	TY	PX	PY

TABLE 4. MONITOR TALLY AND DEFLS AT 4 STAS

	ITR NUM	FICT SPRING	CYC NUM	NOT STAB	NOT CLOS	I,J 4 4	0 0	0 4	4 0
X	1	4.920E 03	1	43		1.195E-02	0	6.298E-04	0
Y		4.920E 03		78	76	5.451E-03	-5.746E-05	-3.113E-04	3.841E-04
X	2	2.460E 04	2	81		8.522E-03	-6.072E-05	-5.283E-04	-2.819E-04
Y		2.460E 04		76	76	5.789E-03	-1.189E-04	-3.142E-04	-3.246E-04
X	3	1.230E 05	3	74		7.334E-03	-1.426E-04	-3.809E-04	-2.665E-04
Y		1.230E 05		68	62	6.118E-03	-1.743E-04	-2.991E-04	-3.159E-04
X	4	6.160E 05	4	65		6.739E-03	-1.837E-04	-2.734E-04	-2.833E-04
Y		6.160E 05		46	39	6.414E-03	-1.921E-04	-2.795E-04	-2.628E-04
X	5	4.920E 03	1	44		6.576E-03	-2.457E-04	-2.788E-04	-2.747E-04
Y		4.920E 03		16	37	6.444E-03	-2.251E-04	-2.696E-04	-2.618E-04
X	6	2.460E 04	2	9		6.562E-03	-2.460E-04	-2.798E-04	-2.711E-04
Y		2.460E 04		4	28	6.457E-03	-2.351E-04	-2.669E-04	-2.651E-04
X	7	1.230E 05	3	8		6.548E-03	-2.410E-04	-2.739E-04	-2.695E-04
Y		1.230E 05		4	17	6.473E-03	-2.398E-04	-2.680E-04	-2.678E-04
X	8	6.160E 05	4	9		6.529E-03	-2.403E-04	-2.694E-04	-2.687E-04
Y		6.160E 05		5	11	6.496E-03	-2.404E-04	-2.690E-04	-2.687E-04
X	9	4.920E 03	1	3		6.515E-03	-2.403E-04	-2.686E-04	-2.686E-04
Y		4.920E 03		0	10	6.500E-03	-2.408E-04	-2.689E-04	-2.694E-04
X	10	2.460E 04	2	0		6.513E-03	-2.405E-04	-2.686E-04	-2.686E-04
Y		2.460E 04		0	9	6.501E-03	-2.407E-04	-2.688E-04	-2.691E-04
X	11	1.230E 05	3	0		6.512E-03	-2.406E-04	-2.687E-04	-2.687E-04
Y		1.230E 05		0	4	6.503E-03	-2.406E-04	-2.688E-04	-2.688E-04
X	12	6.160E 05	4	0		6.510E-03	-2.406E-04	-2.688E-04	-2.688E-04
Y		6.160E 05		0	0	6.505E-03	-2.406E-04	-2.688E-04	-2.688E-04

PROGRAM SLAB 17 - MASTER DECK - WR HUDSON, H MATLOCK REVISION DATE 26 JUL 65
0E051022 HWY SLAB PROJECT SLAB 17 W R HUDSON
RUN EXAMPLE PROBLEMS FOR FINAL CHECK DECK 3 SLAB 17

PROB (CONTD)
201 8X8 SOF , PR=.20 CENTER LOAD, HWY REPORT-6 WRH 29AP5

TABLE 5. RESULTS -- ITERATION 12

I,J		X-DEFL	Y-DEFL	BMX	BMY	REACT	TRERR
-1	-1	-1.943E-04	-1.943E-04	0	0	0	0
0	-1	-2.506E-04	-2.505E-04	0	0	0	0
1	-1	-3.067E-04	-3.067E-04	0	0	0	0
2	-1	-4.812E-04	-4.813E-04	0	0	0	0
3	-1	-6.743E-04	-6.743E-04	0	0	0	0
4	-1	-7.640E-04	-7.639E-04	0	0	0	0
5	-1	-6.742E-04	-6.742E-04	0	0	0	0
6	-1	-4.809E-04	-4.812E-04	0	0	0	0
7	-1	-3.072E-04	-3.068E-04	0	0	0	0
8	-1	-2.504E-04	-2.505E-04	0	0	0	0
9	-1	-1.947E-04	-1.947E-04	0	0	0	0
-1	0	-2.506E-04	-2.506E-04	0	0	0	0
0	0	-2.406E-04	-2.406E-04	0	0	1.564E 01	2.021E-03
1	0	-2.306E-04	-2.306E-04	-4.197E 00	3.056E-10	2.999E 01	-9.718E-03
2	0	-2.641E-04	-2.641E-04	1.638E 00	-2.219E-09	3.434E 01	-6.739E-03
3	0	-2.806E-04	-2.806E-04	2.740E 00	-7.276E-10	3.646E 01	1.745E-02
4	0	-2.688E-04	-2.688E-04	-2.284E 00	-6.985E-10	3.492E 01	1.445E-02
5	0	-2.806E-04	-2.806E-04	2.727E 00	-1.295E-09	3.655E 01	-7.672E-02
6	0	-2.641E-04	-2.641E-04	1.655E 00	-1.397E-09	3.424E 01	9.601E-02
7	0	-2.306E-04	-2.306E-04	-4.214E 00	-1.310E-10	3.005E 01	-7.103E-02
8	0	-2.406E-04	-2.406E-04	0	0	1.562E 01	2.274E-02
9	0	-2.507E-04	-2.507E-04	0	0	0	0
-1	1	-3.068E-04	-3.068E-04	0	0	0	0
0	1	-2.306E-04	-2.306E-04	7.235E-06	-4.195E 00	2.998E 01	1.905E-03
1	1	-1.458E-04	-1.458E-04	2.580E 00	2.580E 00	3.790E 01	4.549E-03
2	1	-5.029E-05	-5.030E-05	1.692E 01	2.456E 01	1.308E 01	-2.777E-03
3	1	1.074E-04	1.074E-04	5.935E 00	6.263E 01	-2.789E 01	-2.968E-02
4	1	2.310E-04	2.311E-04	-2.841E 01	9.665E 01	-6.012E 01	5.312E-02
5	1	1.075E-04	1.074E-04	5.912E 00	6.268E 01	-2.793E 01	3.091E-03
6	1	-5.033E-05	-5.034E-05	1.693E 01	2.450E 01	1.320E 01	-1.133E-01
7	1	-1.459E-04	-1.457E-04	2.603E 00	2.594E 00	3.776E 01	1.512E-01
8	1	-2.306E-04	-2.307E-04	-3.446E-03	-4.193E 00	3.004E 01	-5.606E-02
9	1	-3.067E-04	-3.067E-04	0	0	0	0
-1	2	-4.813E-04	-4.813E-04	0	0	0	0
0	2	-2.641E-04	-2.641E-04	9.725E-04	1.640E 00	3.433E 01	5.795E-03
1	2	-5.030E-05	-5.031E-05	2.456E 01	1.693E 01	1.307E 01	5.382E-03
2	2	2.731E-04	2.731E-04	5.236E 01	5.238E 01	-7.096E 01	-4.441E-02
3	2	8.133E-04	8.134E-04	6.068E 00	1.195E 02	-2.118E 02	3.012E-01
4	2	1.261E-03	1.261E-03	-1.330E 02	2.008E 02	-3.269E 02	-9.502E-01
5	2	8.125E-04	8.137E-04	6.472E 00	1.193E 02	-2.129E 02	1.489E 00
6	2	2.739E-04	2.727E-04	5.191E 01	5.270E 01	-6.991E 01	-1.152E 00
7	2	-5.059E-05	-5.010E-05	2.478E 01	1.675E 01	1.277E 01	3.214E-01
8	2	-2.641E-04	-2.642E-04	8.784E-03	1.667E 00	3.434E 01	4.296E-03

9	2	-4.811E-04	-4.811E-04	0	0	0	0
-1	3	-6.742E-04	-6.742E-04	0	0	0	0
0	3	-2.806E-04	-2.806E-04	-3.976E-04	2.738E 00	3.649E 01	-1.310E-02
1	3	1.074E-04	1.074E-04	6.262E 01	5.947E 00	-2.792E 01	4.367E-03
2	3	8.133E-04	8.134E-04	1.196E 02	5.954E 00	-2.117E 02	2.715E-01
3	3	2.132E-03	2.132E-03	3.410E 00	3.926E 00	-5.529E 02	-1.456E 00
4	3	3.465E-03	3.467E-03	-5.024E 02	6.019E 01	-9.049E 02	3.721E 00
5	3	2.135E-03	2.131E-03	2.127E 00	4.579E 00	-5.493E 02	-5.178E 00
6	3	8.109E-04	8.148E-04	1.210E 02	5.136E 00	-2.150E 02	3.683E 00
7	3	1.080E-04	1.066E-04	6.203E 01	6.392E 00	-2.705E 01	-8.539E-01
8	3	-2.804E-04	-2.804E-04	-3.260E-02	2.683E 00	3.654E 01	-8.526E-02
9	3	-6.747E-04	-6.747E-04	0	0	0	0
-1	4	-7.639E-04	-7.639E-04	0	0	0	0
0	4	-2.688E-04	-2.688E-04	1.538E-04	-2.288E 00	3.491E 01	2.787E-02
1	4	2.311E-04	2.310E-04	9.667E 01	-2.844E 01	-6.006E 01	-1.778E-02
2	4	1.261E-03	1.261E-03	2.005E 02	-1.327E 02	-3.271E 02	-6.930E-01
3	4	3.466E-03	3.467E-03	6.145E 01	-5.037E 02	-9.045E 02	3.309E 00
4	4	6.510E-03	6.505E-03	-1.471E 03	-1.468E 03	8.315E 03	-7.357E 00
5	4	3.461E-03	3.469E-03	6.358E 01	-5.048E 02	-9.099E 02	8.974E 00
6	4	1.264E-03	1.258E-03	1.984E 02	-1.315E 02	-3.226E 02	-5.333E 00
7	4	2.308E-04	2.321E-04	9.726E 01	-2.903E 01	-6.052E 01	3.339E-01
8	4	-2.694E-04	-2.688E-04	7.027E-02	-2.271E 00	3.446E 01	5.236E-01
9	4	-7.641E-04	-7.641E-04	0	0	0	0
-1	5	-6.742E-04	-6.742E-04	0	0	0	0
0	5	-2.806E-04	-2.806E-04	-1.825E-03	2.740E 00	3.654E 01	-6.301E-02
1	5	1.073E-04	1.074E-04	6.266E 01	5.937E 00	-2.796E 01	5.036E-02
2	5	8.134E-04	8.135E-04	1.197E 02	5.924E 00	-2.125E 02	9.802E-01
3	5	2.133E-03	2.131E-03	2.697E 00	4.160E 00	-5.501E 02	-4.287E 00
4	5	3.463E-03	3.469E-03	-5.009E 02	5.960E 01	-9.096E 02	8.546E 00
5	5	2.138E-03	2.129E-03	6.181E-01	5.342E 00	-5.455E 02	-9.088E 00
6	5	8.101E-04	8.158E-04	1.215E 02	4.739E 00	-2.155E 02	4.100E 00
7	5	1.066E-04	1.068E-04	6.256E 01	6.363E 00	-2.885E 01	1.108E 00
8	5	-2.796E-04	-2.809E-04	-8.486E-02	2.813E 00	3.745E 01	-1.012E 00
9	5	-6.726E-04	-6.726E-04	0	0	0	0
-1	6	-4.814E-04	-4.814E-04	0	0	0	0
0	6	-2.641E-04	-2.641E-04	2.617E-03	1.636E 00	3.425E 01	8.581E-02
1	6	-5.019E-05	-5.035E-05	2.450E 01	1.694E 01	1.318E 01	-1.123E-01
2	6	2.730E-04	2.730E-04	5.224E 01	5.243E 01	-7.026E 01	-7.218E-01
3	6	8.124E-04	8.141E-04	6.857E 00	1.192E 02	-2.146E 02	3.179E 00
4	6	1.264E-03	1.259E-03	-1.346E 02	2.015E 02	-3.223E 02	-5.674E 00
5	6	8.099E-04	8.155E-04	7.919E 00	1.184E 02	-2.162E 02	4.905E 00
6	6	2.743E-04	2.720E-04	5.161E 01	5.304E 01	-6.997E 01	-1.050E 00
7	6	-4.905E-05	-5.045E-05	2.416E 01	1.689E 01	1.467E 01	-1.734E 00
8	6	-2.648E-04	-2.636E-04	4.675E-02	1.514E 00	3.346E 01	8.902E-01
9	6	-4.832E-04	-4.832E-04	0	0	0	0
-1	7	-3.067E-04	-3.067E-04	0	0	0	0
0	7	-2.306E-04	-2.306E-04	-1.171E-03	-4.191E 00	3.005E 01	-6.400E-02
1	7	-1.459E-04	-1.458E-04	2.625E 00	2.565E 00	3.778E 01	1.390E-01
2	7	-5.023E-05	-5.026E-05	1.697E 01	2.453E 01	1.289E 01	1.722E-01
3	7	1.079E-04	1.070E-04	5.578E 00	6.286E 01	-2.689E 01	-1.040E 00
4	7	2.298E-04	2.318E-04	-2.778E 01	9.617E 01	-6.148E 01	1.473E 00
5	7	1.083E-04	1.069E-04	5.509E 00	6.310E 01	-2.749E 01	-4.893E-01
6	7	-4.998E-05	-5.057E-05	1.683E 01	2.449E 01	1.386E 01	-7.844E-01
7	7	-1.465E-04	-1.453E-04	2.914E 00	2.370E 00	3.702E 01	9.054E-01
8	7	-2.304E-04	-2.308E-04	8.369E-03	-4.108E 00	3.027E 01	-2.882E-01

9	7	-3.057E-04	-3.057E-04	0	0	0	0
-1	8	-2.506E-04	-2.506E-04	0	0	0	0
0	8	-2.406E-04	-2.406E-04	7.149E-11	3.575E-10	1.562E 01	1.737E-02
1	8	-2.306E-04	-2.306E-04	-4.206E 00	1.455E-11	3.003E 01	-5.303E-02
2	8	-2.641E-04	-2.641E-04	1.636E 00	4.293E-10	3.430E 01	2.947E-02
3	8	-2.807E-04	-2.805E-04	2.780E 00	1.135E-09	3.646E 01	2.511E-02
4	8	-2.685E-04	-2.689E-04	-2.337E 00	2.874E-09	3.485E 01	8.014E-02
5	8	-2.806E-04	-2.807E-04	2.708E 00	7.130E-10	3.684E 01	-3.586E-01
6	8	-2.645E-04	-2.639E-04	1.742E 00	-7.130E-10	3.395E 01	3.983E-01
7	8	-2.303E-04	-2.308E-04	-4.267E 00	7.713E-10	3.009E 01	-1.098E-01
8	8	-2.406E-04	-2.406E-04	-7.149E-11	-3.575E-10	1.563E 01	4.378E-03
9	8	-2.507E-04	-2.507E-04	0	0	0	0
-1	9	-1.945E-04	-1.945E-04	0	0	0	0
0	9	-2.505E-04	-2.505E-04	0	0	0	0
1	9	-3.068E-04	-3.068E-04	0	0	0	0
2	9	-4.811E-04	-4.813E-04	0	0	0	0
3	9	-6.739E-04	-6.738E-04	0	0	0	0
4	9	-7.637E-04	-7.647E-04	0	0	0	0
5	9	-6.763E-04	-6.740E-04	0	0	0	0
6	9	-4.791E-04	-4.807E-04	0	0	0	0
7	9	-3.069E-04	-3.075E-04	0	0	0	0
8	9	-2.515E-04	-2.503E-04	0	0	0	0
9	9	-1.957E-04	-1.957E-04	0	0	0	0

PROB (CONTD)
201 8X8 SOF , PR=.20 CENTER LOAD, HWY REPORT-6 WRH 29AP5

TABLE 5. RESULTS(CONTD) -- ITERATION 12

I,J		TMX	TMY
-1	-1	0	0
0	-1	0	0
1	-1	0	0
2	-1	0	0
3	-1	0	0
4	-1	0	0
5	-1	0	0
6	-1	0	0
7	-1	0	0
8	-1	0	0
9	-1	0	0
-1	0	0	0
0	0	2.742E 00	-2.742E 00
1	0	8.245E 00	-8.247E 00
2	0	1.245E 01	-1.245E 01
3	0	1.132E 01	-1.131E 01
4	0	8.279E-04	1.639E-03
5	0	-1.132E 01	1.132E 01
6	0	-1.245E 01	1.245E 01
7	0	-8.241E 00	8.247E 00
8	0	-2.742E 00	2.740E 00
9	0	0	0

1	1	0	0
0	1	8.246E 00	-8.246E 00
1	1	2.250E 01	-2.250E 01
2	1	3.666E 01	-3.666E 01
3	1	3.983E 01	-3.981E 01
4	1	-3.227E-02	-1.063E-02
5	1	-3.980E 01	3.982E 01
6	1	-3.664E 01	3.666E 01
7	1	-2.253E 01	2.248E 01
8	1	-8.233E 00	8.244E 00
9	1	0	0
1	2	0	0
0	2	1.245E 01	-1.245E 01
1	2	3.666E 01	-3.666E 01
2	2	7.109E 01	-7.107E 01
3	2	9.511E 01	-9.519E 01
4	2	9.510E-02	4.493E-02
5	2	-9.520E 01	9.513E 01
6	2	-7.116E 01	7.106E 01
7	2	-3.655E 01	3.671E 01
8	2	-1.248E 01	1.244E 01
9	2	0	0
-1	3	0	0
0	3	1.131E 01	-1.131E 01
1	3	3.982E 01	-3.981E 01
2	3	9.513E 01	-9.518E 01
3	3	1.710E 02	-1.708E 02
4	3	-1.386E-01	-7.556E-02
5	3	-1.709E 02	1.709E 02
6	3	-9.499E 01	9.522E 01
7	3	-3.996E 01	3.973E 01
8	3	-1.132E 01	1.134E 01
9	3	0	0
1	4	0	0
0	4	-2.189E-03	2.596E-04
1	4	2.239E-03	-3.631E-03
2	4	3.485E-02	2.586E-02
3	4	-9.773E-02	-5.706E-02
4	4	7.729E-02	5.058E-02
5	4	6.506E-02	2.284E-02
6	4	-1.648E-01	-8.230E-02
7	4	6.059E-02	5.622E-02
8	4	6.911E-02	-3.794E-02
9	4	0	0
-1	5	0	0
0	5	-1.131E 01	1.131E 01
1	5	-3.982E 01	3.982E 01
2	5	-9.517E 01	9.515E 01
3	5	-1.709E 02	1.709E 02
4	5	6.813E-02	3.388E-02
5	5	1.708E 02	-1.709E 02
6	5	9.516E 01	-9.514E 01
7	5	3.991E 01	-3.978E 01
8	5	1.125E 01	-1.131E 01
9	5	0	0

-1	6	0	0
0	6	-1.245E 01	1.245E 01
1	6	-3.666E 01	3.666E 01
2	6	-7.110E 01	7.106E 01
3	6	-9.506E 01	9.522E 01
4	6	-1.582E-01	-9.235E-02
5	6	9.520E 01	-9.511E 01
6	6	7.126E 01	-7.101E 01
7	6	3.649E 01	-3.677E 01
8	6	1.244E 01	-1.242E 01
9	6	0	0
-1	7	0	0
0	7	-8.249E 00	8.247E 00
1	7	-2.250E 01	2.249E 01
2	7	-3.662E 01	3.669E 01
3	7	-3.993E 01	3.976E 01
4	7	1.080E-01	6.090E-02
5	7	3.987E 01	-3.980E 01
6	7	3.647E 01	-3.675E 01
7	7	2.259E 01	-2.243E 01
8	7	8.305E 00	-8.283E 00
9	7	0	0
-1	8	0	0
0	8	-2.740E 00	2.740E 00
1	8	-8.245E 00	8.249E 00
2	8	-1.246E 01	1.243E 01
3	8	-1.129E 01	1.134E 01
4	8	-5.604E-02	1.309E-03
5	8	1.132E 01	-1.136E 01
6	8	1.252E 01	-1.241E 01
7	8	8.187E 00	-8.239E 00
8	8	2.712E 00	-2.731E 00
9	8	0	0
-1	9	0	0
0	9	0	0
1	9	0	0
2	9	0	0
3	9	0	0
4	9	0	0
5	9	0	0
6	9	0	0
7	9	0	0
8	9	0	0
9	9	0	0

TIME = 1 MINUTES, 40 AND 43/60 SECONDS

Moving Load Test on Experimental Prestressed Concrete Highway Slab, Part B—Additional Investigations

JOHN R. SMITH and JAMES L. EVANKO, Civil Engineering Department, University of Pittsburgh

This investigation was initiated to determine the loss in prestress in the experimental prestressed concrete highway slab, to determine the extent to which bonding of the strands had been accomplished during the grouting operation and to investigate the effects of corrosion on the strands. Details of the design and construction of the pavement and the results of the static and creep load tests were reported by Moreell et al. (1). The results of the moving load tests were reported by Smith and Lightholder (2).

The investigation was performed about eight years after the pavement was constructed and two years after it was subjected to the moving load tests. Longitudinal cracks had developed over some of the tendons as a result of the moving load tests. Two of these cracks were in the area covered by the present investigation.

The test indicated that there was a loss in prestress in the pavement of about 14 percent. Bond failure occurred between the conduit and the pavement when longitudinal cracks along the conduit were forced open. The developed bond strength between the strands and the grout was about 421 psi. Corrosion covered approximately 30 percent of the surface area of the strands. The average breaking strength of the strands was about 27,200 pounds.

The investigation demonstrated that there was adequate bond developed between the grouted tendons and the concrete to transfer the prestressing loads when transverse cuts are made.

The inherent weakness in the pavement is the longitudinal cracks that develop over the tendons. This condition may be minimized by providing transverse reinforcement or by redistributing the prestressing strands more uniformly across the pavement.

It is recommended that a test section of this pavement be incorporated as a part of a highway system where the performance can be studied under normal traffic conditions.

•IN 1956 and 1957 the Jones and Laughlin Steel Corporation designed and constructed an "Experimental Prestressed Concrete Highway Slab" and ran a series of static and creep load tests on it. During the fall of 1962, the Civil Engineering Department of the University of Pittsburgh placed approximately 580,000 repetitions of moving loads over

Paper sponsored by Committee on Rigid Pavement Design and presented at the 45th Annual Meeting.

a section of the slab containing an expansion joint. The test was performed to determine the behavior of the slab when subjected to repeated applications of moving loads over an extended period of time.

There are several factors related to prestressed pavements that are of interest in the design and construction of highways. These are (a) the loss of prestress, (b) the developed bond stress, and (c) the effect of corrosion on the strength of the pavement.

PURPOSE AND SCOPE OF RESEARCH

The purpose of this investigation is to determine the amount of prestress remaining in the experimental pavement, to determine the bond resistance between the prestressing strands and the concrete, and to evaluate the corrosion that has taken place since the construction of the slab.

The evaluation was accomplished by progressive destruction of a portion of the pavement. Appropriate instrumentation was used to measure the changes in strain as the work proceeded. This required exposure of the tendons in the early stages so that the changes in strain in the strands could be read directly. It also dictated that sufficient concrete be left between the instrument slots and the severed ends of the strands to develop bond resistance between the tendons and the concrete. The critical bond length was determined by progressively reducing the length of bond to failure. Four of the tendons were removed for further study. The strands from three of these were subjected to the standard tensile test. This, together with visual examination of the conduit, grout core and the tendons, provided the information for the evaluation of the bond strength and corrosion.

It was initially established that one of the tendons was not grouted. This, along with the possibility that bond might not be developed, made it desirable to design anchors for the tendons, so that the remainder of the pavement would retain its prestressed condition. In addition, information about such anchors would be valuable in the event that this pavement or a similar pavement was built into a highway system.

ANCHOR FOR TENDONS

Development of the anchorage device incorporated the use of epoxies, sand and a holding fixture. A series of tests was performed on three different diameter bars and $\frac{7}{16}$-in. diameter prestressing strands, using 1-in. pipe as a holding fixture. The inside surface of the pipe and the surface of the bars and prestressing strands were thoroughly cleaned prior to assembly.

Table 1 of the Appendix gives the results of the pull-out tests to which all of the specimens were subjected with the exception of numbers 16 and 18. Specimens 12 through 18 were subjected to a creep test, the results of which are shown in Figure 14 of the Appendix. Specimen number 16 developed faulty instrumentation and was discarded, and number 18 was a four strand test which exceeded the capacity of the 100,000-lb Universal testing machine.

The knowledge gained from these tests was used in the design of the anchors for the tendons. The anchor consists of a 30-in. length of mechanical tubing with a $1\frac{1}{2}$-in. I.D. and a $2\frac{3}{8}$-in. O.D. The tubes were slotted to fit over the tendons. The slots were covered with mechanical tubing having a $2\frac{3}{8}$-in. I.D. and $3\frac{1}{4}$-in. O.D. which was welded in place. A slotted bearing plate 5 in. wide by $1\frac{3}{4}$ in. thick by 6 in. long, grouted in place with a stiff epoxy sand mixture, was used to transfer the load to the concrete. The tendons were bonded into the fixtures with a mixture of seven parts of epoxy patching compound to 10 parts of silicon sand, 100 percent of which passed a No. 20 sieve and was retained on a No. 30 sieve. The assembly is shown in Figure 1.

TEST AREA

The test area shown in Figure 2 was located within the same area that was used for the moving load test. The site was selected because it had been subjected to a considerable amount of traffic during the previous test and it contained two tendons which had developed longitudinal cracks over them. The center of the area was located 29 ft

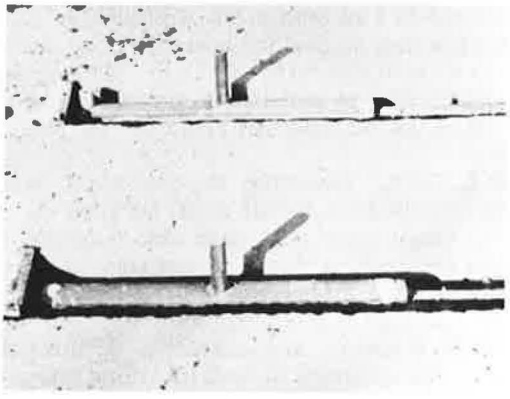

Figure 1. Anchors for the tendons.

west of the expansion joint, midway between the west ramp and the existing holes 15 ft west of the joint.

Access to the tendons was provided by 6- by 49-in. slots. The length was dictated by the anchors and the space needed to manipulate strain measuring instruments. A distance of 81 in. from the end of the slots to the transverse cut was used to insure the development of bond between the tendons and the concrete. The area was covered with a shelter which was heated to maintain the temperature between 55 and 65 F.

INSTRUMENTATION

The instrumentation for the concrete was SR-4, Type A-9 gages surface mounted at the ends of the slots and midway between the slots. These were thoroughly waterproofed and given a protective coating of cerese wax. Each set of gages was wired through a multichannel switch box to a conventional battery-operated strain indicator. The strains in the prestressing strands were taken with a 10-in. Whittemore gage.

OPERATION AND PROCEDURE

The field work began on November 1, 1964. Longitudinal saw cuts were made on each side of the tendons and a 1-in. diameter hole was drilled at each end of the cuts to facilitate the removal of the concrete. The pavement was permitted to dry out thoroughly. The SR-4 strain gages were installed and zero readings were recorded.

The concrete was removed from the slots with light electric chipping hammers. The conduit and grout were stripped from the strands and the anchors were installed in the west slots. Cable clamps were used to provide gage marks for the Whittemore gage.

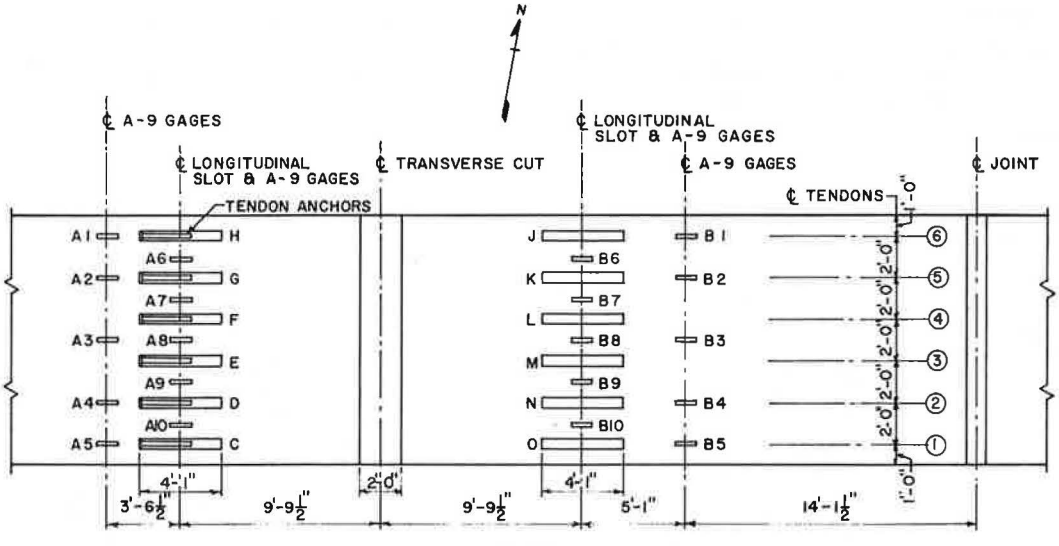

PLAN

NO SCALE

Figure 2. Test area.

The location of the ungrouted tendon was established as tendon No. 2 which ran through slots D and N (Fig. 2). An access slot for this tendon had been provided during construction of the pavement at a point 85 ft west of the transverse cut. The asphalt filler was removed from this hole and it was designated as slot P in Figure 16 of the Appendix. Zero readings were recorded for all of the strands that could be reached with the Whittemore gage.

The transverse cut was made on December 2, 1964. Two cuts, two feet apart, were made across the slab. The saw was permitted to sink down to full depth between the tendons. To facilitate removal of the concrete, longitudinal cuts were also made on each side of the tendons. The concrete between the tendons was removed first and then the concrete, conduit and grout were chipped away from the tendons. Progressive relaxation occurred as each tendon was exposed. The last two tendons to be exposed were the ungrouted tendon No. 2, through slots D, N and P, and tendon No. 3, through slots E and M. As work began on these tendons, the concrete at both locations failed in compression, leaving all but the ungrouted strands relaxed (Fig. 3).

The next step was to cut the tendons. Hack saws, equipped with high-speed tungsten blades, were used. Tendon No. 2 was the first to be cut since it was still highly stressed. The severing of this tendon reduced some of the relaxation in the other tendons (Fig. 4).

The final step was to reduce gradually the length of bond between the transverse cut and the slots until bond failure occurred. Work was started on the east side first. It was decided to remove 12-in. increments of the concrete until a point was reached where bond failure would be impending and then proceed at a slower pace until bond failure was accomplished. Starting at the transverse cut a 12-in. increment was sawed about 1 in. deep. The electric chipping hammers and a sledge were used to break away the concrete. The resulting forces and shock waves caused longitudinal cracks to develop over two additional tendons (Fig. 5). This caused these tendons to relax. The remaining tendons on the east side were released and strain readings on the unstressed strands were recorded.

On the west side the tendon slots were elongated by 6-in. increments with the concrete saw and careful use of the chipping hammers. Strain readings were taken at intervals. Initial failure was indicated at slot F (Fig. 6). About five minutes after the saw cuts were made—work had stopped for the day—the audible failure of the concrete around the conduit was substantiated by visible cracks. This tendon and the one at slot E were the only ones that had longitudinal cracks at the beginning of the tests.

After initial bond failure had been accomplished for the remaining tendons, the strands were freed for total relaxation and the final strain readings were taken. The site was abandoned on December 16, 1964. Graphical representation of the steel and concrete strains is shown in Figures 15 to 20 and Figures 21 to 24, respectively, of the Appendix.

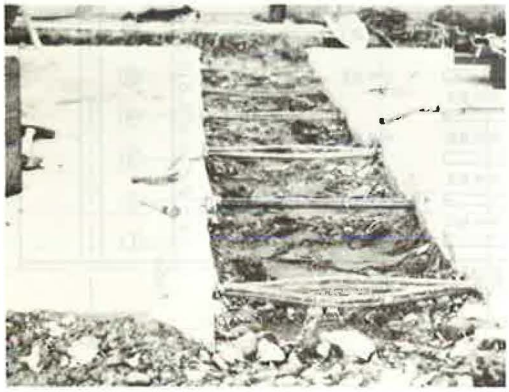

Figure 3. Transverse cut.

Figure 4. Ungrouted tendon severed.

Figure 5. Failure at slot J.

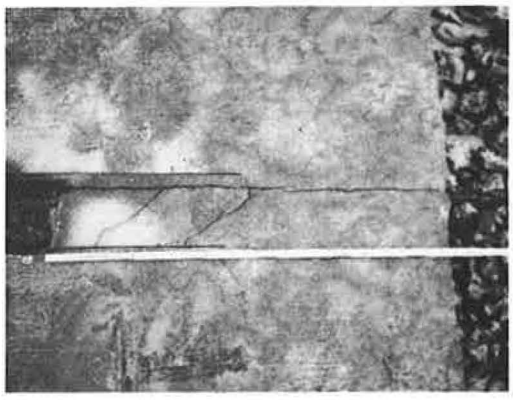

Figure 6. Failure at slot F.

LOSS IN PRESTRESS

Figure 7 shows the average value of the change in stress in the steel and the concrete for each reading. The diagram for the steel stresses shows four separate conditions. C-H and J-O represent the average stress for the grouted tendons to the west and to the east, respectively, of the transverse cut. D and N represent the average stress for the ungrouted tendons west and east of the cut (Fig. 2).

The two curves for each condition agree reasonably well. The final stress for the ungrouted tendon is about 115,700 psi and the average for the grouted tendons is 106,000 psi. One might, at this point, conclude that the loss in prestress would be the difference between the two, since cutting the slots in the pavement would have a negligible effect on the stresses in the ungrouted tendon. However, the stresses reported after the release of the jacks, during the construction of the pavement, indicate a variation in stress from the anchors to the midlength of the slab (1).

The original stresses varied from 116,000 psi at the anchors to 151,000 psi at the midlength with a value of about 124,000 psi in the vicinity of this test section. It is ·umed that this variation was locked into the strands due to the grouting of the ten- The ungrouted tendons, on the other hand, would have had ample opportunity to nore uniformly stressed over the 8-yr period.

` shows the load-deflection relationship between the original area of the slab ·ter the slots were cut. The calculations equate δs to δc and indicate · the load ΔP will be the same for the concrete as it is for the steel. there is no frictional resistance between the concrete and the base

litions the computed prestress in the grouted tendons is about 736 psi. This uses the value P_F = 46,233 lb which is based on the ·train in the tendons of 3,870 microinches. The percent loss in ·ent which compares favorably with the 15 percent found in the litera- ·th frictionless bases.

stresses shown in Figure 7 are not as well grouped as were the steel ·lid lines represent the stresses at the end of the slots and the dashed sses midway between the slots. The (A) values are for those gages ·n and the (B) values represent the gages on the east section. The n slope of these curves indicate that flexural stresses were affecting

BOND

it when the tests were initiated that there would be three different cases ndons were concerned: Case I—the ungrouted tendon, Case II—the

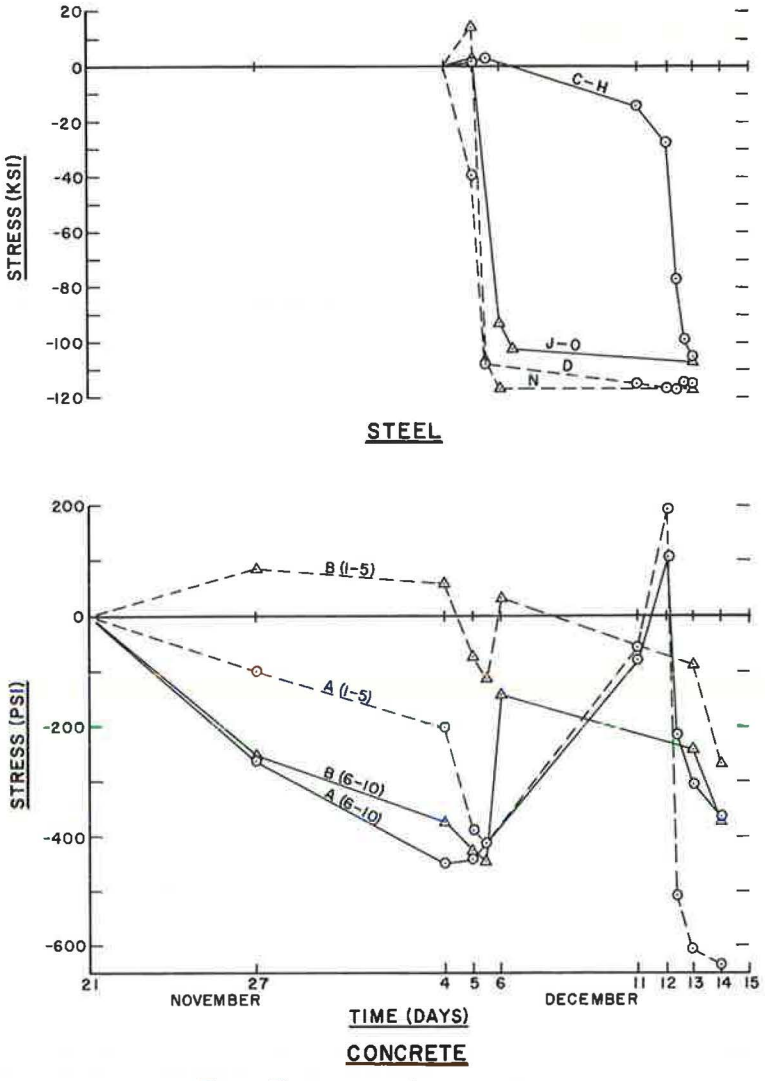

Figure 7. Average change in stress.

grouted tendon with a longitudinal crack, and Case III—the grouted t longitudinal crack. The second and third cases are of primary imp is involved.

The tendons were released when the length of bond was about 20 i lustrated in Figure 6 for Case II. Figure 9 shows the cracks that de and is representative of the type of failure for Case III. In both cases in pulling the conduit through the concrete. The wedging action of the the outside of the conduit forced the pavement apart, resulting in longi at those locations which had no previous cracks.

The force in the tendons at this point was approximately 46, 537 - 3(The resulting unit stress on the surface of the conduit was 46, 223/ (20) 491 psi. The approximate bond stress between the grout and the strand (20) (0. 4375) (4) (3. 14) = 421 psi.

There was an audible adjustment of the load in tendon No. 1, through 31-in. length of bond. This tendon, due to faulty alignment, had one of i

$P_{ORIGINAL} = P_{OS} = P_{OC} = P_O$

$P_{FINAL} = P_{FS} = P_{FC} = P_F$

ΔP = CHANGE IN LOAD TO EFFECT Δ_S AND Δ_C

$\delta_S = \delta_C = \Delta_{OS} - \Delta_{FS} = \Delta_{FC} - \Delta_{OC}$

$$\therefore \frac{P_O L_S}{A_S E_S} - \frac{(P_O - \Delta P) L_S}{A_S E_S} = \frac{(P_O - \Delta P) L_C}{A_{FC} E_C} - \frac{P_O L_C}{A_{OC} E_C}$$

$$\frac{L_S}{A_S E_S} \Delta P = \frac{L_C}{A_{FC} E_C} (P_O - \Delta P) - \frac{L_C}{A_{OC} E_C} P_O$$

$\Delta P = 0.006542 P_O$

$P_O = P_F + \Delta P$; $P_F = (387)(10^{-5})(27.4)(10^6)(0.436) = 46{,}233$ LB.

$P_O = 46{,}537$ LB. ; $\Delta P = 304$ LB.

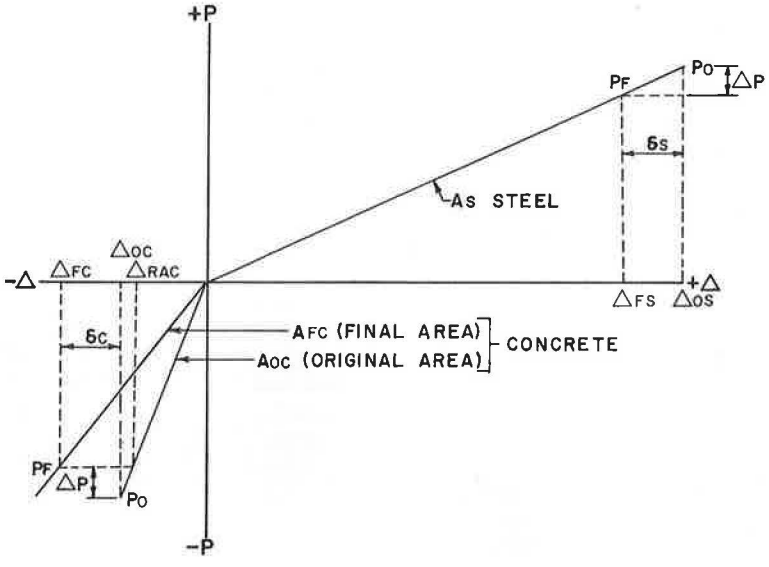

NO SCALE

Figure 8. Load-deflection relationships.

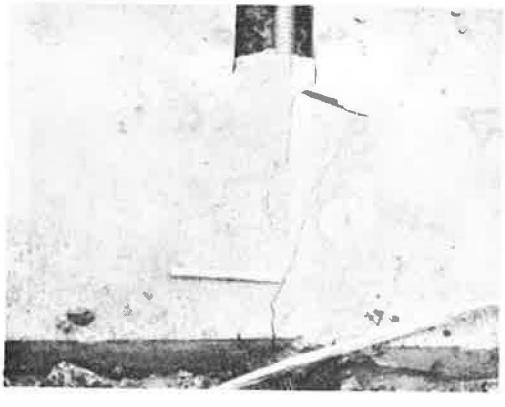

Figure 9. Failure at slot G.

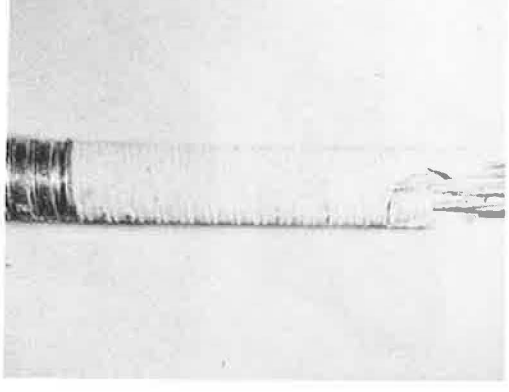

Figure 10. Grout—no initial crack in pavement.

severed during the construction of the slot. Using the same initial load on the tendon and a 31-in. length of bond for three strands, the bond stress would be 362 psi.

The grout was a solid core which completely filled the space inside the conduit (Fig. 10). It was a dark gray with a thin layer of white where it was in contact with the metal conduit. The material was extremely hard and adhered very well to the prestressing strands. It was necessary to use a hammer and cold chisel to remove the grout from the strands. It broke away in segments about 1 in. long. Apparently, cleavage planes had developed normal to the axis of the tendons (Fig. 11). These are probably shrinkage cracks that were pressed together.

Readings taken on the ungrouted tendon at slot P, 85 ft west of the test section, showed little change in strain during the test period. This indicates that the anchors were effective in holding the stress in the tendon. The developed bond stress in the strands was about 306 psi.

CORROSION

Figure 12 shows the condition of the conduit. Case I, at the top of the figure, has from 25 to 30 percent of its surface covered with a light coating of rust. Case II has been completely penetrated with pin holes in the upper area of the picture while the lower area has very little corrosion. In Case III the conduit is free from rust.

Figure 13 shows the condition of the strands. Case I was completely covered with a light film of rust. There was no flaking and very little pitting. In Cases II and III the black oxide coating was very evident. It was spotted with rust which covered as much as 30 percent of the surface in some areas. There was little or no pitting of the base metal. The dark spots on the

Figure 11. Segments of the grout.

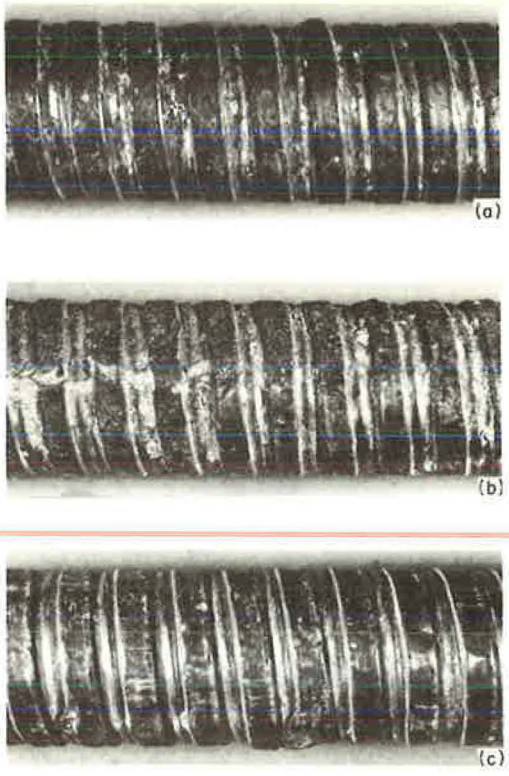

Figure 12. Condition of conduit: (a) Case I, ungrouted tendon; (b) Case II, grouted tendon—initial crack; and (c) Case III, grouted tendon—no crack.

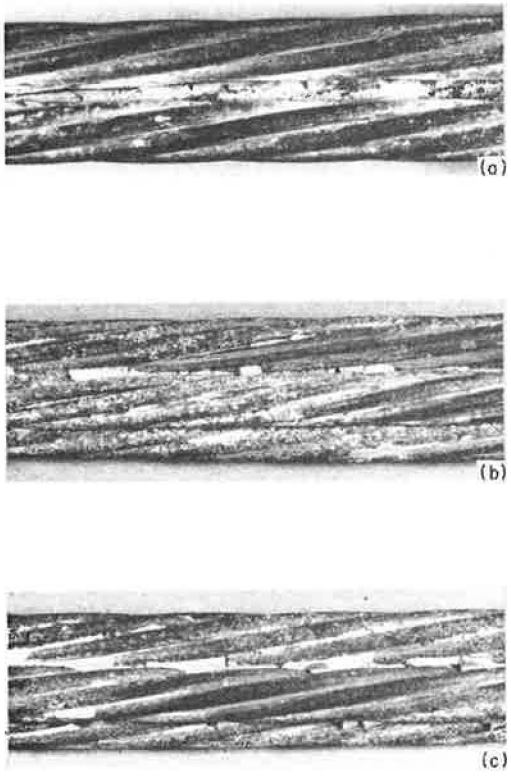

Figure 13. Condition of strands: (a) Case I, ungrouted tendon; (b) Case II, grouted tendon—initial crack; and (c) Case III, grouted tendon—no crack.

surface of the grout in Figure 11 also illustrate the distribution of the rust.

Each of the strands from the three tendons shown in Figure 13 was subjected to the standard tensile test. The value of the ultimate load ranges from 25,600 to 28,80[illegible] lb with an average value for the twelve strands of 27,183 lb. In all of the tests, failure occurred at notches which were caused by the strand vises. The initial tests for these strands indicated an ultimate of 28,700 lb for one reel and 29,800 lb for the other. This indicates a loss in strength of from 5 to 9 percent of the initial values.

The modulus of elasticity for the twelve strands varied from 26,700,000 to 30,200,000 psi with an average value of 28,200,000 psi. This is within 3 percent of the 27,400,000 psi used in the calculations for the design of the slab. Differences in testing techniques could very well account for the loss in ultimate load and the higher value of the elastic modulus.

SUMMARY AND CONCLUSIONS

This investigation on an existing prestressed concrete highway slab was conducted about eight years after the pavement was constructed and two years after it was subjected to the moving load test. The cracks over the tendons in Case II developed during the moving load tests. The loss in prestress during the ensuing eight years is about 14 percent.

The grout was in excellent condition. Pull-out failure was not due to loss of bond stress between the tendons and the grout, but rather to the rupture of the concrete caused by the wedging action of the conduit on the concrete. This occurred when there was about 20 in. of concrete remaining to effect an anchor. The developed bond stress in the tendons at this time was about 421 psi.

Corrosion was present on the surface of the strands. It covered about 30 percent of the surface area. There was little or no penetration into the base metal. The average ultimate strength of 27,183 lb compares favorably with the 27,000 lb specified for ASTM A-416 prestressing strands. It appears that the corrosion had not developed to the extent that it had a detrimental effect on the strength of the pavement.

The test indicates that there was adequate bond to develop the stress in the tendons over a reasonable length. It also illustrates that the plane of weakness that exists in the reduced section of concrete at the tendons is a factor that must be taken into consideration in future designs. This may be minimized by providing transverse reinforcement or by redistributing the prestressing strands more uniformly across the pavement. It also demonstrates that the slab can be successfully cut without destroying the prestressed condition in the remainder of the pavement. It is recommended that a test section of this pavement be incorporated as a part of a highway system where the performance can be studied under normal traffic conditions.

ACKNOWLEDGMENTS

The authors wish to express their appreciation for the advice and assistance of the following individuals: C. D. Jensen and R. K. Shaffer of the Pennsylvania Department

of Highways; H. D. Cashell and H. Higgins of the Bureau of Public Roads; N. G. Marks of Richardson, Gordon and Associates; and J. J. Murray of Jones and Laughlin Steel Corporation.

REFERENCES

1. Moreell, Ben, Murray, John J., and Heinzerling, John E. Experimental Prestressed Concrete Highway Project in Pittsburgh. Proc. Highway Research Board, Vol. 37, pp. 150-193, 1958.
2. Smith, John R., and Lightholder, Richard K. Moving Load Test on Experimental Prestressed Concrete Highway Slab. Highway Research Record 60, pp. 59-76, 1964.

Appendix

TABLE 1

BOND STRENGTH OF EPOXY

Test	Rod Dia. (in.)	Perimeter (in.)	Embedded Length (in.)	Load (lb)	Bond Stress (psi)	Slip-Stick Friction (psi)	Remarks
1	0.250	0.785	4	3,700	1,178	–	Bond failure[a]
2	0.375	1.178	4	8,600	1,825	790	Bond failure[a]
3	0.500	1.571	4	1,100	175	–	Bond failure[a]
4	0.250	0.785	4	350	111	–	Bond failure[a]
5	0.375	1.178	4	9,375	1,990	–	Rod failure[a]
6	0.500	1.571	4	2,050	326	–	Bond failure[a]
7	0.375	1.178	3.94	9,100	1,965	–	Bond failure[a]
8	0.500	1.571	4	13,850	2,205	–	Bond failure[a]
9	7/16 strand	1.374	12.5	4,825	280	–	Bond failure[a]
10	7/16 strand	1.374	12.75	16,000	913	456	Bond failure[b]
11	7/16 strand	1.374	12.75	20,700	1,181	684	Bond failure[b]
12	7/16 strand	1.374	13.0	17,475	998	628	Bond failure[b]
13	7/16 strand	1.374	13.0	15,000	857	798	Bond failure[b]
14	7/16 strand	1.374	13.0	21,650	1,237	1,083	Bond failure[c]
15	7/16 strand	1.374	13.0	13,775	786	856	Bond failure[c]
16	7/16 strand	1.374	13.0	–	–	–	No pull-out test[c]
17	7/16 strand	1.374	26.0	28,050	785	–	Strand failure[c]
18	7/16 strand	5.496	26.0	100,000	702	–	No failure (4 strands)[c]

[a]Epoxy bonding compound.
[b]Epoxy patching compound—1 part epoxy to 1 part sand.
[c]Epoxy patching compound—7 parts epoxy to 10 parts sand.

Notes: The perimeter of the prestressing strands is based on that of a 7/16 dia. circle.
Tests 12-18 were subjected to a creep test before loading to failure.
Tests 1-17—the load was transferred by the epoxy to a 1-in. pipe, 1.315 O.D. and 0.957 I.D.
Test 18—the load was transferred to mechanical tubing, 2.375 O.D. and 1.500 I.D.

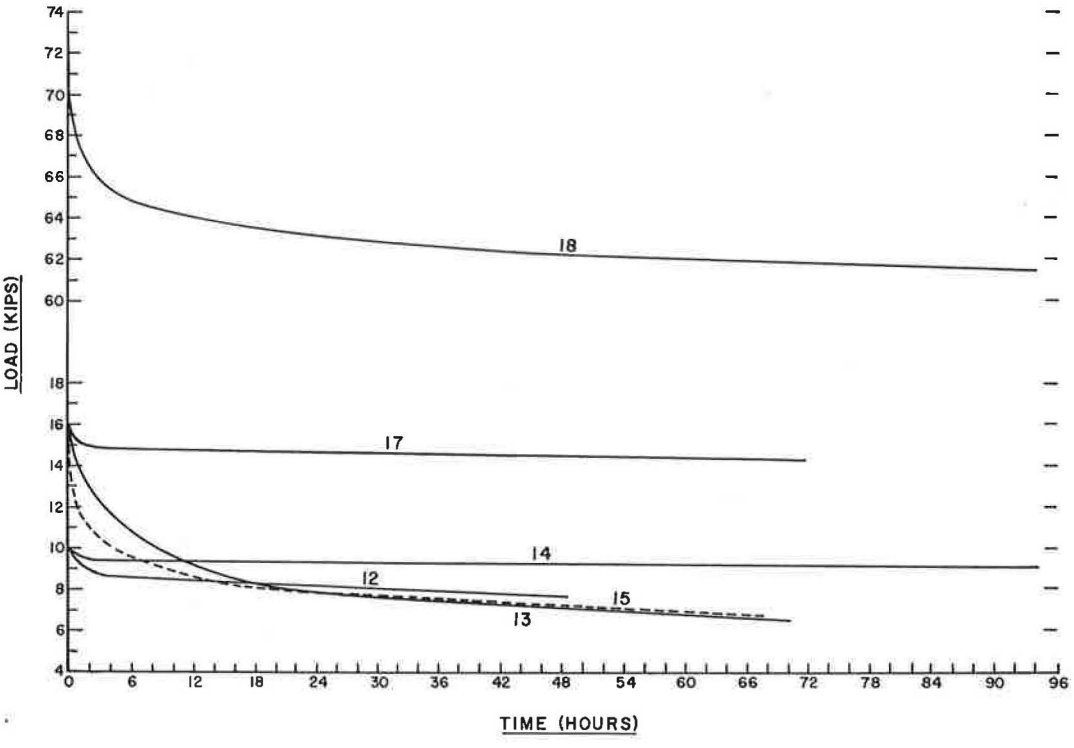

Figure 14. Epoxy creep test.

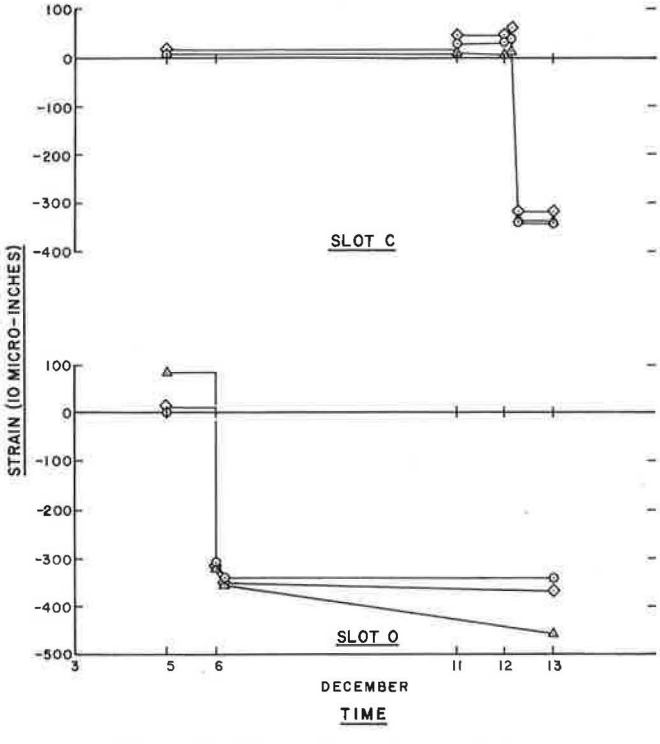

Figure 15. Change in strains, tendon 1.

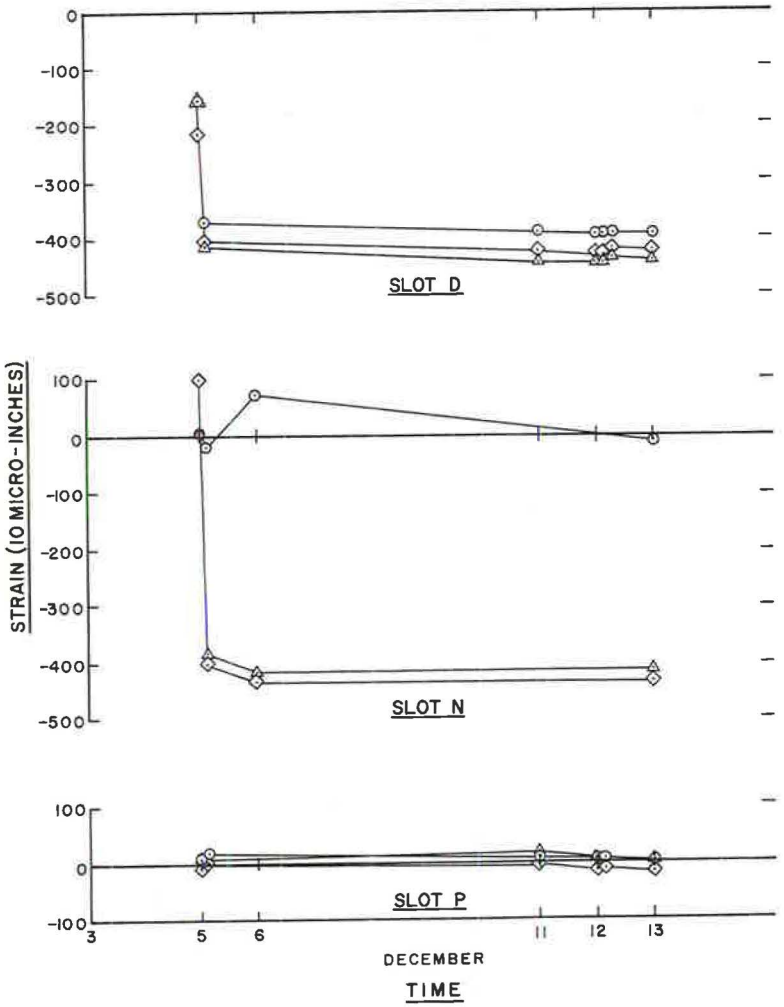

Figure 16. Change in strains, tendon 2.

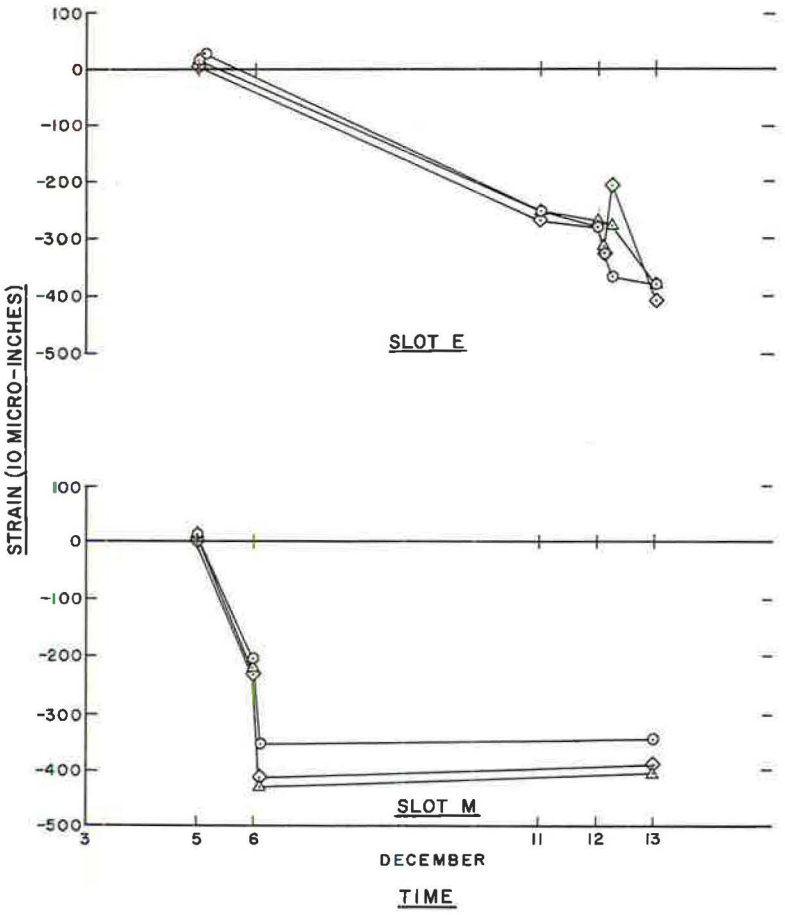

Figure 17. Change in strains, tendon 3.

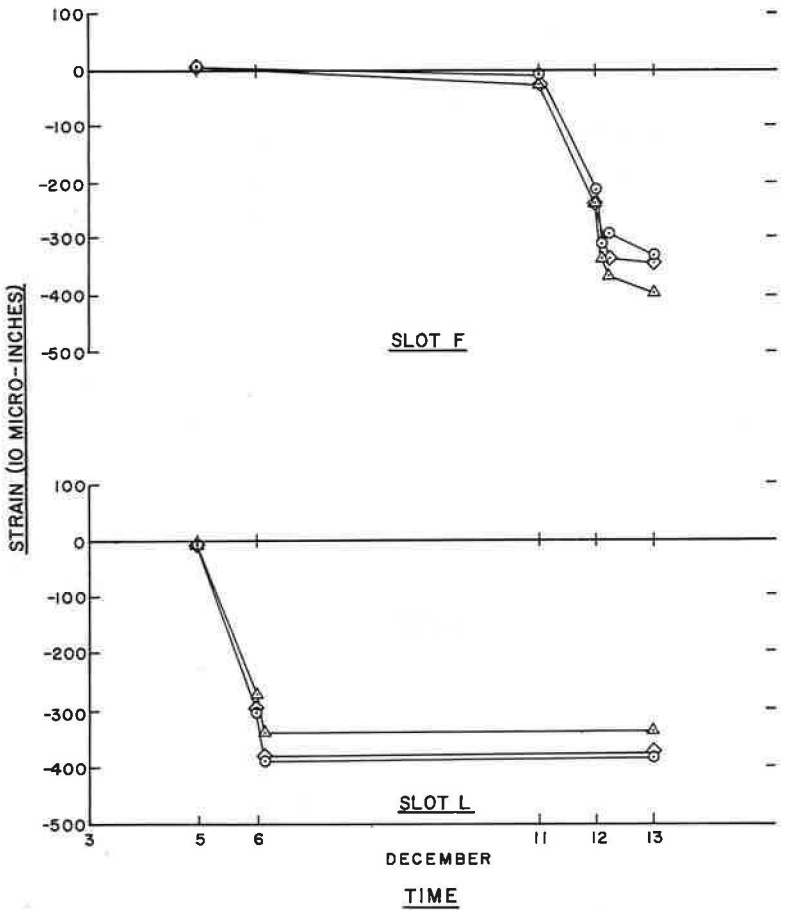

Figure 18. Change in strains, tendon 4.

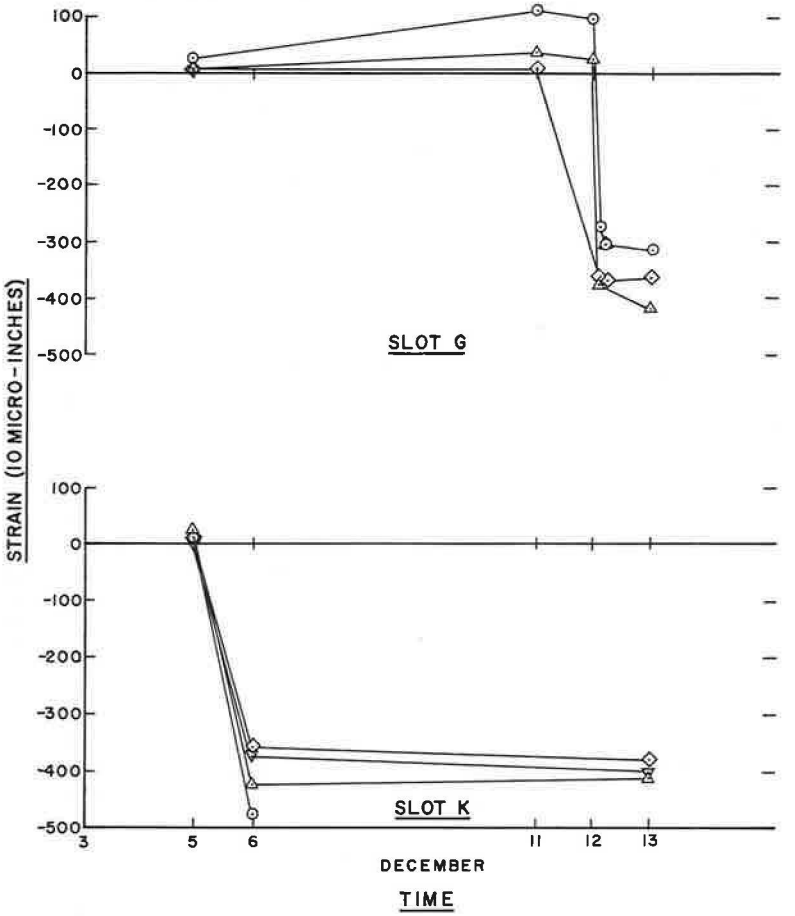

Figure 19. Change in strains, tendon 5.

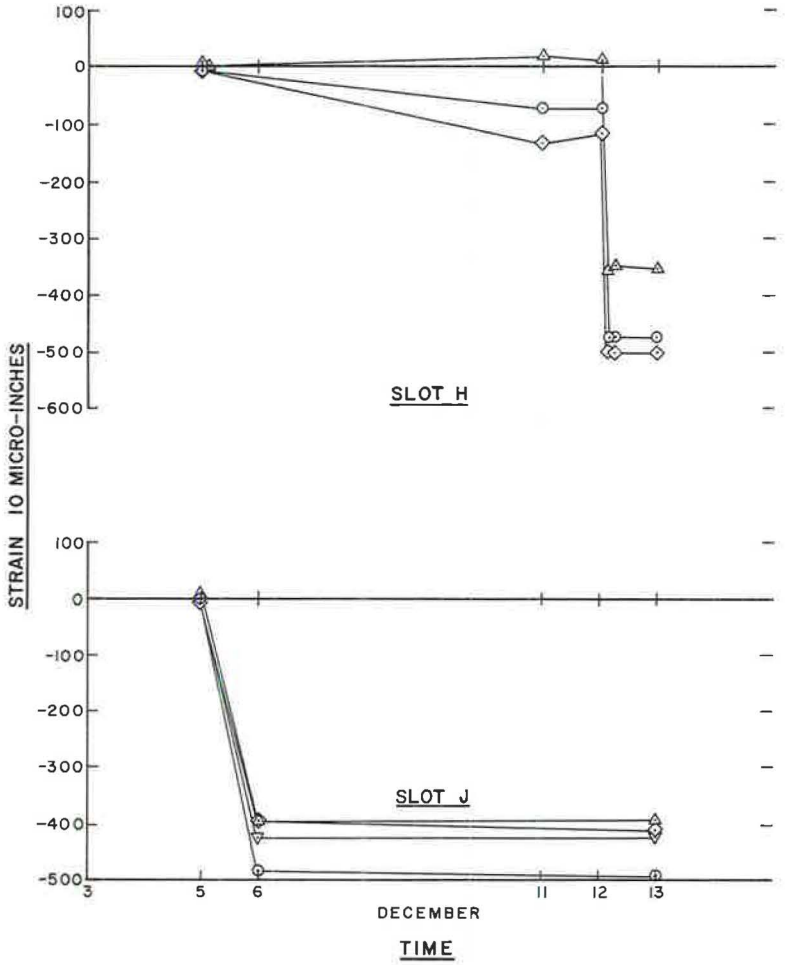

Figure 20. Change in strains, tendon 6.

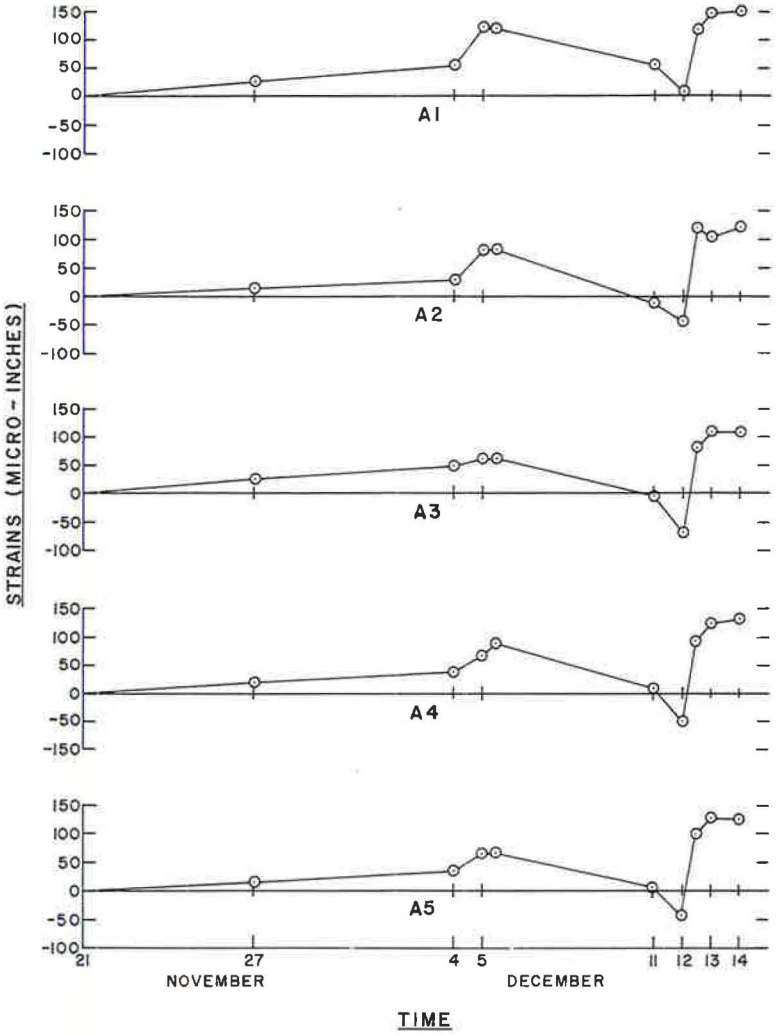

Figure 21. Change in concrete strains, gages A1-A5.

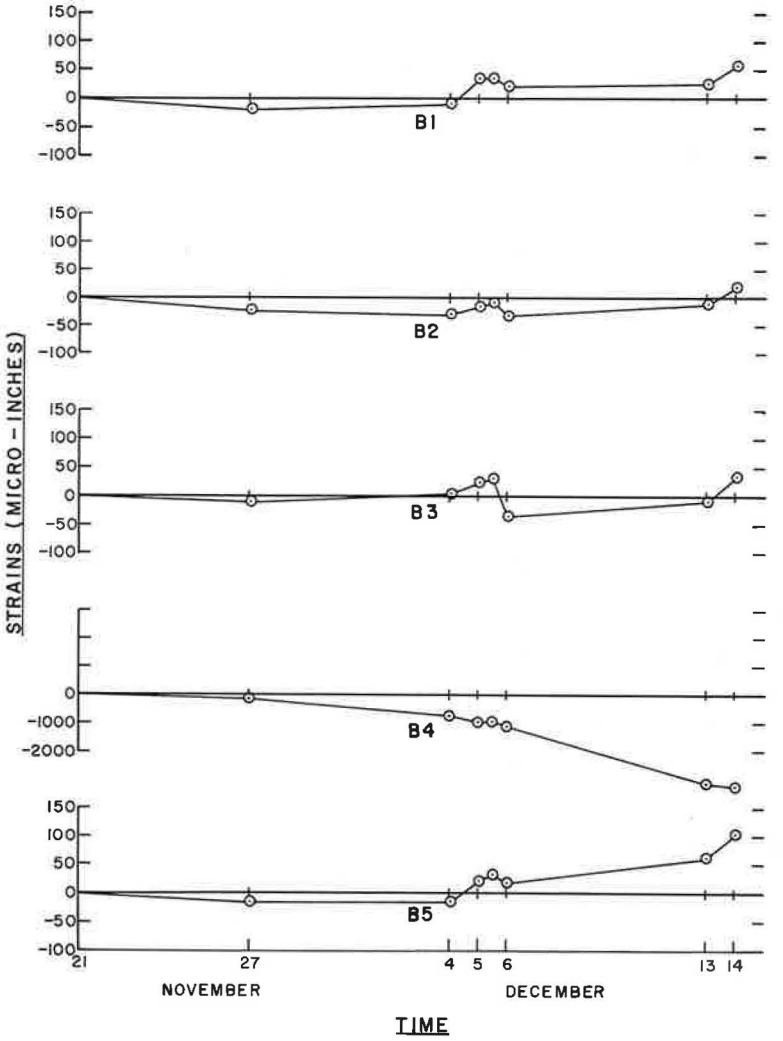

Figure 22. Change in concrete strains, gages B1-B5.

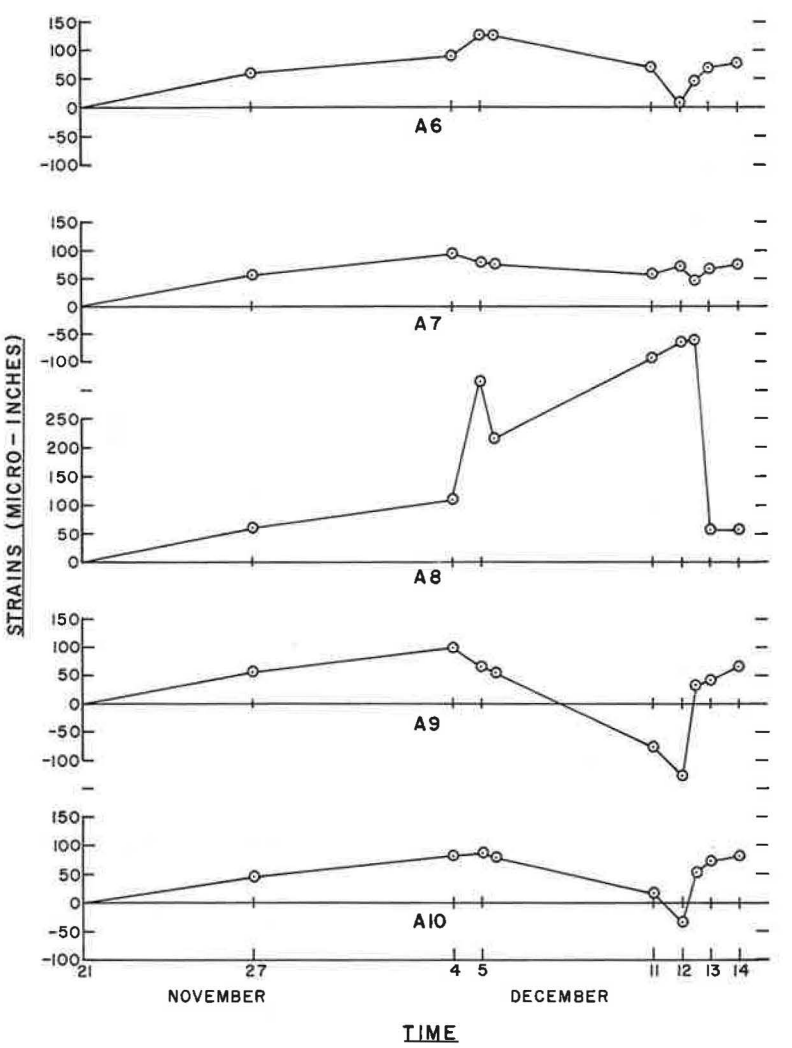

Figure 23. Change in concrete strains, gages A6-A10.

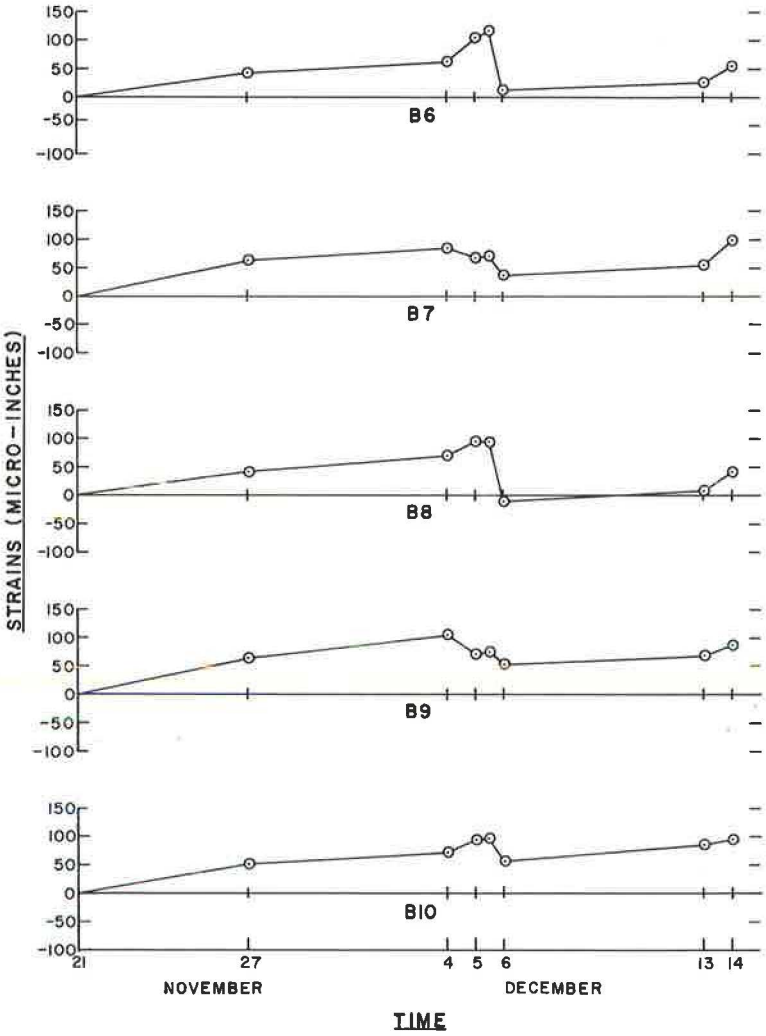

Figure 24. Change in concrete strains, gages B6–B10.

Determining the Relationship of Variables in Deflection of Continuously-Reinforced Concrete Pavement

B. F. McCULLOUGH, Supervising Design Research Engineer, and
HARVEY J. TREYBIG, Engineering Assistant, Texas Highway Department

The AASHO Road Test provided excellent information pertaining to the deflection characteristics of jointed concrete pavements, but the equations are not completely applicable to continuously-reinforced concrete pavement. A comprehensive deflection study of continuous pavement has been conducted in Texas using the Road Test studies as guidelines for the design of the experiments. This is the first report on these deflection studies of CRCP.

The variables studied include load and temperature differential which were explored fully at the Road Test. Other variables studied in this experiment are transverse crack width and transverse crack spacing which are unique to continuous pavement. In addition, a pavement support term is included that encompasses varying conditions of subbase and subgrade type. These variables are studied in terms of both deflection and radius of curvature. An empirical equation for deflection of CRCP is presented which includes all of the variables considered in this study.

•THE FIRST continuously-reinforced concrete pavement (CRCP) was built in Indiana during 1938. Texas was the fifth state to build continuous pavement and today it has more mileage than any other state (1). It was not until the early 1960's that attempts were made to study the deflection characteristics of continuously-reinforced concrete pavement.

This report is on Phase I of a continuing study on the performance of continuously-reinforced concrete pavements presently being conducted by the Texas Highway Department. This report pertains to the static deflection of continuously-reinforced concrete pavement.

The first large-scale deflection study of rigid pavements was at the AASHO Road Test, providing highway engineers with a wealth of information about rigid pavement performance, but the Road Test failed to include continuously-reinforced concrete pavements in the design factorials (2). This means that the vast amount of work done there does not apply directly to the case of continuously-reinforced concrete pavement; therefore, this knowledge must come from other sources. In studying factors affecting the deflection of continuously-reinforced pavements, the AASHO Road Test results can be used as guidelines, but direct comparisons cannot be made.

Rigid pavement research at the AASHO Road Test found the following equation for the deflection of a jointed concrete pavement (3):

$$d = \frac{A_0 L}{10^{A_1 T_D A_2}}$$

Paper sponsored by Committee on Rigid Pavement Design and presented at the 45th Annual Meeting.

where

d = deflection in inches;
L = load in kips;
T = temperature differential in degrees Fahrenheit;
D = pavement thickness in inches; and
A_0, A_1, A_2 = regression constants determined from the data.

The Road Test equation takes into account only load, temperature differential, and slab thickness. For continuously-reinforced pavements this equation is inadequate because of the additional variables associated with this pavement type.

The objective of the project is to determine the deflection characteristics of CRCP under varying conditions of subbase, natural support, pavement thickness, temperature and concrete properties. The scope of this Phase I study is to include the methods of testing for deflections and to develop an algebraic expression for determining the deflection of continuous pavement for any given set of conditions.

DESCRIPTION OF THE EXPERIMENT

Selection of Test Sections

Choice of Site.—The Phase I investigation consisted of three 24-hr deflection studies on pavement sections which had not yet been opened to traffic. These three test sections were of the same design as far as pavement thickness, concrete modulus of elasticity and percent longitudinal steel are concerned. The test sections were selected because of their different supporting characteristics. The test sections were located in three different counties—Colorado, Jefferson and Smith—and will hereafter be referred to by county name. The sections in Colorado and Jefferson Counties were on I-10 and the section in Smith County was on I-20. Figure 1 shows the general location of each of the three test sites.

Description of Sections.—Each of the three selected test sections was 2500 ft long and was chosen in level terrain so that the vertical alignment would not influence the results in any way. Each section was carefully selected so that uniform soil conditions existed throughout. The primary differences between the three pavement sections were the characteristics of the subbase and the subgrade. Table 1 gives the salient features of the three test sections. The classifications of the subgrade are according to the Texas Triaxial Method (4).

Variables Considered

Pavement design involves many parameters and is, no doubt, one of the most complex of all civil engineering problems. Research at the AASHO Road Test was the first major step toward complete control and study of the variables involved in pavement design, but as mentioned earlier CRCP was not included. For ease and clarity in presentation, the variables covered at the AASHO Road Test will be designated as Road Test variables, and the ones included as a part of this investigation will be designated as CRCP variables.

Road Test Variables.—The variables investigated at the Road Test were touched on more lightly in this experiment than the unique variables of CRCP. The Road Test research did an excellent job of investigating pavement thickness and it was felt that thickness was relative, thus this phase of the experiment did not include any studies on thickness.

The other two variables—temperature differential and load—studied at the Road Test were also investigated in relation to CRCP. The load study was merely a check on theory and other research, whereas the temperature study was quite extensive, including equipment development.

CRCP Variables.—Continuously-reinforced concrete pavement has introduced two new variables—crack width and crack spacing—into the field of rigid pavement design. Also considered in this study is the effect of pavement support.

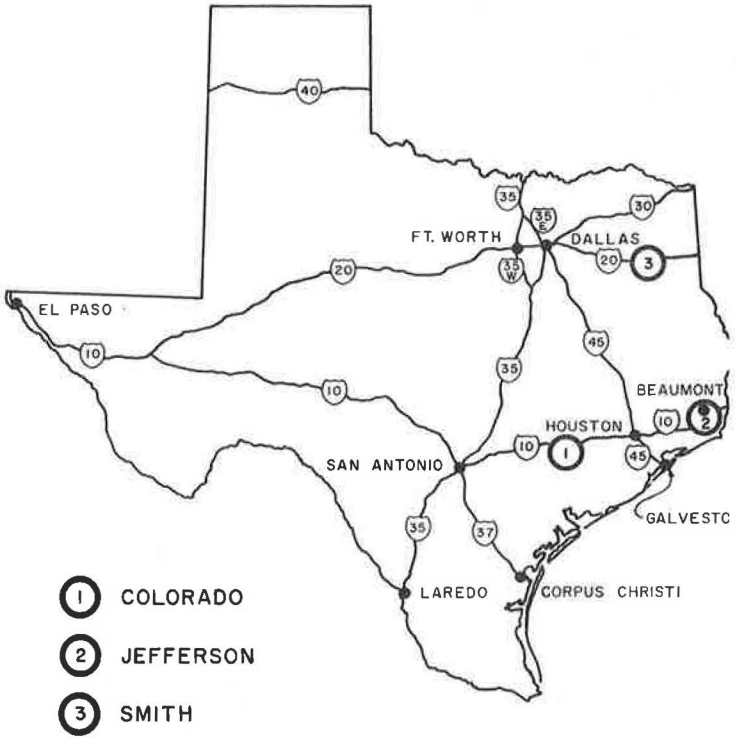

Figure 1. Location of test sites.

TABLE 1

SALIENT FEATURES OF TEST SECTIONS[a]

Highway	County	Subbase		Subgrade, Triaxial Classification
		Thickness (in.)	Type	
I-10	Colorado	6	Cement stabilized gravel[b]	Good Class 4.6
I-10	Jefferson	6	Sand shell	Poor Class 6.0
I-20	Smith	6	Fine grain	Good Class 4.0

[a]All sections are 8-in. continuously-reinforced concrete pavement with 0.5% steel consisting of A-432 #5 bars spaced at 7½ inches for longitudinal steel and A-16 #4 bars at 24-in. c-c for transverse steel.
[b]Stabilized with four percent cement by weight.

EQUIPMENT AND EXPERIMENTAL PROCEDURE

Equipment

The equipment used in the Phase I study of deflection included four Benkelman beams, a Basin beam, a specially equipped truck, special temperature equipment and a microscope. The equipment and its procedure for operation will merely be touched on in this report. For a detailed description and operational procedure of the equipment, refer to (5).

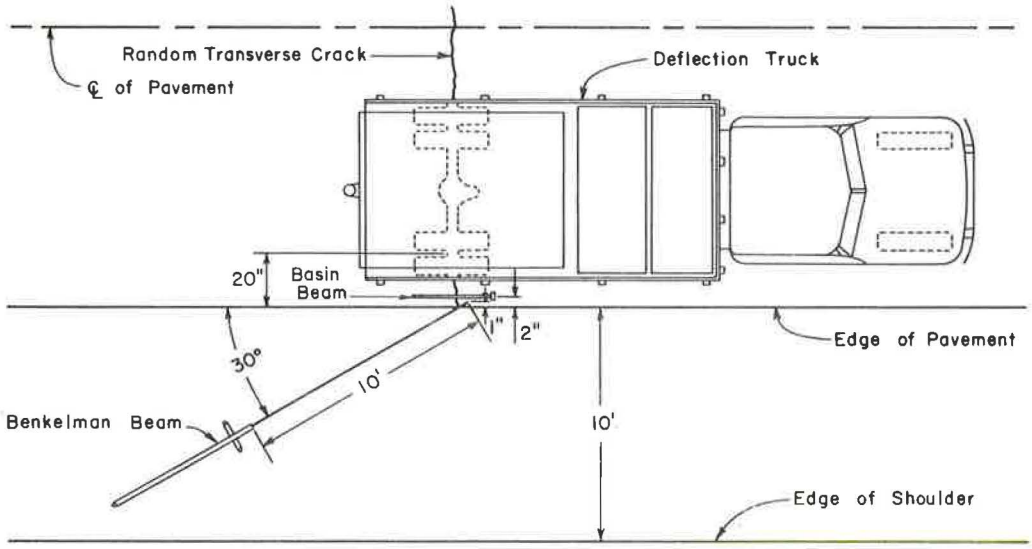

Figure 2. Plan view of equipment arrangement.

Figure 3. Basin beam and Benkelman beams as used on overnight studies.

Benkelman Beams.—Two of the four beams had 10-ft probes, and the other two had 8-ft probes. The Benkelman beams were positioned on the pavement in this study in a manner similar to that used at the AASHO Road Test (3). The beams were positioned at an angle of 30 degrees to the longitudinal edge of the pavement slab with the probe pointing toward the truck. Figure 2 shows a plan view of the position of the Benkelman beam when taking measurements.

Basin Beam.—The Basin beam, which is the instrument used to measure basin deflections in terms of radius of curvature, was designed by the Highway Design Division's Research Section and built by the shops of the Texas Highway Department. The

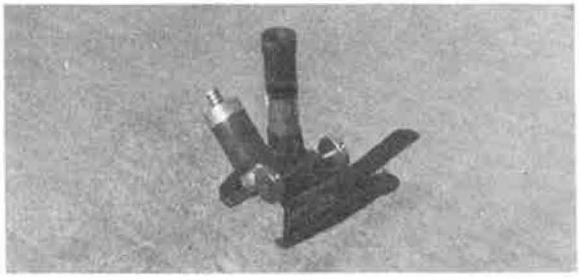

Figure 4. Microscope used to measure crack width.

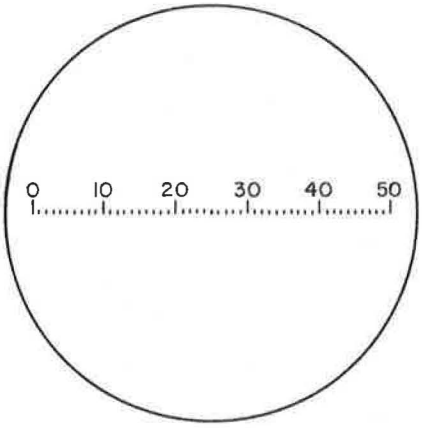

Figure 5. Graduated eyepiece of microscope.

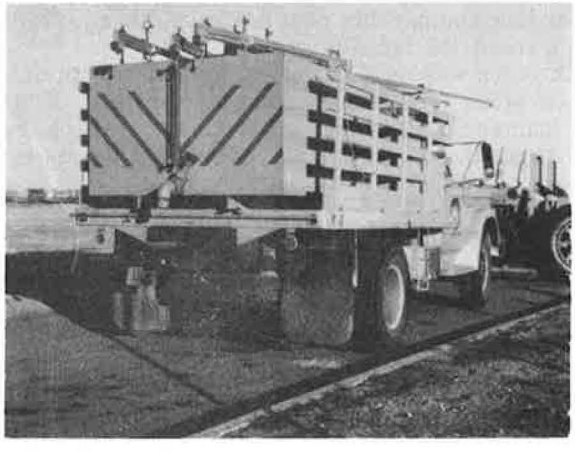

Figure 6. Completed truck carrying Benkelman beams on location.

placement of the Basin beam when taking data is shown in Figure 2 and a photograph is shown in Figure 3. The probe of the dial gage which is in the center of the beam is placed just to either side of the crack in the pavement. The radius of curvature is computed using the geometrical relationship for three points on a circle (5).

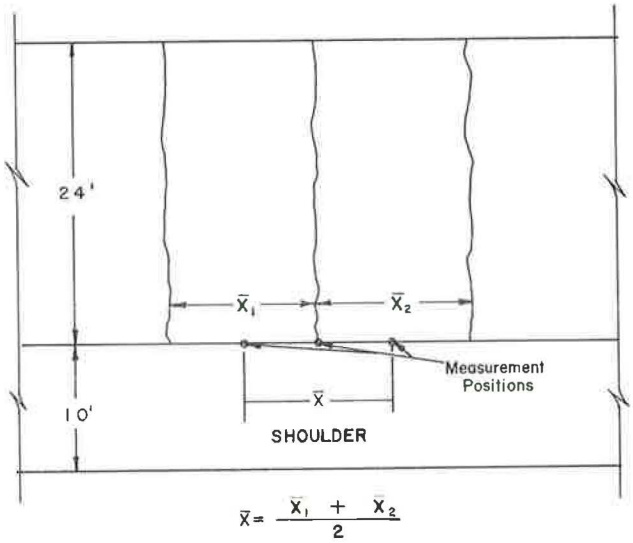

Figure 7. Selection of crack spacing.

Temperature Equipment. —The special temperature equipment used on this project was also designed by the Research Section. It consisted of a small portable 8-in. concrete slab in which two high-speed resistance thermometer bulbs were placed near the top and bottom. The leads from these bulbs were connected to a Minneapolis-Honeywell Electronik Temperature Recorder which recorded the top and bottom temperatures of the portable slab on a continuous strip chart. The development and technique for using this equipment has been covered in a previous report (5).

Microscope. —A specially fabricated microscope with a built-in scale in the eyepiece was used to measure the width of the cracks. By setting the microscope over the crack and focusing on it, the crack width could be read on the inscribed scale to the nearest 0.002 inch. Each time the microscope was used in a given location it was positioned in the same spot in order that comparable data might be taken. Figure 4 shows the microscope and Figure 5 shows the built-in scale.

Truck. —The truck which was used to deflect the pavements in this and continuing studies is a single-axle stake-type truck rated at three tons. It is equipped with a box of lead shot for dead load and also a large water tank so that the magnitude of the load can be varied. Figure 6 shows the truck with the Benkelman beams loaded in the mobile position.

Experimental Procedure

The procedures used at the AASHO Road Test were used as guidelines in developing the procedure for this experiment (3). New procedures were required to study the CRCP variables which are new to rigid pavement design.

Crack Spacing. —On each of the three sections, two small, two medium, and two large crack spacings were selected as points where deflection measurements were to be made. The crack spacings were chosen as is shown in Figure 7 where $\bar{X}_1$ was approximately the same as $\bar{X}_2$. This procedure was followed for the small, medium and large crack spacings. The small crack spacings were from one to four feet, medium from six to eight feet and large from 12 to 31 feet.

Axle Load. —The deflection truck was loaded such that the rear axle load was 18,000 pounds and the tire inflation pressure was 75 psi. The 18,000-lb axle load was adopted because it represents the maximum legal load limit on a single axle in Texas, and it is used as the basis for deriving equivalencies in the AASHO design methods (6). The center of the dual tires on the right side of the truck was kept 20 inches, ±two inches,

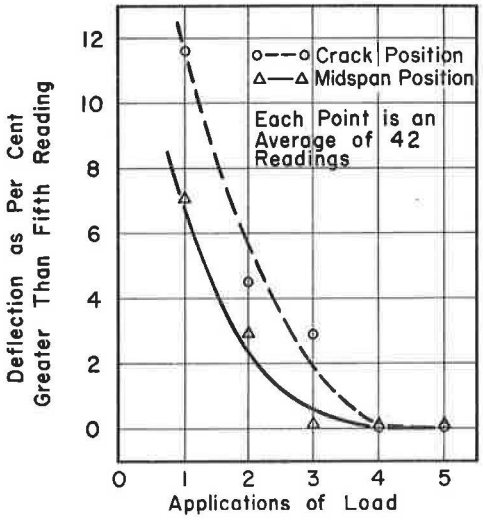

Figure 8. Applications of load vs deflection as percent greater than reading at fifth load application.

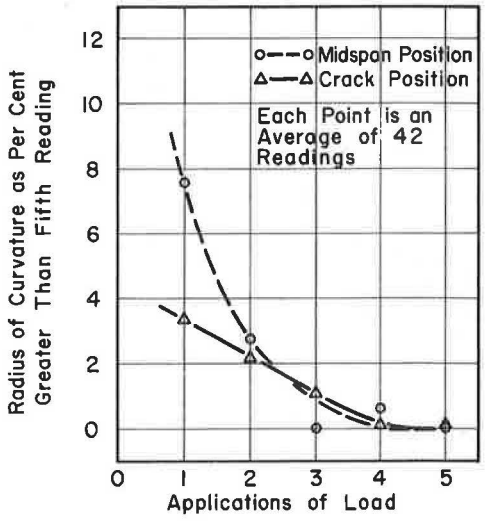

Figure 9. Applications of load vs radius of curvature as percent greater than reading at fifth load application.

from the edge of the pavement. When deflections were measured at the crack, the tire contact area of the outside tire on the right duals was centered over the crack.

Ironing.—Measurements at the AASHO Road Test and experience in Texas have shown that a concrete pavement slab is not always in complete contact with the subbase or subgrade nor is it a uniform distance from it. This phenomenon is conjectured to be due to point-to-point variations in temperature longitudinally down the slab.

A special study was initiated to determine the optimum procedure for measuring deflections with a desired degree of reproduciability. The tests were run on successive days under similar climatic conditions to avoid the variables of the environment, but the test sections were selected so as to encompass a range of support conditions. The measurement procedure consisted of placing the single-axle load in position, zeroing the dial gages, removing the load from the zone of influence and recording the Benkelman and Basin beam readings. This procedure was repeated five times at both the crack and midspan positions every 200 feet, on each of three 2500-ft test sections.

Figure 8 shows the effect of the "ironing" procedure on deflection. Each point on the graph represents the average of 42 measurements. The graph shows that the deflection at both the crack and midspan positions is relatively constant after three passes of the load. Thus at each point at which deflections were measured, the deflection truck was first passed over the area three times in order to attain the desired reproducibility of results.

Figure 9 shows that the ironing procedure had only a slight effect on radius of curvature. The ironing procedure is followed because both deflection and radius of curvature measurements are obtained at the same time.

Measuring Deflections.—The deflections were measured at three points, a, b, and c, as shown in Figure 7. The positioning of the beams for these measurements is shown in Figure 3. All measurements were made in the outside lane with the Benkelman beam probes on the pavement, one inch from the edge and at a 30-deg angle.

After beam placements, the pavement was "ironed out" by making three passes across the test area with the deflection truck. Immediately after ironing, the load was centered on the test crack and all dial gages zeroed, the load removed, and all dial gages read. Deflection readings were taken on the six selected crack spacings for a period of 24 hours on each of the three test sections. Eleven readings were taken with each beam on each crack spacing on each of the three test sections.

Eleven sets of readings on six crack spacings for three test sections produced 198 sets of data. With each set of deflection readings a crack width measurement was made using a microscope with a graduated eyepiece. A continuous recording of the temperature at the top and bottom of the pavement was made throughout each of the three overnight studies.

Deflection with Variable Load.—Deflections were measured in the outside lane by using one Benkelman beam as shown in Figure 2. The test was started with an axle load in excess of 20,000 pounds. The load was varied by reducing the level of the water being used as load. Each time the load was changed, the deflection was measured.

Basin Measurements.—Basin data were taken using the Basin beam. The pavement was ironed out by three passes of the deflection truck after which the Basin beam was placed over the crack and the center of the axle load was lined up vertically with the dial gage. The gage was zeroed, load removed from zone of influence and the dial reading was taken. This procedure was also used at the midspan position. Data were taken over a period of 24 hours so that effects of temperature would be involved. The same special temperature equipment was used here to obtain pavement temperatures as was used when measuring deflections.

PRESENTATION OF RESULTS

The variables of pavement design are studied herein in terms of deflection and radius of curvature. The variables are broken down into two groups—Road Test and CRCP. Road Test refers to variables which were considered on jointed pavements at the AASHO Road Test and CRCP refers to the variables unique to continuously-reinforced concrete pavement.

Deflection

In this section the effect of various parameters such as temperature, load, crack width, and crack spacing on deflection as measured with the Benkelman beam are discussed. First the factors investigated at the Road Test for jointed pavements are presented followed by consideration of factors applicable only to CRCP.

All relationships presented herein are for deflection at the crack position. Deflections at the crack are slightly greater than at midspan, thus for design purposes the crack deflections are analyzed. This difference in deflection is attributed to the presence of the crack.

Road Test Variables.—The studies of load and temperature on CRCP produced results which are analagous to the results of studies at the AASHO Road Test on jointed pavement.

Temperature Differential.—Slab temperature differential is truly a variable as shown by the trend in the data in Figures 10 through 12. The computed linear relationships for each set of data and the coefficients of determination are shown on the respective graphs. These graphs are for each of the test sections and are typical of the relationships fround for the other cracks. Note the inverse relationship between the two variables as was found at the Road Test. Figure 13 shows all three regression lines on one graph. The lines all have approximately the same slope, thus showing the constant relationship between temperature differential and deflection. The vertical position on the graph is indicative of the type of foundation each test pavement had.

Load.—The data shown in Figure 14 show the linear relationship between load and deflection and justify the load term in the model equation presented later herein. Westergaard and others found from their theoretical analyses that the deflection was a direct function of the load (7, 8, 9). Rigid pavement research at the AASHO Road Test also indicated that pavement deflection is a direct function of the load placed upon it (3, 10). Thus the results of this experiment substantiate both theory and other research.

CRCP Variables.—Some of the presently known variables of rigid pavement design which are unique to CRCP are crack width and crack spacing.

Crack Width.—The cracks in concrete due to lineal volume changes vary in width as temperature changes. The mid-depth temperature of the pavement computed from the average of the top and bottom temperatures of the pavement correlates well with the

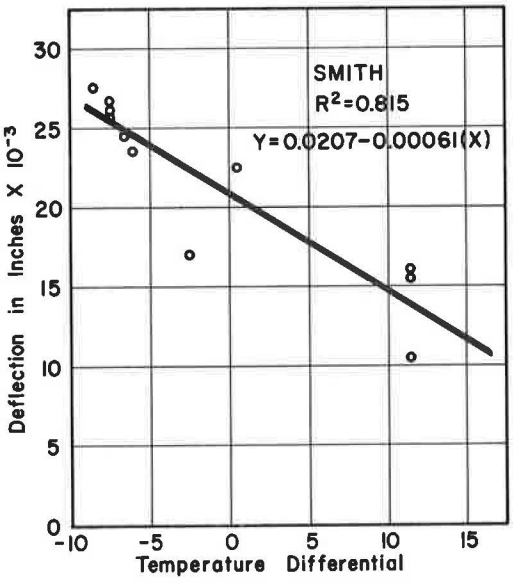

Figure 10. Deflection vs temperature differential—Smith.

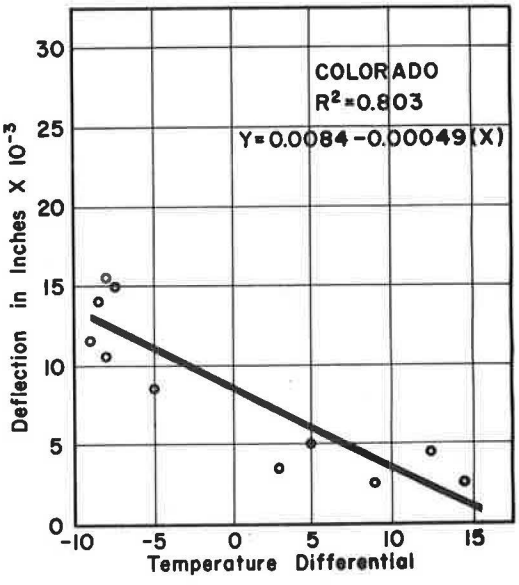

Figure 11. Deflection vs temperature differential—Colorado.

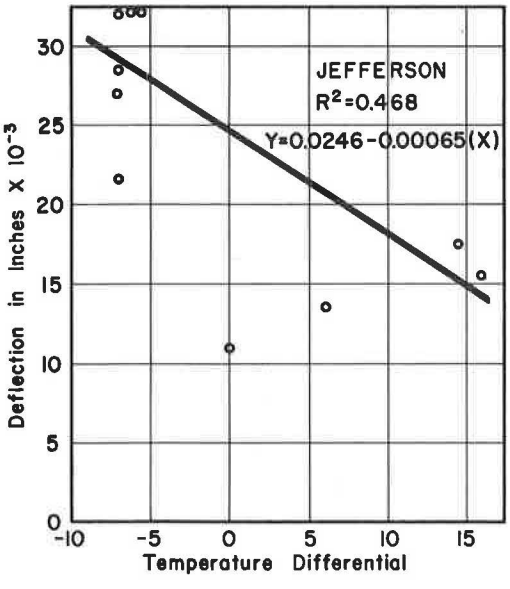

Figure 12. Deflection vs temperature differential—Jefferson.

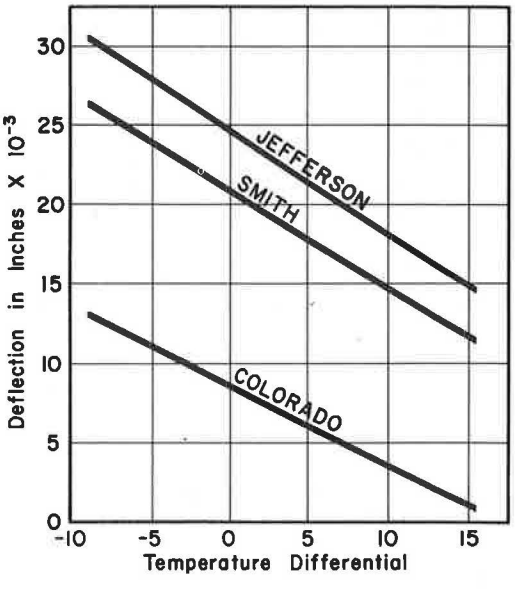

Figure 13. Comparison of regression lines (deflection vs temperature differential) for three projects.

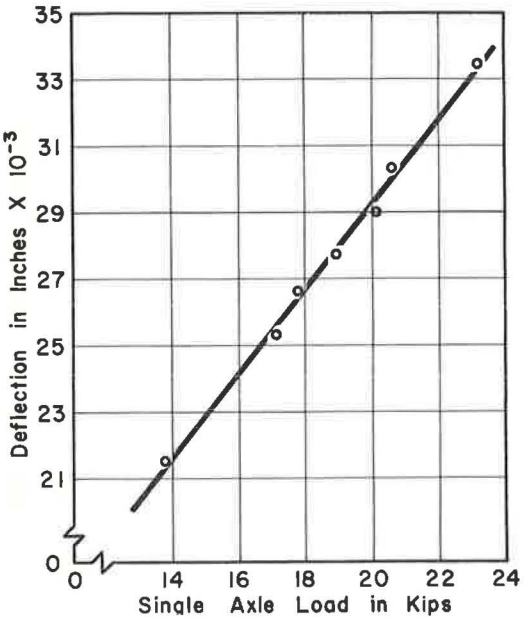

Figure 14. Deflection vs single-axle load.

crack width, thus indicating that the crack width is a function of temperature (11, 12). Figures 15 through 17, which are for like crack spacings, show how the mid-depth temperature affected the crack width on each of the three test sections. These relationships for each test section are typical of relationships found at other cracks. These data corroborate other work in that the crack width increases as the temperature decreases (11, 12, 13). The Smith and Colorado tests involved crack widths of 10 to 35 thousandths of an inch, whereas the Jefferson test section had cracks ranging up to only 10 thousandths of an inch in width. Figure 18 shows the regression lines for mid-depth temperature and crack width for the three test sections in order that a relative comparison can be made. Crack width and mid-depth temperature experienced the same relationship on the Smith and Colorado tests, but the Jefferson test showed the crack width was only slightly affected by temperature.

The crack width might be thought of as a measure of load transfer since the load is transferred by aggregate interlock, and the degree of aggregate interlock is dependent upon the crack width. As a crack closes, the load transfer increases, and the pavement deflects less because of the increased rigidity or degree of slab continuity. Figures 19 through 21 are typical portrayals of how the deflection increases with increases in crack width on each of the projects. Figure 22 gives a relative comparison of the regression lines for equal crack spacings for each of the projects. The same trend is present in all three test sections, but a variation in crack width has a much more pronounced effect in Jefferson County. Data taken from CRCP test sections located throughout the state shows that this relationship between crack width and deflection does exist. Crack width is a function of percent longitudinal steel. Deflection has been found to be a function of percent steel which in turn is a measure of the crack width (14).

As discussed earlier, the mid-depth temperature of the pavement is a relative indicator of crack width; therefore, it may be used as an indirect measure of crack width. Figure 18 shows that as the mid-depth temperature increases the crack width decreases. This same phenomenon is true for deflection. Figures 23 through 25 show the relationship between mid-depth temperature and deflection. Figure 26 shows all three regression lines and shows that as mid-depth temperature increases the deflection decreases in all cases.

Crack Spacing.—The crack spacing on a continuously-reinforced concrete pavement varies at random unless a preformed crack spacing has been provided for in the design and construction. Its relationship to deflection is shown in Figure 27.

Radius of Curvature

Radius of curvature is inversely proportional to the stress in concrete pavement, and studies have shown that it may be used as a relative measure of stress (5). In all subsequent analysis the reader's attention is drawn to the fact that the greater the radius of curvature the smaller the stress. Radius of curvature measurements were not made at the Road Test as such, but pavement stresses due to wheel load were studied in the form of strains which were obtained by use of electrical strain gages.

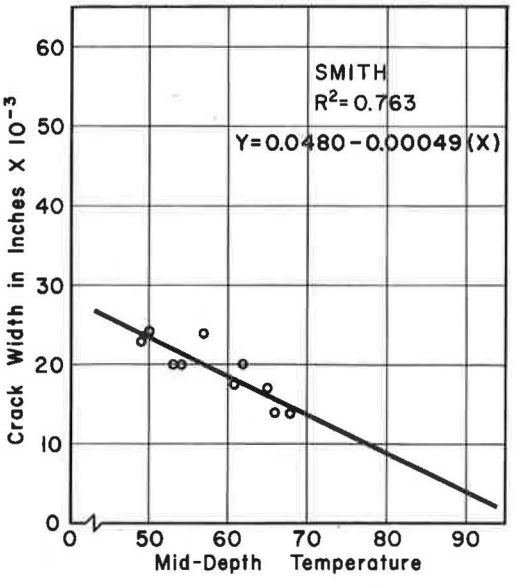

Figure 15. Crack width vs mid-depth slab temperature—Smith.

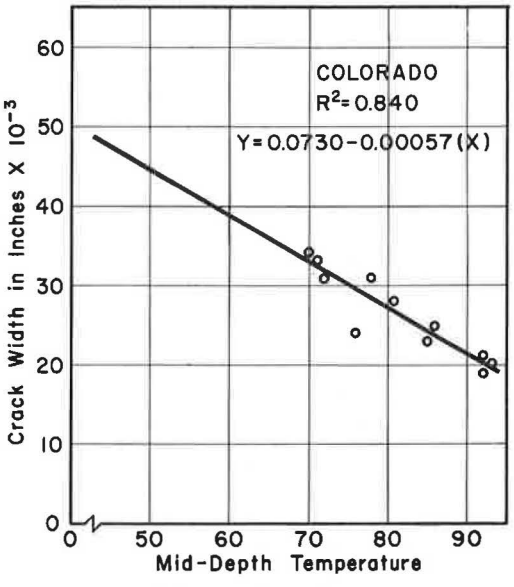

Figure 16. Crack width vs mid-depth slab temperature—Colorado.

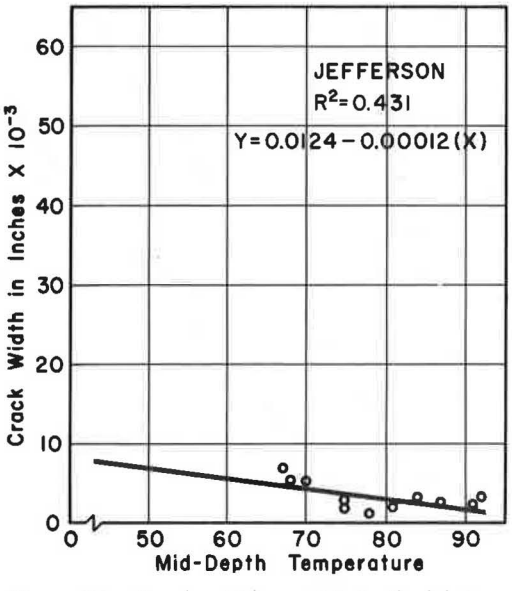

Figure 17. Crack width vs mid-depth slab temperature—Jefferson.

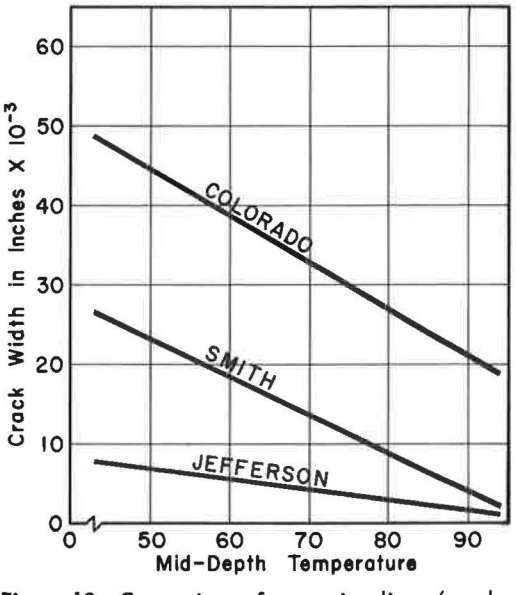

Figure 18. Comparison of regression lines (crack width vs mid-depth temperature) for three projects.

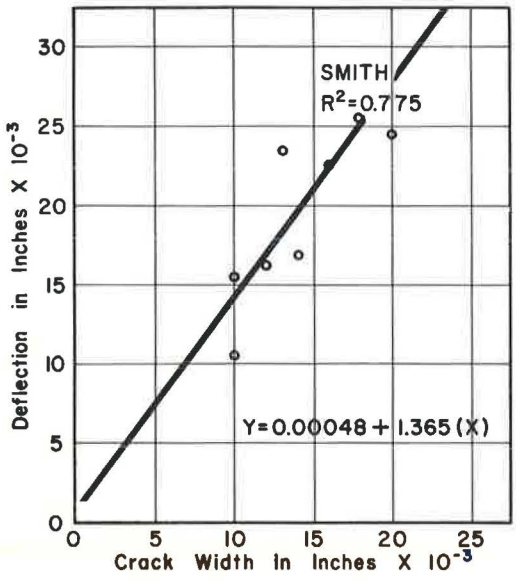

Figure 19. Deflection vs crack width—Smith.

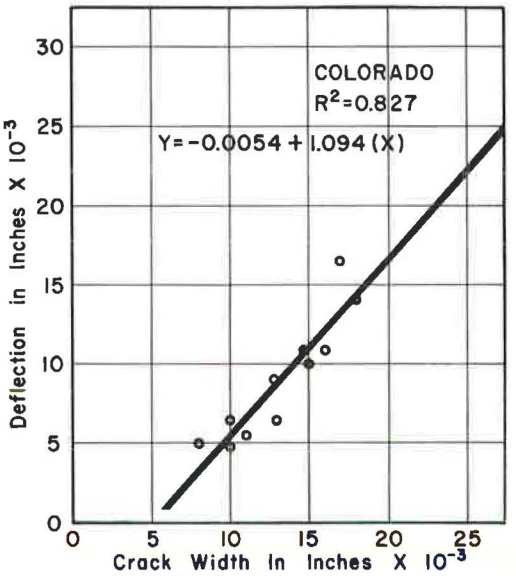

Figure 20. Deflection vs crack width—Colorado.

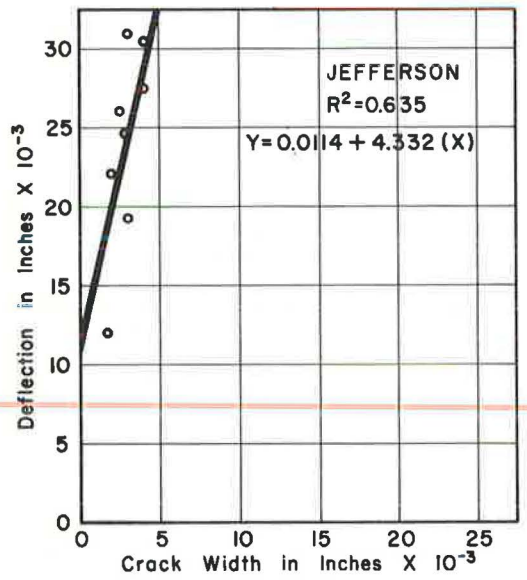

Figure 21. Deflection vs crack width—Jefferson.

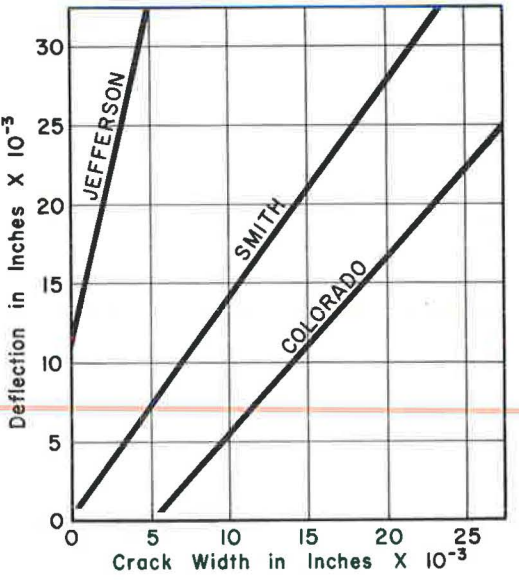

Figure 22. Comparison of regression lines (deflection vs crack width) for three projects.

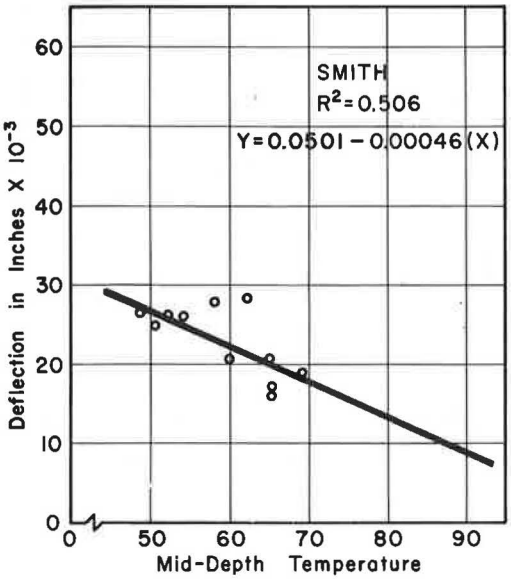

Figure 23. Deflection in terms of mid-depth temperature—Smith.

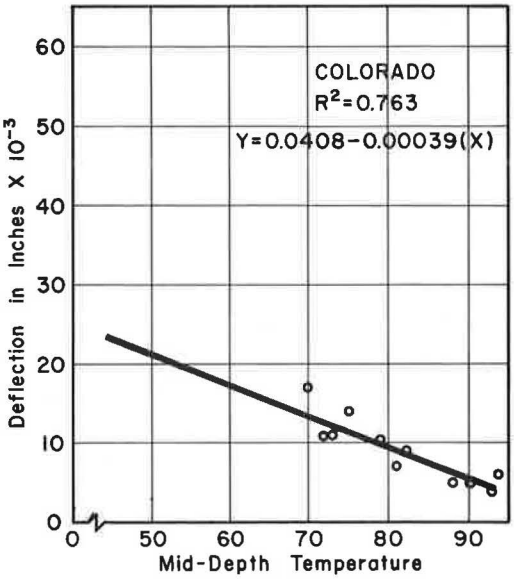

Figure 24. Deflection in terms of mid-depth temperature—Colorado.

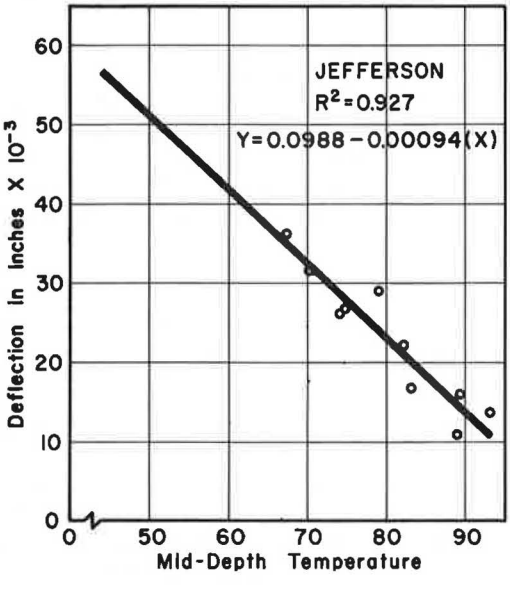

Figure 25. Deflection in terms of mid-depth temperature—Jefferson.

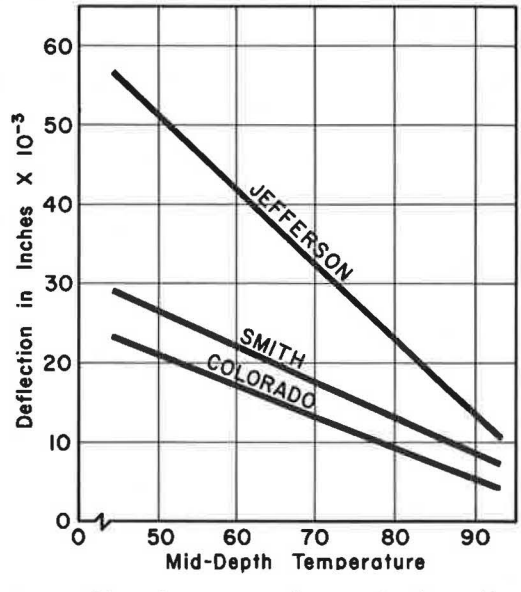

Figure 26. Comparison of regression lines (deflection vs mid-depth temperature) for three projects.

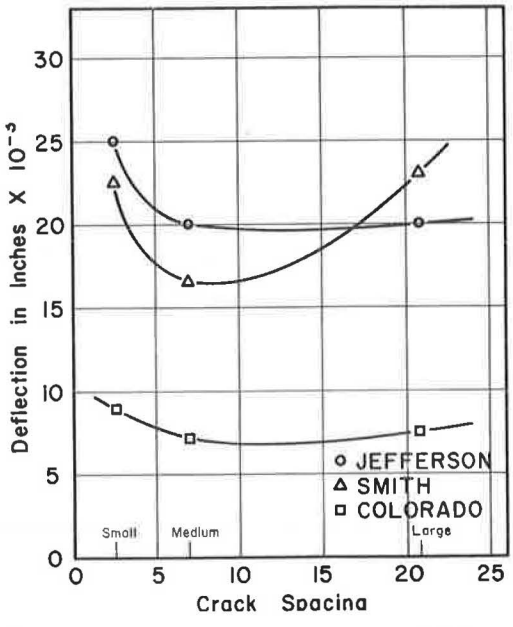

Figure 27. Deflection vs crack spacing.

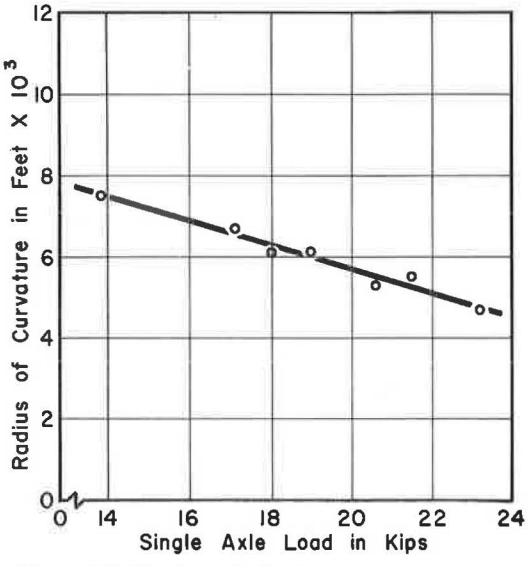

Figure 28. Single-axle load vs radius of curvature.

Road Test Variables. —Studies of single-axle load vs radius of curvature in this experiment indicate an inverse linear relationship between the two. Figure 28 shows the linear relationship between load and radius of curvature. This same linear relationship was found at the Road Test in terms of load and strain. Radius of curvature is an inverse function of stress, which is a direct function of strain, thus the analogy in results does exist.

This investigation showed that radius of curvature or stress is not related to slab temperature differential. This is definitely true for the midspan measurement position. The two groups of data points in Figure 29, representing two typical projects, show that there is no relationship between radius of curvature and temperature differential. This contradicts findings made at the Road Test where it was found that the slab temperature differential had a slight effect on the pavement stress. Their studies indicate that the temperature differential influenced slab stress $\frac{1}{4}$ to $\frac{1}{2}$ as much as it did deflection. At the present time no rational explanation can be given for this apparent discrepancy in findings other than that the sensitivity of the Basin beam is less than electrical strain gages.

Figure 30, which shows the data for the crack position, indicates that the temperature differential might be related to radius of curvature. This illusory relationship of temperature differential and radius of curvature is covered in more detail in the next section.

CRCP Variables. —As discussed previously, crack width is a function of temperature because concrete volume changes are functions of temperature. The mid-depth temperature of the pavement might then be thought of as an indicator of crack width. Figure 31 shows the relationship of the radius of curvature to the mid-depth temperature (crack width) at midspan on two different test sections. Again there is no relationship between temperature and radius of curvature as was the case when comparing temperature differential to radius of curvature. Figure 32 shows a relationship of temperature to radius of curvature at the crack position for two test sections and indicates that temperature has an effect on the radius of curvature, but it must be kept in mind that the continuously-reinforced pavement is cracked and that increases or decreases in temperature have a direct effect on the width of the cracks.

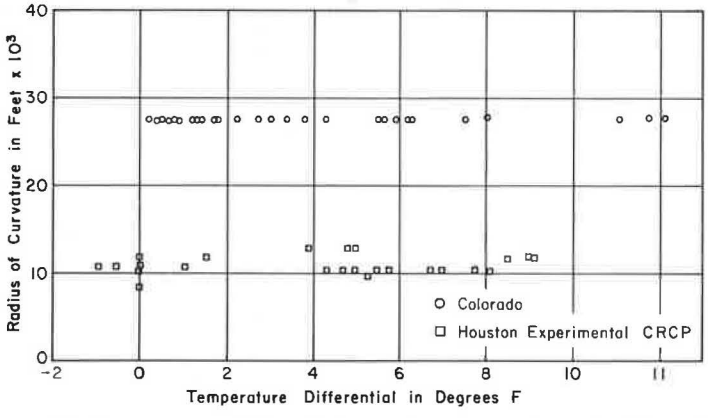

Figure 29. Temperature differential vs radius of curvature at midspan position.

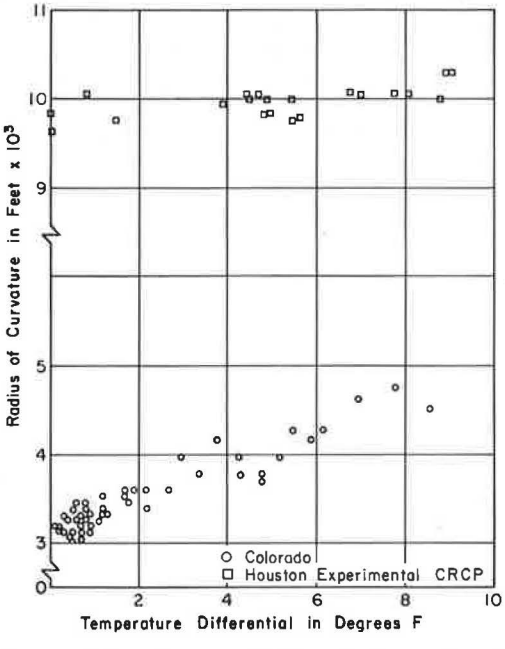

Figure 30. Temperature differential vs radius of curvature at crack position.

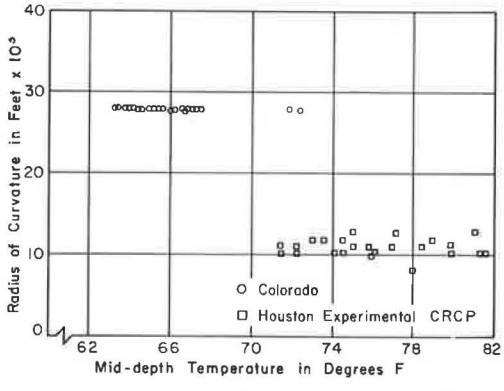

Figure 31. Mid-depth temperature vs radius of curvature at midspan position.

Both temperature differential and mid-depth temperature studies have shown that temperature increases cause an increase in radius of curvature. This phenomenon can be attributed to crack width. If the crack is closed by temperature increase, the pavement begins to react as if the crack were not present. Thus, the radius of curvature does not change with temperature at midspan and the changes in radius of curvature at the crack were caused by changes in crack width rather than temperature.

The crack spacings in this experiment were classified as small, medium, or large as stated earlier. To evaluate crack spacing as a variable, an average deflection condition is selected for a crack width. A comparison of these deflections for the various cracks reveals the influence of crack spacing. Figure 27 shows how the crack spacing affected the deflection in this experiment. The relative vertical position of the curves will vary as the crack width changes. In general, the deflection decreases as the crack spacing increases until a range of five to ten feet is reached. Beyond this range the deflection increases as the crack spacing increases. These data indicate that an optimum crack spacing is in the range of five to ten feet. These observations

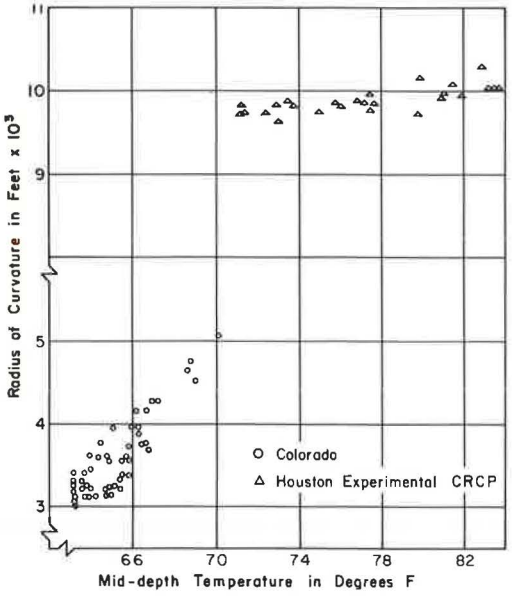

Figure 32. Mid-depth temperature vs radius of curvature at crack position.

tend to verify work reported previously in connection with preformed crack spacings where it was found that the optimum crack spacing was approximately five feet (14).

Development of Equation

Much work was done at the AASHO Road Test to develop equations to predict the deflection of jointed concrete pavements. For continuously-reinforced pavements only one equation will be developed here since the deflection at the crack and mid-span positions are approximately the same with the crack deflection being minutely larger.

Model Selection.—The model selected for the deflection of continuously-reinforced concrete pavement is a modification of the AASHO Road Test model. By adding the CRCP variables, crack width and crack spacing, to the AASHO equation a model would be obtained that was based on considerable research and would also allow direct comparisons. The model selected for continuous pavement was of the form:

$$d = \frac{A_0 L \Delta X^{A_2} \overline{X}^{A_3}}{10^{A_1 T} D^{1.178}}$$

where

d = deflection in inches;
L = single-axle load in kips;
ΔX = surface crack width in inches;
$\overline{X}$ = crack spacing in feet;
T = temperature differential in degrees Fahrenheit between $^3/_4$ inch and 1 $^1/_8$ inches from the top and bottom of the slab, respectively;
D = slab thickness in inches; and
A_0, A_1, A_2, and A_3 = constants computed from the data.

The depth term to the 1.178 power is a result of the rigid pavement research at the AASHO Road Test (3). This power was included in the equation because this experiment did not include a study of pavement thickness. Axle load was studied in terms of deflection, but was not included as a full factorial variable on the test sections. Therefore, in all subsequent regression work an axle load of 18,000 pounds and a pavement thickness of eight inches were inserted in the Road Test equation. These numbers were moved to the left side of the equation and combined with deflection to form the dependent variable. The constants derived from this regression analysis then reflect load and pavement thickness and are directly comparable to the Road Test Equation.

Regression Analysis.—A multiple regression analysis was made on each of the three sets of data from the Colorado, Jefferson and Smith test sections. Through the regression analysis the regression analysis constants in the model were computed. The constants are given in Table 2. The constant A_0 is relative to the pavement support. The Colorado test section had a stabilized subbase, whereas the other two sections did not. Therefore, A_0 for Colorado was less than that for Jefferson or Smith.

The constant A_1 compares very well with the constant on temperature differential in the AASHO equation. In the AASHO equation A_1 is equal to 0.0075 for a single-axle

TABLE 2

CORRELATION CONSTANTS FOR CRCP MODEL OBTAINED FROM MULTIPLE REGRESSION ANALYSIS

MODEL	CONSTANT	COLORADO	JEFFERSON	SMITH
ORIGINAL	A_0	0.028502	0.035803	0.048189
	A_1	0.016679	0.007481	0.010489
	A_2	0.402499	0.119260	0.352490
	A_3	-0.146090	-0.121316	0.028986
MODIFIED	A_0	0.003993	0.016675	0.011115
	A_1	0.015571	0.003881	0.010899
	A_2	7.637913	9.908250	5.207664
	A_3	-0.161818	-0.100224	-0.029021

TABLE 3

STATISTICAL ANALYSIS OF TEST SECTIONS

TEST SECTION	STANDARD ERROR OF THE ESTIMATE	COEFFICIENT OF DETERMINATION	COEFFICIENT OF CORRELATION
Colorado	$\pm$0.00205	0.611	0.782
Smith	$\pm$0.00267	0.641	0.801
Jefferson	$\pm$0.00294	0.343	0.586

load and an edge condition, and the magnitude varies from 0.0075 to 0.015 for various conditions of reinforcement and load position, i.e., edge or joint. The constants obtained for the CRCP model are within this range, with the Jefferson County value being identical to the Road Test edge condition. Therefore, it may be deducted that a continuous pavement responds to slab temperature differentials in the same manner as a jointed pavement.

The constant A_2 reflects the crack width. For the Jefferson test A_2 is small compared to the other two, as was the case of the actual crack widths.

The constant A_3 turned out negative on the Colorado and Jefferson tests. The model indicates a direct relationship between crack spacing and deflection which is not exactly true for the test sections. Figure 27 shows that as crack spacing increases on the Jefferson and Colorado tests the deflection decreases for the bulk of the data, thus explaining the negative A_3.

Modification of Model.—The first selected model was so arranged that if the crack width was zero, the deflection was also zero which is an erroneous boundary condition. Also, the relationship between crack width and deflection was found to be linear; thus the model was slightly modified to correct for these discrepancies. In the modified model ΔX^{A_2} term was changed to $10^{A_2 \Delta X}$ since this function approaches a linear expression and it also satisfies the boundary condition.

Before the multiple regression analyses were rerun on the modified model some of the data points were deleted. With some of the obvious erroneous data (due to bad readings) removed, the multiple regression was rerun, the results of which also appear in Table 2. The only constant to change a large amount was A_2, and again the differences were relative to the magnitudes of the crack width. Also A_3 turned out to be negative for the Smith test as is the case for the other two sections. For the modified model the standard error of the estimate and the coefficients of determination and correlation are presented in Table 3.

DISCUSSION OF RESULTS

Three equations were found for deflection, one for each of the three test sections. The primary difference between the three test sections was in the foundation material or support, i.e., the subbase and subgrade. With soil-supporting characteristics being the only difference in the three pavements, it thus becomes the means whereby the results from the three overnight tests can be combined into one equation.

Soil Support

To tie the three overnight deflection studies together, the term "soil support" was formulated and defined as

$$SS = \left(\frac{U}{T_{sg}}\right)^{1/4}$$

where

SS = soil support;
U = unconfined compressive strength of subbase materials in psi at an age of seven days; and
T_{sg} = Texas triaxial classification of subgrade material.

This form was selected because studies being conducted parallel to this study in connection with subbase support show this model gives the best correlation. Furthermore, logical reasoning would lead to the hypothesis that as the unconfined compressive strength of the subbase increases, the degree of support increases. As the triaxial classification of a material increases, the material is actually weaker and of a poorer quality for use as a highway building material; thus, as the triaxial classification increases, the degree of support decreases (4).

The supporting quality of the subbase and the subgrade bears a direct relationship with deflection as is clearly shown in Figure 33.

The support term was calculated on the basis of in-place values—compressive strength and triaxial class—and the deflection is the average of all reading on the test section. The effect of the variation of support conditions for the regression analysis of each section is reflected in the A_0 term. As shown by the dashed line in Figure 33 both of these trend lines indicate the feasibility of combining the data from the three test sections into one equation.

Subgrade classifications of good, fair, and poor alone cannot be used to explain pavement deflections. Emphasis must be placed on the supporting material immediately beneath the pavement. In cases where the subbase has been stabilized by any one of the four methods presently used by the Texas Highway Department, the deflections do not compare to deflections of a pavement with a nonstabilized subbase with the same class of subgrade. Thus it becomes important in deflection studies that stabilized

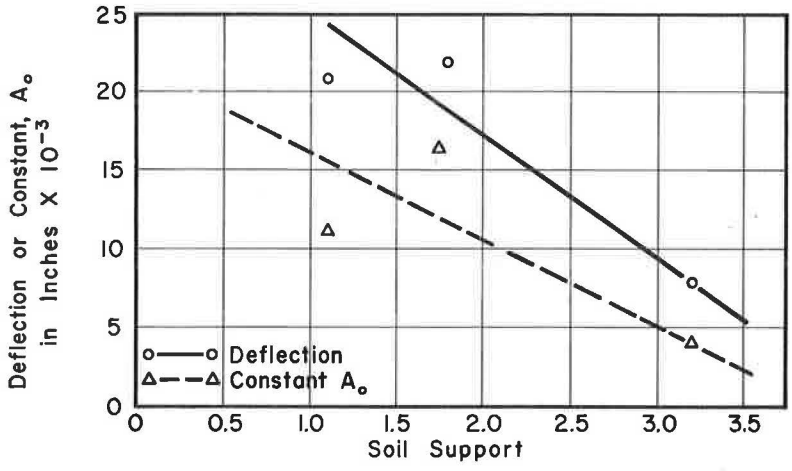

Figure 33. Comparison of deflection and the constant, A_0, as functions of soil support.

TABLE 4

RESULTS OF FINAL REGRESSION ANALYSIS

CONSTANT	COMPUTED VALUE
A_0	0.010617
A_1	0.014724
A_2	4.899716
A_3	-0.099375
A_4	0.850280
STANDARD ERROR OF THE ESTIMATE	±0.0026
COEFFICIENT OF DETERMINATION	0.901
COEFFICIENT OF CORRELATION	0.949

subbases be accounted for. In many cases subgrades are treated with lime either as a construction aid or as a desired improvement of subgrade immediately beneath subbase. When subgrades are treated with lime a second subbase is actually created.

Because deflections are inversely proportional to soil support, the new term "soil support" was placed in the denominator of the model. After the addition of the soil support variable, the model for the deflection at the crack position is

$$d_c = \frac{A_0 L \, 10^{A_2 \Delta X} \overline{X}^{A_3}}{10^{A_1 T} \, D^{1.178} \, SS^{A_4}}$$

where A_4 is a constant computed by data analysis and all the other terms are as previously defined.

Final Analysis

A multiple regression analysis was made using the above equation and the combined data from the three tests. The small crack width on the Jefferson test caused the constant, A_2, to be erroneous. The Jefferson and Smith tests were very much the same from the standpoint of deflection and support. Thus, the Jefferson data were dropped from the final analysis because of the very small crack width.

A multiple regression analysis was made on the remaining data from the Smith and Colorado tests. The results of this analysis are presented in Table 4. Thus the final equation for the deflection at the crack position is based on only two of the overnight deflection studies conducted.

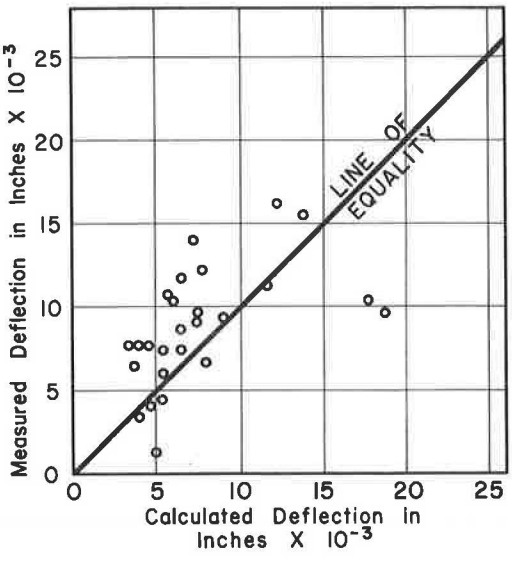

Figure 34. Measured deflection vs deflection calculated by final equation.

TABLE 5

RELATIVE IMPORTANCE OF THE DEFLECTION VARIABLES

Changes in Conditions	Given Conditions *	Load (L)	Thickness (D)	Soil Support (SS)	Crack Width (ΔX)	Temperature Differential (T)	Crack Spacing ($\bar{X}$)	Calculated Deflection	Per Cent Change
	18	8	1.5	0.015	3	5	0.0116	—
SS			3.0				0.0065	-44.0
ΔX				0.030			0.0149	28.4
T					6		0.0115	-0.8
$\bar{X}$						10	0.0115	-0.8

DEFLECTION VARIABLES

* The given conditions prevail other than where specified.

The final equation for the deflection of a continuously-reinforced concrete pavement is

$$d = \frac{0.0106\, L\, 10^{4.8997\Delta X}}{10^{0.0147\, T}\, D^{1.178}\, SS^{0.8503}\, \bar{X}^{0.0994}}$$

The error in this equation is comparable to that in each of the three equations for the three individual tests. The standard error of the estimate for the final equation was 0.00263 which is very close to the values shown in Table 3 for the three tests. The

coefficients of determination and correlation, presented in Table 4, indicate that the equation is valid.

To test the validity of the equation, data were taken from a statewide deflection run and deflections were computed for each test section. The calculated deflections were then plotted against the measured deflections as shown in Figure 34. The points cluster closely around the line of equality, thus showing the equation is valid.

Relative Importance of Variables

An empirical relationship depicting deflection in terms of rigid pavement variables for CRCP has been presented. The relative importance of these variables in terms of deflection is given in Table 5. This table contains a set of given conditions for which the deflection is computed using the final equation developed herein. In the table each variable, besides load and slab thickness which are the two of most importance, respectively, is doubled independently of the remaining variables to show the effect of its change on deflection. The variables are presented in order of decreasing importance. Thus, the order of the relative importance of the variables is load, thickness, soil support, crack width, temperature differential, and crack spacing.

SUMMARY

This Phase I study on the performance of continuously-reinforced concrete pavement warrants the following conclusions:

1. The deflection of continuously-reinforced concrete pavement is a function of the load applied, crack width, crack spacing, temperature, pavement thickness and the supporting characteristics of the subbase and subgrade.
2. An empirical equation has been derived that enables a designer to approximate deflections in terms of the above enumerated parameters. A designer may then use the equation to prescribe a set of conditions that will insure the pavement deflection will be less than a desirable maximum.
3. The order of the relative importance of the variables is load, slab thickness, soil support, crack width, temperature differential, and crack spacing.
4. When measuring deflections the pavement should be "ironed out" three times before taking data.
5. Concrete pavements deflect in predictable patterns that can be measured with the Benkelman beam and Basin beam if proper precautions are taken.
6. From a deflection standpoint an optimum average crack spacing appears to be in a range of five to ten feet.
7. Deflection is a direct linear function of load and radius of curvature is an inverse linear function.
8. Radius of curvature calculations need not be corrected for slab temperature differential.

Needed Research

The equation presented herein is intended to represent the best utilization of the presently available knowledge and data concerning the deflection of continuously-reinforced concrete pavements. The deflection equations are empirical and must be used as such.

An attempt has been made herein to evaluate the support provided by the subbase and subgrade, but studies should continue on this and other variables such as weather and other environmental conditions. With the advanced data processing methods available today, vast amounts of data can be handled rapidly, thus facilitating the research minded who are interested in pushing back the frontier of pavement design.

ACKNOWLEDGMENTS

This research was conducted under the supervision of M. D. Shelby, Research Engineer, and the general supervision of T. S. Huff, Chief Engineer of Highway Design.

The authors wish to acknowledge and extend their thanks to C. A. Weise, Senior Resident Engineer, District 13; Warren N. Dudley, Senior Laboratory Engineer, District 20; and George Wall, Assistant District Engineer, District 10, whose able assistance and cooperation made the success of this investigation possible.

The able assistance of various members of the Research Section who were instrumental in the success of this study is gratefully acknowledged.

REFERENCES

1. Status Report on Continuously Reinforced Concrete Pavement Built or Under Contract in the U. S. Concrete Reinforcing Steel Institute, Oct. 30, 1963.
2. Highway Research Board. The AASHO Road Test: History and Description of Project. HRB Special Report 61A, 56 pp., 1961.
3. Highway Research Board. The AASHO Road Test: Report 5—Pavement Research. HRB Special Report 61E, 352 pp., 1962.
4. Texas Highway Department. Manual of Testing Procedures, Vol. 1.
5. McCullough, B. F. Development of Equipment and Techniques for a Statewide Rigid Pavement Deflection Study. Research Report No. 46-1, Texas Highway Dept., Jan. 1965.
6. AASHO Interim Guide for the Design of Rigid Pavement Structures. AASHO Committee on Design, April 1962.
7. Westergaard, H. M. Stresses in Concrete Pavements Computed by Theoretical Analysis. Public Roads, Vol. 7, No. 2, April 1926.
8. Pickett, Gerald, Raville, Milton E., Janes, William C., and McCormick, Frank J. Deflections, Moments and Reactive Pressures for Concrete Pavements. Kansas State College Bull. No. 65, Engineering Experiment Station, Oct. 15, 1951.
9. Spangler, M. G. Stresses in the Corner Region of Concrete Pavements. Iowa Engineering Experiment Station Bull. 157, 1942.
10. Hudson, W. R. Value of Single Load Response in Rigid Pavement Design. Paper presented at Texas Section ASCE, May 10, 1963.
11. McCullough, Benjamin F. The Early Service Life Characteristics of a Continuously Reinforced Concrete Pavement in Comal County, Texas. Research Report No. 62-4, Texas Highway Dept., 1962.
12. Shelby, M. D., and McCullough, B. F. Determining and Evaluating Stresses in an In-Service Continuously-Reinforced Concrete Pavement. Highway Research Record 5, pp. 1-49, 1963.
13. Nixdorf, Richard H., and Lepper, Henry A., Jr. Maryland Investigation of Continuously Reinforced Concrete Pavement, 1959-64 Strain Observations. Univ. of Maryland, College Park, July 1964.
14. McCullough, B. F. Evaluation of Single Axle Load Response on an Experimental Continuously Reinforced Concrete Pavement. Research Report No. 46-3, Texas Highway Dept., April 1965.

Application of AASHO Road Test Findings to the Design of Flexible Pavement Structures in South Carolina

T. Y. CHU, Professor of Civil Engineering, and
W. K. HUMPHRIES, Assistant Professor of Civil Engineering, University of South Carolina; and
OREN S. FLETCHER, Research Engineer, South Carolina State Highway Department

Field and laboratory investigations conducted in South Carolina for the development of a tentative procedure for subgrade evaluation are described. The tentative procedure involves the use of undrained triaxial tests for evaluating the modulus of deformation of subgrade materials. From this modulus, the soil support value of a subgrade is determined, permitting the application of the AASHO Interim Guide general design procedure to the design of flexible pavement structures in South Carolina.

•AMONG VARIOUS design methods derived from the findings of the AASHO Road Test, a general design procedure was developed by the AASHO Operating Committee on Design and presented in the AASHO Interim Guide for the Design of Flexible Pavement Structures (1). This design procedure, however, does not include methods for subgrade evaluation. Due to the wide variance in the type of subgrade soils and the different environmental conditions encountered in various states, it is apparent that a subgrade evaluation method suitable for one state may not be applicable to other states. As indicated in the AASHO Interim Guide, each state is urged to develop a specific method for evaluating the soil support value of subgrade materials.

In South Carolina, a study for developing a subgrade evaluation method was initiated in 1962. After considering a number of test methods, the triaxial test was selected because of its versatility concerning test conditions and the capability of measuring the strength and stress-strain characteristics of subgrade materials. Field and laboratory investigations were then conducted for establishing a specific test procedure for determining the soil support value.

The general approach in conducting the field and laboratory investigations was as follows: Along existing highways having adequate traffic records, sites with pavement serviceability indexes of approximately 2 or 2.5 were selected for this study. A limited number of sites with higher serviceability indexes were also investigated for comparison purposes. On the basis of the actual thickness of pavement components, traffic history, and a selected regional factor, the soil support value for the subgrade material at each site was estimated from the AASHO Interim Guide design charts (similar to Figs. 4 and 5 except without the modulus of deformation scale). The estimated soil support values were then correlated with laboratory test data obtained from subgrade samples representing actual field conditions with respect to density and moisture content.

In the AASHO Interim Guide design charts, the AASHO Road Test embankment soil and crushed stone base material were assigned certain soil support values. In this study, triaxial tests were also conducted with samples of these materials to provide the necessary reference data. Results from the field and laboratory investigations were then analyzed to establish a tentative procedure for determining the soil support value

Paper sponsored by Committee on Flexible Pavement Design and presented at the 45th Annual Meeting.

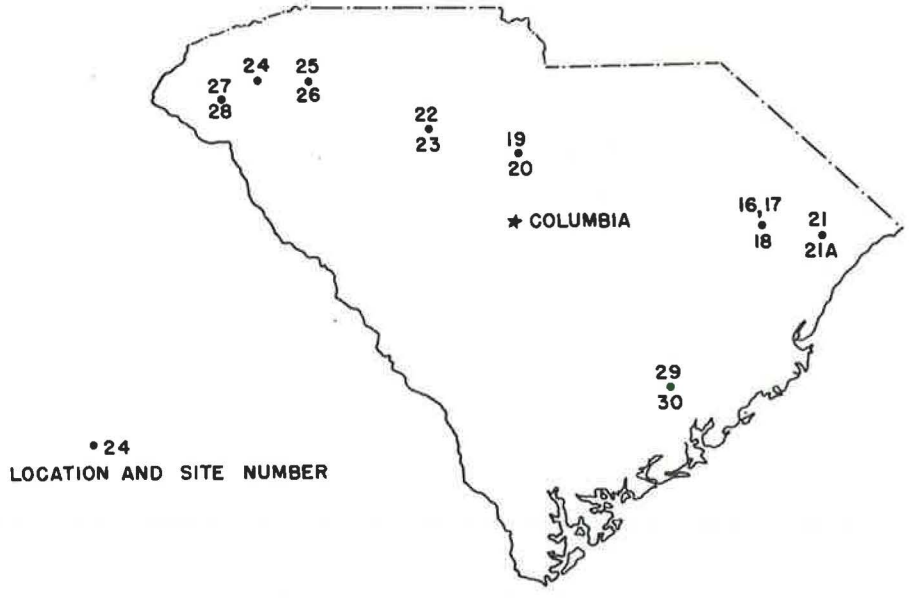

Figure 1. General location of sites investigated in South Carolina.

of various types of subgrade soils encountered in South Carolina. Using this procedure for subgrade evaluation, the AASHO Interim Guide general procedure can be applied for flexible pavement design in South Carolina.

FIELD INVESTIGATIONS

Sixteen sites along existing highways in different geographical regions in South Carolina were selected for this study. In determining the specific location of each site, an attempt was made to select primarily the sections of existing highways where the pavement had reached a relatively low serviceability index. Efforts were made, however, to avoid locations where the inferior performance of the pavement might have been caused by abnormal conditions of the pavement components such as shoving or disintegration of bituminous surfaces. The location and general information for each site are given in Figure 1 and Table 1.

The serviceability indexes given in Table 1 were determined by visual inspection of the pavement conditions. The serviceability index of 2.5 assigned to Site 24 (1960) and Sites 27 and 28 (1961) was, however, based on the assumption that poor pavement conditions were encountered at that time and, therefore, resurfacing was required. These three sites are located in the areas where poor pavement conditions were observed in 1960 and 1961 as discussed in the report by Rostron (3).

The sampling and in-place density tests at each site were made in the following manner: Along the outer wheelpath in the selected location, a section of the existing pavement approximately three feet square was cut out by a rotary concrete saw. After removing the pavement, the in-place density and moisture content of the subgrade were determined. Due to difficulties in obtaining undisturbed samples*, only bag samples of the subgrade were taken from the test area. Samples of the pavement components were also taken to assist in the evaluation of the pavement structure. The density and moisture content data obtained from the field tests are included in Table 3. In areas

*For best representation of the subgrades under existing pavements, the use of undisturbed samples is preferable. It is extremely difficult, however, to obtain samples without appreciable disturbance when high densities of the subgrade materials are encountered. The problem of undisturbed sampling would be most critical in the case of the cohesionless soils found in many locations covered in this study.

TABLE 1

INFORMATION ON VARIOUS SITES SELECTED FOR PAVEMENT INVESTIGATIONS

Site	General Description	Pavement Condition	Serviceability Index
16	Gently rolling topography. Westbound lane in cut approx. 2 ft in depth. High groundwater level (approx. 2 ft below pavement surface in June 1964).	Severe alligator cracking, very rough riding surface.	2
17	Gently rolling topography. Roadway on 5-ft fill.	Limited cracking, smooth riding surface.	3.5
18	Gently rolling topography. Westbound lane in cut approx. 3 ft in depth.	Severe alligator cracking.	2.5
19	Rolling topography. Roadway on 3-ft fill.	Alligator cracking, ¼-in. average rut depth.	2.5
20	Rolling topography. Southbound lane in cut approx. 10 ft in depth.	Alligator cracking.	2.5
21	Flat area adjacent to a pond. High groundwater level (approx. 4 ft below pavement surface in Oct. 1964).	Many patched areas, ½-in. average rut depth.	2
21A	Same as above (groundwater level approx. 3 ft below pavement surface in Oct. 1964).	Many patched areas, ½-in. average rut depth (1-in. maximum rut depth).	2.5
22	Rolling topography. Westbound lane in cut approx. 30 ft in depth.	Alligator cracking, ¼-in. average rut depth.	2.5
23	Rolling topography. No appreciable cut or fill.	Alligator cracking, ¼-in. average rut depth.	2.5
24	Rolling topography. Eastbound lane in shallow cut (less than 5 ft).	According to previous investigations (3), poor pavement conditions were observed in 1960. The analysis period shown in Table 7 is from 1956 to 1960.	2.5 (1960) 3.5 (1964)
25	Rolling topography, SE-bound outer lane in cut approx. 15 ft in depth.	Severe alligator cracking and many patched areas before resurfacing in Sept. 1964. Benkelman beam tests were made after resurfacing.	2 (before resurfacing) 4 (after resurfacing)
26	Rolling topography. SE-bound outer lane in cut approx. 7 ft in depth Groundwater level approx. 5 ft below pavement surface in Oct. 1964.	Same as above.	2 (before resurfacing) 4 (after resurfacing)
27	Rolling topography. Eastbound outer lane in cut approx. 30 ft in depth.	According to previous investigations (3), poor pavement conditions were observed in 1960. The analysis period shown in Table 7 is from 1958 to 1961.	2.5 (1961) 3.5 (1964)
28	Rolling topography. Eastbound outer lane in cut approx. 15 ft in depth.	According to previous investigations (3), poor pavement conditions were observed in 1960. The analysis period shown in Table 7 is from 1958 to 1961.	2.5 (1961) 3.5 (1964)
29	Flat area. Roadway on low fill (approx. 2 ft in height). Groundwater level approx. 2 ft below pavement surface in Aug. 1964.	Alligator cracking, some areas patched.	2.5
30	Flat area. Roadway on low fill (approx. 3 ft in height). Ground water level approx. 3 ft below pavement surface in Aug. 1964.	Alligator cracking, ¼-in. average rut depth.	2.5

where the groundwater level had been relatively high, observation wells were installed to check the elevation of the water table. Information concerning the groundwater levels is included in Table 1.

Benkelman beam deflection tests were conducted at each site by the normal procedure (4) and the complete deflection data were presented in a separate report (14). Because of the effects of many variables on pavement deflection, it is difficult to establish a specific relationship (on a quantitative basis) between the Benkelman beam deflection and the modulus of deformation of the subgrade materials presented elsewhere in this paper. In general, relatively high pavement deflections were encountered in areas of micaceous subgrade soils. This is apparently due to the low modulus of deformation of the micaceous soils (see Tables 2 and 4). Furthermore, the deflection data from the

TABLE 2

PROPERTIES OF SUBGRADE MATERIALS

Site	General Description of Material	Sieve Analysis: Percent Passing Sieve No.			Atterberg Limits		AASHO Classification	Sp. Gr.	Ignition Loss* (%)
		10	40	200	L.L.	P.I.			
16	Brown silty sand	100	91	35	—	NP	A-2-4	2.67	0.12
17	Gray silty sand	100	91	21	—	NP	A-2-4	2.68	0.02
18	Brown silty sand	100	99	42	35	7	A-4	2.69	0.04
19	Brown micaceous silty sand	100	71	33	26	4	A-2-4	2.74	0.76
20	Brown micaceous silty sand	100	71	23	—	NP	A-2-4	2.72	0.74
21	Brown silty clay	98	92	42	43	23	A-7-6(4)	2.73	—
21A	Brown silty clay	98	85	49	38	19	A-6(3)	2.65	—
22	Brown micaceous silty sand	100	63	26	—	NP	A-2-4	2.66	0.99
23	Brown silty sand	100	65	29	19	3	A-2-4	2.62	0.18
24	Reddish-brown micaceous silty sand	100	68	31	40	6	A-2-4	2.75	4.86
25	Reddish-brown micaceous silty sand	100	82	21	—	NP	A-2-4	2.72	3.42
26	Red micaceous silty sand	100	86	44	33	5	A-4	2.72	3.25
27	Pink micaceous silty sand	100	66	29	—	NP	A-2-4	2.67	3.33
28	Reddish-brown micaceous sandy silt	100	75	53	43	14	A-7-6(2)	2.76	0.63
29	Black silty sand	100	93	25	—	NP	A-2-4	2.64	—
30	Black silty sand	100	89	24	—	NP	A-2-4	2.56	—

*The ignition loss was determined by the procedures recommended by Rostron (3).

sites with sandy subgrade soils indicate the general trend that greater pavement deflections occur in areas of lower serviceability index.

LABORATORY INVESTIGATIONS

The properties and classifications of the subgrade materials sampled from all sites are given in Table 2. Laboratory compaction test data for these materials are included in Table 3. The triaxial tests for all subgrade samples were performed using the following procedure.

Specimens 4 in. in diameter and 8 in. high were molded at the field moisture content by using the rammer as specified for the compaction test (AASHO Test Method T-99). Each specimen was compacted in five layers of equal thickness. The number of rammer blows for each layer was adjusted in such a manner that the density of the compacted specimen would be close to the field density. The compacted specimens were kept at the molding moisture for one day before being used for triaxial tests. Undrained tests

TABLE 3

FIELD AND LABORATORY DENSITY AND MOISTURE DATA—SUBGRADE MATERIALS

Site	Field Test Data			Laboratory Compaction Test (AASHO T-99)		Field Density as Percent of Max. Dry Density
	Dry Density (pcf)	Moisture Content (%)	Degree of Saturation (%)	Max. Dry Density (pcf)	Opt. Moist. Content (%)	
16	128.3	10.2	92	122.0	12.0	105
17	112.2	6.8	38	116.5	9.0	96
18	104.2	20.4	91	115.0	15.2	91
19	128.2	10.6	88	123.5	10.7	104
20	116.0	10.1	60	115.4	13.6	100
21	115.6	16.1	94	110.5	16.8	104
21A	113.2	16.5	97	119.0	14.0	95
22	119.1	7.2	49	115.6	13.0	103
23	113.2	8.9	54	121.4	10.8	93
24	89.5	19.1	57	101.0	20.0	89
25	95.1	17.6	61	99.8	23.0	95
26	95.4	22.8	80	102.4	21.6	93
27	107.9	18.0	89	105.6	17.6	102
28	110.1	18.8	93	107.2	18.8	102
29	119.7	13.0	92	113.4	14.4	105
30	108.9	15.3	85	108.8	15.3	100

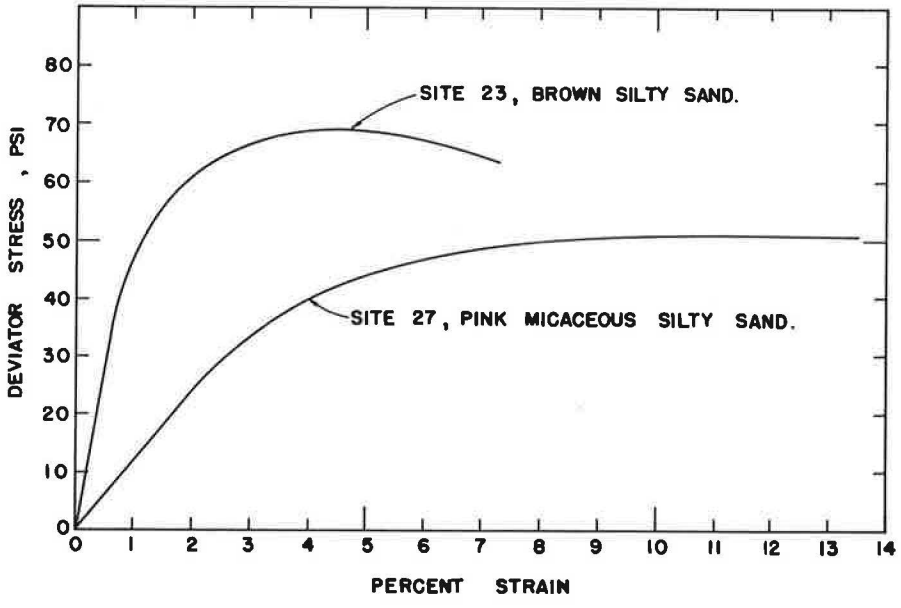

Figure 2. Typical stress-strain curves for two different types of subgrade material encountered in South Carolina.

were then performed at a rate of strain of approximately one percent per minute. During testing, the lateral pressure on the specimen was kept constant. For each series of tests, lateral pressures of 5, 10, and 20 psi were used. Sufficient data on the applied load and corresponding deformation of the specimens were obtained during the test for determining the modulus of deformation* from the stress-strain curve as shown in Figures 2 and 9. The data from a series of triaxial tests were also used to plot the Mohr circles and to determine the Mohr envelope as shown in Figure 3.

Table 4 summarizes the results from triaxial tests on all subgrade samples conducted according to the above procedure. A comparison of the data in this table with the information given in Table 2 shows that for the majority of the sites investigated, the dry density and the moisture content of the specimens tested are very close to the values determined from the field tests. It is recognized that even with similar densities and moisture contents, the strength and stress-strain characteristics of specimens prepared in the laboratory may not be the same as those of the subgrade materials under the actual field conditions. For best representation of the subgrade materials, the use of undisturbed samples would be preferable. Undisturbed samples, however, were not used in this study for reasons discussed earlier in this paper.

The moduli of deformation and related data obtained from the triaxial tests on AASHO Road Test embankment soil and crushed stone base material are given in Table 5. Test data from other sources are included in the table for comparison purposes. The properties of the embankment soil and crushed stone base material were reported by Shook and Fang (5).

A limited number of triaxial tests were conducted after the specimens had been subjected to capillary absorption. After preparing a specimen in the mold, the weight of the specimen together with the mold was determined. The specimen was kept in the mold and a piece of filter paper with a porous stone was placed under the specimen.

*The modulus of deformation is the secant modulus determined from the stress-strain curve. It is computed by dividing the deviator stress by the corresponding strain. The modulus of deformation is used in the Kansas method for the design of flexible pavements (10, 11).

TABLE 4

TRIAXIAL TEST DATA—SUBGRADE MATERIALS

Site	Specimen Number	Dry Density (pcf)	Testing Moisture (%)	Degree of Saturation (%)	Lateral Pressure (psi)	Modulus of Deformation (psi) at Deviator Stress Shown			Maximum Deviator Stress (psi)
						5 psi	10 psi	20 psi	
16	1	128.4	9.6	87	5	4,300	4,300	4,300	103.0
	2	129.4	9.3	88	5	4,300	4,300	4,300	114.5
	3	129.6	8.4	80	10	5,500	5,500	5,500	115.3
	4	129.7	9.1	87	10	5,500	5,500	5,500	107.7
	5	129.6	9.1	87	20	6,130	6,130	6,130	Not tested to failur
	6	128.5	9.4	85	20	6,000	6,000	6,000	133.0
17	1	116.6	6.8	42	5	4,000	4,000	4,000	41.3
	2	115.5	6.7	41	5	4,600	4,600	4,600	42.5
	3	116.6	7.0	44	10	5,300	5,300	5,300	62.7
	4	115.3	6.9	42	10	5,010	5,010	5,010	56.0
	5	115.5	6.9	42	20	6,670	6,670	6,670	96.5
18	1	110.0	14.8	76	10	4,600	4,600	4,600	68.0
	2	109.5	14.8	75	10	3,450	3,450	3,450	73.8
19	1	122.5	11.3	79	5	1,800	1,800	1,800	51.4
	2	121.5	11.4	77	5	1,680	1,680	1,680	48.1
	3	123.3	11.3	81	10	1,850	1,850	1,850	60.3
	4	121.1	11.4	77	10	2,080	2,080	2,080	58.1
	5	123.5	11.0	79	20	2,500	2,500	2,500	70.7
	6	122.3	11.4	79	20	2,450	2,450	2,450	103.8
20	1	118.7	12.3	88	5	2,500	2,500	2,500	66.6
	2	118.9	12.4	79	5	2,850	2,850	2,850	77.1
	3	119.3	12.4	81	10	3,080	3,080	3,080	95.8
	4	118.0	12.7	80	10	3,600	3,600	3,600	94.0
	5	118.1	12.3	77	20	6,000	6,000	6,000	134.8
	6	118.4	12.6	80	20	6,680	6,680	6,680	143.8
21	1	115.0	16.4	95	5	1,300	1,000	650	42.6
	2	114.8	16.4	94	10	1,600	1,350	640	51.0
	3	113.7	16.8	94	20	1,950	1,950	1,750	62.0
	4	114.6	16.4	94	20	2,100	2,100	1,500	55.5
21A	1	113.5	16.9	99	5	1,150	860	560	36.0
	2	113.5	16.8	99	10	1,330	1,330	1,000	42.5
	3	113.5	16.7	98	10	1,150	1,000	630	38.0
	4	113.5	16.7	98	20	1,150	1,150	770	47.0
	5	113.5	16.8	99	20	1,420	1,130	570	43.0
22	1	116.0	7.0	44	5	3,530	3,530	3,530	55.0
	2	116.1	7.4	46	5	2,780	2,780	2,780	51.9
	3	117.0	7.0	45	10	4,500	4,500	4,500	74.8
	4	116.4	7.1	45	10	4,300	4,300	4,300	69.0
	5	116.3	7.3	46	20	5,270	5,270	5,270	101.0
	6	116.0	7.1	44	20	5,270	5,270	5,270	101.0
23	1	113.9	8.5	52	5	3,000	3,000	3,000	44.6
	2	115.1	8.3	53	5	3,700	3,700	3,700	50.4
	3	115.1	8.5	54	10	5,000	5,000	5,000	68.9
	4	114.9	8.4	53	10	4,300	4,300	4,300	66.2
	5	115.1	8.6	55	20	7,250	7,250	7,250	91.8
	6	115.0	8.4	53	20	7,200	7,200	7,200	94.2
24	1	92.0	19.1	61	5	1,450	1,450	1,300	32.4
	2	90.9	18.9	59	10	1,500	1,330	420	39.0
	3	91.8	18.2	58	10	1,450	1,450	940	34.0
	4	91.1	18.5	58	20	1,730	1,730	1,510	45.5
	5	90.7	18.8	58	20	1,820	1,820	1,370	45.5
25	1	98.4	17.6	66	5	1,600	1,400	970	30.1
	2	96.8	18.0	65	5	1,600	1,400	1,030	34.2
	3	97.1	18.0	66	10	1,900	1,900	1,730	43.2
	4	98.6	17.2	65	10	1,600	1,600	1,520	42.2
	5	97.5	17.5	65	20	2,100	2,100	2,100	65.0
	6	96.3	17.1	61	20	2,400	2,400	2,400	63.8
26	1	96.9	22.3	81	5	1,520	1,520	1,520	42.9
	2	97.3	22.3	82	10	1,630	1,630	1,630	49.8
	3	95.3	21.9	77	10	1,750	1,750	1,750	48.5
	4	96.5	22.5	81	20	2,690	2,690	2,690	62.5
27	1	108.0	17.1	86	5	800	800	710	34.5
	2	107.3	17.3	84	5	890	890	890	35.8
	3	108.2	16.9	84	10	1,550	1,550	1,300	44.0
	4	107.1	17.3	84	10	1,360	1,200	1,200	51.2
	5	108.0	17.2	86	20	1,790	1,790	1,790	67.5
	6	107.0	17.2	83	20	1,670	1,670	1,670	58.0
28	1	103.9	19.9	84	5	1,550	1,550	1,160	55.0
	2	105.1	20.1	88	10	1,420	1,420	1,060	59.0
	3	105.0	19.7	86	10	1,800	1,800	1,470	59.1
	4	105.0	19.8	86	20	1,330	1,330	1,300	68.0
29	1	116.0	13.3	85	5	1,670	1,520	1,410	65.0
	2	116.4	12.9	83	5	1,430	1,430	1,330	55.9
	3	115.9	13.0	82	10	2,050	2,050	2,050	74.6
	4	116.5	13.9	90	10	1,600	1,600	1,600	66.2
	5	115.8	13.3	84	20	3,000	3,000	3,000	103.7
	6	115.8	13.2	83	20	3,200	3,200	3,200	100.5
30	1	107.9	14.9	80	5	1,630	1,630	1,630	55.7
	2	108.4	14.9	82	5	1,600	1,600	1,500	55.6
	3	108.7	14.4	80	10	2,700	2,700	2,700	69.0
	4	107.9	14.8	80	20	5,400	5,400	5,400	91.1

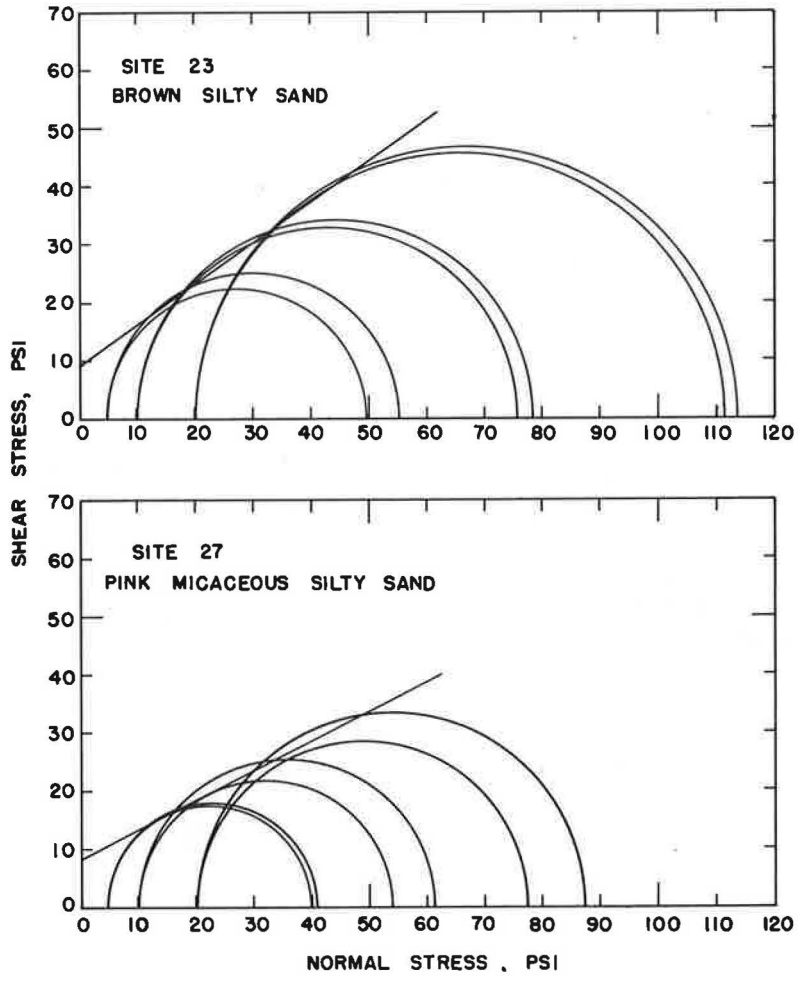

Figure 3. Mohr envelopes, subgrade soils from Sites 23 and 27.

The assembly was then kept in a rectangular pan in which the water level was maintained ½ in. below the bottom of the specimen. During the capillary absorption period, a surcharge weight was placed on the specimen to give a vertical pressure of 1 psi. Each specimen was kept in the pan until there was no more capillary flow into the specimen as detected by weighing the assembly periodically. The data concerning the length of the capillary absorption period, the change in moisture content during this period, and the results from triaxial tests made after capillary absorption are presented in Table 6.

ANALYSIS OF DATA OBTAINED AND FORMULATION OF SUBGRADE EVALUATION PROCEDURE

Estimation of Soil Support Value from Existing Pavement Structure and Traffic Data

While the AASHO design procedures (1, 9) were developed for determining the thickness of flexible pavements for proposed construction, in this study the design charts were used for estimating the soil support values of subgrade materials under existing pavements. The following procedure was used for estimating the soil support value.

TABLE 5

MODULUS OF DEFORMATION AND RELATED DATA OF AASHO ROAD TEST MATERIALS

Source of Test Data	Dry Density of Specimen as Molded (pcf)	Testing Moisture (%)	Degree of Saturation (%)	Modulus of Deformation (psi) at Deviator Stress Shown			Maximum Deviator Stress (psi)
				5 psi	10 psi	20 psi	
Material: AASHO Embankment Soil							
Triaxial tests performed in this study[a]	112.5	14.9	81	1,200	1,200	1,020	47.0
	114.0	14.3	82	1,360	1,360	1,080	50.0
G. F. Sowers[b]	See reference (8)			1,040 (modulus of elasticity)			—
Kansas State Highway Commission[c]	119.8	15.2					
	119.6	15.5	—	1,300	See reference (5)		—
	120.4	15.2					
Material: AASHO Crushed Stone Base Material							
Triaxial tests performed in this study[a]	139.0	4.0	48	10,300	10,300	10,300	149.2
	139.2	3.3	40	11,600	11,600	11,600	140.0
Kansas State Highway Commission[c]	138.9	7.4					
	138.9	6.8	—	10,000	See reference (5)		—

[a]Bag samples of the AASHO Road Test materials were used in preparing the specimens for the triaxial tests. It was intended to test the embankment soil at approximately the average field moisture and field density of the subgrade in the main loop sections of the AASHO Road Test (6), and to test the crushed stone material at approximately the average moisture and density values of the base as determined during the Road Test (7). Specimens of the crushed stone base material were prepared by using the material passing ¾-in. sieve (materials retained on ¾-in. sieve replaced by ¾-in. to No. 4 sieve fraction). The lateral pressure during testing was 10 psi.

[b]Based on data from undrained triaxial tests on undisturbed samples of the embankment soil obtained from several locations at the site of the AASHO Road Test. Specimens were tested at a controlled strain rate of 0.8 to 1 percent per minute. The lateral pressure during testing was 10 psi (8).

[c]Specimens were prepared in the laboratory by using representative samples of the embankment soil and the crushed stone material. The normal Kansas triaxial test procedure requires the saturation of the test specimens and the use of a lateral pressure of 20 psi. The rate of deformation was 0.005 and 0.1 in. per minute for the embankment soil and the crushed stone base, respectively. The lateral pressure during testing was 20 psi (5).

TABLE 6

TRIAXIAL TEST DATA OF SUBGRADE MATERIALS AFTER CAPILLARY ABSORPTION

Site	Dry Density of Test Specimen as Molded (pcf)	Moisture Content (%)		Number of Days for Capillary Absorption	Triaxial Test After Capillary Absorption				
		Before Capillary Absorption	After Capillary Absorption		Lateral Pressure (psi)	Modulus of Deformation (psi) at Deviator Stress Shown			Maximum Deviator Stress (psi)
						5 psi	10 psi	20 psi	
18	111.1	15.3	16.6	4	10	3,350	3,350	3,350	53.3
	109.2	14.4	16.7	4	10	3,750	3,750	3,550	not tested to failure
21A	112.8	15.3	16.0	10	10	1,000	630	340	33.5
28	105.8	19.7	20.7	11	10	1,830	1,830	1,090	47.5
29	115.5	12.1	13.2	6	10	1,060	900	800	73.0
30	109.7	15.2	16.7	9	10	2,680	2,680	2,680	79.0
	108.3	15.7	16.6	9	10	2,400	2,400	2,400	74.2
AASHO Embankment Soil	112.2	14.9	15.3	14	10	1,150	1,100	550	43.0

TABLE 7

TRAFFIC DATA[a]

Site	Years in Analysis Period	Approx. Accumulated Equiv. 18k Single Axle Load Applications in Analysis Period	Average Equiv. Daily 18k Single Axle Load Applications in Analysis Period	Computed Equiv. Daily 18k Single Axle Load Applications for Determining SN[b]
16, 17, 18	9	109,000	33.2	14.9
19	5	196,000	107.2	26.8
20	5	159,000	87.3	21.8
21, 21A	12	158,000	36.0	21.6
22, 23	4	214,000	147.0	29.4
24	4	634,000	433.6	86.7
25, 26	7	760,000	296.5	104
27, 28	3	276,000	252.0	37.8
29, 30	4	184,000	125.9	25.2

[a]The equivalence factors given in the AASHO Interim Guide for the Design of Flexible Pavement Structures (1) were used in determining the equivalent 18k single axle load applications.

[b]Because a 20-year traffic analysis period was used in the AASHO design charts, the equivalent 18k applications for determining SN were computed as follows:

$$\text{Computed Equiv. Daily 18k Applications} = \frac{(\text{Average Equiv. Daily 18k Applications}) \times (\text{Years in Analysis Period})}{20}.$$

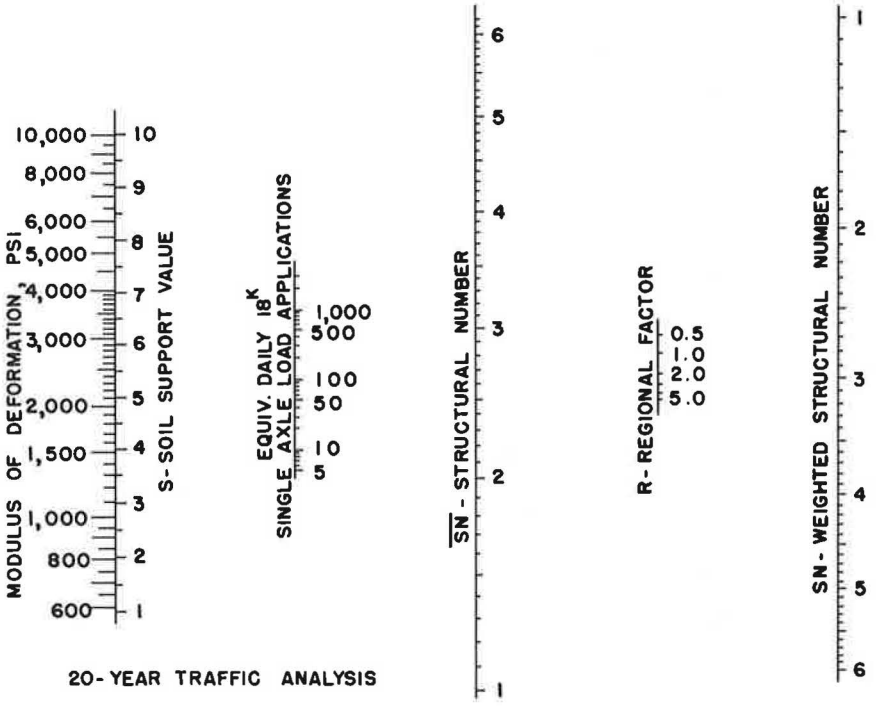

Figure 4. Design chart for terminal serviceability index of 2.0 (based on AASHO Interim Guide except for addition of modulus of deformation scale).

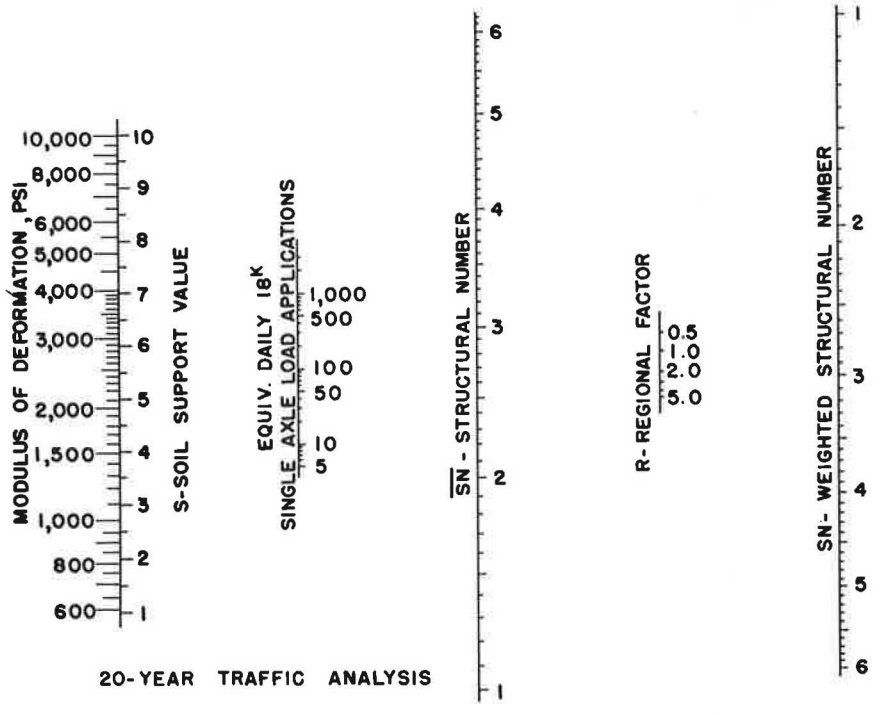

Figure 5. Design chart for terminal serviceability index of 2.5 (based on AASHO Interim Guide except for addition of modulus of deformation scale).

TABLE 8

COEFFICIENTS OF RELATIVE STRENGTH USED

Pavement Component	Coefficient of Relative Strength	Remarks
Asphalt Concrete	0.44*	0.27 for old asphalt concrete underlying new bituminous surfacing
Bituminous Surface Treatment	0.30	0.25 for old surface treatment underlying new bituminous surfacing
Sand Asphalt Base	0.25*	
Bituminous Stabilized Soil	0.20	0.07 for bituminous stabilized soil in inferior condition
Granular Base or Subbase	0.07*	
Crushed Stone Base	0.14*	

*Values based on information given in (9).

TABLE 9

PAVEMENT STRUCTURE, TRAFFIC, AND ESTIMATED SOIL SUPPORT VALUE AT VARIOUS SITES IN SOUTH CAROLINA

Site	Analysis Period	Pavement Component	Thickness (in.)	Coeff. of Relative Strength	SN of Each Pavement Component	SN of Pavement Structure	Equiv. Daily 18k Single Axle Load Applications	Serviceability Index	Estimated Soil Support Value
16	1955-1964	Bit. Surface Treatment	1	0.30	0.30	1.31	14.9	2	7.6
			1.25	0.25	0.31				
		Bit. Stabilized Soil (Inferior Condition)	5	0.07	0.35				
		Granular Subbase	5	0.07	0.35				
17	1955-1964	Bit. Surface Treatment	1	0.30	0.30	2.37	14.9	3.5	*
			1.25	0.25	0.31				
		Bit. Stabilized Soil	6	0.20	1.20				
		Granular Subbase	8	0.07	0.56				
18	1955-1964	Bit. Surface Treatment	1	0.30	0.30	1.70	14.9	2.5	6.2
			0.75	0.25	0.19				
		Bit. Stabilized Soil	5	0.20	1.00				
		Granular Subbase	3	0.07	0.21				
19	1959-1964	Bit. Surface Treatment	1	0.30	0.30	2.03	26.8	2.5	5.8
			5.5	0.25	1.38				
		Granular Subbase	5	0.07	0.35				
20	1959-1964	Bit. Surface Treatment	1	0.30	0.30	2.14	21.8	2.5	5.3
			5.5	0.25	1.38				
		Granular Subbase	6.5	0.07	0.46				
21 & 21A	1952-1964	Bit. Surface Treatment	2	0.30	0.60	2.40	21.6	2	4.2
		Sand Asphalt Base	4	0.25	1.00				
		Bit. Surface Treatment	1.5	0.25	0.38				
		Granular Subbase	6	0.07	0.42				
22 & 23	1960-1964	Asphalt Concrete	1	0.44	0.44	1.86	29.4	2.5	6.7
		Bit. Surface Treatment	4	0.25	1.00				
		Bit. Stabilized Soil (Inferior Conditon)	6	0.07	0.42				
24	1956-1960	Asphalt Concrete	2	0.44	0.88	2.69	86.7	2.5	5.4
			1.5	0.27	0.41				
		Crushed Stone Base	10	0.14	1.40				
25	1957-1964	Asphalt Concrete	3	0.44	1.32	2.44	104	2	5.9
		Crushed Stone Base	8	0.14	1.12				
26	1957-1964	Asphalt Concrete	3	0.44	1.32	2.58	104	2	5.6
		Crushed Stone Base	9	0.14	1.26				
27	1958-1961	Asphalt Concrete	3.5	0.44	1.54	2.94	37.8	2.5	3.7
		Crushed Stone Base	10	0.14	1.40				
28	1958-1961	Asphalt Concrete	3.5	0.44	1.54	2.80	37.8	2.5	4.1
		Crushed Stone Base	9	0.14	1.26				
29	1960-1964	Bit. Surface Treatment	1	0.30	0.30	2.30	25.2	2.5	5.0
			4	0.25	1.00				
		Bit. Stabilized Soil	5	0.20	1.00				
30	1960-1964	Bit. Surface Treatment	1	0.30	0.30	2.18	25.2	2.5	5.3
			3	0.25	0.75				
		Sand Asphalt Base	2.5	0.25	0.63				
		Bit. Stabilized Soil	2.5	0.20	0.50				

*Soil support value for Site 17 (Serviceability index = 3.5) not estimated because AASHO design charts are for serviceability indexes of 2 and 2.5 only.

At each site, the construction records and traffic data were analyzed to determine the equivalent daily 18k single axle load applications. The traffic data and the method for computing the 18k load applications are given in Table 7. The structural number of the existing pavement was computed on the basis of the actual thickness and the coefficient of relative strength of each pavement component. In addition, the serviceability index of the existing pavement was determined by visual inspection of the pavement conditions. On the basis of this information and a selected regional factor, the soil support value of the subgrade material below the existing pavement was determined from one of the AASHO design charts. The design charts for serviceability indexes of 2 and 2.5 are shown in Figures 4 and 5. The modulus of deformation scale on the opposite side of the soil support value scale shown in the figures is discussed elsewhere in this paper.

In applying the above procedure for estimating the soil support value of the subgrade under existing pavements, it is necessary to assign a specific coefficient of relative strength for each pavement component. Although the AASHO Design Committee has recommended certain values for the coefficients of relative strength of common types of paving materials, the specific coefficient for any particular type of paving material is to be determined according to specific local conditions. Extensive field and laboratory investigations would be required to establish a rational procedure for determining the coefficients of relative strength of various types of paving materials. The specific coefficients of relative strength used in this study are listed in Table 8. Some of the values given in the table were based on the information reported by Liddle (9). The remaining values were selected primarily by judgment. (To assist in the selection of the coefficients of relative strength, a limited number of Hveem stabilometer and cohesiometer tests were performed by using cored samples of the pavement components (14). The Marshall test, which was believed unsuitable for testing the pavement components consisting of bituminous surface treatments, was not conducted in this study.)

While a regional factor should be assigned to each site in order to obtain an accurate estimate of the soil support value, extensive investigations are again required for establishing a specific method for the determination of regional factors. According to the general guide for estimating the regional factor as described in the AASHO design procedure (1, 9), the regional factors for all sites investigated would be close to 1.0. The value of 1.0 was used for estimating the soil support values at all sites investigated.

The estimated soil support value of the subgrade at each site and the basic information used in the analysis are summarized in Table 9.

Comparison of Alternative Procedures for Subgrade Evaluation

In the analysis of the triaxial test data, consideration was given to two alternative procedures for subgrade evaluation. The first alternative is to establish the Mohr envelope from the Mohr circles and to determine the soil support value according to a tentative subgrade evaluation chart shown in Figure 6. The second alternative is to determine the soil support value according to the modulus of deformation obtained from the stress-strain curve.

To compare the two alternatives for subgrade evaluation, a specific method for determining the soil support value according to the modulus of deformation is required. In developing the design charts by the AASHO Design Committee, the soil support values of the AASHO Road Test embankment material and the crushed stone base material were given the numerical values of 3.0 and 10.0, respectively. These values, together with the modulus of deformation data given in Table 5, served as a basis for correlating the soil support values with the moduli of deformation for all types of subgrade materials. In establishing a specific method for determining the soil support value, the following assumptions and empirical procedures were used:

1. To simplify the test procedure and to provide a uniform basis for subgrade evaluation, the modulus of deformation was determined by undrained tests with a constant lateral pressure of 10 psi and a rate of strain of approximately one percent per minute.
2. On the basis of the laboratory data from the AASHO Road Test materials (Table 5), the soil support values of subgrade materials having moduli of deformation of 10,000 and 1,100 psi were given the numerical values of 10.0 and 3.0, respectively.

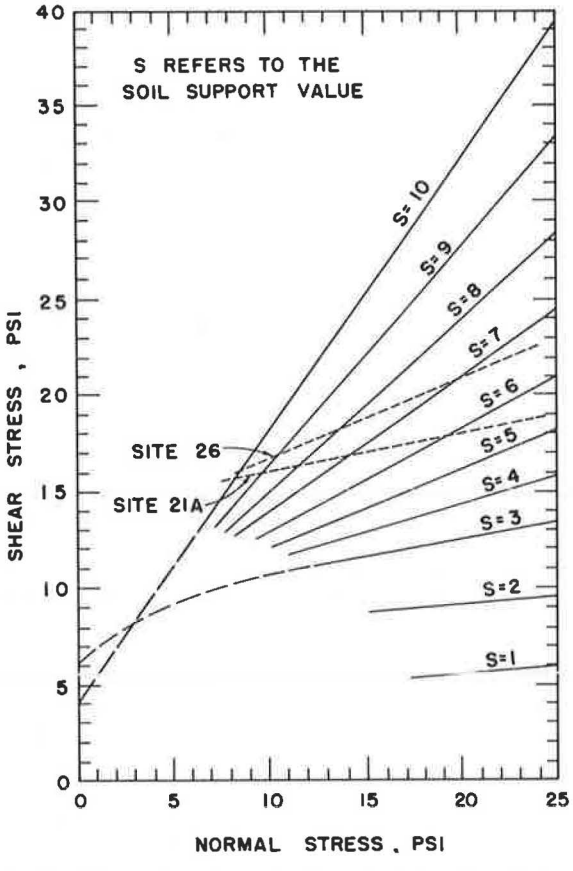

Figure 6. Tentative subgrade evaluation chart based on Mohr envelope.

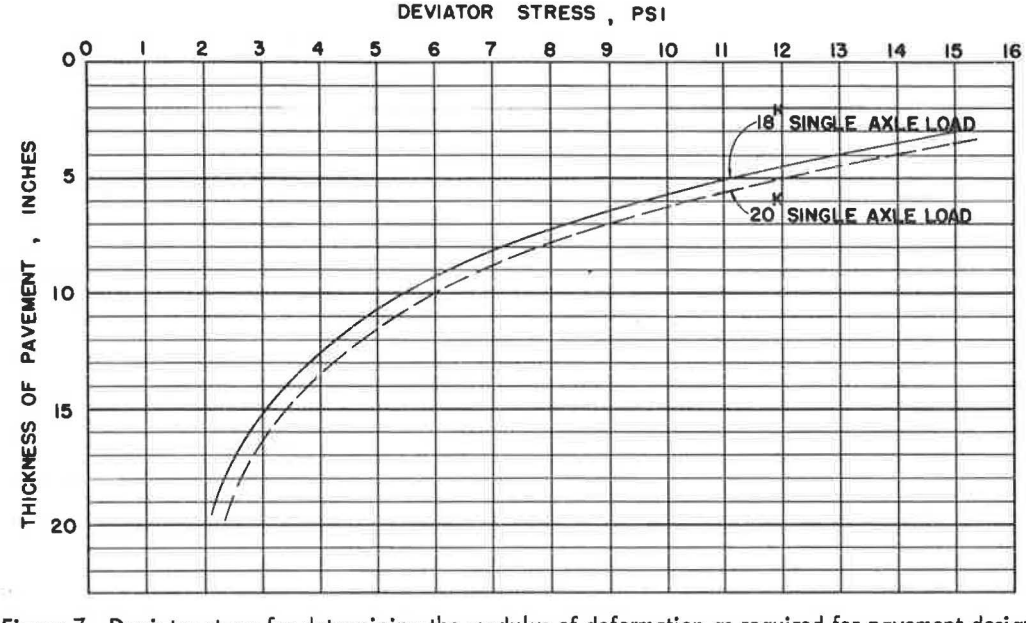

Figure 7. Deviator stress for determining the modulus of deformation as required for pavement design.

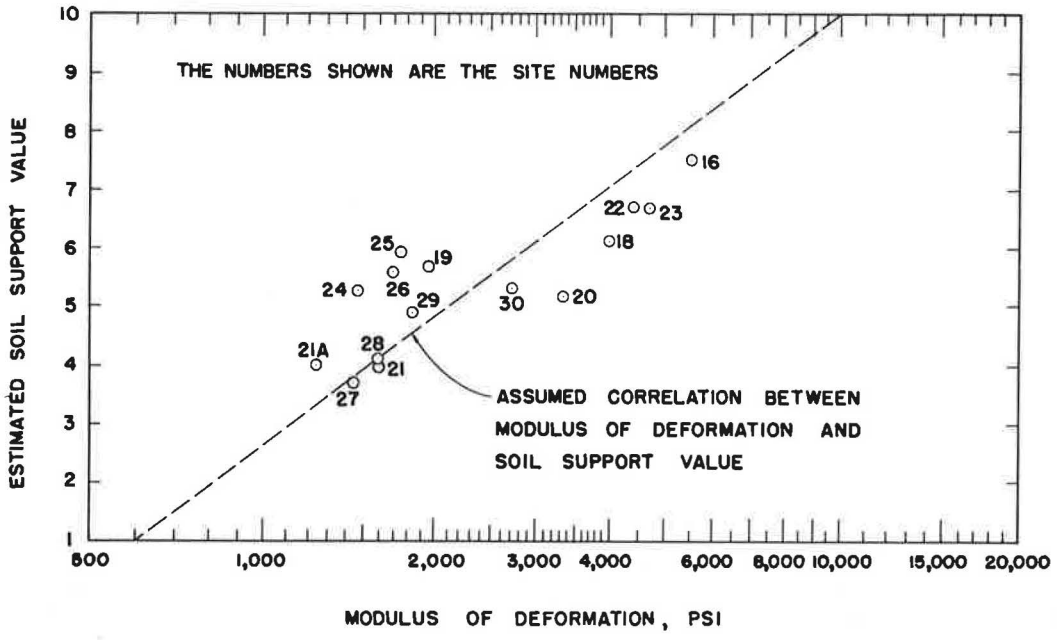

Figure 8. Correlation of estimated soil support value with the modulus of deformation of subgrade materials.

3. It was assumed that the soil support value would vary directly with the logarithm of the modulus of deformation as shown by the dashed line in Figure 8. The assumed relationship is also shown by the soil support value and the modulus of deformation scales in Figures 4 and 5.

4. Because of the variation of the modulus of deformation with the deviator stress, it would be necessary to compute the deviator stress in the subgrade due to anticipated wheel loads. The approximate deviator stresses near the center of the "pressure bulbs" below pavements of various thicknesses are shown in Figure 7. The deviator stresses shown were computed by assuming a tire inflation pressure of 70 psi and that the Boussinesq theory is applicable for this analysis. The analysis was simplified by using the stress charts developed by Foster and Ahlvin (12). Figure 7 shows that the difference in the deviator stress caused by 18k or 20k single axle loads is very small. To be consistent with the 18k single axle load used in expressing the traffic data, the use of the 18k curve in Figure 7 is recommended.

In considering the limitations of the basic information and the assumptions, interpolations, and extrapolations involved in establishing the modulus of deformation scale, it is evident that the reliability of this procedure should be verified by correlating field information with laboratory test data. For this purpose, the estimated soil support value for each site was plotted against the modulus of deformation as shown in Figure 8. The modulus of deformation for each site was determined according to the deviator stress indicated in Figure 7 and the laboratory data given in Table 4 by a procedure explained in Appendix A. The dashed line in Figure 8 represents the assumed relationship between the soil support value and the modulus of deformation. While the information shown is insufficient for any definite conclusion, the dashed line appears to be a reasonable representation of the general relationship between the soil support value and the modulus of deformation.

A comparison of the estimated soil support values given in Table 9 with the values determined according to the assumed relationship with the modulus of deformation is given in Table 10. It is difficult to make a similar comparison between the estimated soil support values and the values determined according to the Mohr envelopes due to

TABLE 10

COMPARISON OF ESTIMATED SOIL SUPPORT VALUES WITH ACTUAL VALUES DETERMINED BY TRIAXIAL TESTS ON SUBGRADE MATERIALS

Site	Estimated Soil Support Value, S_e	Actual Soil Support Value, S_a	S_e/S_a
16	7.6	8.1	0.94
18	6.2	7.1	0.87
19	5.8	4.8	1.21
20	5.3	6.5	0.82
21	4.2	4.2	1.00
21A	4.2	3.4	1.24
22	6.7	7.4	0.91
23	6.7	7.6	0.88
24	5.4	3.9	1.38
25	5.9	4.5	1.31
26	5.6	4.4	1.28
27	3.7	3.8	0.97
28	4.1	4.1	1.00
29	5.0	4.6	1.09
30	5.3	5.8	0.91

the fact that some Mohr envelopes cross a number of the soil support value lines shown in Figure 6. The Mohr envelopes for the subgrade materials from two sites shown in Figure 6 serve to illustrate the difficulty in determining the soil support values. In this respect, the use of the modulus of deformation for subgrade evaluation is a preferable procedure. With this procedure, a specific soil support value for a given modulus of deformation can be obtained directly from the scale shown in Figure 4 or 5.

While triaxial tests using three different lateral pressures are usually made for establishing the Mohr envelope, tests with only one lateral pressure (10 psi) are sufficient for determining the modulus of deformation. The use of the modulus of deformation for subgrade evaluation would, therefore, reduce the time and material required in performing the triaxial tests.

In the case of micaceous soils, such as the subgrade material from Site 27 (Figs. 2 and 3), the modulus of deformation is relatively low but the ultimate shearing strength as represented by the Mohr envelope may be relatively high. For such materials, the use of the Mohr envelope would result in a much higher soil support value than that evaluated according to the modulus of deformation. The information from field investigations indicates that the lower soil support value determined from the modulus of deformation is a more reliable representation of the load-carrying capacity of the subgrade than the higher value obtained from the Mohr envelope. The procedure for subgrade evaluation based on its modulus of deformation appears to be applicable to all types of materials, including micaceous soils.

On the basis of the above comparison, the alternative of using the modulus of deformation for subgrade evaluation was selected. Tentative procedures for determining the modulus of deformation of subgrade materials and the use of such information for the design of flexible pavement structures are given in Appendix A.

Additional laboratory test data concerning the stress-strain characteristics of subgrade materials are given in Appendix B. The information is of interest in that it may serve as a basis for the refinement of the tentative subgrade evaluation procedure in the future.

Preparation of Test Specimens to Simulate Field Conditions

In performing triaxial tests for the design of proposed flexible pavements, it is desirable to test the specimens at moisture contents representing the anticipated conditions under the pavement. While methods are available for predicting the subgrade moisture content on the basis of extensive field data concerning groundwater and drainage conditions, weather information, and the capillary characteristics of subgrade materials, considerable preparatory work would be necessary to establish certain reference data in order to simplify the procedure for routine testing. For the immediate application of the triaxial tests for the design of pavement structures, a relatively simple procedure such as capillary absorption or saturation by evacuation is preferable. Under normal conditions, the moisture content of the specimens resulting from capillary absorption is believed to be closer to the probable field moisture content than that obtained by saturation.

In this study, a limited number of triaxial tests were performed with specimens after capillary absorption. The data obtained from such tests (Table 6) indicate that the moduli of deformation are approximately the same or slightly lower than those obtained from tests on specimens representing the field conditions (Table 4). While no

definite conclusion can be reached on the basis of the limited data, the treatment of test specimens by capillary absorption appears to be a conservative approach for the purpose of simulating the field conditions of subgrade soils.

As mentioned above, all specimens used in this study were compacted to the density determined from in-place density tests. In South Carolina, a minimum dry density of 95 percent of the maximum dry density (AASHO T-99) is specified for subgrade construction (13). Table 3 shows that at the majority of the sites investigated, the actual density of the subgrade is near or above the 95 percent density requirement. In performing triaxial tests for the design of new pavements, it is necessary to compact the subgrade materials to the minimum density as indicated in the specifications.

NEED FOR FURTHER STUDIES

The tentative subgrade evaluation procedure as described was formulated on the basis of limited field and laboratory investigations. Further studies are required, therefore, to verify or to refine the basic assumptions, such as the assumed relationship between the soil support value and the modulus of deformation. The reliability of the pavement design procedure is also dependent upon factors not covered in this study, such as the coefficients of relative strength for pavement components and the determination of regional factors. Further investigations in these areas in the form of satellite or similar studies are needed to provide the necessary information for improving the overall design procedure.

SUMMARY

A tentative procedure for subgrade evaluation as required in the AASHO Interim Guide design procedure is presented. To determine the soil support value of the subgrade material, triaxial tests are to be conducted with specimens representing the anticipated density and moisture conditions of the subgrade. The test data are then used for computing the modulus of deformation of the subgrade material. With this information, the soil support value of the subgrade can be determined according to a correlation with the modulus of deformation. Results from the limited field and laboratory investigations conducted in this study indicate that the tentative method may be used for evaluating the soil support value of various types of subgrade materials encountered in South Carolina.

ACKNOWLEDGMENTS

The research reported in this paper was conducted at the University of South Carolina under the sponsorship of the South Carolina State Highway Department and the U. S. Bureau of Public Roads. Some laboratory experiments were performed by personnel of the South Carolina State Highway Department Materials Laboratory. Samples of the AASHO Road Test materials were furnished by the Illinois Division of Highways through Mr. John E. Burke, Engineer of Research and Development. The authors wish to express their appreciation to all who have given advice and assistance in this study.

REFERENCES

1. AASHO Committee on Design. AASHO Interim Guide for the Design of Flexible Pavement Structures, Oct. 12, 1961.
2. McDowell, C. Road Test Findings Utilized in Analysis of Texas Triaxial Method of Pavement Design. The AASHO Road Test: Proceedings of a Conference Held May 16-18, 1962, St. Louis, Mo. HRB Spec. Rept. 73, p. 314, 1962.
3. Rostron, J. P. Cracking and Performance of Asphaltic Wearing Surfaces of Certain Highway Sections. Bull. 100, Engineering Experiment Station, Clemson College, June 30, 1963.
4. Benkelman, A. C., Kingham, R. I., and Fang, H. Y. Special Deflection Studies on Flexible Pavement. The AASHO Road Test: Proceedings of a Conference Held May 16-18, 1962, St. Louis, Mo. HRB Spec. Rept. 73, p. 102, 1962.

5. Shook, J. F., and Fang, H. Y. Cooperative Materials Testing Program at the AASHO Road Test. AASHO Road Test Technical Staff Papers, HRB Spec. Rept. 66, p. 59, 1961.
6. Highway Research Board. The AASHO Road Test: Report 5, Pavement Research. HRB Spec. Rept. 61E, 1962.
7. Highway Research Board. AASHO Road Test Data System 4180, Measurements of Moisture Content, Density, CBR on Base and Subbase. April 1960, August 1960, and March 1961 Trench Studies.
8. Sowers, G. F. Stress Bearing Capacity and Flexible Pavement Thickness Design Based on the AASHO Road Test and Georgia Pavement Evaluation Test. Rept. 6, Engineering Experiment Station, Georgia Inst. of Technology, 1964.
9. Liddle, W. J. Application of AASHO Road Test Results to the Design of Flexible Pavement Structures. Proc. of Internat. Conf. on Structural Design of Asphalt Pavements, Univ. of Michigan, 1962.
10. State Highway Commission of Kansas. Design of Flexible Pavements Using the Triaxial Compression Test. HRB Bull. 8, 1947.
11. Yoder, E. J. Principles of Pavement Design. John Wiley and Sons, New York, 1959.
12. Foster, C. R., and Ahlvin, R. G. Stresses and Deflections Induced by a Uniform Circular Load. Proc. HRB, Vol. 33, p. 467, 1954.
13. South Carolina State Highway Department. Standard Specifications for Highway Construction, 1964 edition.
14. Chu, T. Y., and Humphries, W. K. The Application and Refinement of Triaxial Tests on Subgrade Materials for the Design of Flexible Pavement Structures. Univ. of South Carolina, 1965.
15. Vesić, A. S., and Domaschuk, L. Theoretical Analysis of Structural Behavior of Road Test Flexible Pavements. National Cooperative Highway Research Program Report 10, Highway Research Board, 1964.

Appendix A

TENTATIVE TEST AND DESIGN PROCEDURES

The general procedure for the testing of subgrade soils and the use of such information for the design of flexible pavement structures are presented in the form of a design example. Assume that the design of flexible pavements for a section of a proposed highway is desired. The triaxial test and design procedures as required for determining the thickness of the pavement are described separately.

Triaxial Tests

1. Preparation of Test Specimens.— Two identical specimens are prepared from each soil sample. For each sample, prepare a batch of moist soil containing the optimum moisture content. If the moisture content of the soil during field compaction is expected to be appreciably different from the optimum content, use the anticipated, instead of the optimum, moisture content. Keep the material at the mixing moisture content overnight before molding the specimens. Compact the moist soils with adequate compactive effort to obtain the specified density. Each specimen should be prepared in such a manner that uniform conditions may be obtained throughout the specimen. Irregular conditions, especially at the top and bottom of the specimen, should be avoided.

2. Capillary Absorption.—Each specimen is subjected to capillary absorption before being used for triaxial tests. This step is similar to the general procedure for capillary absorption used by the Texas Highway Department for "Standard Triaxial Compression Test" (2).

3. Determination of Moduli of Deformation.—Each specimen is subjected to undrained triaxial test at a constant rate of strain of approximately 1 percent per minute until

failure occurs. (The possible use of the ultimate strength for subgrade evaluation is discussed in the note at the end of Appendix A.) Upon completion of the undrained test, samples are taken from the top, middle, and bottom portions of the specimen for moisture content determinations. For each specimen, compute the stresses and strains from the load-deformation data obtained during the undrained test, plot the stress-strain curve as illustrated in Figure 9A, and determine the modulus of deformation for deviator stresses of 5, 10, and 20 psi. In this example, the average moduli of deformation of the specimens are plotted against the deviator stresses as shown in Figure 9B. If the modulus of deformation remains constant for deviator stresses up to 20 psi, it would not be necessary to plot the modulus of deformation vs deviator stress curve (Fig. 9B).

Design Procedure

The procedure described below mainly explains the use of the modulus of deformation data for determining the thickness of flexible pavements. It is assumed that for a particular section of the proposed pavement, the modulus of deformation data for the subgrade material are as shown in Figure 9.

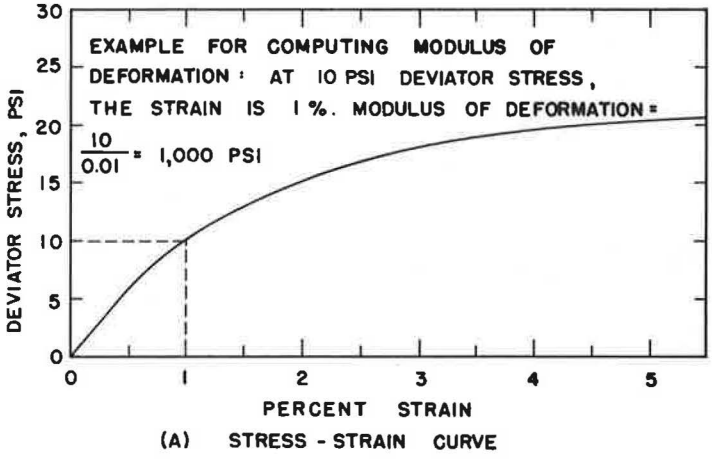

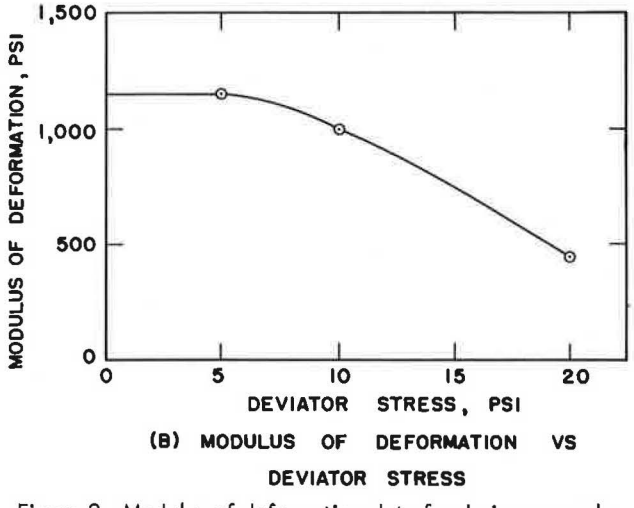

Figure 9. Modulus of deformation data for design example.

1. Establish the terminal serviceability index for the proposed highway, select a regional factor, and determine the equivalent 18k single axle load applications according to the procedures given in the AASHO Interim Guide (1). In this example, assume the desired terminal serviceability index = 2.5; the regional factor = 1.0; and computed 18k load applications (20-year traffic analysis) = 50.

2. Determine the soil support value according to the modulus of deformation data and an assumed deviator stress. In this example, the modulus of deformation data are shown in Figure 9; the assumed deviator stress = 5 psi; the modulus of deformation (from Fig. 9B) = 1150 psi; and the soil support value (from Figure 5) = 3.1.

3. Determine SN from AASHO design chart. In this example, the soil support value (S) = 3.1; 18k load applications = 50; the regional factor (R) = 1.0. From Figure 5, SN = 3.35.

4. Convert SN to pavement thickness according to established coefficients of relative strength. If the total thickness of the pavement structure is, for example, 11 in., the deviator stress for determining the modulus of deformation would be close to 5 psi (Fig. 7). Therefore, no adjustment of the modulus of deformation used in step 2 is required. If the design thickness is, for example, 6 in., the deviator stress given in Figure 7 would be approximately 10 psi. In this case, the modulus of deformation used in step 2 should be changed to 1,000 psi, the soil support value would then become 2.7, and the SN value should be revised accordingly. Such adjustments of the modulus of deformation and SN values are, however, seldom necessary in the design of flexible pavements for moderate to heavy traffic.

Note.—The tentative procedure for subgrade evaluation described is based on the assumption that, so far as the properties of the subgrade are concerned, the deformation characteristics (expressed in terms of the modulus of deformation) instead of the ultimate strength (related to the maximum deviator stress) is the controlling factor affecting the performance of flexible pavements. In the various locations investigated, this appears to be a reasonable assumption. In the event a subgrade soil has a moderate modulus of deformation but an extremely low ultimate strength (as indicated by a very low maximum deviator stress), the deformation characteristics may not be the controlling factor as assumed. For such exceptional cases, it would be necessary to consider the adverse effect of the low ultimate strength on the performance of flexible pavements. A method for evaluating the soil support value on the basis of the ultimate strength of subgrade soils was developed by Sowers (8).

Appendix B

MISCELLANEOUS DATA RELATED TO STRESS-STRAIN CHARACTERISTICS OF SUBGRADE SOILS

Effect of Repeated Loading on Modulus of Deformation

Figure 10 shows a set of stress-strain curves from five repeated loadings in an undrained triaxial test performed with a compacted silty clay. The test procedures were similar to those presented in Appendix A except that the specimen was subjected to the five repeated loading and unloading cycles. For each cycle, the deviator stress was increased to a maximum value of approximately 10 psi and then released. As expected, the slope of the straight line portion of the stress-strain curve obtained from the first loading is not as steep as that for the subsequent loadings. The modulus of deformation determined from the first loading is, therefore, lower than that obtained from the subsequent loadings. It will be noted that for the material tested the moduli of deformation determined from the second and subsequent loadings approach a constant value. This general trend concerning the deformation characteristics under repeated loadings has been observed in testing a number of compacted soils.

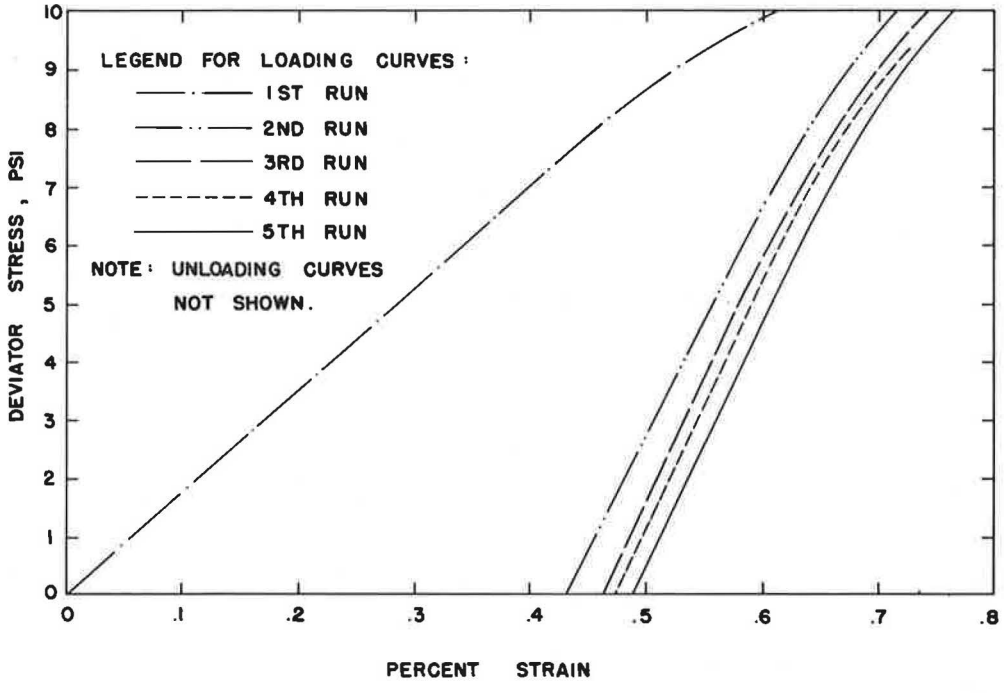

Figure 10. Typical stress-strain curves from five repeated loadings in undrained triaxial test.

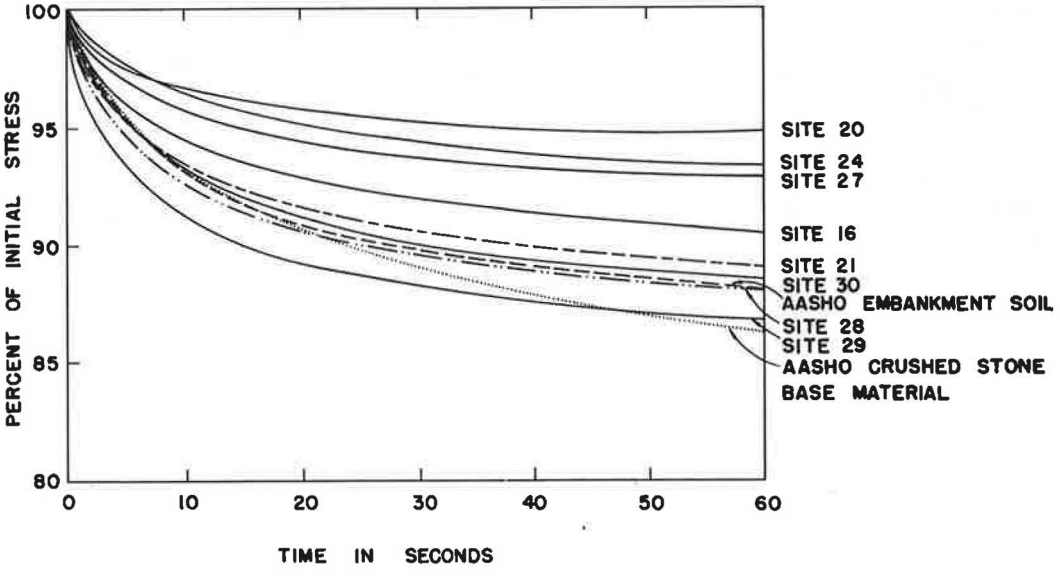

Figure 11. Reduction in the deviator stress of subgrade materials when constant strain is maintained during triaxial test.

The determination of the modulus of deformation from the stress-strain curves obtained from the first and subsequent loadings and the laboratory data on the deformation characteristics of the AASHO Road Test subgrade and pavement components were reviewed by Vesić and Domaschuk (15) in connection with the theoretical analysis of the structural behavior of road test flexible pavements. In analyses concerning the elastic deflections of flexible pavements, the modulus of deformation determined from repeated loadings would be more significant than that of the first loading. In establishing the subgrade evaluation procedure in Appendix A, consideration was given to the use of the modulus of deformation determined from repeated loadings instead of that from the first loading. The information relative to the repeated loading deformation characteristics alone appears to be inadequate for evaluating the soil support value of subgrade materials because both the elastic and the plastic deformations of a subgrade may affect the performance of flexible pavements.

Change in Deviator Stress Under Constant Strain

In a series of triaxial tests with compacted specimens of subgrade materials, observations were made on the change in the deviator stress of each specimen when the strain of the specimen was kept constant. The following procedure was followed in making the observations:

1. The undrained test was performed according to the procedure described in Appendix A until a deviator stress of nearly 40 psi was reached.
2. The loading machine was stopped so that the strain of the specimen being tested would remain constant during the observation period. The lateral pressure was maintained at 10 psi.
3. The change in the deviator stress was recorded at 5-sec intervals.

Data from the observations are shown in Figure 11. The deviator stresses shown are expressed in percent of the initial deviator stress acting on each specimen. While an appreciable decrease in the deviator stress during the observation period is noted in all cases, the change in deviator stress of the specimens prepared from micaceous soils (Sites 20, 24, and 27) is less than that of specimens prepared from other types of materials, with the exception of Site 28. Although the material from Site 28 is also a micaceous soil, the relatively high content of particles passing No. 200 sieve and the medium plasticity of the soil indicate that the clay fraction in the soil may have an appreciable effect on the characteristics of the soil.

The limited information shown in Figure 11 is insufficient for relating the observed characteristics of the soils to the performance of the flexible pavements. The information indicates, however, that it might be possible to include a simple step in the triaxial test procedure for evaluating a special property of subgrade soils. This property may be a controlling factor affecting the degree of prestressing in the subgrade. The degree of prestressing is believed to be one of the important factors influencing the deflection of flexible pavements.

Theoretical Analysis of Structural Behavior of Road Test Flexible Pavements*

ALEKSANDAR SEDMAK VESIĆ, Professor of Civil Engineering, Duke University (formerly of Georgia Institute of Technology), and
LEONARD DOMASCHUK, Research Assistant, Georgia Institute of Technology

ABRIDGMENT

•THE MAIN objective of this study is to present a rational, mechanistic interpretation of measurements and observations made on flexible pavements in the AASHO Road Test and other similar experimental investigations. The analysis is centered around stresses and deflections of the pavement system, with due attention to the mechanisms of pavement failure and associated phenomena. The paper is divided into five chapters.

Chapter 1 consists of a comprehensive critical review of the existing theories of structural behavior of flexible pavements. For the purpose of discussion all the theoretical methods of pavement design are divided into two major groups: (a) ultimate strength methods, and (b) elasticity methods. Advantages and shortcomings of both groups as well as of individual better-known methods of each group are discussed in detail.

Chapter 2 contains selected data on the structural behavior of the AASHO Road Test flexible pavements. The data are assembled in accordance with the three major objects of analysis, namely: (a) stress distribution in the pavement system, (b) resilient pavement deflections, and (c) cumulative plastic deflections and structural failure of pavements.

Chapter 3 presents available data on index properties, strength and deformation characteristics of the pavement materials and the subgrade. Chapter 4 is an analysis of all the assembled data, subdivided in a manner similar to that used in Chapter 2. Major conclusions are outlined in Chapter 5.

Vertical stress distribution data show that stresses vary with pavement temperature and degree of saturation of the subgrade, as well as with vehicle speed. Generally, the stresses are lower at lower temperatures, at lower degrees of saturation, and at higher vehicle speeds. At creeping vehicle speeds, and over the major part of the year, excepting frost periods, vertical stresses follow the patterns predicted by the Boussinesq theory for a homogeneous solid. Under loads they are considerably higher than those predicted by the Burmister theory of a layered solid.

Deflection data indicate that the deflection basins have a very limited extension and are not at all comparable in size to those predicted by the layered solid theories. This finding is in agreement with previous observations as well as with the stress measurement results. It is indicative of a limited load-spreading ability and a limited slab action of conventional bases and subbases.

Structural failure data are analyzed with emphasis on the mechanics of rutting. It is found that the rutting of AASHO Road Test flexible pavements was caused primarily by distortion within the pavement structure, as long as the subgrade stress remained below a critical level. This finding justifies the selection of the limiting subgrade stress as a design criterion.

*The paper of which this is an abridgment is available from the Highway Research Board as NCHRP Report 10, "Theoretical Analysis of Structural Behavior of Road Test Flexible Pavements" (31 pp., $2.80).

Paper sponsored by Committee on Flexible Pavement Design and presented at the 45th Annual Meeting.

It was further concluded that the phenomenon of structural failure of flexible pavements is governed by the relative resilience or compressibility of the subgrade soil with respect to the shear strength of the pavement structure. Depending on the thickness and strength of that structure with respect to the subgrade, punching shear failure or general shear failure may occur in extreme cases.

In the remainder of Chapter 5 implications of the findings of this study with respect to existing design procedures are discussed and recommendations for future research are given. The need for more fundamental research in the area of mechanics of flexible pavements is stressed. It is suggested that a general design method for flexible pavements must include consideration of both elastic and plastic phenomena.

Observations on Flexible Pavement Deflections in Maryland

W. G. MULLEN, North Carolina State University, and
W. R. CLINGAN and E. T. PAULIS, Maryland State Roads Commission

Reported are observations on two phases of a long-term study of high-type flexible pavements in Maryland. Included are observations of deflection measurements using the Benkelman beam technique on (a) selected pavements over periods up to ten years and (b) one-shot fall deflection for all new pavements constructed since 1960. Analysis of deflection distribution by magnitude with respect to subgrade soil type, spring and fall measurements, inner and outer wheelpaths and pavement thickness is included. Correlation is developed between deflection distribution by magnitude and general subgrade soil type. Significant differences were found between deflections of inner and outer wheelpaths and between spring and fall measurements by wheelpath. Relations between deflections and performance, subgrade moisture content and change in ADT were examined for significance.

•BEGINNING in 1955 a cooperative research program was undertaken by the Maryland State Roads Commission Bureau of Research with the Bureau of Public Roads to study deflection behavior of selected existing flexible type pavements by utilizing the Benkelman beam technique that was developed during the WASHO Road Test. This work continues, and a progress report (1) was issued in July 1965. Previously, papers by Lee (2) in 1956 and by Williams and Lee (3) in 1958 were published relating progress and tentative interpretation of results.

In 1960 the study was expanded to include observations on newly completed flexible pavements in addition to the existing pavements selected in 1955. At this time the entire study was included as a project under the HPS-HPR program. Each year all newly completed flexible pavements have been added to the program so that initial deflection observations are available.

In the fall of 1963, a physical sampling investigation of the pavement layers, base and subgrade of one of the pavements in the original study, US 40 between Frederick and Hagerstown, was undertaken. Results of this analysis are omitted from this paper in the interest of brevity. Analysis of another of these pavements, I-70S between Frederick and Washington, has been reported under a separate study (4).

A number of interesting findings have resulted from this study. Included are observations that spring deflections are higher than fall deflections, outer wheelpath readings are higher than inner wheelpath readings, and most significant, for the range of pavement thickness encountered in Maryland, magnitude and dispersion of deflections fall into different categories according to subgrade soil types. Deterioration and distress in a pavement are not signaled by a change in deflection magnitude, nor does volume of traffic have any noticeable effect upon deflection.

Physiography

The six physiographic provinces found in Maryland are shown on the map (Fig. 1). Information for the plotting of boundaries has been obtained from Woods and Lovell (5), Maryland Geological Survey (6, 7) and Mathews and Shirley (8).

Paper sponsored by Committee on Flexible Pavement Design and presented at the 45th Annual Meeting.

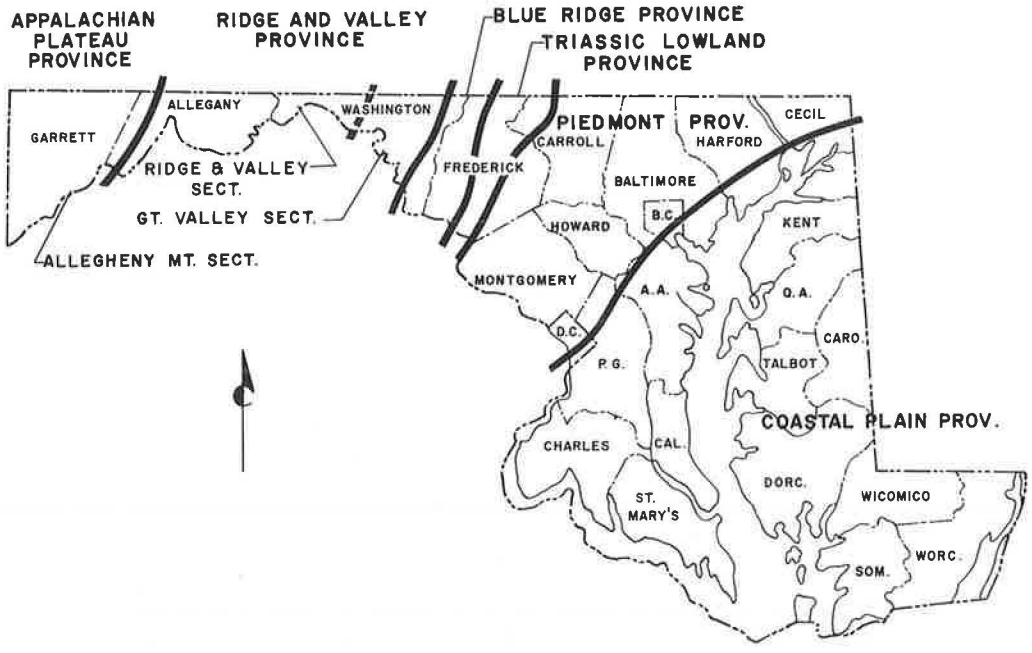

Figure 1. Physiographic map of Maryland.

Of the six provinces, the Coastal Plain is composed of sediments deposited in deep layers that tilt slightly downward to the southeast. The soils of the other five provinces are largely residual, having been formed from the underlying rocks. The rocks range in age from the Precambrian rocks of the Piedmont to the later and younger Pennsylvanian and Permian rocks of the coal measures in the Allegheny Mountain section of the Appalachian Plateau Province.

Climate

The mean annual temperature in Maryland varies from the upper 40's in the westernmost part of the state to the middle 50's in the lower eastern shore. Precipitation averages between 40 and 45 inches. Distribution is affected somewhat by the topography with slight rain shadows developing east of the Allegheny Mountains of the Appalachian Plateau through the Ridge and Valley Sections of Allegheny and Washington Counties.

Freezing and frost action are problems from western portions eastward through the Piedmont. In Frederick and Montgomery Counties, near the center of the state both geographically and climatically, frost penetration below pavement layers into the subgrade has been computed to vary from 0 to 25 inches depending upon the severity of the weather (4).

LONG TERM STUDY PAVEMENTS

There are six highway locations included in the original extensive measurement category of the investigation begun in 1955. Descriptions of these pavements are given in Table 1, and typical pavement sections are shown in Figure 2. General layout of the test sites has been reported previously (2).

The technique of the Benkelman beam or load-deflection test is well known and in the tests reported here measurements were made using an 11.2-kip wheel load with tires inflated to 80 psi. Maximum deflection and recovery were recorded for both inner and outer wheelpaths.

A great mass of deflection data has been accumulated during the progress of the study which has been compiled in a separate report (9). Reproduction of deflection

TABLE 1

TEST PAVEMENTS

Highway No.	Location	Length (miles)	Pavement Thickness (inches)	Year Completed	Predominant Soils, AASHO Class.	Condition and Remarks, 1965	Defl. Site No.
US 40W	Frederick to Hagerstown	16.5	17	1947	A5, A4-7	Good	71
US 40E	Frederick to Ridgeville	12.0	20½-22½	1956[a]	A5	Fair—Surface Cracking	48
I-70S (US 240)	Frederick to Germantown	16.0	15-17	1952-54	A5, A4-7	Poor—Reconstruction 1964-65	53
US 301 (Md. 71)	Md. 305 to Md. 300	10.5	15½	1955	A2-4	Poor—Resurfaced 1 in. 1958-61[b]	38
US 301 (Md. 71) Black Base	Md. 300 to Unicorn Bridge	4.5	15½	1957	A2-4	Poor—Cracking, Rutting	14
US 15	Thurmont Bypass	4.5	22	1957	A5	Fair—Surface Treated 1960	14
Md. 404	Queen Anne's Bypass	0.5	13½	1957	A2-4	Poor—Surface Cracking[c]	9

[a]Opened as stage construction on surface-treated base in 1955; 7½ in. bituminous concrete added in 1956.
[b]Part of this section resurfaced in 1958, the remainder in 1961.
[c]Resurfaced 1 in. bituminous concrete in May 1965 during preparation of this report.

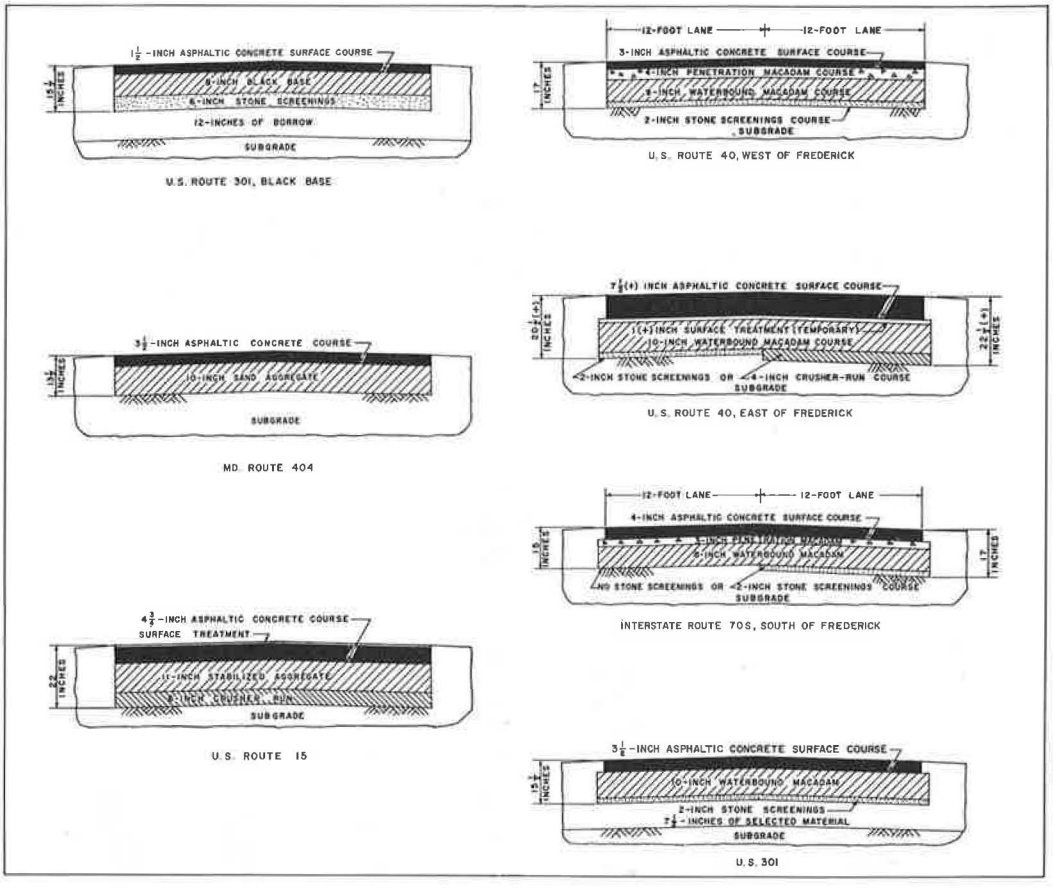

Figure 2. Pavement sections.

data here has been held to the minimum necessary for analysis, and is presented in Table 2. Subgrade soils have been grouped into general categories and distribution of deflections according to category is tabulated in Table 3. Average daily traffic for the period of service for each highway is given in Table 4.

TABLE 2

AVERAGE DEFLECTIONS BY HIGHWAY

Highway No.	1955	1956	1957	1958	1959	1960	1961	1965	High	Low	Avg.
					Spring Deflections (1/1000 in.)						
US 40W	28	27	23	23	27	—	29	29	29	23	27
US 40E[a]	(71)[b]	31	25	27	28	—	28	22	31	22	27
I-70S[a]	41	40	37	35	41	—	42	(24)[c]	42	35	39
US 301	—	36	28	26	26	—	26	24	36	24	28
US 301 BB	—	—	23	19	21	—	25	22	23	19	22
US 15	—	—	—	—	61	—	64	(46)[d]	64	61	63
Md. 404	—	—	—	—	24	—	25	24	25	24	25
					Fall Deflections (1/1000 in.)						
US 40W	22	22	20	23	22	24	—	—	24	20	22
US 40E[a]	26	23	21	—	22	—	—	—	26	21	23
I-70S[a]	32	29	26	32	30	30	—	—	32	26	30
US 301	36	27	22	27	22	26	—	—	36	22	26
US 301 BB	—	—	—	18	16	17	—	—	18	16	17
US 15	—	—	—	59	45	(29)[d]	—	—	59	45	52
Md. 404	—	—	—	19	19	—	—	—	19	19	19

[a]Data for shoulder lane only; median lane data similar.
[b]Deflections on surface treated base—not included in averages.
[c]Deflections on leveling course and base of resurfacing—not included in averages.
[d]Deflections on surface treatment—not included in averages.

Spring and Fall Deflections

The data from Table 2 are plotted in Figure 3, where the average of all spring readings is compared with the average of all fall readings on a highway-by-highway basis for the entire period of testing. It is evident that the average of spring deflections is higher than the average of fall deflections for the period of testing, and, further, that on a year-by-year basis spring deflections are consistently higher than fall deflections.

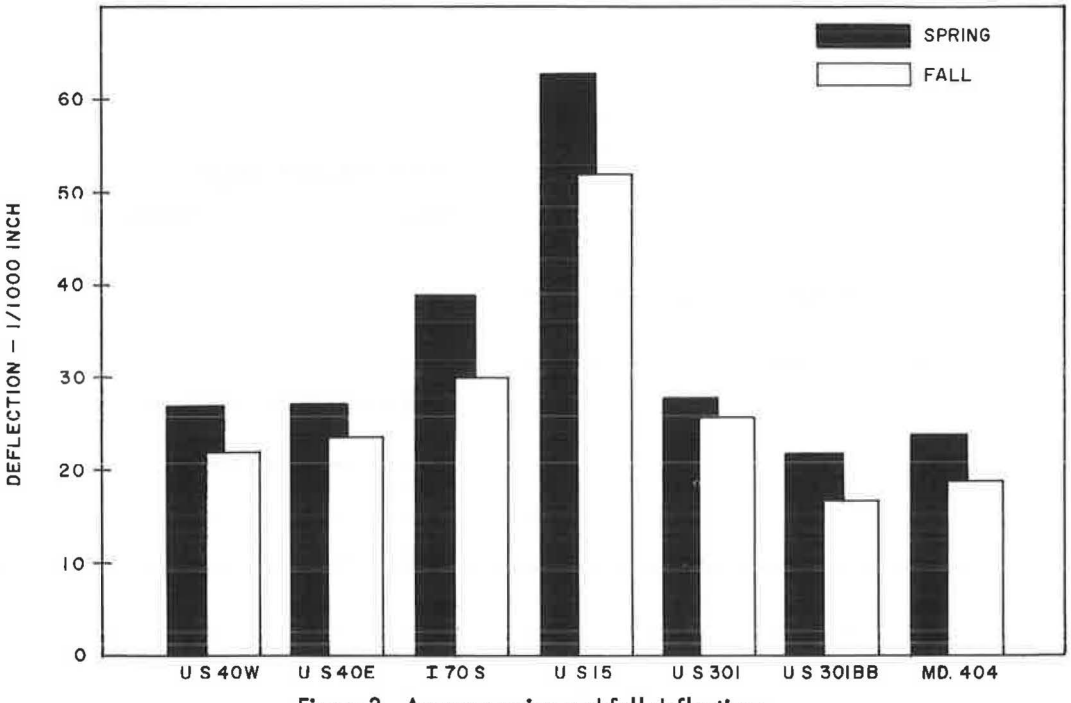

Figure 3. Average spring and fall deflections.

Figure 4. Drainage of subgrade on US 301, fall 1955.

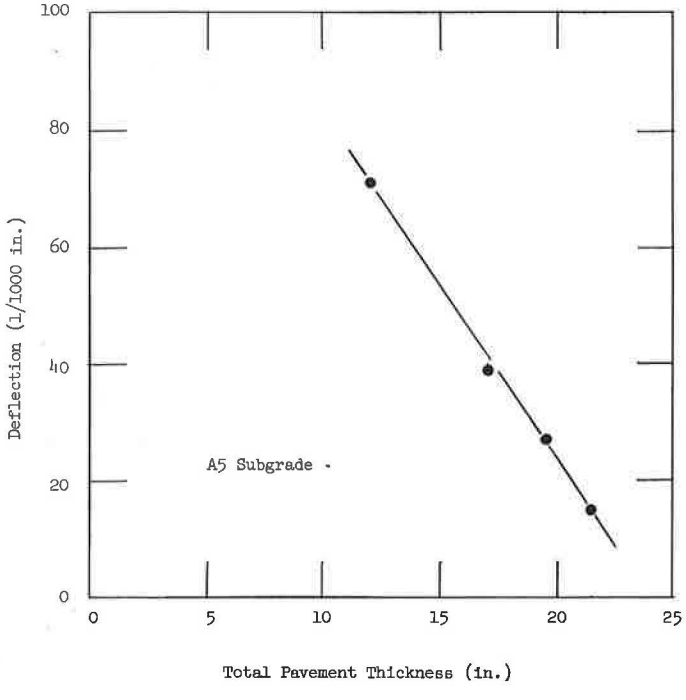

Figure 5. Spring deflection vs pavement thickness over A5 subgrade.

This effect is fairly well documented (10) and is generally attributed to loss of supporting value of the subgrade soil over the winter due to moisture gain and frost action. Decrease of fall deflections over spring deflections, conversely, is generally attributed to loss of moisture during summer and recompaction or reconsolidation of the subgrade from traffic action.

It is also fairly apparent that there is some difference in the magnitude of difference between spring and fall readings for different highways. Examination of the data does not reveal a correlation with climate but there seems to be a relation between the predominant subgrade soil and the variation between spring and fall readings. This effect will be treated more extensively later.

Distress vs Deflection

Of the seven pavements considered in this part of the study, it may be seen in Table 1 that there has been distress or deterioration at some stage of the history of all except US 40W. By and large, despite this distress, it is seen from the data in Table 2 that there has been no appreciable change in average annual deflection that may be attributed to the development of distress.

In two cases, however, it seems apparent that the average deflections have been appreciably reduced by drainage and/or waterproofing of the pavement structure. In one of these cases, US 301, a substantial reduction of deflection followed installation of subgrade drains at several locations in late 1955. Figure 4 shows trenching and release of trapped subgrade water preparatory to installation of a drain. The effect on deflection of opening similar drains was also observed for US 15.

Pavement Thickness

Pavement thickness for the various highways included in Table 1 ranges from $13\frac{1}{2}$ to $22\frac{1}{2}$ in. Comparison of total pavement thickness to average spring and fall deflection is inconclusive in establishing a relationship.

However, within one soil group, A-5, it has been possible to compare changes in thickness to changes in spring deflection. US 40E subgrade is predominantly A-5 silt, as is the major portion of the subgrade for that portion of I-70S studied. US 40E was originally opened to traffic over a surface treated base course and subbase. Subsequently $7\frac{1}{2}$ in. of bituminous concrete was added in binding and wearing courses. Spring deflections are included in Table 2. I-70S has been resurfaced and 1965 spring readings were obtained after addition of a $2\frac{1}{2}$-in. leveling and binder course of bituminous concrete.

The data for these thickness changes, plotted in Figure 5, reveal a fairly good straight-line relationship. An attempt to develop a similar relationship for the addition of an inch of resurfacing for US 301 over a sandy soil was not successful. The implication here is that subgrade soil type is an important parameter influencing pavement deflection. It may be that deflection magnitude changes occur on sandy soils until a certain minimum confinement is attained and thereafter additional confinement in the form of added pavement thickness does not further reduce deflection. On the other hand, the bearing value of a silty soil is not improved by confinement in the same manner as a granular soil, and reduction in deflection here probably results from the increase in pavement stiffness with increases of thickness.

Soil Groups

It was possible to group the subgrade soils into three categories, sandy soils, silty soils, and silty clay soils. Deflection data by soil group are given in Table 3. It has been observed from these data that fall deflections are lower than spring deflections due probably to more favorable climatic and soil conditions. It may be assumed, then, that fall deflections are more indicative of soil and pavement properties to the exclusion of climatic effects than are spring deflections. For this reason fall deflections were analyzed according to soil groups for both inner and outer wheelpaths. Results are plotted in Figures 6-8.

TABLE 3

DISTRIBUTION OF 1955-61 FALL DEFLECTIONS BY SOIL TYPE

Deflection Range (1/1000 in.)	AASHO Soil Type													
	A2, A3, A2-4, A4-2 Sandy Soils				A4, A5 Silty Soils						A7-4, A4-7 Silty-Clay Soils			
	US 301	Md. 404	Total	Percent	US 40W	US 40E	I-70S	US 15	Total	Percent	US 40W	I-70S	Total	Percent
(a) Inner Wheelpath														
0-9	—	—	—	0	1	2	—	—	3	0.4	13	—	13	8.8
10-19	21	1	22	11.8	16	58	22	—	96	12.3	72	7	79	53.7
20-29	108	24	132	70.5	69	140	90	5	304	39.1	14	25	39	26.5
30-39	26	2	28	15.0	57	67	96	7	226	29.1	10	4	14	9.5
40-49	5	—	5	2.7	24	14	39	7	84	10.8	1	—	1	0.7
50-59	—	—	—	0	5	3	19	6	33	4.2	1	—	1	0.7
60-69	—	—	—	0	—	—	12	7	19	2.4	—	—	—	0
70+	—	—	—	0	—	—	5	8	13	1.7	—	—	—	0
(b) Outer Wheelpath														
0-9	—	—	—	0	—	2	—	—	2	0.3	4	—	4	2.7
10-19	1	1	2	0.9	1	62	12	—	75	9.9	57	1	58	39.2
20-29	103	22	125	53.9	34	135	67	3	239	31.5	29	23	52	35.1
30-39	74	4	78	33.6	39	71	102	3	215	28.3	12	11	23	15.1
40-49	25	—	25	10.8	43	18	62	4	127	16.7	8	1	9	6.1
50-59	2	—	2	0.9	33	6	1	6	46	6.1	2	—	2	1.4
60-69	—	—	—	0	8	1	3	4	16	2.1	—	—	—	0
70+	—	—	—	0	9	—	10	20	39	5.1	—	—	—	0

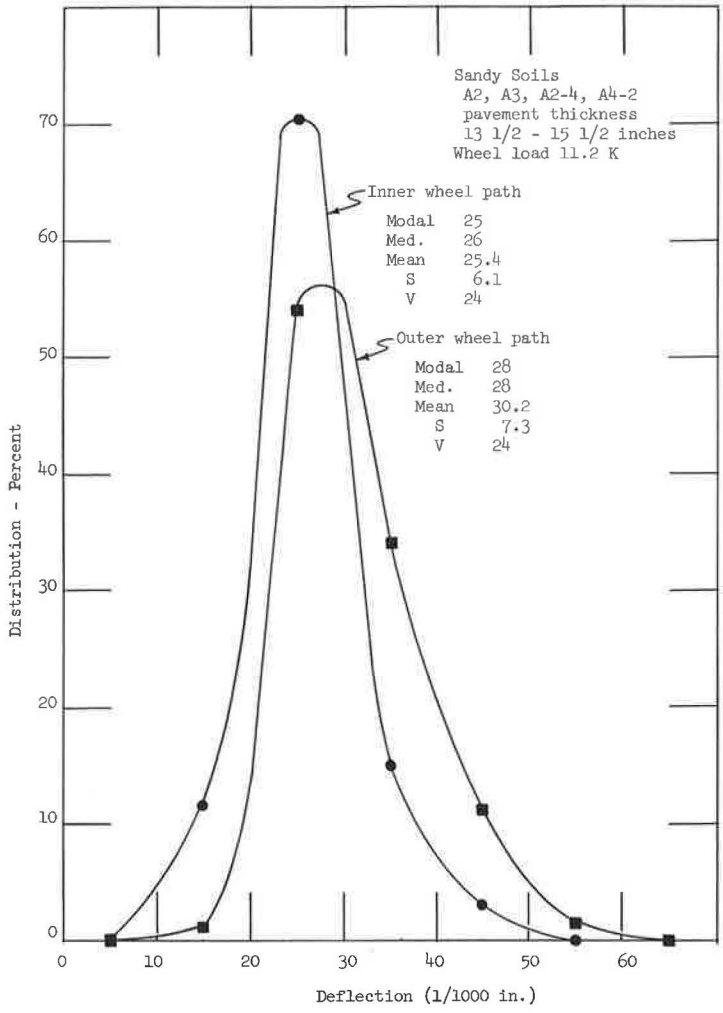

Figure 6. Fall deflection distribution for sandy soils.

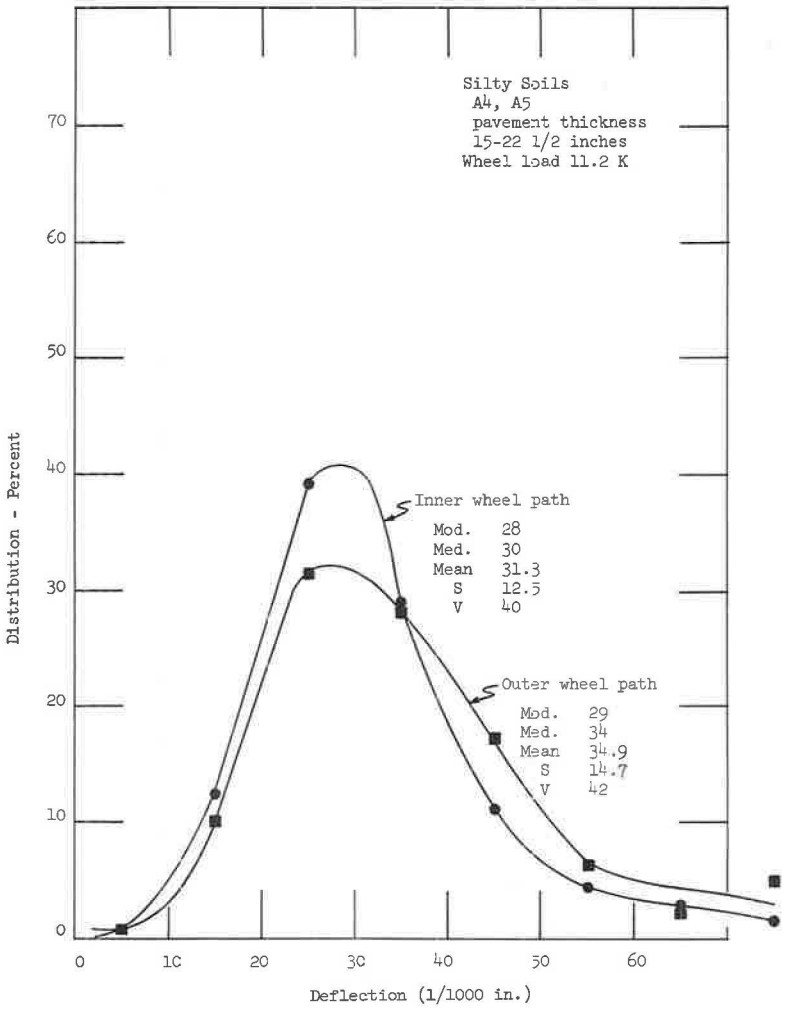

Figure 7. Fall deflection distribution for silty soils.

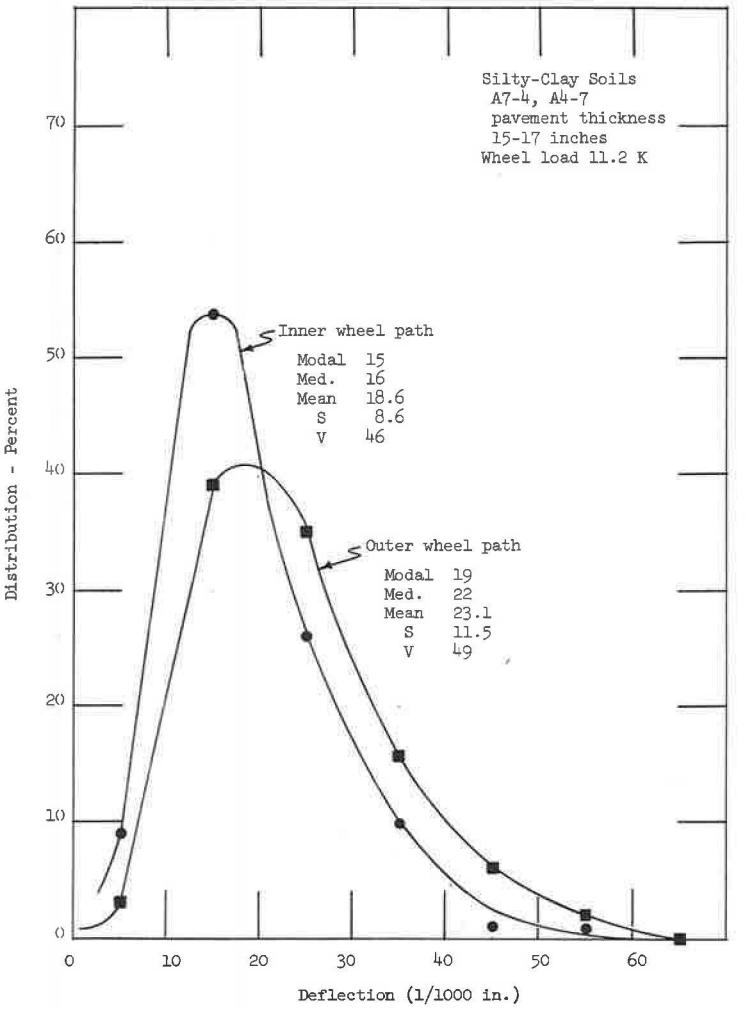

Figure 8. Fall deflection distribution for silty-clay soils.

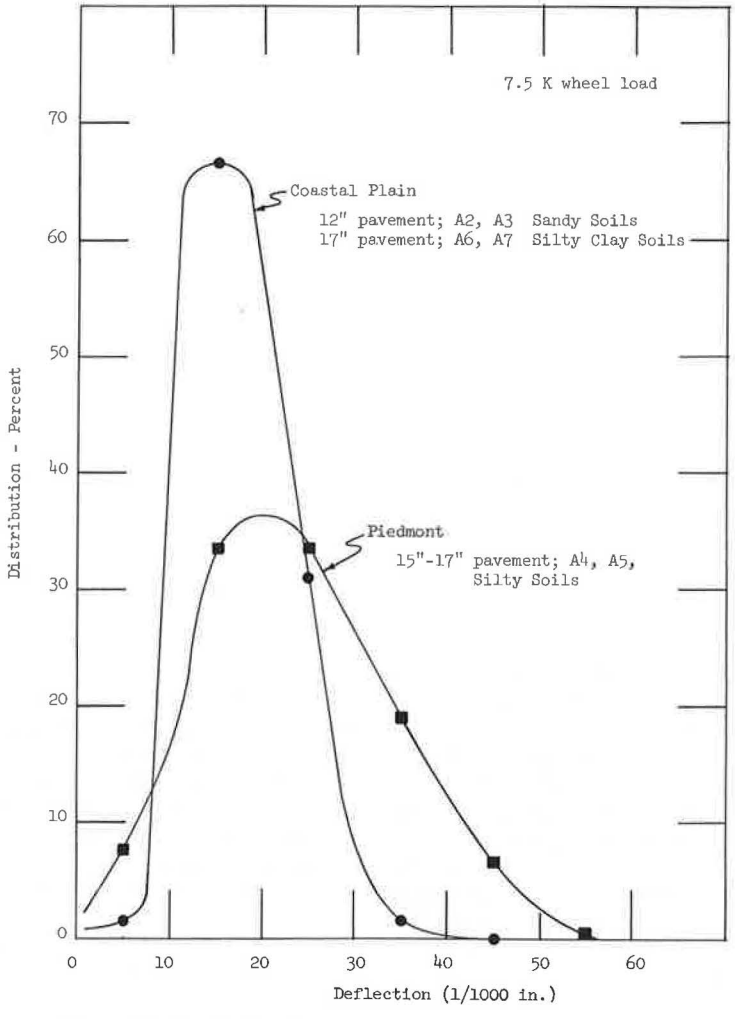

Figure 9. North Carolina deflection data, after Hicks (11).

TABLE 4

AVERAGE DAILY TRAFFIC

Year	US 40W	US 40E	I-70S	US 301	US 301 BB	US 15	Md. 404
1947	3000	–	–	–	–	–	–
1948	3400	–	–	–	–	–	–
1949	3800	–	–	–	–	–	–
1950	4300	–	–	–	–	–	–
1951	5200	–	–	–	–	–	–
1952	6000	–	400	–	–	–	–
1953	6400	–	4100	–	–	–	–
1954	6800	–	4900	–	–	–	–
1955	7200	6600	5200	–	–	–	–
1956	7700	7600	5400	3300	–	–	–
1957	7800	7300	6200	3900	3400	1800	1800
1958	8100	7900	6600	2800	2700	2600	1800
1959	8400	8700	7000	3000	2800	3300	2000
1960	8900	9400	8000	3600	3400	4700	3600
1961	9600	9600	8300	3900	3800	4700	3800
1962	10700	10300	9500	4700	3900	4700	3400
1963	11100	10400	11100	5300	4000	4600	3600
1964	11800	9800	11400	3700	2700	4900	3100

TABLE

FALL DEFLECTIONS BY SOIL

AASHO

Category	A2, A3, A2-4, A4-2 Sandy Soils						A4, A5 Silty Soils				
	Inner Wheelpath		Outer Wheelpath		Avg. Percent	Cum. Percent	Inner Wheelpath		Outer Wheelpath		Avg. Percent
	Frequency	Percent	Frequency	Percent			Frequency	Percent	Frequency	Percent	
Deflection Range (1/1000 in.):											
0-9	6	0.9	2	0.3	0.6	0.6	4	1.8	2	0.9	1.4
10-19	271	39.0	170	25.9	32.4	33.0	65	29.5	36	16.6	23.1
20-29	332	47.8	310	47.2	47.5	80.5	82	37.4	80	36.9	37.2
30-39	66	9.4	128	19.4	14.4	94.9	44	20.0	55	25.3	22.7
40-49	20	2.8	39	6.0	4.4	99.3	15	6.8	26	12.0	9.4
50-59	1	0.1	8	1.2	0.6	100	10	4.5	18	8.3	6.4
60-69	0	0	0	0	0		0	0	0	0	0
Statistics:											
No., n	696		657				220		217		
Mean, $\bar{X}$	22.5		25.9				26.4		30.6		
Median, $\bar{X}$ med.	21.4		24.8				25.0		28.9		
Modal, $\bar{X}$ mod.	21.8		22.4				24.4		26.5		
Est. S	7.6		8.1				11.1		12.4		
Coef. Var. V %	33.7		31.3				42.0		40.5		

It is observed from these figures that outer wheelpath readings are different from the inner wheelpath deflections for each soil. The outer wheelpath determinations exhibit more dispersion, and higher mean, median and modal values than for the inner wheelpath. The outer wheelpath is at the lower edge of the pavement for subgrade drainage purposes and the subgrade has a lesser degree of confinement than does that under the inner wheelpath. It may be that a higher moisture content exists in the subgrade under the outer wheelpath to account for some of the deflection dispersion and the difference in confinement may be another contributing factor.

Of particular interest is the characteristic shape assumed by the two frequency distribution curves for each soil group. The sandy soils are basically from the Coastal Plain, the silty soils from the Piedmont, and the silty-clay soils are residual soils formed from limestones of Frederick Valley of the Triassic Lowland and the limestones of Hagerstown Valley. It is also interesting to note that the silty-clays exhibit the lowest mean value, the sandy soils next lowest and the silty soils have the highest mean and the greatest dispersion. The outer and inner wheelpath distributions are more nearly alike for the silty soil than for the other two soil groups.

The three plots, Figures 6-8, would tend to demonstrate that, for the range of pavement thicknesses tested, soil type has the greatest influence on pavement deflection of all the variables considered.

The silty-clays when undisturbed are blocky in structure and well drained. When this soil is compacted at optimum moisture content over a fairly well drained subsoil, it is relatively impermeable, and, therefore, it is not highly susceptible to moisture changes and to frost action.

Silty soils are compressible and are highly susceptible to moisture changes and to frost action. These properties probably account for the wide dispersion of deflection values for these soils.

Sandy soils when confined exhibit good bearing qualities, are fairly well drained, are relatively insensitive to changes in moisture content and are almost entirely free of frost susceptibility. These observations seem to be confirmed by the narrow dispersion exhibited in the plot of deflection data for these soils.

Corroboration for the observance of differences in deflection distribution for different soil groups is found in work reported by Hicks (11). Figure 9 is a plot from his data illustrating the difference between Piedmont soils and Coastal Plain soils for North Carolina.

5
TYPES—NEW PAVEMENTS

Soil Type												
	A4-7, A7-4 Silty-Clay Soils						A6, A7 Clayey Soils					
Cum. Percent	Inner Wheelpath		Outer Wheelpath		Avg. Percent	Cum. Percent	Inner Wheelpath		Outer Wheelpath		Avg. Percent	Cum. Percent
	Frequency	Percent	Frequency	Percent			Frequency	Percent	Frequency	Percent		
1.4	41	8.8	14	3.1	6.0	6.0	17	11.4	4	2.8	7.1	7.1
24.5	228	48.7	201	45.3	47.0	53.0	42	28.2	42	29.9	29.1	36.2
61.7	133	28.4	160	36.1	32.3	85.3	62	41.7	58	41.3	41.5	77.7
84.4	39	8.4	54	12.1	10.3	95.6	22	14.8	26	18.3	16.6	94.3
93.8	20	4.2	12	2.6	3.4	99.0	4	2.6	10	7.0	4.8	99.1
100	7	1.5	4	0.8	1.1	100	2	1.3	1	0.7	1.0	100
	0	0	0	0	0		0	0	0	0	0	
	468		445				149		141			
	20.5		21.9				22.3		24.9			
	18.5		20.4				22.6		24.1			
	15.5		20.5				22.5		22.3			
	10.1		8.9				10.2		9.7			
	49.3		40.6				45.7		39.0			

Traffic

Average daily traffic history for each of the test pavements is found in Table 4. It is evident that traffic has increased yearly for all of the highways except US 301 and US 301 BB where the opening of an alternate north-south route through the state has caused at least a temporary decrease in ADT.

Despite the changes in ADT, deflection averages have not changed significantly for the duration of these observations, and it seems at this time that traffic volume cannot be counted as a major variable affecting pavement deflection.

NEW PAVEMENTS

Beginning in 1960, as new pavements have been constructed, initial fall deflection readings have been obtained. An analysis of the deflection data obtained on these newer pavements tends to supplement and to confirm the findings from the analysis of the long-term study pavements.

An attempt has been made to include in the analysis all pavements for which data exist. However, a few have been excluded because the subgrade soil type varied widely within the project. When the highways were subdivided by soil groupings, a grouping of clayey soils (A-6, A-7) appeared that was not present for the analysis of the long-term study pavements.

Statistical methods used in this report are discussed in the Appendix. Data are given in Table 5.

Results and Discussion

The results obtained from an analysis of the deflection data from these newer pavements tend to corroborate the results from the deflection studies of the long-term study pavements. Figures 10 through 13 and a rejection of the null hypothesis (see Appendix) show that outer wheelpath deflections are greater than those for the inner wheelpath. The test of the null hypothesis is a means of measuring the difference, if any, of two sets of data. Two factors that may influence this difference are the confinement of the subgrade under the inner wheelpath as opposed to the relative "unconfinement" of the subgrade under the outer wheelpath and the lower elevation of the outer wheelpath that places it in a position to collect more subgrade moisture. From Table 5 it may be seen

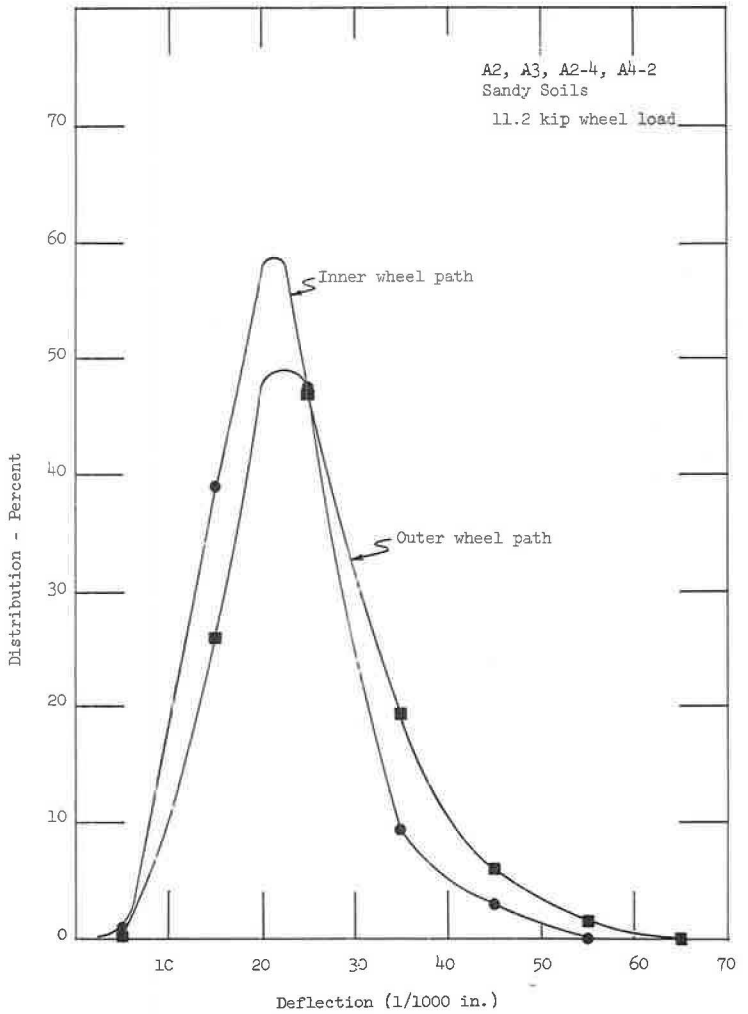

Figure 10. Fall deflection distribution for sandy soils, new pavements.

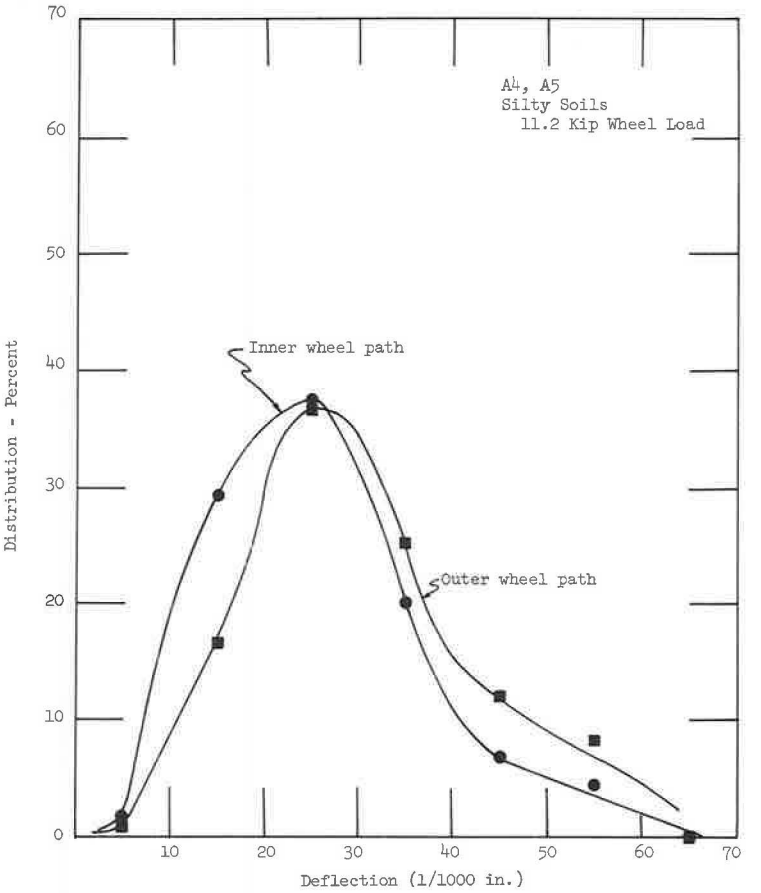

Figure 11. Fall deflection distribution for silty soils, new pavements.

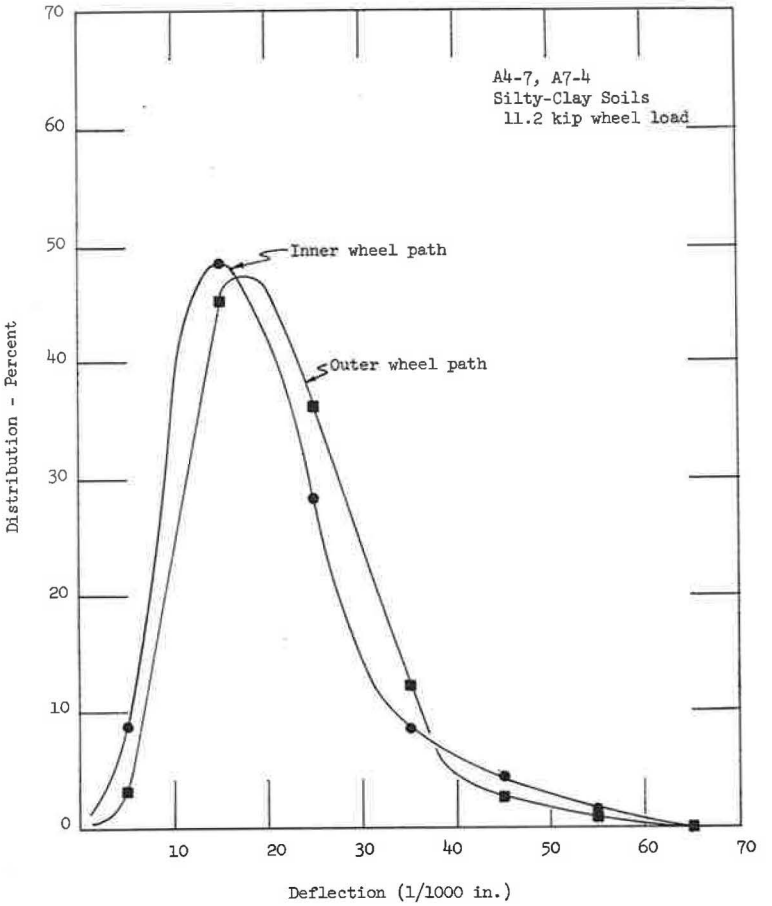

Figure 12. Fall deflection distribution for silty-clay soils, new pavements.

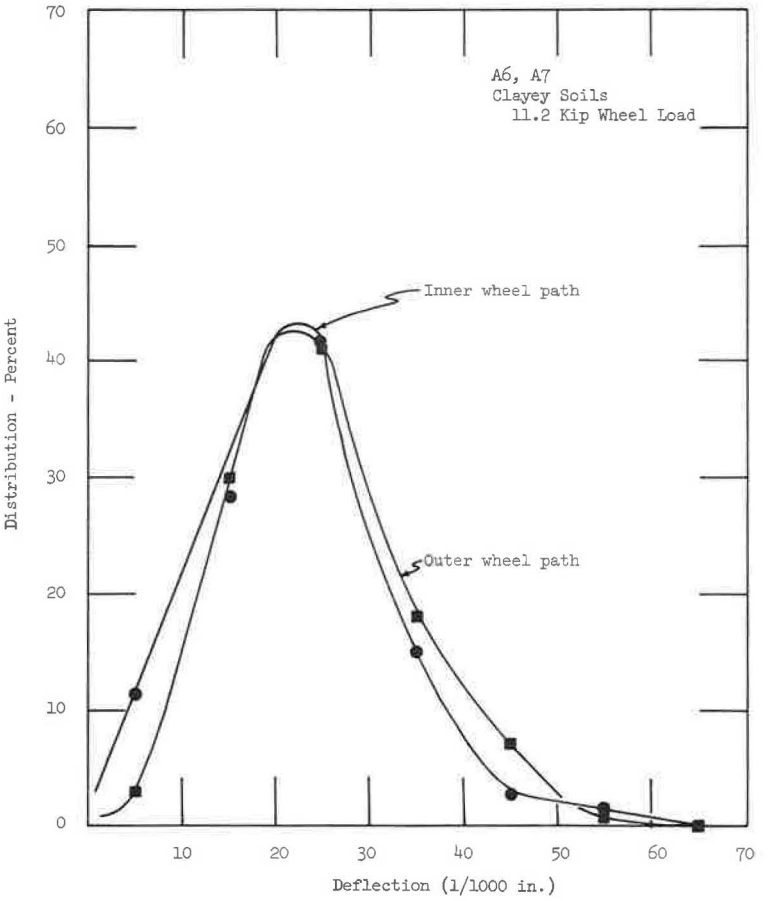

Figure 13. Fall deflection distribution for clayey soils, new pavements.

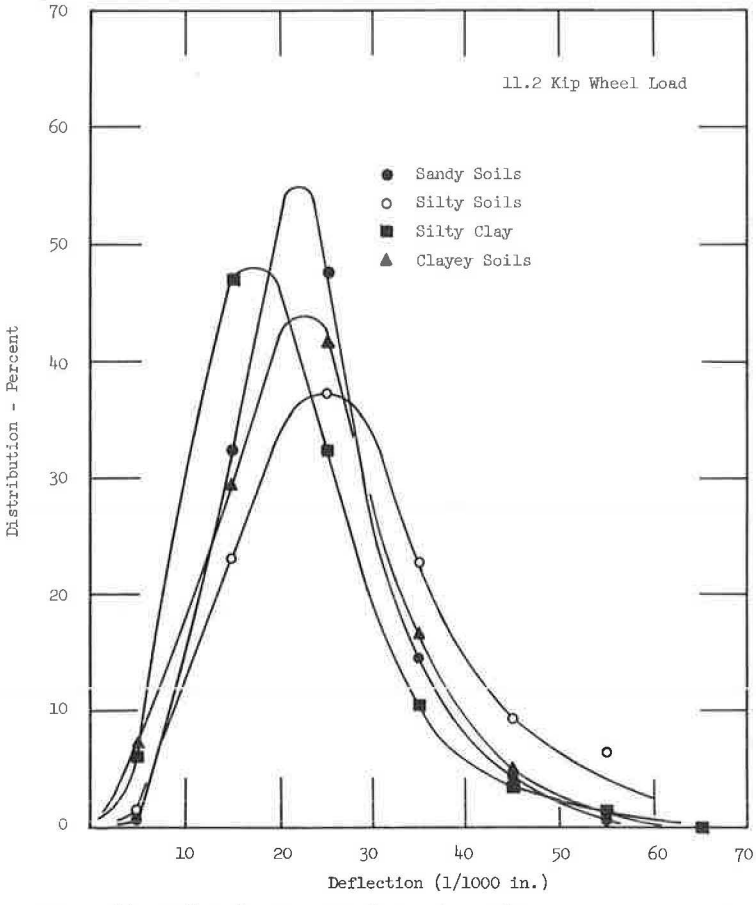

Figure 14. Fall deflection distribution by soil types, new pavements.

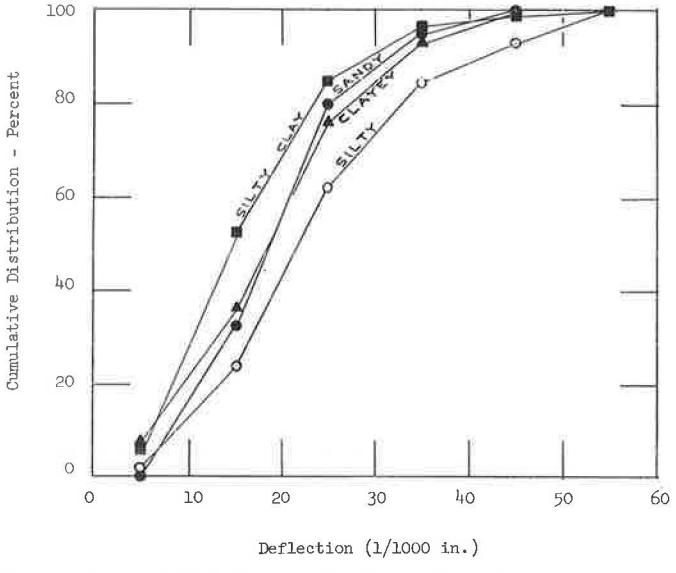

Figure 15. Cumulative fall deflection distribution by soil type, new pavements.

that the greatest difference in the mean deflection between the inner and outer wheelpaths occurs in silty soils. The fact that silt is the soil included here that tends to be the most sensitive to moisture change and also most susceptible to frost heaving probably contributes to the relatively higher outer wheelpath deflections.

From Figures 14 and 15 and Table 5, it may be seen that pavement deflections range from low to high as the subgrade material ranges from silty-clays through sandy and clayey soils to silt, essentially the same effect observed in the analysis of the long-term study pavements.

Also noted is the peakedness of the distribution curve for sandy soils in Figure 10 together with the standard deviation and coefficient of variation in Table 5. These data tend to support the contention that sand should be less susceptible to changes in climatic conditions or pavement thickness than silt. The same contention may be made for clay and for silty-clay but to a lesser degree. The peakedness of the curve also indicates that the deflection of a flexible pavement over a sandy subgrade may be anticipated with a greater degree of confidence than the deflection of a pavement over a silty subgrade. Again, this observation may be made for pavements over silty-clay or clay subgrades but with a lesser degree of confidence than for pavements over subgrades.

SUMMARY

For the range of pavement thicknesses encountered in Maryland among both long-term study pavements and newly constructed pavements, it may be assumed with reasonable confidence that subgrade soil type is a major factor influencing the magnitude and range of deflections. Further, the deflection magnitude and dispersion is greater for the outer wheelpath than for the inner wheelpath for a given pavement thickness and subgrade soil type.

For the long-term study pavements, it was found that spring deflections are higher and more dispersed than fall deflections for the same wheelpath. Also, deflections have not been measurably affected by increase in ADT, nor has onset of distress been signaled by a change in deflections. An apparent inverse proportion has been observed between total pavement thickness and deflection magnitude for pavements over an A-5 subgrade, but this has not been observed for any other subgrade soil type. Finally, deflections have been significantly decreased in magnitude where a known wet subgrade has been drained.

ACKNOWLEDGMENTS

This research was performed under the overall supervision of Allan Lee, Chief, Bureau of Research, Maryland State Roads Commission. Stuart Williams and James A. Kelley of the U.S. Bureau of Public Roads are to be thanked for their advice and consultation during the course of this project. George E. Frangos of the Maryland State Roads Commission was instrumental in guidance of the statistical analysis found in this report. Charles E. Starkey, Bureau of Research, Maryland State Roads Commission, supervised the field testing. The district and resident engineers of the Maryland State Roads Commission were very helpful and cooperative in supplying personnel to perform the field testing. Also to be thanked are Mrs. Irma W. Keith and Miss Barbara Jean Hood for their typing and Frank Stromberg who did all of the drafting for this report.

REFERENCES

1. Mullen, W. G., Clingan, W. R., and Paulis, E. T. Statewide Investigation of Flexible Pavements, First Interim Report. Maryland State Roads Commission HPS-HRP Project in cooperation with U.S. Department of Commerce, Bureau of Public Roads, July 1965.
2. Lee, A. Experience with Flexible Pavements in Maryland. HRB Bull. 136, p. 1, 1956.
3. Williams, S., and Lee, A. Load-Deflection Study of Selected High-Type Flexible Pavement in Maryland. HRB Bull. 177, p. 1, 1958.

4. Mullen, W. G., Paulis, E. T., and Kennedy, W. M. Condition Surveys Along I-70S, First Interim Report. Maryland State Roads Commission HPS-HPR Project in cooperation with U.S. Department of Commerce, Bureau of Public Roads, 1964.
5. Woods, K. B., and Lovell, C. W. Physiographic Regions of North America. Map, 1958.
6. Maryland Geologic Survey. Maps of Maryland Counties.
7. Maryland Geologic Survey. Complete Highway Reports, 1898-1910.
8. Mathews, E. B., Shirley, H. G. Report on Road Materials of Maryland. National Research Councils' Road Materials, 1917.
9. Lee, A., et al. Deflection Test Data Tabulation. Maryland State Roads Commission HPS-HPR Project—Statewide Investigation of Flexible Pavements. 1965, unpublished.
10. Yoder, E. J. Principles of Pavement Design. John Wiley and Sons, 1959.
11. Hicks, L. D. Flexible Pavement Deflection Study in North Carolina. Proc. HRB, Vol. 39, p. 403, 1960.

Appendix

STATISTICAL METHODS

We usually perform statistical analysis upon data in order to learn something about the broader field which the data represent. The techniques of statistical analysis are such that we may, with a stated degree of confidence, generalize from what is found in the figures at hand to the wider phenomenon which they represent. In technical language, we regard a set of data as a sample drawn for a larger universe. After the sample has been studied, the question arises as to what conclusions may be drawn concerning this universe.

The process by which, on the basis of samples, we draw a conclusion about the universe from which the sample is taken is called inference. Thus, statistical inference is always a conclusion concerning the value of the statistical measures describing the data of the universe—the mean, the standard deviation, and the like. Whatever the specific problem, a statistical inference is a judgment of one sort or another about the values of certain measures which describe the universe in the same way that similar measures describe the sample.

A measure of the central tendency or the tendency of a set of data to group about a particular value in the form of a bell-shaped curve is often useful. There are three commonly used methods of measurement, and all three are given in the statistical data presented in this report. The most frequently used measurement of central tendency is the mean ($\overline{X}$). This is the arithmetic mean or average. There is one disadvantage in that if there exist in the data some extreme values the calculated mean may not be indicative of the data. Two other measurements of central tendency are the median and the mode. The median ($\overline{X}$ med.) is the middle value of the data and the mode ($\overline{X}$ mod.) is that value which occurs most frequently. As the frequency distribution curve appoaches a normal curve, the mean, median, and mode approach the same value.

Other statistical measurements used in this report were the standard deviation (S) and the coefficient of variation (V). These are both measures of the dispersion of a group of data. The coefficient of variation is the standard deviation divided by the mean and multiplied by 100 or, in other words, it is the standard deviation expressed as a percentage of the mean. As an example of the usefulness of the standard deviation, certain statements may be made concerning those frequency distributions which are approximately normal: 50 percent of the data will fall within the range of $\overline{X} \pm 0.6745$ S, 68.3 percent will be included by $\overline{X} \pm 1.0$ S, and 95.5 percent of the values will be in the range of $\overline{X} \pm 2.0$ S.

In the study of engineering problems we are often concerned with the comparison of two or more groups of figures. The more complex forms of investigation will be ignored and the relatively simple technique of comparing the means of two sets of data will be utilized. In comparing two means, the basic question is whether the differences which appear in the actual data may be considered significant or not. The general method for dealing with such a problem is the test of the null hypothesis.

The question of whether the observed difference between the means of two groups of data is significant or not refers to the character of the two universes from which the respective sections of the data have been drawn. If the difference in the sample means is so great as to lead us to conclude that the means of the two universes are not equal, we say that the observed difference is significant. If, in contrast, the sample means are so close together that such a conclusion cannot be drawn (that is, that the means of the two universes are equal), we say that the observed difference is not significant. The whole problem of making such a test is referred to as one of "significant differences."

The null hypothesis—that the mean of the differences distribution of many pairs of samples is zero—tests the question of whether the difference between two sets of data is significant or not. Based on the properties of the normal distribution, when dealing with large samples ($n > 30$), the two samples are examined for differences of the means that are great enough to discredit the null hypothesis. The characteristics of the data used to evaluate this hypothesis are $\overline{X}$ and S.

Example:

	Sample 1	Sample 2
$\overline{X}$	100	80
S	8	6
n	64	49

1. $\sigma_d^2 = \frac{S_1^2}{n_1} + \frac{S_2^2}{n_2}$

$\sigma_d^2 = \frac{8^2}{64} + \frac{6^2}{49}$

$\sigma_d^2 = 1 + 0.735$

$\sigma_d = 1.32$

2. $d = \overline{X}_1 - \overline{X}_2$

$d = 100 - 80$

$d = 20$

3. $Z = \frac{d - 0}{\sigma_d}$

$Z = \frac{20 - 0}{1.32}$

$Z = 15$

At a 99 percent confidence level, $Z = 2.33$. Therefore, reject the null hypothesis.

Using the procedure in the example and the data for the standard deviation S and the mean $\overline{X}$ (from Table 7, Ref. 1, p. 34), the following values for Z and P are obtained:

Soil	Z	P
Sandy	7.94	0.999
Silty	3.72	0.999
Silty-Clay	2.22	0.987
Clayey	2.27	0.988

Z is a measure of the difference in the means of the inner and outer wheelpaths for a soil type, and P is the probability that the difference found is a significant difference and not a difference which may have occurred by chance. As can be seen by the high values of P, there is an extremely small probability that the observed difference occurred by chance. Instead, this shows there is a significant difference between the deflection readings obtained for the inner wheelpath and those obtained for the outer wheelpath, thereby supporting the conclusion of higher deflections being obtained in the outer wheelpath than in the inner wheelpath.

Discussion

F. P. NICHOLS, JR., Assistant Engineering Director, National Crushed Stone Association—The authors should be complimented on their fine paper. The statistical inferences they have drawn from their accumulated mass of deflection data in Maryland generally support the inferences drawn in neighboring Virginia and reported here three years ago (12). I refer particularly to the importance of the soil area, the major influence of subgrade soil type on deflection values, and the relatively minor influence of base type and thickness within a given soil area.

The Benkelman beam seems to be getting wider and wider use as an indicator of flexible pavement performance. Besides this paper, four others scheduled in a Maintenance Department session (13) describe uses of the Benkelman beam or advocate the use of even quicker test methods because of reasonably close correlations between results on the same pavements by both methods. The beam is a useful tool, but like most tools it can be misused or its results may be misinterpreted. An intelligent appraisal of test data is essential.

To begin with, corrections must be made for errors which may creep into the results of tests performed by either the WASHO or the rebound method. When the pavement to be tested has appreciable slab strength because of a particularly stiff base, such as one stabilized with cement or asphalt, there is usually some movement of one or both of the datum beam's support legs during the course of a test. Uncorrected, this movement might lead to an appreciable overestimate of the true deflection value in the WASHO method, or some underestimate in the rebound method.

The Canadian Good Roads Association has published (14) a standard test procedure by which it is possible to obtain the correct value of total rebound deflection regardless of possible slight movement of the front support legs. Three dial readings are recorded: (a) an initial reading when the load is directly over the probe, (b) an intermediate reading with the load stopped at a point 8 ft 10 in. beyond the probe, and (c) a final reading after the load has passed completely out of range. The apparent, or uncorrected rebound value, X_A, is twice the difference between readings (a) and (c). The support leg movement, Y, is essentially equal to twice the difference between readings (b) and (c). From the geometry of the device it is determined that the true rebound value, X_T, may be computed thus:

$$X_T = X_A + 2.91Y$$

Though the support leg movement Y is usually quite small, if indeed there is any at all, the value of 2.91 by which it must be multipled makes the correction of significant importance in preventing overestimates of the strength of pavements with stabilized base layers.

Finally, even if all corrections are made there is still danger of misinterpreting the importance of low deflections on certain pavements. For example, a comparison may be cited between corrected rebound deflection values from a 9000-lb wheel load on two typical Virginia pavements. The first has been carrying traffic, which now includes over 500 trailer trucks and buses daily in one direction, without appreciable serviceability loss since late in 1961. Its design included the following:

Asphaltic concrete binder and surface	4.5 in.
Dense graded crushed granite	6.0 in.
Granular soil borrow, CBR 20	6.5 in.
Cement treated subgrade	6.0 in.
Total	23.0 in.

Average rebound deflection values measured in three successive years during the spring thaw period on the above pavement were:

1963	0.044 in.
1964	0.041 in.
1965	0.044 in.

The second pavement was designed to provide economical service on a very lightly traveled primary highway carrying only 8 or 10 heavy vehicles per day, and seems to be fulfilling its purpose, though now only in its second winter. Its design includes only:

A triple surface treatment	1 in. ±
Roadside borrow (A-4) stabilized with cement	5 in.
Cement-treated subgrade	7 in.
	13 in.

Rebound deflection values measured soon after construction and again the following spring have averaged:

Fall 1964	0.015 in.
Spring 1965	0.027 in.

Which of the above examples is the stronger? Which would withstand the greatest number of repetitions of the maximum legal axle load? On the basis of deflection alone, one would have to say that the somewhat more rigid but definitely more brittle soil cement is the stronger. But experience and common sense should say that the better balanced, more flexible design of the first example should be the most serviceable, in the truest sense of the word. These examples are cited just to point out the limitations of the Benkelman beam in assaying composite strength.

References

12. Nichols, F. P., Jr. Deflections as an Indicator of Flexible Pavement Performance. Highway Research Record 13, p. 46, 1963.
13. Highway Research Board. Evaluation of Pavements by Deflection Studies for Maintenance Purposes. Highway Research Record 129, 1966.
14. Canadian Good Roads Association. Pavement Evaluation Studies in Canada. Proc. International Conf. on Structural Design of Asphalt Pavements, Univ. of Michigan, 1962, pp. 137-218.

W. G. MULLEN, Closure—The prepared discussion by Mr. Nichols is appreciated, and the point he raised with respect to the rebound interpretation is indeed significant. Though it is not stated in our paper, both initial deflections and rebound recoveries were recorded and due cognizance was taken of these values in analysis of the Maryland data.

With reference to the example of layer design vs deflection that Mr. Nichols cites, we would agree that in our experience deflection was not relatable to performance, nor was change in deflection related to change in performance. Our major finding was that deflection seems to be related to subgrade soil type for the pavements encountered in Maryland.

Pulse Velocities in Flexible Pavement Construction Materials

PHILLIP G. MANKE, Assistant Professor of Civil Engineering, Oklahoma State University, and
BOB M. GALLAWAY, Research Engineer, Texas Transportation Institute

•IN RECENT years engineers have become increasingly interested in the use of vibratory techniques for in situ testing of roads and road construction materials. Although these techniques are still in the development stage, they show promise of becoming rapid nondestructive testing methods for the evaluation of road material quality and for assessing the probable performance of an entire pavement structure.

Burmister's theoretical equations (1) for the stresses and displacements in layered elastic systems show that the stresses and deflections imposed by traffic on a roadway depend on the relative values of the modulus of elasticity and the thickness of the respective layers forming the pavement structure. Theory also indicates that the dynamic moduli of elasticity of the layers as well as their thickness can be determined from vibrational measurements made in the field both during and after construction (2, 3).

While a considerable number of experimental and theoretical studies of the propagation of vibrations in pavement structures have been made, the development of dynamic testing techniques as an engineering method has been slow. This is due primarily to the difficulties of interpreting the relationships between velocity of propagation and frequency of vibrations generated at the surface with the dynamic moduli of elasticity and thicknesses of the layers. Divergence of opinion among the respective investigators on the interpretation of results in terms of the mechanical properties has also been a contributing factor to the slow development of these techniques (4).

The present study employs a laboratory vibrational technique to determine the velocity of propagation of a compressional wave through common road construction materials. This investigation is a part of National Cooperative Highway Research Program Project 1-6, conducted by the Texas Transportation Institute. One of the objectives of NCHRP Project 1-6 is to study and evaluate the effectiveness of vibratory testing systems for estimating the stiffness and thickness of individual pavement layers in place. The Shell road vibration machine, a high-frequency electromagnetic vibrator developed by the Royal Dutch Shell Company of Amsterdam, Holland, is one such device being studied.

A series of flexible pavement structures designed for the specific purpose of calibrating the Shell vibratory equipment was constructed at the Texas A&M Research and Development Annex near Bryan, Texas. This test facility was statistically designed to furnish a selection of pavement sections composed of subgrade, subbase and base layers of varying thickness and type of material with a variable depth of asphaltic concrete surfacing.

The test facility consisted of 27 pavement sections constructed in three parallel lanes of nine sections each. Each pavement section was 12 ft wide and 40 ft long. The thickness and type of material composing the various layers of the respective sections are given in Table 1.

Typical flexible pavements are composed of layers arranged so that the moduli of elasticity decrease with depth. In designing the test facility it was desired to vary this arrangement in the base and subbase layers so as to have some sections in which a

Paper sponsored by Committee on Flexible Pavement Design and presented at the 45th Annual Meeting.

TABLE 1

DESIGN OF TEST SECTIONS

Sec. No.	Actual Design					
	Layer Thickness (in.)			Material Type[a]		
	Surface	Base	Subbase	Base	Subbase	Subgrade
1	5	4	4	C	R	NC
2	1	12	4	C	R	NC
3	1	4	12	C	R	NC
4	5	12	12	C	R	NC
5	5	4	4	R	C	NC
6	1	12	4	R	C	NC
7	1	4	12	R	C	NC
8	5	12	12	R	C	NC
9	5	4	4	R	R	GC
10	1	12	4	R	R	GC
11	1	4	12	R	R	GC
12	5	12	12	R	R	GC
13	5	4	4	C	C	GC
14	1	12	4	C	C	GC
15	1	4	12	C	C	GC
16	5	12	12	C	C	GC
17	3	8	8	L	L	SC
18	1	8	8	L	L	SC
19	5	8	8	L	L	SC
20	3	4	8	L	L	SC
21	3	12	8	L	L	SC
24[b]	3	8	8	R	L	SC
25	3	8	8	C	L	SC
26	3	8	8	L	R	SC
27	3	8	8	L	C	SC
28	3	8	8	L	L	NC
29	3	8	8	L	L	GC

[a]Materials Code: Surface—Hot-mix asphaltic concrete, all sections; base and subbase—R = raw (untreated) crushed limestone, L = lime-treated crushed limestone, C = cement-treated crushed limestone; Subgrade—NC = natural clay, GC = clayey gravel, SC = sandy clay.

[b]Nos. 22 and 23 were duplicate sections and were not constructed.

layer having a high modulus was overlaid by a layer with a low modulus. It was also desirable to obtain as wide a range of elastic moduli as possible in the three materials used in the subgrade layers.

Pulse velocity measurements were made on laboratory specimens of the respective materials using the equipment and procedure described herein. These velocities were considered indicative of the relative elastic moduli and aided in the selection and positioning of the subgrade materials and in determining the amount and type of stabilizing agent to be used with the crushed limestone for the base and subbase layers.

ELASTIC WAVE VELOCITY

The theory of transmission of impulses through a solid body has been studied extensively in connection with the propagation of earthquake waves through the earth. In an

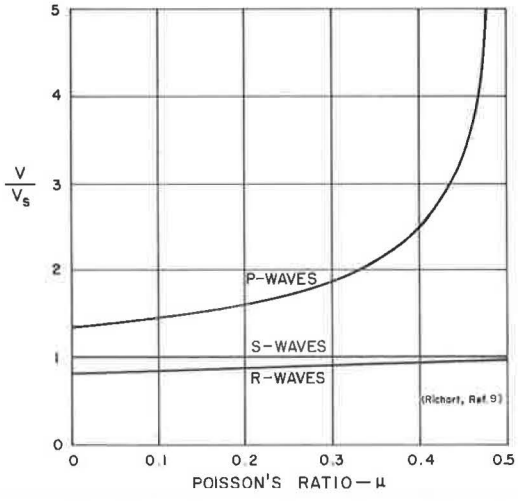

Figure 1. Relation between Poisson's ratio (μ), and velocities of propagation of compression (P), shear (S), and Rayleigh (R) waves in a semi-infinite elastic medium.

extended solid any generated impulse can be shown to separate into two groups of waves: a longitudinal or compressional wave, in which the particles vibrate in a direction parallel with the direction of wave transmission, and a transverse or shear wave, in which the particles vibrate in a direction perpendicular to the direction of wave transmission. In some instances a surface wave may be generated at the interface between two different media, either on a free surface or in a layered system. The general mode of vibration of surface waves is either an elliptical motion in the vertical plane in the direction of wave transmission (Rayleigh waves) or transverse to the direction of propagation in the horizontal plane (Love waves) (5). Compressional and shear waves travel with a velocity determined by the elastic constants and the density of the medium. The longitudinal or compressional wave travels with the greatest velocity.

The motion that is produced in an elastic body by a suddenly applied force is not transmitted immediately to all parts of the body. Initially, the most remote parts of the body are undisturbed and the deformations that are produced by the stress are propagated through the body in the form of elastic waves. The theory of the propagation of these waves is developed from the fundamental static stress-strain relationships of elastic bodies. The theoretical development of the equations of plane wave propagation can be found in most texts on elastic theory (6), seismic waves (7), or sound transmission (8).

The equations of motion in terms of particle displacement in a homogeneous, isotropic, elastic medium define the transmission of two types of waves, i.e., compressional and shear waves. In the case of a compressional type wave the velocity of propagation, V_c is expressed by

$$V_c = \sqrt{\frac{E(1-\nu)}{\rho(1+\nu)(1-2\nu)}} \qquad (1)$$

and in the case of a shear type wave the velocity of propagation, V_s is

$$V_s = \sqrt{\frac{E}{2\rho(1+\nu)}} \qquad (2)$$

where

E = Young's modulus,
ν = Poisson's radio, and
ρ = mass density.

The relation between compressional, shear, and Rayleigh wave velocities and Poisson's ratio in a semi-infinite elastic medium is shown in Figure 1 (9).

Equations 1 and 2 have been employed directly or in slightly modified form by many investigators to compute the dynamic modulus of elasticity of various materials. The use of these equations is based on the assumption that the materials behave as perfectly elastic solids. This is not strictly true, since most materials exhibit plastic as well as elastic properties.

Long et al. (10) reported good agreement between dynamic modulus values computed from pulse velocities in concrete and those determined from static flexural strength tests. However, there appears to be some doubt as to the value of dynamic moduli calculated from measured pulse wave velocities. Batchelder and Lewis (11) derived no benefit from calculating modulus values from pulse velocity measurements in their study of freeze-thaw deterioration of concrete specimens. They found the changes in velocity with deterioration of the specimen to be a more accurate indication than calculated values of moduli of elasticity. Whitehurst (12) also states that it appears that the pulse velocity (compressional or shear wave velocity) itself is as good a criterion for comparison as any other value which might be calculated from it.

EXPERIMENTAL DETAILS

Equipment

The equipment used to measure compressional wave velocities consisted of four major components: (a) a pulse generator, (b) a source transducer, (c) a receiver transducer, and (d) an oscilloscope. These four components are shown in Figures 2 and 3, and schematically in Figure 4.

A schematic wiring diagram of the pulse generator is shown in Figure 5. The generator has two functions: (a) to provide the electrical pulse necessary to actuate the source transducer, and (b) to trigger the oscilloscope. Operating on 110-volt, 60-cycle alternating current, the pulse generator provided an 1100-volt, 60-cps DC spike pulse to the source transducer. The spike pulse was obtained by the discharge of a condenser through a thyratron tube. The pulse generator also provided an 11-volt DC signal (1/100 of the pulse voltage) to the triggering circuit of the oscilloscope at the same instant that the compressional pulse was transmitted to the specimen.

The source and receiver transducer assemblies were constructed identically. The transducer was a $1\frac{1}{2}$-in. diameter by $\frac{1}{8}$-in. thick lead titanate zirconate ceramic disc. This commercially available (Clevite Corporation) piezoelectric disc with a resonant frequency of 140 kc/sec was glued with epoxy cement between two brass discs of the same size. A solid lucite cylinder was cemented to one face of this assembly. The total cylindrical assembly was $1\frac{1}{2}$ in. in diameter and $2\frac{1}{8}$ in. tall.

The brass discs were the terminal electrodes of the assembly. The disc between the lucite cylinder and the ceramic disc served as the positive terminal and the other brass disc as the negative terminal. The ground terminal was placed in contact with the specimen being tested and served to protect the ceramic crystal as well as to prevent the passage of current through the material. An electrical pulse was applied across the ceramic disc, exciting thickness modes of vibration, and transmitting a compressional wave or pulse into the bottom of the cylindrical specimen.

When this wave reached the top of the specimen, the particle disturbance of the material was transmitted to the receiver, a duplicate of the source transducer, connected directly to the vertical input connection on the oscilloscope. This piezoelectric transducer converted the mechanical energy to an electrical signal which was amplified and displayed on the oscilloscope.

The oscilloscope was a Tektronix type RM545B unit with a type B wide-band high gain plug-in unit (peramplifier unit). This type of instrument features two time base generators which can be used in delayed sweep operations for highly accurate time measurements. With the preamp unit, the oscilloscope has a calibrated vertical deflection sensitivity of 0.005 volts/cm to 20 volts/cm, and a horizontal time sweep range of 2 microsec/cm to 1 sec/cm with an accuracy within ±3 percent. The rise time of the amplifier is 18 nanosec (1×10^{-12} sec).

Procedure and Accuracy

The procedure used for determining the compressional wave velocity was relatively simple. A compressional pulse was introduced into one end of a cylindrical specimen and the length of time it took the pulse to travel to the other end was accurately measured. The velocity V_c was the ratio of the length of the specimen to the travel time of the pulse.

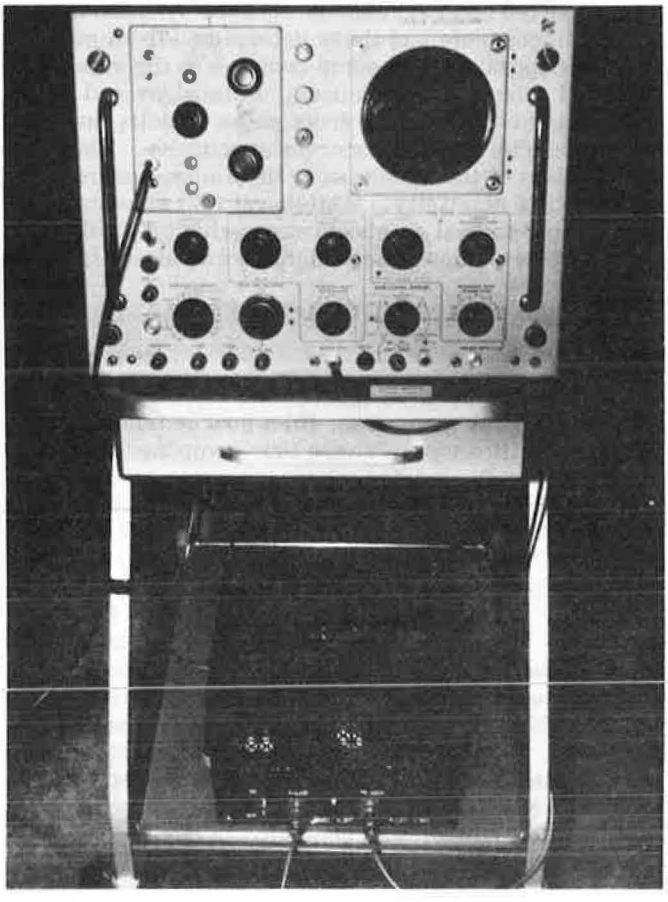

Figure 2. Oscilloscope and pulse generator on mobile cart.

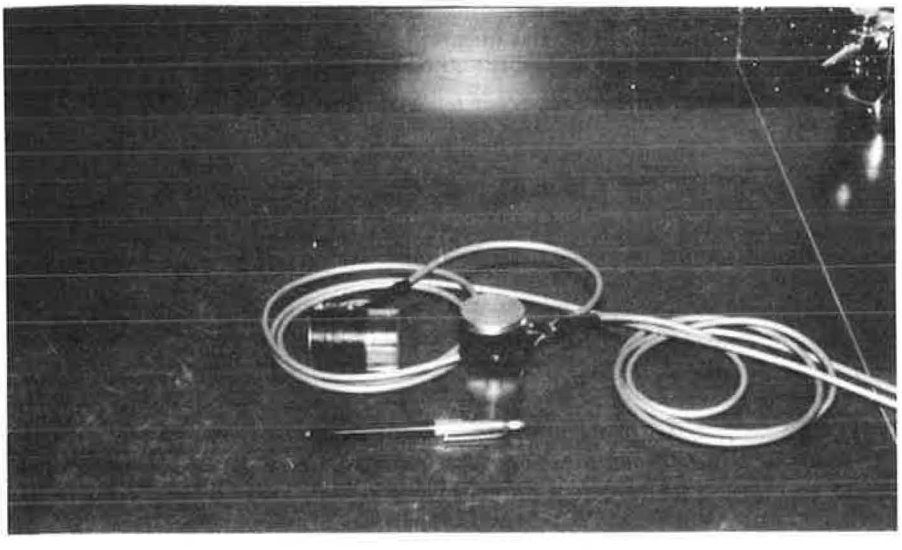

Figure 3. Source and receiver transducer assemblies.

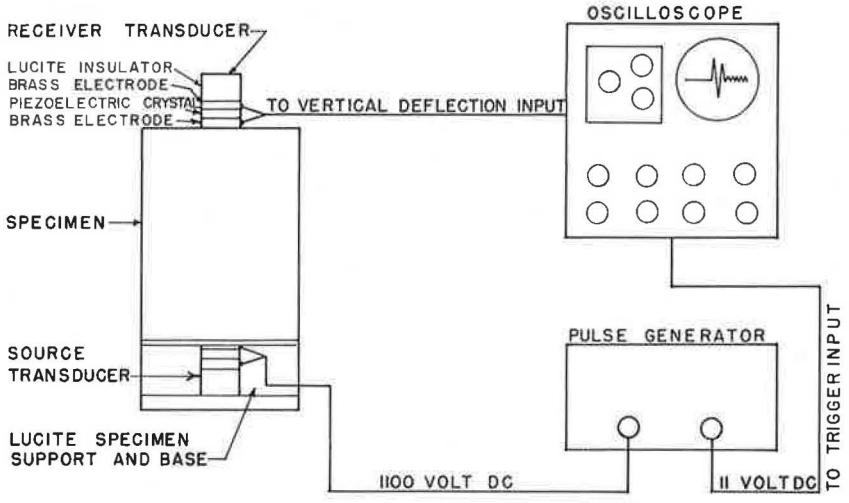

Figure 4. Schematic diagram of equipment components and test arrangement.

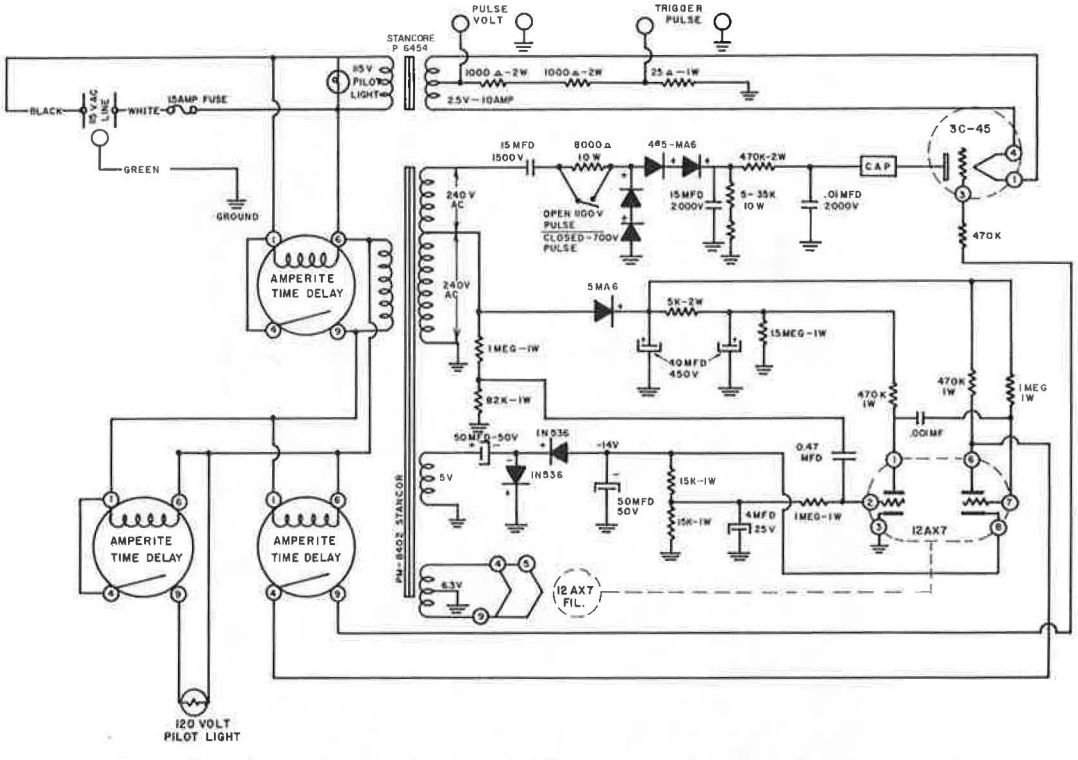

Figure 5. Schematic wiring diagram of pulse generator (courtesy of A. M. Gaddis).

A cylindrical specimen was placed on top of the source transducer and the receiver was placed in the center of the top face of the specimen. The propagation path was along the vertical axis of the specimen and the pulse traveled from the bottom to the top. To improve the coupling between the transducers and the material being tested a light coat of vaseline or silicone grease was applied to the face of the transducers

before they were placed in contact with the specimen. The oscilloscope was initially triggered by the pulse generator at the same time that voltage was applied across the source transducer. When the triggering circuit of the oscilloscope was actuated, it caused an electron beam to travel in a straight line from left to right across the face of the cathode ray tube. As the input compressional wave reached the receiving transducer, a voltage was generated which caused the electron beam of the oscilloscope to deflect vertically. The travel time of the compressional wave through the specimen was measured from the beginning of the electron beam trace to the beginning of the vertical deflection or "first arrival."

A photograph of two typical electron beam traces is shown in Figure 6. The top trace is for a specimen of sandy clay and the bottom trace is for a specimen of clayey gravel. The measured travel time of the compressional wave in the sandy clay was 200 microsec and the computed velocity was 3407 fps. For the clayey gravel specimen, the travel time was 350 microsec and the computed velocity was 1950 fps.

The electron beam trace was a steady display on the oscilloscope screen. The travel time was determined by moving the display to the left and reading the time per cm of length of the initial horizontal portion of the trace directly from the oscilloscope dials. This time reading was then corrected for the travel time in the transducer assemblies. The correction was made by subtracting a "transducer constant" from the gross travel time read from the dials. This constant was the length of time required for the wave to travel through the two brass ground plates of the source and receiver transducer assemblies.

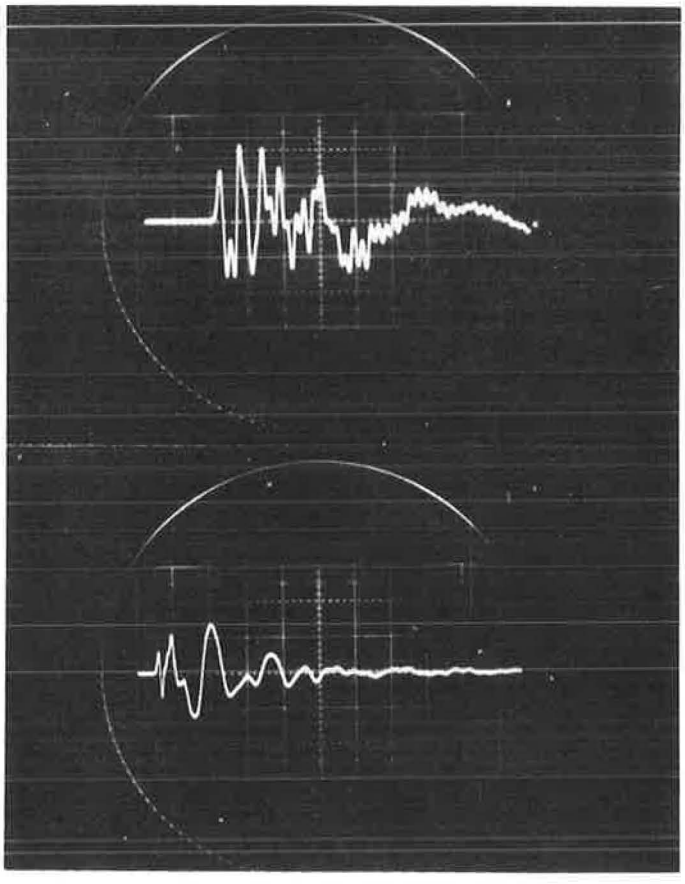

Figure 6. Typical pulse traces for sandy clay (top) and clayey gravel (bottom).

TABLE 2

STEEL STANDARD OBSERVATIONS

Length of Steel (in.)	Gross Travel Time (microsec)	Velocity (fps)
3.025	17.1	19,240
5.956	30.0	19,090
12.008	56.8	18,950

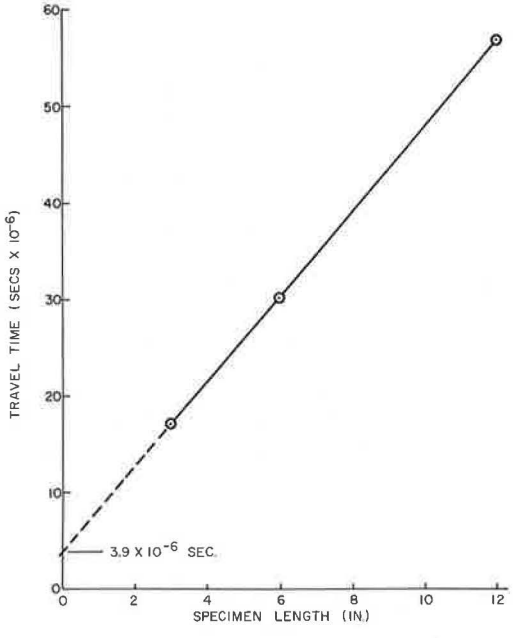

Figure 7. Determining transducer constant by extrapolation from steel specimen observations.

The transducer constant was obtained by placing the assemblies in direct contact and measuring the travel time as described above. For the set of transducers used throughout the study this constant was 4.14 microsec. To check this value, travel times corresponding to the first arrivals through steel samples of different lengths were determined. By plotting travel time against gage length and extrapolating to zero length the transducer constant was determined. Results were in excellent agreement with the direct measured value.

The steel specimens were cut from the same bar of $1\frac{1}{2}$-in. diameter SAE 1020 cold-rolled steel. The travel time observations and calculated velocities are shown in Table 2. Figure 7 shows the plot of these measurements and their extrapolation to zero length. These steel specimens were measured frequently throughout the study and served as standards to demonstrate that the equipment was giving consistent readings.

Actually the "first arrival" is not an abrupt deflection of the horizontal electron beam trace. Even when the received signal is very strong it arrives gradually rather than suddenly with only a slight positive increase in slope initially. The "toe" of this slope recedes to the left toward shorter times as the amplification is decreased and wavelength is increased. This gradual onset of the first arrival is the principal limitation on the accuracy of the velocity determination. With high amplification the uncertainty of locating the beginning of the toe could be reduced to about 0.04 microsec in favorable cases.

The total transit time measurements ranged from a minimum of 4 microsec to a maximum of 600 microsec. For all of the velocity determinations made, the readings could be repeated to within ± 2 divisions of the multiplier dial. The corresponding time interval depended upon the setting of the delay time dial and varied from ± 0.04 microsec to ± 4.0 microsec. Over the range of transit times measured, the accuracy of the readings is within ± 1 percent.

Materials

Subgrade, Subbase, and Base. —Three different types of locally available materials were used for the subgrade portions of the test sections. These materials consisted of a highly plastic black clay indigenous to the construction site, siliceous gravel with a small amount of clay binder and a red sandy clay—the latter two materials coming from pits located a few miles from the site of construction. The base and subbase material was a crushed limestone from a quarry near New Braunfels, Texas. Depending upon the design of a given section (see Table 1), this material was placed in the untreated condition or was stabilized with 3 percent lime or 4 percent portland cement.

A summary of the gradation, Atterberg limits and classification of each of these materials is shown in Table 3. Gradation curves for the materials are shown in Figure 8.

Surfacing. —Each of the test sections was surfaced with hot mix asphaltic concrete conforming to the Texas Highway Department specifications (13) for a modified Type E sheet asphalt surface course mixture. The aggregate used in this mixture was a combination of a wet-bottom boiler slag with limestone rock asphalt screenings and fly ash. The materials were blended as follows: 75 percent (by weight) slag aggregate, 20 percent (by weight) rock asphalt screenings, and 5 percent (by weight) fly ash. The sieve analysis of the individual materials is presented in Table 4 and the gradation curve of the blend is shown in Figure 9.

The asphalt binder used was a standard paving grade asphalt cement meeting the specifications of the Texas Highway Department (14) for grade AC-20, and The Asphalt Institute specifications (15) for a penetration grade of 60-70. Viscosity-temperature information for the asphalt cement is listed in Table 5.

Specimens and Compaction

The method of compaction and the size of the laboratory specimens of the subgrade, subbase, and base materials conformed to those specified in Test Method Tex-113-E (June 1962) of the Texas Highway Department (16). This method uses an automatic compaction device (Fig. 10) with a base plate to hold a 6-in. ID, 8½-in. tall forming mold. The automatic tamper is equipped with a 10-lb ram that falls 18 in. The striking face of the ram is a 40-deg segment of a 3-in. radius circle. The compactive effort in terms of number of blows per layer or total energy input, expressed as foot-pounds per cubic inch of specimen, is specified for various types of material. Four layers of material are compacted to yield a specimen approximately 8 in. in height and 6 in. in diameter.

Specimens of the clayey gravel (GC), sandy clay (SC) and untreated crushed limestone (R) were compacted using 50 blows of the 10-lb ram per 2-in. lift of material. The black clay (NG) specimens were compacted with 25 blows per 2-in. layer. Specimens made using these compactive efforts were used in determining the moisture-density relations of the various materials and for the Texas triaxial compression tests (Test Method Tex-117-E). Specimens of the cement-treated and lime-treated crushed limestone received a compactive effort of 25 and 50 blows per layer, respectively. These specimens were tested according to the procedures outlined in Soil-Cement and Soil-Lime Compressive Strength Test Methods (Tex-120-E and Tex-121-E).

In addition to the 6-in. diameter specimens described above, a number of larger specimens 12 in. in diameter and 5 to 10 in. in height were made using the sandy clay, clayey gravel, and untreated crushed limestone materials. The purpose of these large-diameter specimens was to evaluate the effects of thickness, layer interface and particle orientation on the compressional wave velocity. In order to obtain a more representative value of velocity, particularly for studying the particle orientation and interface

TABLE 3

FLEXIBLE BASE AND SUBGRADE MATERIALS

Material Description	Black Clay (NC)	Red Sandy Clay (SC)	Gravel Clay (GC)	Crushed Limestone
Gradation:				
Percent passing				
1 3/4 in.	100	100	100	100
1 1/4 in.	100	100	98	98
7/8 in.	100	100	97	96
3/8 in.	100	100	91	62
No. 4	100	100	82	55
No. 10	100	100	65	45
No. 40	100	100	33	22
No. 100	93	45	11	14
No. 200	87	33	8	11
Atterberg limits:				
Liquid limit	58	34	18	14
Plasticity index	38	14	3	2
Classification:				
Texas	5.0	4.0	3.6	1.0
AASHO	A-7(20)	A-2(1)	A-1(0)	A-1(0)

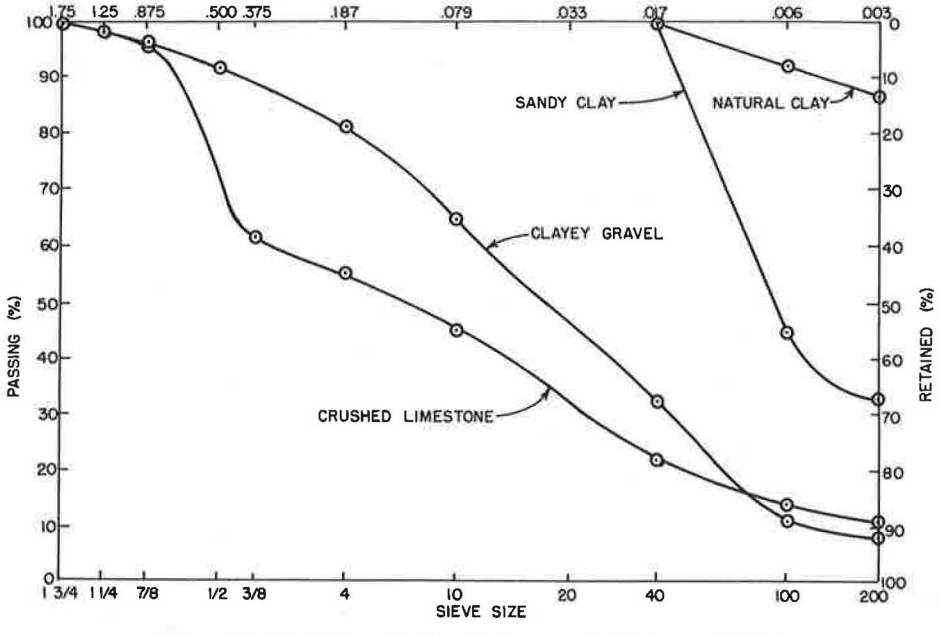

Figure 8. Gradation of subgrade, base and subbase materials.

TABLE 4

SIEVE ANALYSIS OF AGGREGATES IN SURFACE COURSE MIXTURE

Sieve Size	Slag Aggregate, Percent Passing	Asphalt Screenings, Percent Passing	Fly Ash, Percent Passing
3/8 in.	100	100	100
No. 4	99.1	100	100
No. 10	80.2	96.8	100
No. 40	19.7	35.1	96.2
No. 80	11.5	11.2	80.0
No. 200	6.1	3.0	56.0

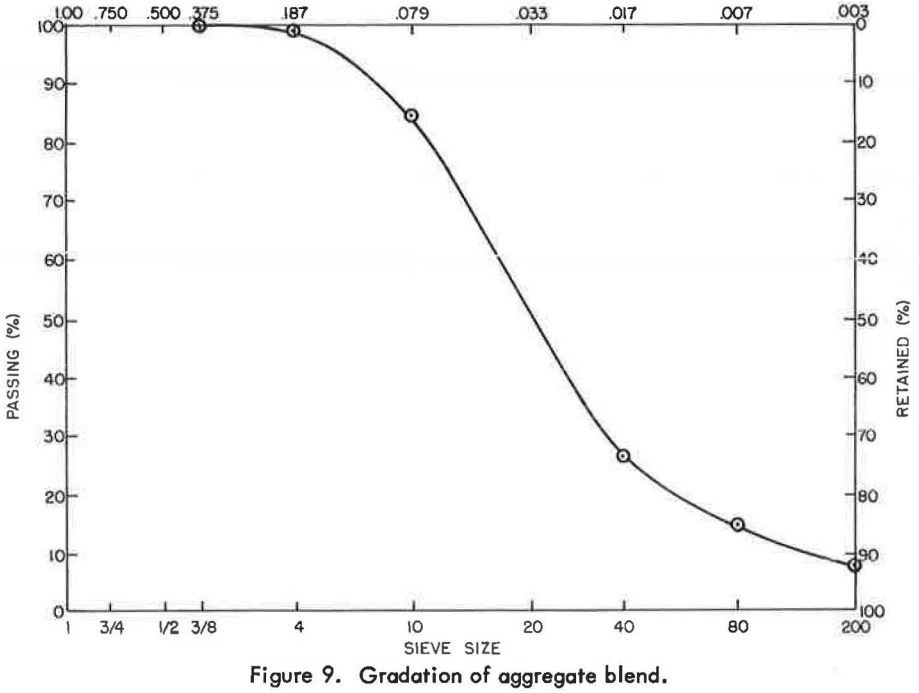

Figure 9. Gradation of aggregate blend.

TABLE 5

VISCOSITY-TEMPERATURE RELATIONSHIP OF ASPHALT CEMENT
(Designation: Texas, AC-20; Asphalt Inst., 60-70)

Penetration 100 gm/5 sec/77F	Specific Gravity at 77F	Temp. F	Absolute Viscosity, Poises
60	1.015	50	$^{a}9.20 \times 10^{7}$
		77	$^{a}1.96 \times 10^{6}$
		140	$^{b}2.30 \times 10^{3}$
		275	$^{b}0.52 \times 10^{1}$

[a]Determined using sliding plate microfilm viscometer.
[b]Determined using capillary-tube viscometer.

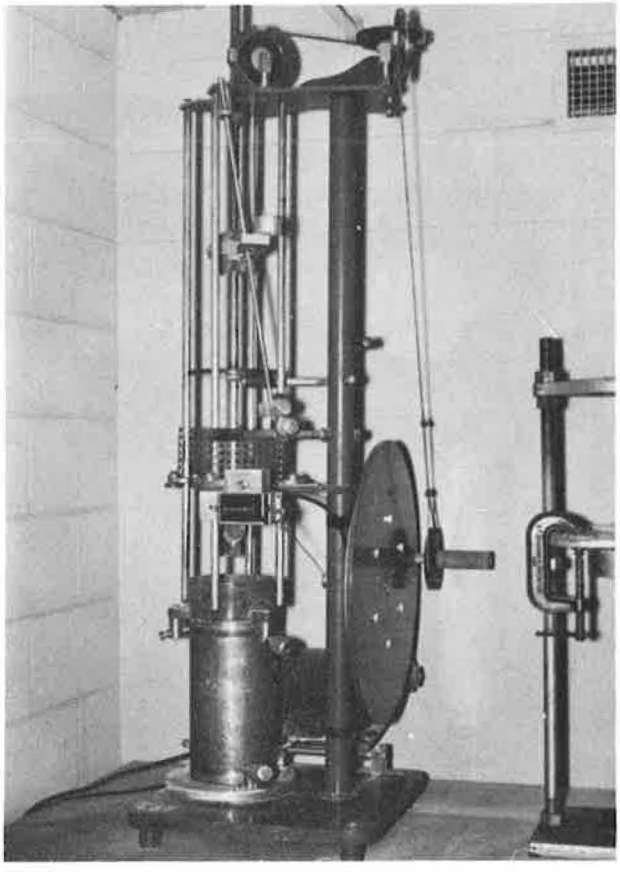

Figure 10. Texas Highway Department compaction device.

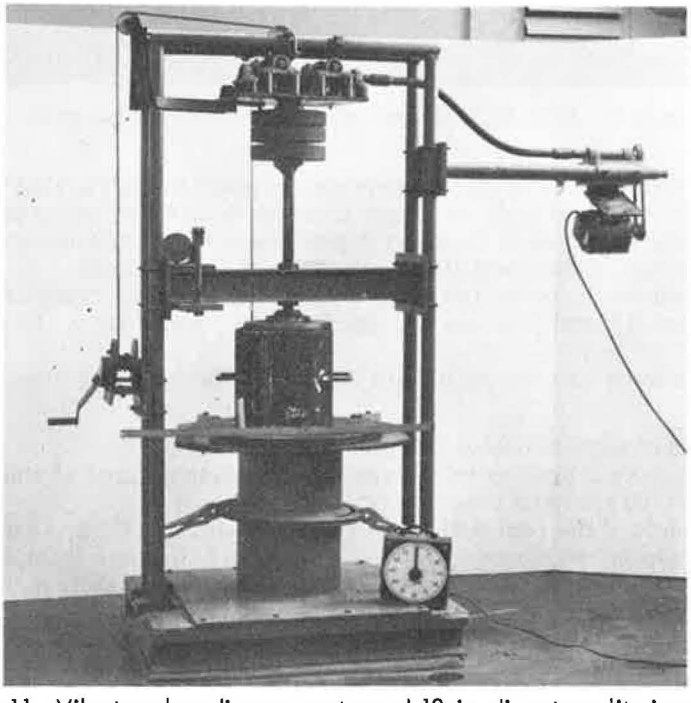

Figure 11. Vibratory-kneading compactor and 12-in. diameter split-ring mold.

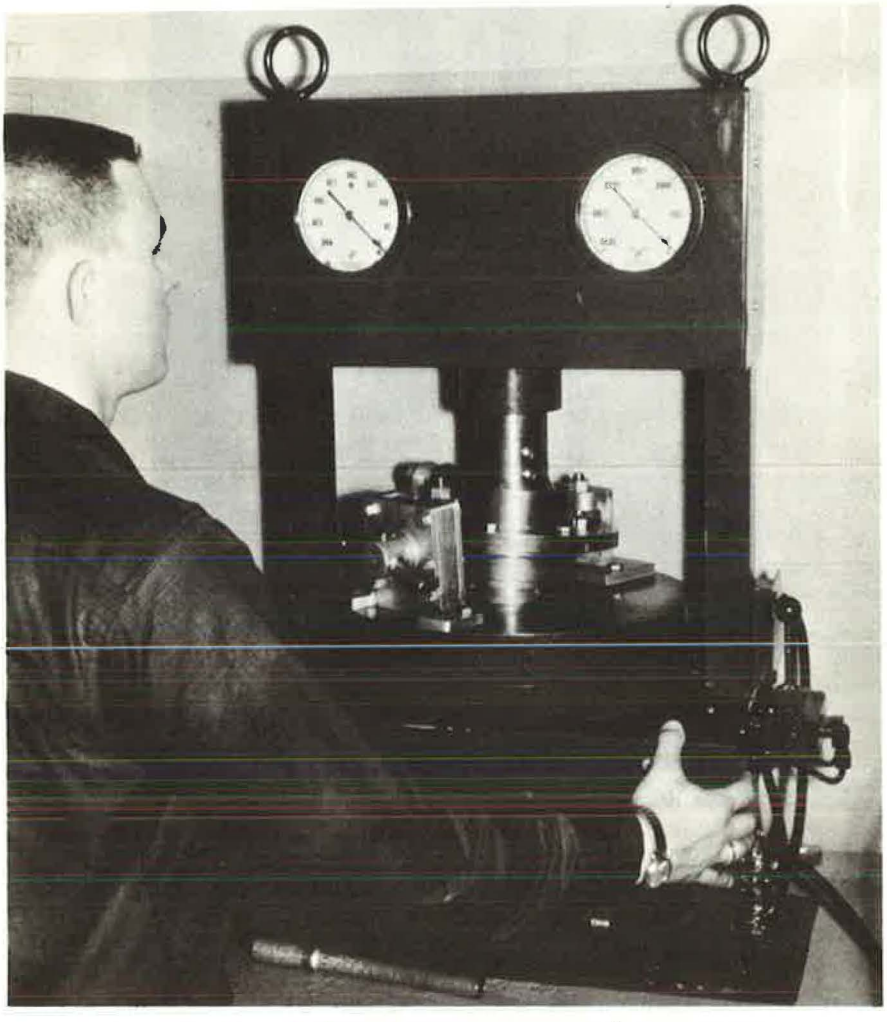

Figure 12. Texas Highway Department gyratory-shear compactor.

effects, it was considered desirable to increase the path length traveled by the pulse. Also, it was considered that with the large-diameter mold there would be less influence on orientation of the particles in the central portions of the compacted material from the restraining effects of the mold at the periphery of the specimen.

These specimens were compacted using a vibratory-kneading compactor, as described by Jimenez (17) and Jimenez and Gallaway (18), and a 12-in. ID split-ring forming mold, shown in Figure 11.

The specimens were compacted in 2-in. lifts using the following compaction procedure:

1. A dead load of approximately 280 pounds was applied.
2. A dynamic force caused by the rotation of eccentric masses of about 500 pounds at a frequency of 1200 rpm was then applied.
3. The base plate of the compactor was canted ($\frac{3}{16}$ in. in $17\frac{1}{2}$ in.) and the mold was turned counterclockwise continuously during the period of dynamic compaction.
4. The duration of compaction used was 2 min per approximately 8,000 grams of material.

5. A final period of dynamic compaction (30 sec) with the base plate in the horizontal position was used in order to square the faces of the specimen.

The compactive effort was indeterminate because the state of density of material varied during compaction and changed the inertial forces of the compactor.

Specimens of the individual materials were molded separately and tested to determine the average velocities in both the vertical (perpendicular to the plane of compaction) and horizontal (parallel to the plane of compaction) planes of the specimens. Following this, several two-layered specimens were made. The first or bottom layer of these specimens consisted of a 5-in. compacted thickness of a subgrade material and the top layer was a 5-in. compacted thickness of the untreated crushed limestone aggregate.

The compacted asphaltic concrete specimens were 4 in. in diameter and 2 in. thick. These specimens were made using the Texas Highway Department method of compacting test specimens of bituminous mixtures (Test Method Tex-206-F, Part II, Tentative, June 1964). This method imparts a kneading action to the mixture being molded and compactive effort is applied until the densified mixture has a certain resistance to load.

The motorized gyratory-shear molding press is shown in Figure 12. Compactive effort is applied by hydraulic pressure and rotation of the mold in a canted position until one stroke of the pump handle causes a pressure indication on the low-pressure gage of 150 psi or more. When this end point is reached, a pressure of 1588 psi is applied to the specimen with the mold in a horizontal position and then released slowly. In order to vary the specimen densities obtained with this molding press, end points of 100 and 200 psi were also used.

The size of all the specimens used in this study was well suited for the determination of the compressional wave velocity of the respective materials. Several investigators (19, 20, 21) using pulse velocity techniques have demonstrated that the first arrival travels at the theoretical velocity V_c in materials for which the elastic constants can be determined independently. Using materials such as glass, steel, and aluminum and observing specimens of different sizes, they have found that this velocity is independent of length and diameter of the specimen and transducer frequency within certain ranges of dimensions and experimental accuracy. According to Birch (20), the ratio of length to diameter of the specimen should not exceed 4 or 5, because for larger values less energy arrives with the velocity V_c as more energy is converted to disturbances arriving later than the first arrival.

This is due to conversion to other types of waves at the boundaries of the specimen. Part of the longitudinal waves emanating from the source transducer are reflected at grazing angles of incidence at the material-air interface. This reflection leads to a conversion of part of the compressional energy into shear waves, which, in turn, can be reconverted to compressional waves by reflection at the specimen boundary. The amount of energy converted from one wave type to another depends on the angle of incidence of the wave and on Poisson's ratio of the material (22).

RESULTS AND DISCUSSION

The results of the compressional wave velocity determinations for all the materials used in this study are shown graphically in Figures 13 through 23 and in tabular form in Tables 6 and 7.

The individual factors investigated and their influence on wave velocity are discussed separately except where a combination seemed logical. For the base and subgrade materials a discussion is presented for the effects of (a) moisture content and density, (b) confining pressure, (c) temperature, (d) stabilizing agents and (e) layer interface and particle orientation. For the asphaltic concrete surface course mixtures the effects of (a) temperature and asphalt content, and (b) voids on velocity are discussed.

Effects of Moisture and Density

The relations of moisture content to density and wave velocity at atmospheric pressure in the natural clay and sandy clay materials are shown in Figures 13 and 14. These two materials exhibit similar types of velocity-moisture relationships. The velocity in

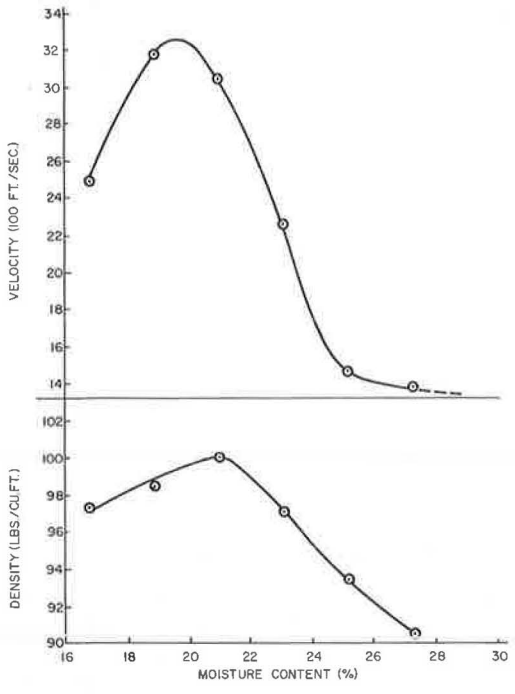

Figure 13. Relation of moisture content to dry density and compressional velocity for natural clay.

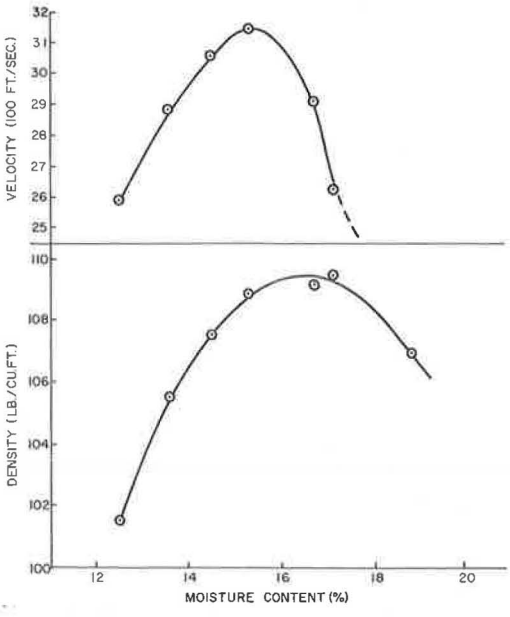

Figure 14. Relation of moisture content to dry density and compressional velocity for sandy clay.

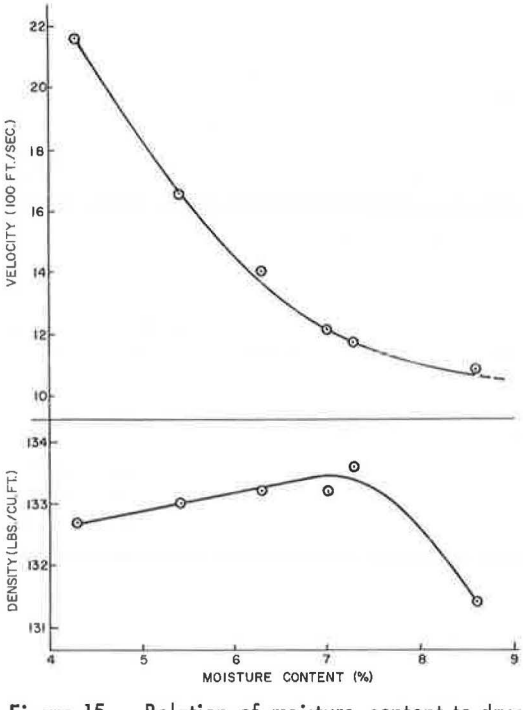

Figure 15. Relation of moisture content to dry density and compressional velocity for clayey gravel.

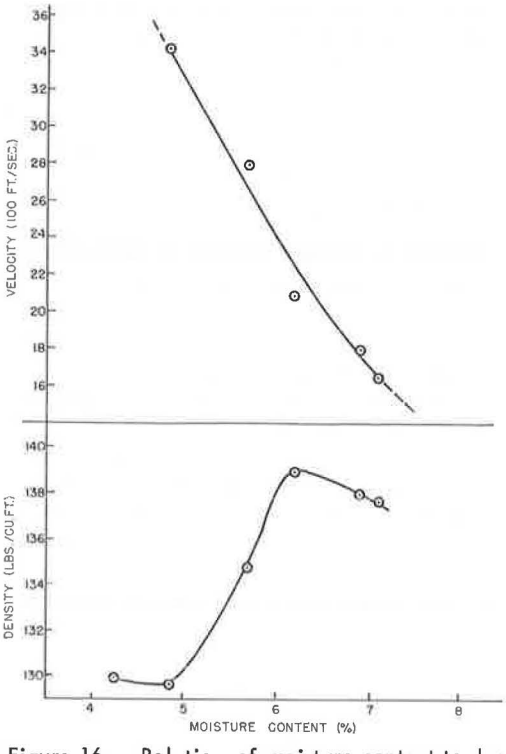

Figure 16. Relation of moisture content to dry density and compressional velocity for crushed limestone.

these materials increases with moisture content to a maximum value and then decreases rapidly as the moisture content continues to increase. The maximum velocity is attained before the materials reach maximum density. In the case of the natural clay, this occurs at a moisture content of approximately 1.4 percent less than optimum and in the case of the sandy clay about 1.1 percent less than optimum.

These results do not agree exactly with previous pulse velocity experimental work by Leslie (23). Leslie reported the same general type of velocity-moisture relationships in silty clay specimens. However, in his specimens the maximum velocity occurred at maximum density and optimum moisture content for the material. Differences in equipment and material characteristics may be responsible for this slight disagreement in experimental results. Leslie used the standard Proctor method to compact his specimens and the discrepancy is probably due to the difference in compaction procedures.

The increase in velocity with moisture content up to approximately the optimum value in the clays is apparently related to the nature and thickness of the water films surrounding the particles. Water may be held as a film around a colloidal clay particle either by direct adsorption of the dipole water molecules on the surface of the particle or may be the result of the hydration of ions of an electrolyte that are associated with the particle (24). In any event, when these films are thin the molecular forces of adsorption are quite strong and the apparent viscosity of the water is high. As the films become thicker, i.e., more water is added, the attractive force lessens and the water becomes less viscous with distance from the particle.

Within a certain moisture range for a given clay material the tension effects of the water films between the colloidal particles impart to the clay its cohesive properties. The cohesion between particles is greater when the water films are thin and decreases as the films increase in thickness. These water films also aid in the compaction of clay materials, functioning as a lubricant to promote the orientation of the particles into a denser state. Thus, below the optimum moisture content the velocity increases with an increase in moisture, due to densification of the material aided by the lubricating action of the water films and better coupling between particles related to the cohesive forces associated with thin water films.

The two more granular materials also show similar types of velocity-moisture curves (Figs. 15 and 16). The velocity steadily decreases as the moisture content increases and apparently bears little relation to the density of the material or its optimum moisture content. In the crushed limestone there is a decrease of approximately 1,800 fps or almost a 50 percent reduction in velocity with an increase of only two percent in moisture content. The clayey gravel shows the same percentage decrease with an increase of approximately four percent in moisture content.

At low moisture contents, the material at the top surface of the specimens of crushed limestone was relatively loose and powdery. In this condition it was difficult to obtain good coupling between the receiver transducer and top of the specimens, and the velocity could not be determined for the specimen at 4.2 percent moisture content.

Hardin and Richart (25) in their work with Ottawa sand found that the velocity for saturated specimens and specimens drained prior to testing was less than that for dry specimens. From their results they concluded that the velocity was decreased by the mass of water which moved along with the solid framework of the specimen as it vibrated and that at low pressures the water reduced the stiffness of the material frame and further reduced the velocity. These concepts are logical and appear to explain the results obtained with the more granular materials in this study.

Effects of Pressure

The variation of the compressional wave velocity with pressure was determined for the red sandy clay and the clayey gravel subgrade materials. Specimens of each of the materials were made at two different moisture contents below optimum and tested at various combinations of vertical and lateral pressure in a Texas triaxial cell (16).

This cell is a lightweight stainless-steel cylinder, $6\frac{3}{4}$ in. ID and 12 in. in height, fitted with a standard air valve and a tubular rubber membrane 6 in. in diameter. The

tubular rubber membrane is clamped at each end of the cylinder and functions as an inflatable liner of the cell. The specimens were placed in the cell and loaded axially by means of a screw jack press. Lateral stress was applied to the specimens by means of air pressure in the cell.

Specimens were subjected to vertical stresses of 0, 5, 10, 15, and 20 psi. At each of these vertical stresses, the velocity was determined first with no lateral restraint on the specimen, then the cell was pressurized and determinations made at lateral stresses of 5, 10, 15, and 20 psi. The application of the lateral stress was accompanied by a tendency of the specimen to elongate axially. In order to keep the height of the specimen constant, the load was increased slightly to maintain the same deformation gage reading observed when there was no lateral stress on the specimen. No correction for this increase in vertical stress was made so that the confining pressure cannot be considered completely uniform.

The clayey gravel specimens were subjected to a 2.5-psi lateral stress before the 15- and 20-psi vertical stresses were applied. This was done to prevent possible failure of the specimens before the testing was completed.

The data from these tests are shown in log-log curves with the velocity in feet per second plotted as the ordinate and confining pressure in pounds per square foot as the abscissa (Figs. 17 and 18).

The variation of velocity with pressure was determined from these plots using the following equation:

$$V_c = C\sigma^e \tag{3}$$

where

V_c = the compressional wave velocity, fps;
C = a constant;
σ = confining pressure, psf; and
e = slope.

Figure 17 shows the results for the red sandy clay specimens. At low pressures the velocity is affected only slightly by confining pressure. A slight break in the curves occurred at 1440 psf and the velocity varies with approximately the 0.04 power of the confining pressure for the specimen with 15.5 percent moisture and the 0.03 power for the specimen at 13.5 percent moisture in the range of 1440 to 2880 psf.

The results obtained for the clayey gravel specimens are shown in Figure 18. The effect of confining pressure is more pronounced on this material as is indicated by the greater slopes of the curves. A break in these curves occurred at 720 psf and the velocity varies with the 0.15 power of the confining pressure for the specimen at 5 percent moisture and the 0.19 power for the specimen at 7 percent moisture in the range of 720 psf to 2880 psf.

These results are in fair agreement with results of the other investigators. Hardin and Richart (25) found that for clean sands the compressional velocity varies with approximately the 0.25 power of confining pressure. Matsukawa and Hunter (26) found the same value for dry sand specimens in the range of 40 to 400 psf. At higher pressures (600 to 10,000 psf) Shannon et al. (27) found the velocity to vary with approximately the 0.33 power of confining pressure in dry Ottawa sand. Wilson and Miller (28) found a variation of about the 0.17 to 0.20 power for compressional waves in various soil specimens in the pressure range of 600 to 10,000 psf.

Effects of Temperature

Specimens of the sandy clay and clayey gravel materials were prepared at different moisture contents and then tightly sealed in aluminum foil to prevent the escape of moisture. The compressional wave velocities of these specimens were determined at 100, 75, 38 and 30 deg F at atmospheric pressure. These temperatures covered the range that was considered likely to be experienced by these materials in a road subgrade.

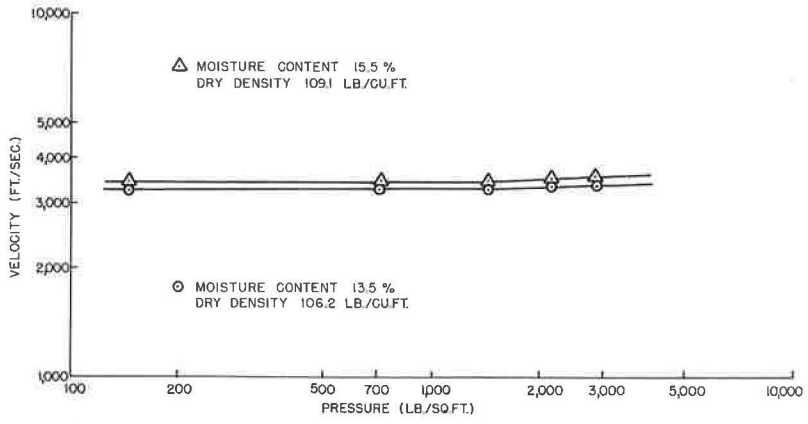

Figure 17. Variation in velocity of compressional wave with confining pressure and moisture content for sandy clay.

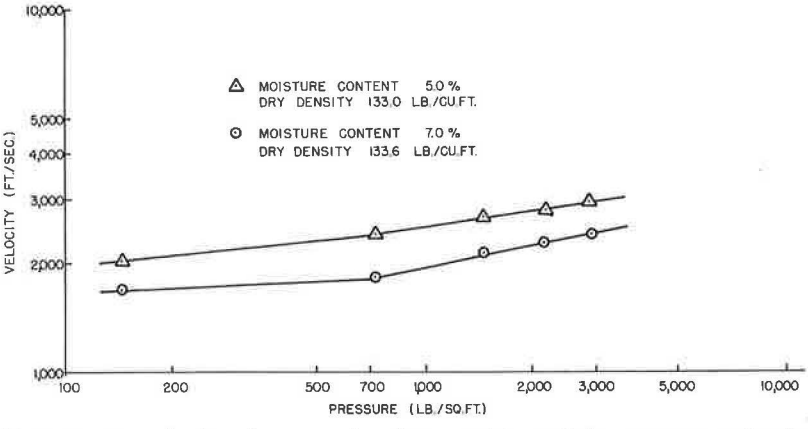

Figure 18. Variation in velocity of compressional wave with confining pressure and moisture content for clayey gravel.

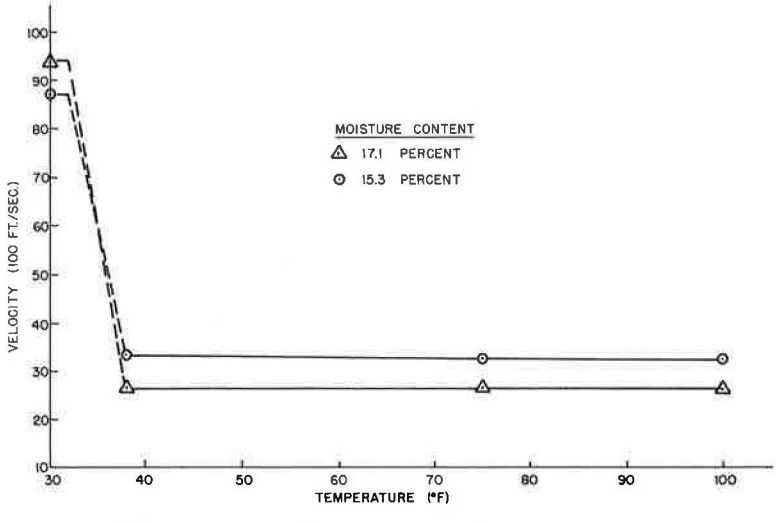

Figure 19. Variation of compressional wave velocity with temperature in sandy clay.

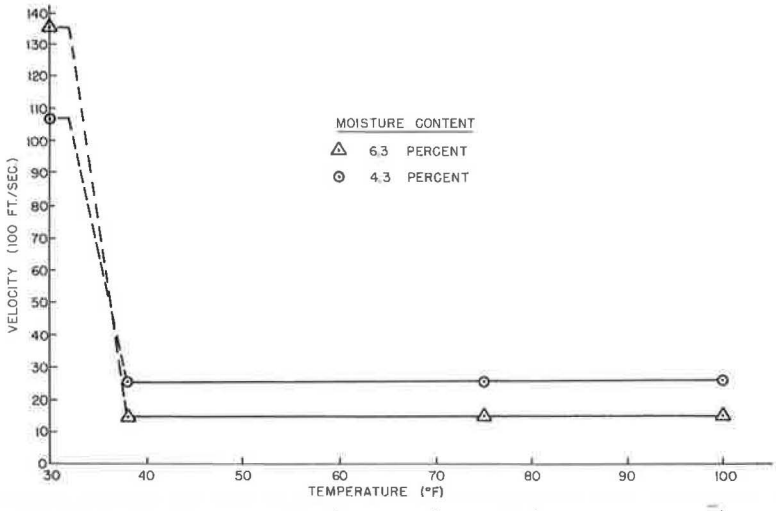

Figure 20. Variation of compressional wave velocity with temperature in clayey gravel.

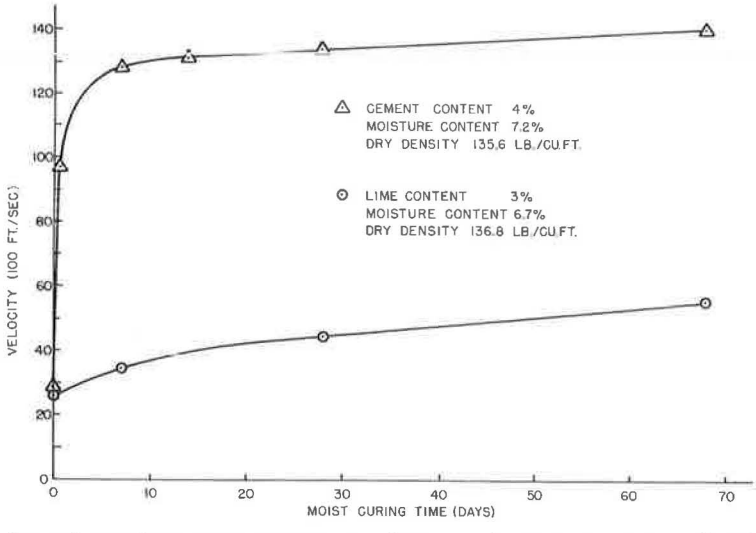

Figure 21. Effect of curing on compressional wave velocity in treated crushed limestone.

The results are shown in Figures 19 and 20. The velocities remained essentially constant in the range of 100 to 38 F but increased drastically as soon as the water in the interstices of the material became frozen. A great increase in the amplitude of the received pulse was also observed. The ice is an effective cementing agent and increases the acoustical coupling between the material particles. Thus the more rigid matrix is able to transmit the compressional wave at a much higher velocity and with less attenuation. The velocities observed in the respective specimens remained constant between 30 and -10 F.

That portion of the curves between 32 and 38 F is shown as a dashed line. Although it is reasonable to assume that the curves are linear, there may be a nonlinear relationship of velocity with temperature related to the change in viscosity of the water in the voids of the material in this temperature range.

Wave velocities could not be determined for the specimens after thawing. The expansion of the water in freezing was enough to disrupt the intergranular contact achieved by compaction to the point that attenuation losses prevented the transmission of a readable pulse signal.

It is interesting to notice that in both materials the specimens with the higher moisture content had the lower velocities at the higher temperatures and had the higher velocities after freezing.

Effect of Additives

The effects of cementitious additives and moist curing time on the compressional wave velocity in the crushed limestone material are shown in Figure 21. Although the specimen densities obtained after the addition of the cement and lime are somewhat lower than those of the untreated material, the initial velocities determined immediately after molding are higher. This suggests that the finer materials in an aggregate mixture play an important part in the transmission of the wave energy.

As seen in the figure the velocities of the lime and cement treated specimens increase with curing time although at much different rates. The velocity in the cement-treated specimen was about 3.7 times the velocity of the lime-treated specimen at the end of 7 days' moist curing.

These results were not unexpected but do serve to illustrate the effects of increased rigidity or stiffness on the wave velocity due to cementation of the particles. Good solid contact between the grains is requisite to good transmission of the wave energy and high velocities.

Effects of Layer Interface and Particle Orientation

The purpose of the large 12-in. diameter specimens was to study the effects of thickness, layer interface, and particle orientation. Velocity measurements were made on these specimens in the vertical direction after each lift of material was compacted. After molding of the specimen was completed, the split-ring mold was removed and horizontal measurements made at several locations at mid-height of the specimen. In the layered specimens these horizontal measurements were also made in both materials immediately adjacent to the interface between them. Typical data obtained for the two-layered specimens are listed in Table 6.

The results of this series of tests were not conclusive. In general, the thickness of material or the total path length of the pulse in a given material had little or no effect on the velocities determined with the equipment used in this study. The presence of an interface between compacted lifts of the same material affected the velocity very little. However, the top of each compacted lift was scarified to eliminate a smooth interface before the compaction of the next lift. This assured good contact between lifts and may account for this slight effect.

Little difference was observed in velocities measured perpendicular to the plane of compaction and those measured parallel to the plane of compaction in the sandy clay and clayey gravel. The observed horizontal velocities in the gravel were slightly less than those in the vertical direction. In the crushed limestone which contained larger and more elongated particles, the horizontal velocities averaged about 200 fps or approximately 7 percent higher than those measured in the vertical direction. This indicates that the orientation of the particles with their long axes parallel to the plane of compaction does have some effect on velocity although it was less than anticipated.

The theoretical velocities shown in Table 6 were computed from the following equation:

$$\frac{1}{\overline{V}} = \frac{\varphi}{V_2} + \frac{1+\varphi}{V_1} \qquad (4)$$

where

$\overline{V}$ = average velocity of system,

V_1, V_2 = average velocities of the two materials where $V_1 > V_2$, and

φ = fractional length of material with slowest velocity in the total path length.

TABLE 6

TYPICAL VERTICAL AND HORIZONTAL COMPRESSIONAL WAVE VELOCITIES IN TWO-LAYERED TWELVE-INCH DIAMETER SPECIMENS

Specimen No.	Layer and Type of Material	Measurement Path		Measured Velocity (fps)	Theoretical Velocity[b] (fps)	Dry Density (lb/cu ft)	Moisture Content (%)
		Location[a]	Length (in.)				
5	Lower—Sandy Clay	AB	5.375	2,350	—	98.9	20.0
		FG	12.000	2,347	—		
		HI	12.000	2,294	—		
	Upper—Crushed Limestone	AC	7.500 (2.125 is LS)	2,441	2,445	127.5	5.0
		AD	9.625 (4.250 is LS)	2,253	2,506		
		AE	10.687 (5.312 is LS)	2,141	2,519		
		JK	12.000	2,976	—		
		LM	12.000	3,048	—		
6	Lower—Clayey Gravel	AB	5.000	2,863	—	134.9	5.2
		FG	12.000	2,770	—		
		HI	12.000	2,747	—		
	Upper—Crushed Limestone	AC	7.125 (2.125 is LS)	2,113	2,825	127.5	5.0
		AD	9.250 (4.245 is LS)	1,971	2,801		
		AE	10.312 (5.312 is LS)	2,017	2,793		
		JK	12.000	2,525	—		
		LM	12.000	2,625	—		

[a]Cross section through a diameter of specimen showing measurement path location.

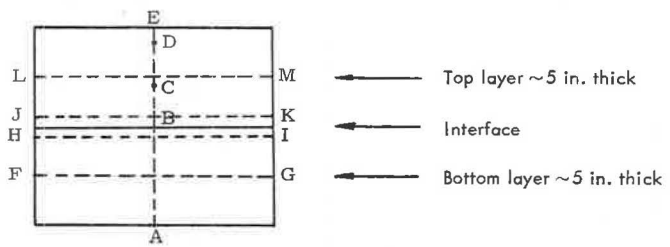

[b]See Eq. 4. The velocity in the crushed limestone was 2,712 ft/sec.

TABLE 7

DESIGN VALUES OF TYPE E (MODIFIED) MIXTURE WITH 60 PENETRATION ASPHALT MOLDED BY TEXAS GYRATORY-SHEAR METHOD

Asphalt Content (%)	Specimen Density (gm/cc)	Impregnated S.G.	Relative Density (%)	Total Voids (%)	Hveem Stability (%)	Cohesiometer Value (gm/in.)
6.0	2.210	2.391	92.4	7.6	36	219
7.0	2.223	2.358	94.3	5.7	37	261
8.0	2.244	2.336	96.1	3.9	36	276

This equation was adopted from one used by Wyllie et al. (29) to calculate "time-average" velocities in layered systems of aluminum and lucite discs. According to Wyllie et al., in elastic media systems this equation gives the theoretical velocity if the wave travel is directly through the specimen normal to the layers and if there is no slippage or separation of interfaces. The difference in measured and theoretical velocities indicate that these theoretical conditions were not met in the specimens tested.

While slippage or separation at the interface between the two materials could not be determined, there was a considerable decrease in the amount of energy transmitted across the interface. After the addition of the first 2-in. lift of crushed limestone, the amplitude of the received pulse was decreased to about $^1/_{10}$ of the amplitude observed prior to the addition. This energy loss is largely attributed to reflection of the wave energy at the interface between the two layers (8). No effect of the interface between layers on wave propagation in the horizontal plane was found in this series of tests.

Effect of Temperature and Asphalt Content in Surface Course Mixture

As expected, the compressional wave velocities in the asphaltic concrete surface course mixture were influenced considerably by temperature. Three sets of specimens at different asphalt contents were compacted and tested. The design values for the mixtures are shown in Table 7. The results of the velocity determinations on mixtures containing 6, 7, and 8 percent asphalt at various temperatures are shown in Figure 22. Each data point represents the average value for three specimens.

In the range of approximately 50 to 120 F, the velocity decreases almost linearly with temperature at a rate of about 30 fps per one degree rise in temperature. Below 50 F there is a slight upward trend of the curves and above 120 F the curves appear to level off at some minimum velocity for the mixtures.

Although measurements were not made at temperatures below 39 F there is reason to believe that the curves will show a reversal of curvature between 50 F and 20 F and that below 20 F they will continue their upward trend reaching a constant value or maximum velocity at some extremely low temperature. This belief is fostered by the results obtained by Goetz (30). Although Goetz reported only the variation in "sonic modulus of elasticity" (Young's modulus) values with temperature between -10 F and 70 F, since there is a direct relationship between velocity and modulus of elasticity the variation of velocity with temperature should be essentially the same. However, due to the difference in testing techniques, further investigation is needed before a definite conclusion is reached.

The mechanical behavior of a bituminous paving mixture is complicated by its deformation characteristics at different temperatures. At sufficiently high temperatures such a mixture may be considered a plastic material. At normal room temperature the mixture may exhibit both plastic and elastic characteristics and when the temperature is lowered sufficiently it behaves in an elastic manner. Goetz found a "transition zone" or reversal of curvature in the modulus curves of his mixtures that occurred between 20 F and 40 F. He considered this transition to indicate that the plastic nature of the mixtures was dominant at temperatures above 40 F and that elastic behavior was

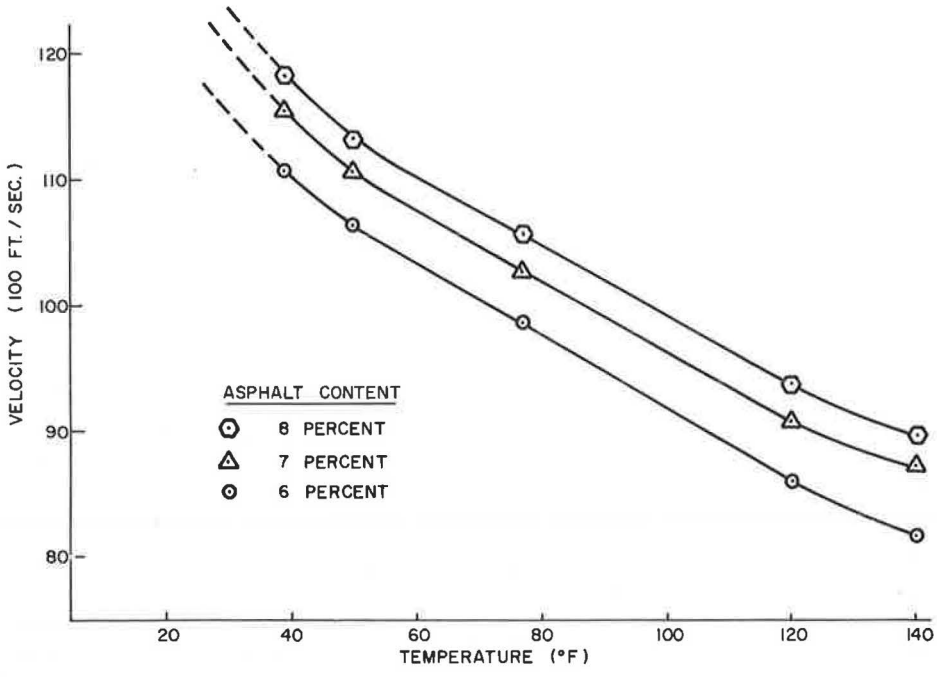

Figure 22. Variation of compressional wave velocity with temperature in asphaltic concrete surface course mixture.

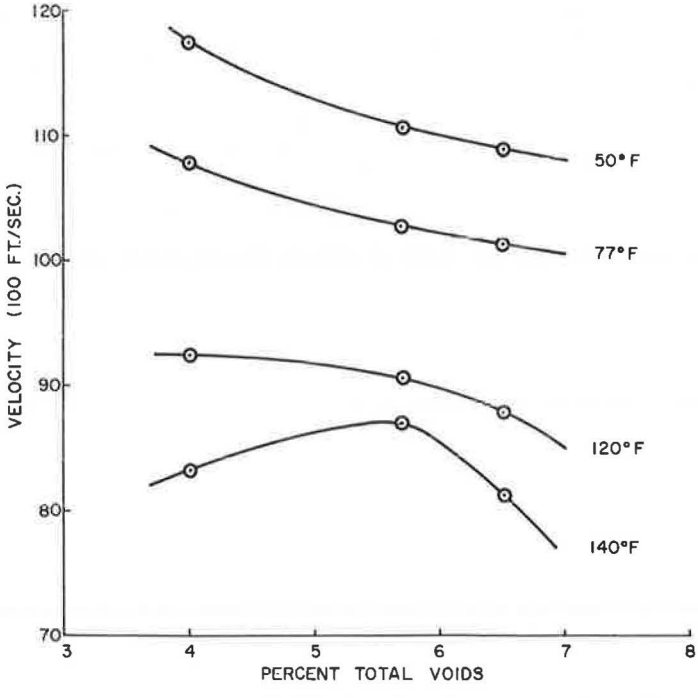

Figure 23. Relation of voids to wave velocity at various temperatures for surface mixture at 7 percent asphalt content.

dominant below 20 F. The change in slope of the curves in Figure 22 at about 120 F may be interpreted as an indication of the viscous tendencies of the mixture, this change occurring at the approximate softening point of the asphalt.

The results obtained by Goetz show no consistent relation between the resonant frequency test values and the amount of asphalt in the mixtures. The pulse technique results, however, show a relatively regular and uniform relation between the velocities of the mixtures at different asphalt contents. Although the velocity is incrementally increasing with asphalt content in the mixtures tested in this study, it is expected that a limit to this effect exists for any aggregate-asphalt mixture. As soon as the asphalt content is increased to the point that the voids between aggregate particles become filled and the aggregate framework is destroyed, the velocity should be lowered considerably. Evidence of this decrease in velocity was found in studying the influence of voids.

Effects of Voids in Surface Course Mixture

A series of specimens of the surface course mixture were compacted so as to obtain three different relative densities at the same asphalt content. The percent total voids in these specimens was determined at 77 F. This series of specimens was tested at different temperatures to determine the relation of total percent voids in the mixture to wave velocity at the various temperatures. The results of these compressional wave velocity determinations are shown in Figure 23. Each data point represents the average value for three specimens.

As seen in the figure, voids caused a reduction in the wave velocity in the specimens at the 50 F and 77 F test temperatures, i.e., velocity decreased with an increase in voids. The change in character of the curves between 77 F and 120 F is believed to be another manifestation of the viscous and expansive nature of the asphalt binder. At some intermediate temperature there is probably a linear relationship between velocity and percent total voids for this mixture (Fig. 23) but at 120 F, the approximate softening point of the asphalt, there is a decided change in the characteristics of the curves.

When asphalt is heated it undergoes a considerable amount of volumetric expansion as well as a decrease in viscosity. Thus, in a compacted mixture the asphalt may expand with increasing temperature to the point that air voids in the mixture are at a minimum but the corresponding decrease in viscosity may still result in reduced velocities of the compressional wave. This is due not only to the decrease in velocity in the asphalt itself with increasing temperature, but also to the loss of cohesiveness of the mixture and the consequent reduction in coupling of the aggregate particles.

It is interesting to note that the smallest total fluctuation in velocity over the range of temperatures was exhibited by the mixture compacted to the 150 psi end point and containing 5.7 percent air voids.

SUMMARY AND CONCLUSIONS

This investigation was considered a pilot study of a pulse velocity measurement technique and an attempt to determine the suitability and applicability of such a technique as a testing procedure for the evaluation of various types of flexible pavement construction materials. Within the limits of this statement of purpose the study has been reasonably successful. A more thorough investigation of some of the factors involved in and influencing wave velocity measurements and their interpretation in terms of material properties will be required. However, it is believed that the results of this study will give direction to future work in this area of vibrational testing, Further, it is hoped that these results will be of benefit in achieving the desired objectives of the parent research project with which this study was associated.

Within the limits of the materials and testing procedures employed, the following conclusions may be drawn:

1. The velocities of elastic waves in clays and more granular highway construction materials are related to the properties of the respective material in a complex manner.
    a. In general, the wave velocity is diminished as the moisture content is increased.

b. In compacted materials, increased density should result in higher velocities but elastic wave propagation is complicated by the properties of the fluid in the voids and any anisotropic nature of the compacted medium.
c. External or confining pressure results in increased wave velocities.
d. Over the range normally experienced by subgrade and base materials in a pavement structure, temperature has little or no effect on wave velocity. However, temperatures below freezing result in drastic increases in wave velocity provided the material contains some moisture.
e. Cementitious materials in the voids of a granular medium increase the coupling between particles and thus increase the wave velocity.

2. In bituminous mixtures the viscoelastic character of the binder influences the wave propagation.
   a. Velocities increase with increased asphalt content up to an expected limiting content for a given aggregate mixture.
   b. In these mixtures velocity decreases with increasing temperature.
   c. Velocities increase with increased densification or reduction in percent total voids of the mixture.
   d. Using pulse velocity measurements, it may be possible to define the temperature ranges in which the plastic, elastic and viscous properties of the bituminous mixture are dominant.
3. The pulse velocity technique using both shear and compressional modes of vibration suggests itself as a promising possibility for finding the elastic constants of flexible pavement construction materials. Determination of Poisson's ratio and elastic modulus values, particularly in bituminous mixtures that undergo changes in physical state, might provide a better understanding of both the design requirements and field performance of these materials.
4. The pulse velocity technique, as a form of nondestructive testing, is already established as a valuable tool of the engineer. Its application to the field of engineering materials, particularly flexible pavement construction materials, has not been fully explored and its full potential in this area is yet to be realized.

REFERENCES

1. Burmister, D. M. The General Theory of Stresses and Displacements in Layered Soil Systems. Jour. of Applied Physics, Vol. 16, pp. 89-94, 126-127, 296-302, 1945.
2. Jones, R. Measurements and Interpretation of Surface Vibrations on Soil and Roads. HRB Bull. 277, pp. 8-29, 1960.
3. Heukelom, W., and Foster, C. R. Dynamic Testing of Pavements. Jour. of Soil Mechanics and Foundations Div., ASCE, Vol. 87, No. SM1, Part I, pp. 1-28, 1960.
4. Jones, R., and Whiffin, A. C. A Survey of Dynamic Methods of Testing Roads and Runways. HRB Bull. 277, pp. 1-7, 1960.
5. Van Santen, G. W. Introduction to a Study of Mechanical Vibration. Elsevier Press, Houston, 1953.
6. Timoshenko, S., and Goodier, J. N. Theory of Elasticity, 2nd Edition. McGraw-Hill, New York, 1951.
7. White, J. E. Seismic Waves: Radiation, Transmission and Attenuation. McGraw-Hill, New York, 1965.
8. Officer, C. B. Introduction to the Theory of Sound Transmission. McGraw-Hill, New York, 1958.
9. Richart, F. E., Jr. Foundation Vibrations. Jour. of Soil Mechanics and Foundations Div., ASCE, Vol. 86, No. SM4, Part I, pp. 1-34, Aug. 1960.
10. Long, B. G., Kurtz, H. J., and Sandenaw, T. A. An Instrument and a Technique for Field Determination of the Modulus of Elasticity and Flexural Strength of Concrete (Pavements). Proc. ACI, Vol. 41, pp. 217-231, 1945.
11. Batchelder, G. M., and Lewis, D. W. Comparison of Dynamic Methods of Testing Concretes Subjected to Freezing and Thawing. Proc. ASTM, Vol. 53, pp. 1053-1065, 1953.

12. Whitehurst, E. A. Pulse-Velocity Techniques and Equipment for Testing Concrete. Proc. HRB, Vol. 33, pp. 226-242, 1954.
13. Texas Highway Department. Standard Specifications for Road and Bridge Construction, 1962.
14. Texas Highway Department. Revised Specifications for Asphalt Cement, 1964.
15. The Asphalt Institute. The Asphalt Handbook, Manual Series No. 4, 1965.
16. Texas Highway Department. Manual of Testing Procedures, Vol. 1.
17. Jimenez, R. A. An Apparatus for Laboratory Investigations of Asphaltic Concrete Under Repeated Flexural Deformations. Report submitted to the Texas Highway Department under Research Project HPS-1-25-D, January 1962.
18. Jimenez, R. A., and Gallaway, B. M. Preliminary Report of an Apparatus for the Testing of Asphaltic Concrete Diaphragms. Proc. AAPT, Vol. 31, pp. 477-499, 1961.
19. Mason, W. P., and McSkimin, H. J. Attenuation and Scattering of High Frequency Sound Waves in Metals and Glasses. Jour. Acoustical Soc. of America, Vol. 19, pp. 464-473, 1947.
20. Birch, F. The Velocity of Compressional Waves in Rocks to 10 Kilobars: Part I. Jour. of Geophysical Research, Vol. 65, No. 4, pp. 1083-1102, 1960.
21. Hughes, D. S., Pondron, W. L., and Mims, R. L. Transmission of Electric Pulses in Metal Rods. Physical Review, Vol. 75, No. 10, pp. 1552-1556, 1949.
22. Hueter, T. F., and Bolt, R. H. Sonics. John Wiley and Sons, New York, 1955.
23. Leslie, J. R. Pulse Techniques Applied to Dynamic Testing. Proc. ASTM, Vol. 50, pp. 1314-1323, 1950.
24. Baver, L. D. Soil Physics, 3rd Edition. John Wiley and Sons, New York, 1963.
25. Hardin, B. O., and Richart, F. E. Elastic Wave Velocities in Granular Soils. Jour. of Soil Mechanics and Foundations Div., ASCE, Vol. 89, No. SM1, pp. 33-65, Feb. 1963.
26. Matsukawa, E., and Hunter, A. N. The Variation of Sound Velocity with Stress in Sand. Proc. Physical Soc., Sect. B, Vol. 69, Part 8, No. 440B, pp. 847-848, 1956.
27. Shannon, W. L., Yamane, G., and Dietrich, R. J. Dynamic Triaxial Tests on Sand. Proc. First Panamerican Conference on Soil Mechanics and Foundation Engineering, Mexico City, 1959.
28. Wilson, S. D., and Miller, R. P. Discussion of Foundation Vibrations, by F. E. Richart, Jr. Trans. ASCE, Vol. 127, Part I, pp. 913-917, 1962.
29. Wyllie, M. R. J., Gregory, A. R., and Gardner, L. W. Elastic Wave Velocities in Heterogeneous and Porous Media. Geophysics, Vol. 21, pp. 41-70, 1956.
30. Goetz, W. H. Sonic Testing of Bituminous Mixtures. Proc. AAPT, Vol. 24, pp. 332-348, 1955.

Fatigue and Deflection of Asphaltic Concrete

O. A. WHITE, Engineer of Materials and Research, Oregon State Highway Department

ABRIDGMENT

•IN THE FALL of 1956 a comprehensive study was begun on the fatigue and deflection properties of asphaltic concrete for the purpose of evaluating pavement characteristics and design criteria. The project was arranged in three parts: (a) field tests to determine deflections of existing pavements under load; (b) laboratory tests on beams cut from pavements tested for deflection under load to determine the deflection life remaining and other physical characteristics; and (c) laboratory tests on molded specimens to determine deflection fatigue life and other characteristics as affected by aggregate gradation and asphalt content.

Phase I—Deflection Tests

Deflection tests were made using a Benkelman beam and truck loaded to 18,000 lb on a single rear axle. Static measurements were made at 2 points 50 ft apart in each wheel track for each area of test. Over 1000 measurements were made in the fall and again in the spring at the same marked points. Forty-three construction projects were measured and pavement conditions noted at one or more areas of test for each project. A final pavement condition survey was made in 1964. Additional tests were made on other projects since the spring of 1957 to determine the effect of pavement age, pavement thickness, different wheel loads, and base aggregate degradation. Data concerning the type and source of base rock were obtained from the files for each project measured.

Tables 1, 2 and 3 give various comparisons of deflections for each of five types of bases. The values of deflection are averages of all readings in the category indicated for each type of base. The number of points measured for type of base were: 20 over borrow material, 130 over volcanic cinders, 84 over crushed river gravel, 174 over crushed pit gravel, and 150 over crushed quarry rock.

TABLE 1

SPRING AND FALL MEASUREMENTS—DEFLECTION IN INCHES

Type of Base	Fall Avg.	Spring Avg.	Range of Deflection for Group		Percent of Points With Spring Deflections Higher Than Fall Deflections
			Spring	Fall	
Borrow	0.0398	0.0609	0.0316	0.0805	100
Cinder	0.0416	0.0427	0.0195	0.0760	56.3
Crushed River Gravel	0.0244	0.0257	0.0120	0.0380	76.1
Crushed Pit Gravel	0.0193	0.0216	0.0115	0.0362	65.6
Crushed Rock	0.0179	0.0210	0.0077	0.0395	70.6

Table 4 shows the relationship between the degree of deflection and failure.

Figure 1 shows the relationship between load and deflection on two different types of base construction. The fill area is composed of a pumice type material taken out of the cut.

Sponsored by Committee on Flexible Pavement Design.

TABLE 2

OUTSIDE AND INSIDE WHEEL TRACK DEFLECTIONS

Type of Base	Fall Deflections (in.)		Spring Deflections (in.)		Percent Inside Deflection Higher Than Outside	
	Avg. Outside	Avg. Inside	Avg. Outside	Avg. Inside	Fall	Spring
Borrow	0.0402	0.0394	0.0756	0.0562	40.0	0.0
Cinder	0.0402	0.0430	0.0438	0.0417	37.5	28.5
Crushed Gravel	0.0227	0.0221	0.0252	0.0262	42.8	38.2
Crushed Pit Gravel	0.0185	0.0202	0.0220	0.0203	34.4	53.2
Crushed Rock	0.0184	0.0175	0.0220	0.0197	62.8	25.7

TABLE 3

TYPE OF BASE AND FAILURE

Type of Base	Total Avg. Defl. Spring + Fall (in.)	Percent Failed Points		
		Fall 1956	Spring 1957	Spring 1964
Borrow	0.0503	60.0	100.0	100.0
Cinder	0.0422	56.2	87.5	96.8
Crushed River Gravel	0.0240	4.7	19.0	28.5
Crushed Pit Gravel	0.0204	0.0	0.0	18.7
Crushed Rock	0.0201	0.0	2.8	17.1

TABLE 4

DEGREE OF DEFLECTION AND FAILURE

Deflection Range	Percent of Points Failed		
	Fall 1956	Spring 1957	Spring 1964[a]
0.0 - 0.0200	0.0	3.0	2.3
0.0201 - 0.0300	2.3	9.3	38.6
0.0301 - 0.0400	35.3	36.0	75.0
0.0401 and greater	78.9	100.0	100.0

[a]Percentages based on spring and fall measurements within deflection range. Thus the 2.3% indicated for the 0.0-0.020 range includes the 1.5% of total spring and fall measurements plus one project failed since 1957.

Table 5 shows the effect of pavement overlays and age on deflection. The increase in deflection immediately after placing is attributed to an increase in moisture content caused by condensation under the hot layer.

Table 6 shows the effect on deflection of increased deleterious fines formed in the base rock by attrition from traffic. Values of 2.5 in. maximum height and 25 percent maximum pass No. 20 would appear to be acceptable limits for the degradation test.

Table 7 shows the predicted decrease in deflection, using the constant 0.0038-in. decrease in deflection per inch of pavement increase, and the actual deflection obtained on three different points. (Data and procedures used to determine the value of 0.0038-in. decrease in deflection for each inch of asphaltic concrete added are given in the text of the complete report.)

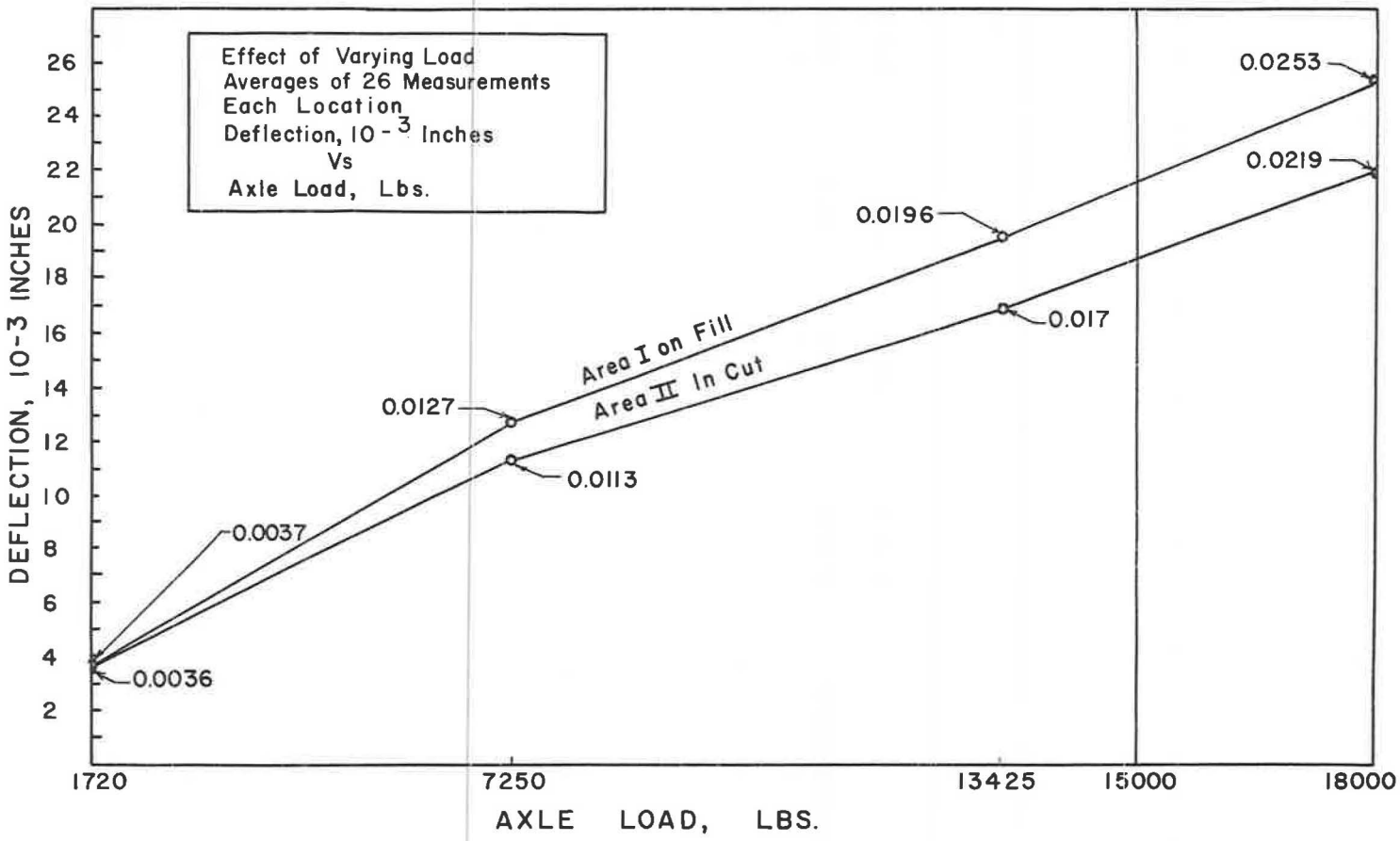
Effect of Varying Load
Averages of 26 Measurements
Each Location
Deflection, 10 - 3 Inches
Vs
Axle Load, Lbs.
DEFLECTION, 10-3 INCHES
26
24
22
20
18
16
14
12
10
8
6
4
2
0.0253
0.0219
0.0196
0.017
0.0127
0.0113
0.0037
0.0036
Area I on Fill
Area II In Cut
1720
7250
13425
15000
18000
AXLE LOAD, LBS.

Figure 1.

TABLE 5

REPEATED DEFLECTION TESTS

Project	Oil Mat	New Grade	Avg. Deflections ($^{1}/_{1000}$ in.) at Age				
			1 Day Base Lift, 2 In.	1 Day Top Lift, Total 3 In.	2 Weeks	1 Yr	2 Yr
1	41. 4		55. 5	44. 6	40. 7		31. 0
1		38. 6	30. 3	29. 2	29. 0		25. 6
2	35. 7					30. 5	27. 3

TABLE 6

REPEATED DEFLECTIONS OVER DEGRADING MATERIAL
(IN THOUSANDTHS OF AN INCH)

Project 1: Hwy 30, MP 138 to 142

Oregon Degradation Test Results on Base Material at MP 138:
Age—3 yr, Fall 1956; Height—3. 0 in.; Pass No. 20—26. 2%

	1956	1957	1960
Avg. Range (16 points)	20-26	18-28	28-46

Project 2: Hwy 15, MP 85

Point	1961	1963	Degradation	
			Height (in.)	Pass No. 20 (%)
1 Travel Lane SB	16	24	3. 2	18. 7
2 Travel Lane NB	18	24	3. 0	18. 8
3 Passing Lane SB	16	16	2. 0	16. 1
4 Passing Lane NB	16	16	3. 1	16. 7

TABLE 7

CALCULATED AND MEASURED DEFLECTIONS—9 KIP WHEEL LOAD

Project	Original Deflection	Overlay Thickness, In.	Constant	Theoretical Decrease	Predicted Deflection	Actual Deflection	
1	0. 0414	3. 5	0. 0038	0. 0133	0. 0281	0. 031	2 yr.
2	0. 0386	3. 5	0. 0038	0. 0133	0. 0253	0. 0256	2 yr.
2	0. 0357	1. 5	0. 0038	0. 0057	0. 0300	0. 0305	1 yr.
						0. 0273	2 yr.

Phase II—Field-Cut Beams

Three beams, 4 in. wide by 28 in. long, were cut from each of the projects measured for deflection under load in 1956 and 1957. Two of each set of beams were tested in the laboratory for fatigue of repeated flexure; one beam flexed 0. 020 in. and the other 0. 040 in. The third beam was tested to determine the coefficient of thermal expansion and beam strength at -10 F. Reclaimed asphalt tests, and tests to determine asphalt content, void content, and gradation were made on samples cut from the flexed and broken beams.

No correlation could be found between the number of deflections required for failure and pavement characteristics or ingredient characteristics. Several variables existed which could not be evaluated for their effect on fatigue life. These variables included the number and degree of deflections prior to cutting the beam, asphalt film thickness, asphalt consistency or hardness prior to cutting the beams, and improvements made on the deflection machine to remove distortion and extrusion of the test specimen.

Differences in coefficient of thermal expansion and modulus of rupture between specimens composed of cinder aggregate and nonvesicular aggregate are as follows:

Specimen	Avg. Coef. of Linear Expansion (in./in./deg F)	Avg. Modulus of Rupture, psi, at -10 F
Cinder Aggregate	1.51×10^{-5}	479
Nonvesicular Aggregate	1.268×10^{-5}	814

The hardening of the asphalt, as indicated by the reclaimed asphalt penetration, varied from 8 to 74 penetration points and averaged 42. 7 points for the 42 pavements tested. Due to the variables of aggregate characteristics, asphalt content, void content, mixing temperature and length, pavement age, weather conditions, and asphalt source, the reclaimed asphalt tests of penetration, thin film, and absolute viscosities are not capable of any valid comparison.

Phase III—Laboratory-Molded Specimens

Seventy-five sets of specimens were made in the laboratory. Tests were made to determine fatigue of deflection at two constant deflection amounts, void content, linear coefficient of thermal expansion, modulus of rupture at -10 F, and tests on reclaimed asphalt. Constants in the test specimens were aggregate source, asphalt source, material preparation, specimen fabrication, specimen handling, and test procedures. Controlled variables were aggregate gradation and asphalt content, consisting of 25 specific gradations at three asphalt contents.

Results of tests in terms of the number of deflections required to break the specimen were rated from 1 to 25 for each asphalt content and are presented in chart form. The total combined ratings for all 75 specimens show the best and second best in ability to withstand deflection on mixtures with 26 and 27. 5 percent of aggregate passing the No. 10 sieve.

The patterns formed by void contents on charts are relatively consistent for all conditions but there is no evidence of connection between void content and fatigue durability.

The coefficients of linear expansion of laboratory-made specimens are comparable to those of the field-cut beams. A relationship exists between asphalt content and linear expansion, as given in the table:

Identification	Coef. of Lin. Exp. (in./in./deg F x 10^{-5})	Range, x 10^{-5}
Lab-Made 5.0% Asph.	1.286	1.07-1.46
Lab-Made 5.5% Asph.	1.305	1.13-1.46
Lab-Made 6.0% Asph.	1.430	1.27-1.64
Avg. Lab-Made	1.340	1.07-1.64
Field Cut	1.286	1.00-1.53

The average modulus of rupture at -10 F and deflection at failure is 742.5 psi and 0.0385 in. Figures for the field-cut beams are 814 psi and 0.0473 in., respectively.

Tests on reclaimed asphalt show a range of penetration drop from 6 to 40 penetration points. There is a slight trend for less penetration drop with increased working on the fatigue machine.

Influence of AASHO Road Test Local Factors On Present Serviceability Index for Flexible Pavement Systems

ROBERT L. KONDNER, RAYMOND J. KRIZEK, and NAUSHERWAN HASAN
Northwestern University

ABRIDGMENT

•USING DATA from approximately 134 flexible pavement sections of the AASHO Road Test, a correlation is developed between flexible pavement performance and local factors considered, such as pavement structural composition, applied load, and number of load applications. Pavement performance is represented by a present serviceability index which has been correlated with a panel serviceability rating. The general expression used to describe the present serviceability index as a function of the number of load applications for given conditions of applied axle load and pavement structure assumes a constant rate of pavement deterioration during the majority of the year and a very rapid deterioration associated with spring thaw periods. The coefficients included in each of the above expressions are then determined as functions of applied axle load and a pavement thickness index. Specific values for all coefficients are presented for the environmental conditions of the AASHO Road Test, and illustrative examples are given to indicate the usefulness of this concept in the rational design of flexible pavement systems. Quantitative values for these coefficients for other localities, other material properties, and other environmental conditions may be obtained through a comprehensive satellite test program.

Sponsored by Committee on Strength and Deformation Characteristics of Pavement Sections.

Alternate Measures of Pavement Unserviceability

B. G. HUTCHINSON, Assistant Professor, University of Waterloo, Waterloo, Ontario

A most significant contribution of the AASHO Road Test to the rationalization of pavement design is the pavement serviceability-performance concept described by Carey and Irick (3). This pavement rating procedure has gained widespread acceptance in pavement studies, specifically in the Canadian pavement evaluation studies. Hutchinson (8) has pointed out some of the deficiencies of this subjective rating procedure and recommended the execution of further experimental studies to establish the significance of these deficiencies.

This paper examines the concept of pavement unserviceability and explores alternate techniques for measuring the serviceability characteristics of highway pavements. The requirements of a serviceability criterion are formally established and existing knowledge on human response to motion is reviewed in the light of these requirements. The results of an experimental program that involved the measurement of human tracking behavior are given and compared with parallel subjective ratings and measures of road roughness.

•THE PRINCIPAL features of the operating behavior of highway pavements that are of immediate interest to pavement design and evaluation studies are changes in the serviceability of a pavement throughout its life, and the limiting value of serviceability at which pavement failure occurs. A suitable model of pavement performance can be expressed in terms of three variables: the pavement unserviceability U, the unserviceability level U* at which pavement failure occurs, and the failure age A at which U* occurs. The essence of this model is conveyed by Figure 1. The term unserviceability, rather than serviceability, is used in this paper since it results in a more convenient scaling of these characteristics. Higher unserviceabilities are associated with higher roughness characteristics.

PAVEMENT UNSERVICEABILITY

It is well known that when a vehicle travels along a pavement, motions are generated in the body of a vehicle that are a function of the vehicular suspension characteristics, the vehicle speed and the magnitude and configuration of pavement roughness. This motion and vibration lead to discomfort and fatigue in driving operations, and Magid (9) points out that serious physiological disorders may result from protracted exposure to this vibration.

While there is a general consensus that the measurement of pavement unserviceability involves assessing some aspect of human response to motion, pavement unserviceability has not yet been defined explicitly in operational terms. A primary requirement in the measurement of any variable is the development of an operational definition of the variable.

The moving highway vehicle may be considered as an ensemble of two components, a man and a vehicle. The man reacts to certain inputs to him such as pavement markings, highway signs, other vehicles, weather conditions and the like. From his reactions to these stimuli, the man controls certain inputs to the vehicle (such as steering, throttle, brakes and so on) to produce a desired output which is ordered vehicle movement. The output of this subsystem of man and vehicle can only be evaluated relative to the objectives of the overall system which is highway transportation.

Paper sponsored by Committee on Pavement Condition Evaluation, and by Committee on Surface Properties—Vehicle Interaction, and presented at the 45th Annual Meeting.

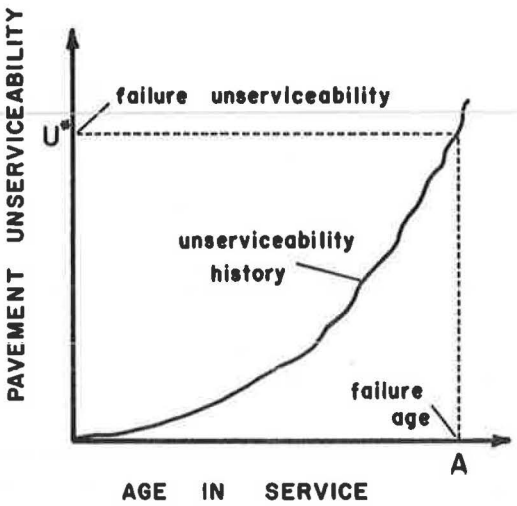

Figure 1. Pavement performance model.

The objectives of this system and many other large engineering systems can only be stated in broad and general terms. The development of an objective technique for evaluating the output of these systems becomes extremely difficult, if not impossible. In fact, the interactions between an engineering system and its environment may be too complex to measure in any other manner than by the judgments of experts. Such an approach was pursued in the AASHO Road Test formulation of pavement unserviceability.

At the present time, the objectives of highway transportation can only be defined in very general terms such as the provision of safe, comfortable, convenient, and economical highway transportation. An approach frequently used in engineering to overcome this type of problem is to decompose the system into its components and to develop measurable subcriteria for these components that seem to be compatible with the ultimate objectives of the total system.

In the absence of a more complete understanding of human behavior in highway vehicles it is impossible to isolate with certainty the critical human variables of the highway-vehicle-driver system. The only realistic approach at the present time is to define a human response characteristic that appears to be related logically to the overall objectives of highway transportation and one which is particularly sensitive relative to the objectives of highway transportation.

REQUIREMENTS OF AN UNSERVICEABILITY CRITERION

Since it is only feasible to estimate pavement unserviceability magnitudes indirectly through the use of a secondary variable, it is necessary to establish the requirements of this criterion in order to guide the selection of the most appropriate criterion. These requirements are as follows:

1. The criterion must be objective unless the feasible objective measures assess only trivial attributes of the system. It is well known that subjective estimates are susceptible to large systematic errors.
2. The measurement technique required to establish magnitudes of the criterion must be operational for widely dispersed pavement sections and must provide estimates of pavement unserviceability that are universally applicable and invariant.
3. The unserviceability criterion should reflect maximum sensitivity in discriminating between unserviceability magnitudes, but should minimize the differences in the measure between individuals.
4. The criterion measures should achieve at least interval measurement scale status because of the manner in which the measures are used in pavement design and evaluation.

HUMAN RESPONSE MEASURES

A fundamental problem in assessing human response to any type of stimulus is to establish exactly how human sensation magnitudes vary with intensities of the stimulus. It is not possible to measure sensory magnitudes directly and these must be estimated by observing an external verbal or symbolic response by a subject. In addition, the relation between these sensory magnitudes and the ability of an operator to perform a particular task is not well understood. Hutchinson (8) has pointed out that for conceptual clarity existing psychophysical theory presupposes the existence of a judgment

continuum, paralleled by a sensory continuum, and through this relationship, the judgment or response continuum is also related to the stimulus continuum.

Guilford (7) provides an exhaustive review of psychophysical scaling procedures that have been developed and used to establish functional relations between these continua. While they differ in detail, all psychophysical scaling methods may be considered as the combined effect on the response of a subject of an experimenter's operations of stimulation and instruction. Instruction refers to the response that is elicited from a subject, and the major differences in scaling methods are due to the difference in the response elicited and the particular methodology used. The present status of psychophysical measurement and other techniques for measuring human response characteristics may be summarized as follows:

1. It has not been rigorously established what behavioral observations of a subject constitute a valid measure of a subject's sensation.
2. A variety of psychophysical scaling procedures have been developed for eliciting verbal reports from subjects, which all have as their objective the minimizations of distortions between the judgment and sensory continua.
3. A number of relations have been generated between numerical estimates obtained in the above manner and the magnitudes of associated physical stimuli. However, the usefulness of these relations in predicting human behavior under general environmental conditions has not been adequately demonstrated.
4. A number of recent investigations suggest that objective physiological measures of sensation may be developed in the future, but at the present time, little is known about their relation to human performance.
5. The majority of recent work in engineering psychology has been somewhat more pragmatic. It has been oriented toward establishing decrements in the performance of a task by a subject when the subject is exposed to various levels of a particular stimulus. The task is either the real world task of interest, or some abstraction of the task that closely parallels it.

HUMAN RESPONSE TO MOTION

Human response to whole body vibration and motion has been assessed in the past by many criteria such as subjective tolerances, mechanical body response and the like. In this section, the implications of current knowledge on human response to motion are briefly reviewed. This knowledge and the previously established requirements for the unserviceability criterion are then used to select the most appropriate criterion.

Mechanical Body Response

When humans are subjected to motion, the vibrations first of all have a mechanical effect on the body. The magnitude of this mechanical body response depends on the dynamic properties of the body and the magnitude and nature of the motion. Physiological and psychological effects are known to result from the mechanical effects depending on the magnitude and duration of the motion.

Coermann (4) suggests that one approach to the study of mechanical body response is to consider it as a complex system of masses, elastic elements, and viscous dampers. He has pursued these studies by measuring mechanical impedance. This is a technique that is used to describe the transmission of mechanical energy within a complex mechanical system. Coermann has developed a mechanical analog of the human body (Fig. 2) which illustrates the natural frequencies of various portions of the body.

Figure 3 illustrates some of Coermann's experimental observations in which the impedance is plotted against frequency for a subject in various situations. For purposes of comparison, the mechanical impedance of a 150-lb mass is shown along with the impedance characteristics of a simple one mass-spring system. The important features of these experimental results are the fact that the body responds like a pure mass at low frequency vibrations up to 2 cps and the high impedance at about 6 cps.

The mechanical properties of the body cannot be viewed in isolation with respect to the problem at hand, and are only important with respect to the responses that they

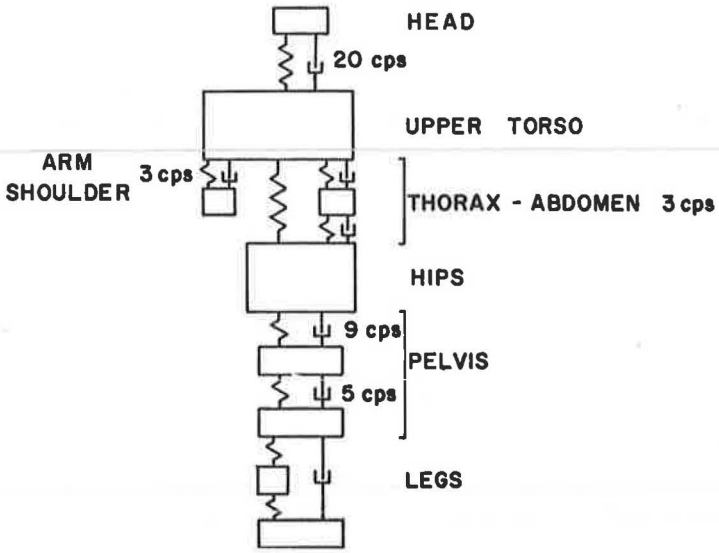

Figure 2. Mechanical analog of human body.

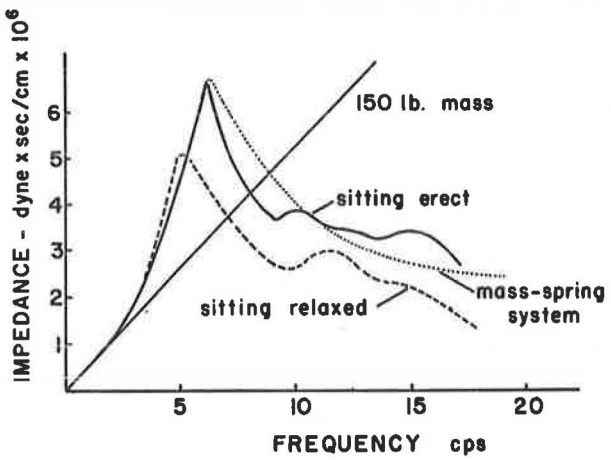

Figure 3. Mechanical impedance of several systems.

elicit. The significance of these findings will be discussed after the nature of subject response measurements is examined.

Subjective Response

A number of investigations have been undertaken in an attempt to assess the magnitude and nature of subjective judgments to motion. Various subjective responses from the threshold of perception to the feeling of pain have been defined and used to classify these sensations to motion.

Goldman (6) reviewed much of the early data and averaged response data from a number of investigations and has interpreted and classified information in terms of three types of subjective response: perceptible, unpleasant and intolerable. The results

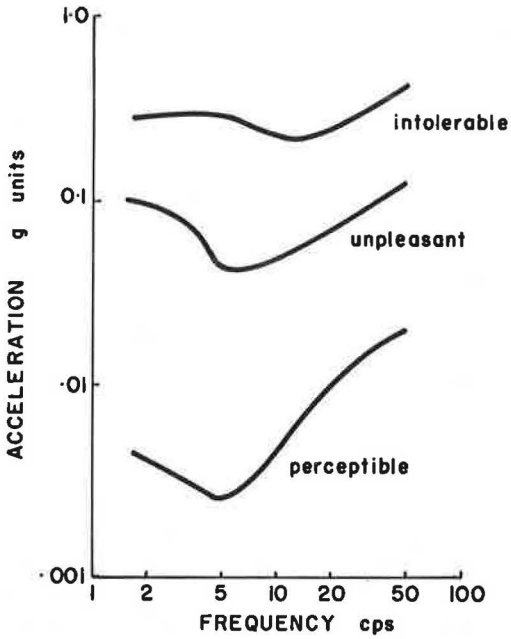

Figure 4. Subjective response data (6).

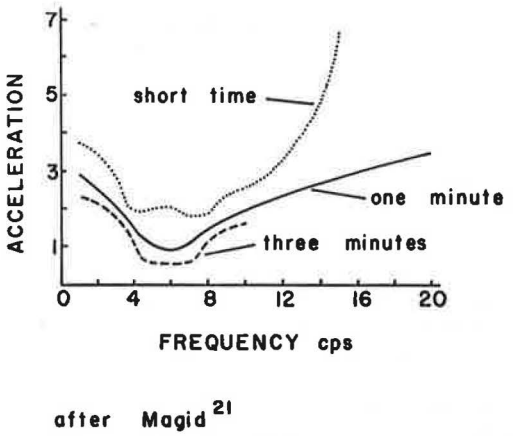

after Magid [21]

Figure 5. Short-term subjective tolerance data.

of his compilation are shown in Figure 4. A great deal of variation is apparent in these trends as conveyed by Figure 4, and the relations must be considered to be indicative of general trends only. Goldman suggested that much of this variation resulted from variations in experimental procedures as well as the difficulties inherent in explicitly defining subjective response classes.

More recent studies have been undertaken by Parks (11) and Magid (9). The important feature of both of these experimental programs was the reinforcement of Goldman's observations.

Probably the most significant experiments are those carried out by Coermann (4) in which both mechanical body response and short time tolerances were measured simultaneously. Figure 5 summarizes Coermann's data, and the findings of Parks and Magid are also shown in the graph. The information contained in this graph indicates the dependence of subjective tolerances and mechanical body response measurements.

Stevens (14) has argued that for physical continua such as vibration and motion that involve changes in intensity, the sensory scale value S obtained from verbal reports is to a close approximation a power function of the physical energy p of a stimulus for a large number of stimuli

$$S = a\, p^b \tag{1}$$

Stevens has shown that for a variety of modalities the exponent b is a reproducible quantity, while the parameter a depends on the units of both the physical and response scales. Stevens has suggested a technique of subjective measurement which has been used by Versace (15) to measure the subjective responses of passengers to automobile motion. It is a procedure in which a subject equates the apparent strengths of the sensations produced in two different modalities. Suppose that the values of two scales are p_1 and p_2, and the subjective magnitudes are related to the physical stimuli by the power functions

$$\begin{aligned} S_1 &= a\, p_1^b \\ S_2 &= c\, p_2^d \end{aligned} \tag{2}$$

and that cross modality matching is defined as meaning equal subjective values; that is, $p_1 = p_2$ if $S_1 = S_2$ and

$$p_1 = \left(\frac{a}{c}\right)^{1/b} p_2{}^{d/b} \tag{3}$$

Consequently, if one of the power functions, say for p_1, has been established in the laboratory for a particular subject, then the nature of the other power function relating S_2 and p_2 may be readily established from experimental cross modality data and Eq. 3.

Versace (15) has reported some experimental results in which passengers were required to adjust a continuous sound intensity to match their subjective estimates of the intensity of automobile motion generated by various road roughness configurations. While Versace has generated a limited amount of systematic data, the fundamental question that remains unanswered involves the meaning that can be attached to the verbal responses that a subject emits to a stimulus. This question is fundamental to all scaling procedures that rely on verbal reports.

Tracking Tasks

An alternate approach to assessing human response to physical stimulation is to measure the ability of subjects to perform various tasks when exposed to different intensities of a physical stimulus. The use of tracking tasks to measure human response has gained most impetus from the area generally known as human factors engineering.

The conventional type of tracking task usually requires a subject to track some type of externally generated input function using a specific type of control mechanism in which the experimenter is interested. The control mechanism generates an output function, and the difference between the input and output function is usually referred to as the tracking error. The goal of the subject exposed to such a task is to minimize the tracking error under the various environmental conditions.

While tracking tasks have been used extensively in an engineering context, they have never been defined other than by convention. At the present time, no adequate theory of tracking behavior exists, and the use of tracking tasks to assess human behavior remains an arbitrary procedure. However, their contribution lies in the fact that the task of the subject is the actual task of interest, or some task that closely approximates the essential features of the real task. In addition, these tracking tasks yield reliable data when they are executed under carefully controlled test conditions, and the measurements are objective.

SELECTION OF CRITERION

Each of these procedural classes for assessing human response was reviewed in the light of the previously established requirements for an unserviceability criterion in order to isolate the most appropriate criterion. A tracking task was selected for the following reasons:

1. The primary task of the driver of a highway vehicle involves tracking; the operator must react to a variety of stimuli such as pavement markings, signs and other vehicles to produce an ordered movement in his vehicle.
2. The more sophisticated subjective estimate procedures that have been developed to minimize the influence of systematic errors on judgments depend on an ordered sequential application of stimuli to a subject. This requirement excludes the use of these techniques for field experiments on dispersed pavement sections.
3. The cross-modality matching technique provides a means for overcoming the problem mentioned in 2. However, the significance of these measurements can only be judged relative to their ability to predict changes in driver performance.
4. Tracking tasks in which procedural variables have been properly selected can be used to assess human response on any pavement section independently of other pavement sections.

5. Tracking tasks eliminate many of the systematic errors to which subjective estimate procedures are susceptible.
6. Subjective responses arise from the mechanical reaction of the body and tracking tasks measure a combination of mechanical response and the influence of sensory responses on motor behavior.

EXPERIMENTAL EQUIPMENT AND PROCEDURES

The tracking task that was developed is shown in Figure 6. The mechanism consists of an electrically driven paper chart feed that can be easily mounted in a variety of highway vehicles. The input function is drawn on the chart paper, and each subject is required to track this input signal with a hand-held felt pen while attempting to null the tracking error.

Adams (1) points out that the variables which influence human tracking behavior may be classified into two groups: task variables and procedural variables. Task variables concern those factors which are equipment centered, and relate to the physical attributes of the tracking task. The procedural variables relate to the human subject and involve such factors as instructions to the subject and the number of practice runs.

Task Variables

The first task variables established were those dealing with the properties of the input function. Morgan (10) has reviewed human tracking response characteristics associated with step, ramp, sine and complex wave inputs. Human operators are most capable of tracking ramp inputs with little error after a small amount of training. The most desirable frequency range for an input function is $\frac{1}{5}$ to $\frac{1}{2}$ cps, and in view of the comments by Young (17) regarding the slope of the input function, a triangular wave form of 1.2-cm amplitude, 30-cm wavelength, and a chart speed of 6 cm/sec was

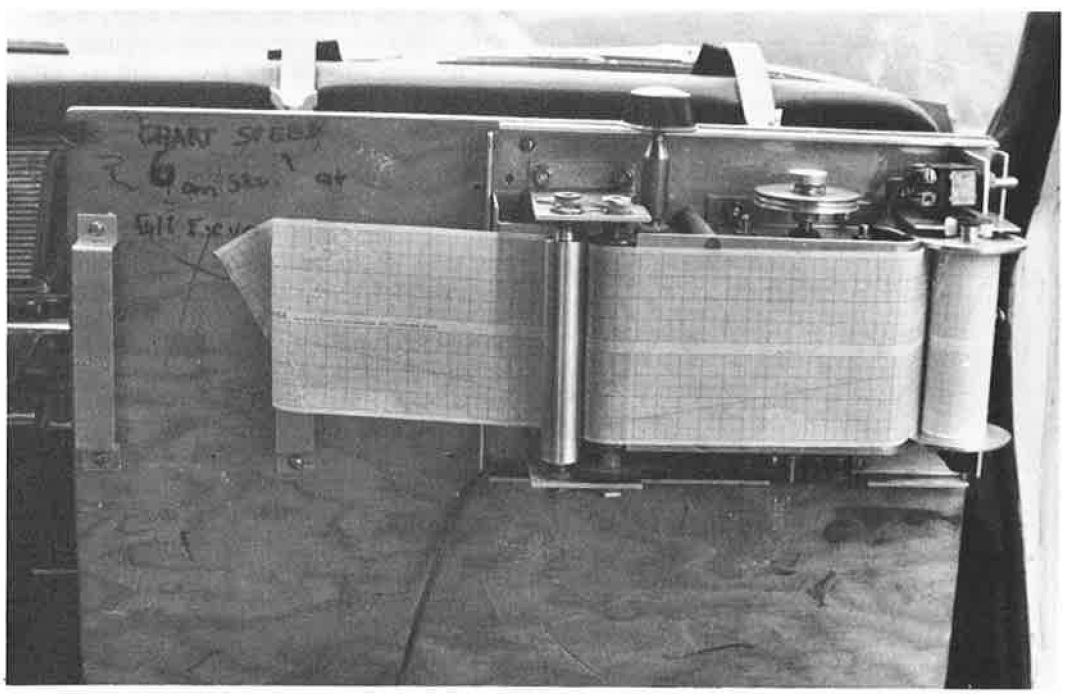

Figure 6. Tracking device.

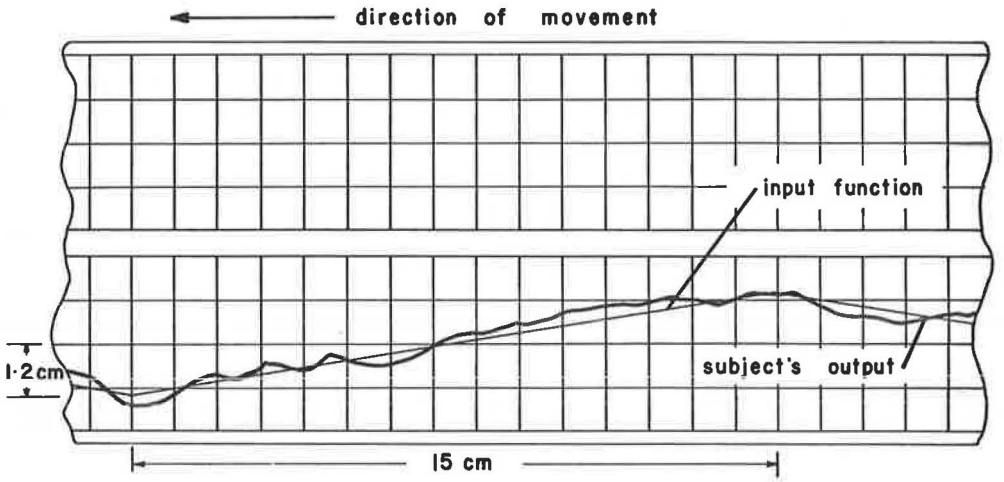

Figure 7. Characteristics of input function.

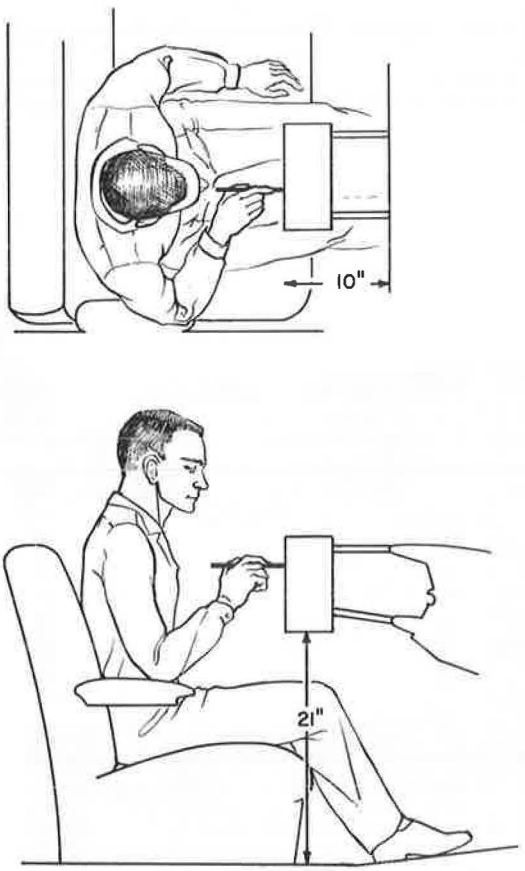

All dimensions are standard for the 1963 Pontiac Laurentian sedan

Figure 8. Arrangement of tracking task.

selected for the input function. The properties of the input function are shown in Figure 7. The selection of these input function parameters was guided by the previously established requirement that differences between the performance of subjects should be minimized.

The tracking device was rigidly attached to the instrument panel of the test vehicle (Fig. 8). The tracking device was located opposite the front passenger seat, and positioned such that a subject's elbow rested on the arm rest of the door, and no contact existed between a subject's forearm and body.

The felt pen was held by a subject at a point two inches from the felt nib and in the normal writing position. No part of the subject's hand was in contact with the tracking mechanism and each subject was constrained by a seat belt. The relationship of vehicle, tracking task and subject is shown in Figure 9. The test vehicle was a 1963 Pontiac Laurentian sedan. The vehicle speed during all test runs was maintained at 60 mph.

Direct tracking of the input signal by a subject, in preference to the use of an intervening control mechanism, was selected for two reasons. The first reason was to insure that human responses were not distorted by the response characteristics of any control mechanism. Second, Morgan (10) points out that a subject's motivation in the execution of a task depends on the degree to which an operator exercises

Figure 9. General arrangement of subject, tracking device and vehicle.

control over an output signal, as well as the speed with which an operator obtains feedback on his performance.

Procedural Variables

Eight male university students were selected from the summer students employed by the Department of Highways of Ontario. The students were right-handed and their ages ranged from 20-25 years. The primary procedural variable examined concerned the orientation and training of subjects.

A great deal of experience with tracking tasks has indicated that the abilities of subjects to perform a tracking task improve rapidly with training. Simple tasks performed

under good working conditions result in small performance errors that are reduced very little with practice. In complex tasks, performance ability may increase over a long period of time, but the majority of improvement will take place during initial practice sessions.

The orientation and training program consisted of general instruction in the task as well as initial practice runs on pavement test sections. Two training test sections were established in the vicinity of Metropolitan Toronto and were similar in layout to the regular test sections. Each subject was required to perform the tracking task during six trials on each of the two test sections. Previous studies carried out during the developmental period had revealed that performance ability became asymptotic at about 4 or 5 test runs.

Each pavement test section was 1500 feet in length and was preceded by a 1000-ft long initial section and succeeded by a 200-ft long runout section. The tracking task was activated before the total test section complex and each subject was instructed to commence tracking as the test vehicle crossed the start line. The subject performed the task for the complete 2700 feet. A subject performed the tracking task at each test section three times in succession. To minimize the systematic errors associated with procedural influences (the time between test runs, tracking instability at the start of test runs and so on), a number of procedural precautions were taken. A subject's performance was only evaluated from his behavior during the second and third test runs, and tracking errors were scored only for the central 1500 feet of the test section layout.

Ten pavement test sections were located throughout the Ontario provincial highway system possessing a range of roughness characteristics. The test sections were clustered in two groups of five sections. The pavements within each test section were located within a radius of about 10 miles so that randomization in the order with which test sections were traversed could be accomplished. The group of pavements at which each subject began his circuit of the test sections was selected randomly. Five randomly selected subjects repeated the task on all test sections.

SCORING TRACKING ERROR

Poulton (12) has examined methods of scoring tracking error and points out that two types of tracking error must be examined: errors of position and errors of timing. An error in position may be regarded as arising from an operator not reversing his tracking action sufficiently quickly. An error in timing refers to the fact that the operator may reproduce the input function faithfully but the output function may be displaced by a constant amount. Figure 10 conveys the nature of these two error types. The problem that arises in assessing tracking behavior is concerned with what error should be measured, and then how should the error be measured?

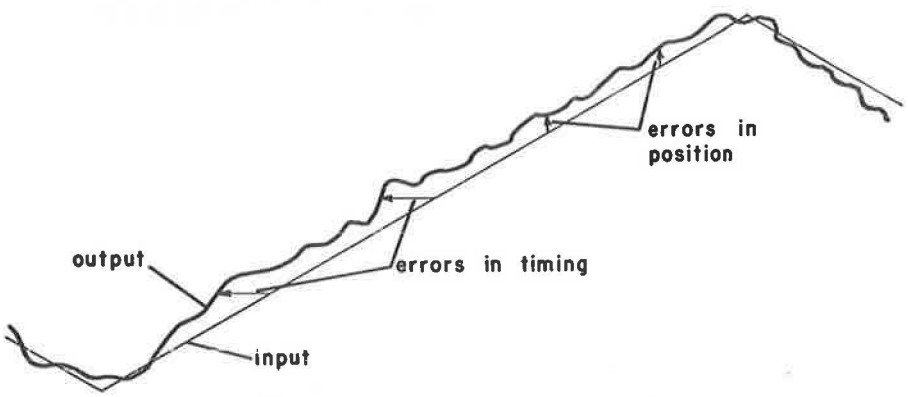

Figure 10. Types of tracking error.

TABLE 1

MEAN SQUARE TRACKING ERROR—REPLICATION NO. 1

Subject No.	Pavement Section										Σ
	0	1	2	3	4	5	6	7	8	9	
1	2.1	3.1	2.1	3.2	1.9	1.9	1.6	3.4	2.8	1.7	46.7
	1.7	2.9	2.1	3.3	1.3	2.1	1.6	2.8	3.6	1.5	
2	2.0	2.1	1.8	2.3	1.6	1.2	1.9	3.4	3.9	1.6	42.4
	1.6	1.9	1.7	2.6	1.6	1.3	2.0	3.3	3.0	1.6	
4	1.3	2.7	2.6	2.8	1.7	1.2	1.5	4.1	2.9	2.1	43.0
	1.2	2.0	2.2	2.8	1.6	1.0	1.3	3.7	2.6	1.6	
5	1.7	2.6	2.0	3.5	2.1	1.6	1.6	3.0	2.6	1.5	45.1
	1.4	3.2	1.6	3.9	2.2	1.8	1.6	2.7	2.9	1.6	
6	1.6	2.7	2.3	2.2	1.6	1.6	1.9	3.0	2.9	1.9	46.1
	1.6	2.7	2.2	3.2	1.4	2.2	2.0	3.9	3.5	1.7	
7	1.8	2.9	2.0	2.6	1.9	1.3	1.6	3.6	3.0	2.3	46.2
	1.8	2.9	1.9	3.2	1.5	2.5	2.0	2.1	3.8	1.5	
8	2.0	2.8	2.1	3.4	1.7	1.4	1.4	4.5	3.8	1.7	50.2
	2.5	2.3	2.2	2.7	2.0	1.4	2.2	4.4	3.3	2.4	
9	1.0	2.6	1.4	2.7	1.3	1.5	1.4	3.2	4.6	2.1	45.7
	1.0	3.0	2.4	3.3	1.6	1.7	1.9	3.0	3.9	2.1	
	26.3	42.4	32.6	47.7	27.0	25.8	27.5	54.1	53.1	28.9	365.4
Mean	1.65	2.65	2.03	2.98	1.69	1.61	1.72	3.38	3.30	1.80	45.7

TABLE 2

MEAN SQUARE TRACKING ERROR—REPLICATION NO. 2

Subject No.	Pavement Section										Σ
	0	1	2	3	4	5	6	7	8	9	
1	1.0	3.4	1.6	3.3	2.6	1.5	1.6	3.5	3.1	1.4	43.9
	2.0	2.5	1.6	2.5	2.5	1.0	1.6	3.3	2.5	1.4	
5	1.4	3.2	1.9	2.6	2.0	2.0	1.7	2.8	2.2	2.0	42.5
	1.4	3.0	2.2	2.9	1.5	1.5	1.3	3.0	2.2	1.7	
6	2.1	2.3	1.9	3.5	1.8	1.8	1.9	3.4	3.4	1.6	47.5
	1.9	2.7	1.3	3.2	1.7	1.5	2.0	4.2	3.9	1.4	
7	1.2	2.2	2.2	2.7	1.9	1.6	1.7	3.4	3.8	1.9	48.1
	1.4	2.9	3.1	3.6	1.6	1.5	2.0	4.0	3.7	1.7	
8	2.2	3.5	1.3	4.0	1.8	1.8	2.0	4.3	3.0	1.7	52.2
	1.6	3.7	2.0	3.9	1.9	1.7	1.8	4.6	3.4	2.0	
	16.2	29.4	19.1	32.2	19.3	15.9	17.6	36.5	31.2	16.8	46.8
Mean	1.62	2.94	1.91	3.22	1.93	1.59	1.76	3.65	3.12	1.68	

TABLE 3

PRESENT PERFORMANCE RATINGS

Rater	Pavement Section									
	0	1	2	3	4	5	6	7	8	9
1	8.0	4.0	7.3	6.9	7.7	6.0	9.0	3.1	4.2	7.8
2	8.9	6.2	6.0	6.3	7.0	7.5	8.5	3.6	3.9	8.5
3	8.0	4.6	6.6	4.8	6.6	4.5	7.2	3.6	5.0	7.8
4	7.9	6.1	7.8	6.8	7.5	6.0	8.0	4.0	5.0	7.0
5	7.0	5.5	6.6	6.0	7.0	4.8	7.5	4.7	5.0	6.0
	39.8	26.4	34.3	30.8	35.8	28.8	40.2	19.0	23.1	37.1
PPR	8.0	5.3	6.9	6.2	7.2	5.8	8.0	3.8	4.6	7.4

The major component of highway vehicle motion is vertical and in view of the comments by Poulton (12) on the response strategies of subjects, the mean square error in position was selected as a criterion of human performance. The mean square error in position was obtained by calculating the mean and mean square deviation within each half wavelength, and then correcting the mean square deviation to a zero mean deviation. The performance of each subject on each test run was expressed as the mean square error in position for the central portion of each tracking record. The raw tracking scores for each subject on each test section are given in Table 1 and 2 for the two replications.

SUBJECTIVE ESTIMATES

The regular pavement rating team of the Department of Highways of Ontario also assessed the serviceability characteristics of each pavement test section according to the standard procedure of the Canadian Good Roads Association (2). This procedure is an adaptation of the AASHO Road Test procedure and it uses a ten-point rather than a five-point rating scale. The pavement ratings reported by this panel are given in Table 3.

ANALYSIS OF EXPERIMENTAL RESULTS

The tracking task described earlier, which has been used to obtain measures of human response under the various environmental conditions, was based on the following premises:

1. The human response measure is a reliable criterion and the major systematic errors to which the measurement procedure is susceptible have been removed by the selection of appropriate task and procedural variables.
2. The measure of human response is a valid criterion for estimating pavement unserviceability.
3. The human performance measure is systematically related to parallel measures of pavement roughness.

The validity of these premises is examined in this and the succeeding sections of the paper.

The mean square tracking errors listed in Table 1 were subjected to an analysis of variance and the results of this analysis are given in Table 4. This table shows that the source of variation in the mean square tracking error due to pavements is significant as well as the pavement × subject interaction. Table 5 contains the results of the

TABLE 4

ANALYSIS OF VARIANCE TABLE—REPLICATION NO. 1

Sources	Sum of Squares	Degrees of Freedom	Variance	F Ratio	Significance
Pavements	75.519	9	8.391	73.61	—[a]
Subjects	2.010	7	0.287	2.52	—[b]
Pavements × Subj.	14.949	63	0.237	20.8	—[a]
Observations	9.130	80	0.114		
Total	151.36	159			

[a]Significant at 1 percent level.
[b]Not significant.

TABLE 5

ANALYSIS OF VARIANCE TABLE—BOTH REPLICATIONS

Sources	Sum of Squares	Degrees of Freedom	Variance	F Ratio	Significance
Pavements	98.002	9	10.889	93.07	—[a]
Subjects	3.072	4	0.768	6.56	—[a]
Replications	0	1	—	—	—[b]
Pavements × Subj.	10.053	36	0.279	2.38	—[a]
Pavement × Rep.	1.344	9	0.149	1.27	—[b]
Subject × Rep.	0.604	4	0.151	1.29	—[b]
Observations	11.645	100	0.117		
Total	189.991				

[a]Significant at 1 percent level.
[b]Not significant.

analysis of variance for both replications. To simplify the analysis, only the results common to the five subjects were included. This analysis also revealed that the sources of variation due to both pavements and subjects as well as the pavement × subject interaction were significant.

It is important to note that both the pavement × replication and the subject × replication interactions were found to be nonsignificant. The nonsignificance of these two sources of variation indicate that the systematic errors to which this type of experimental technique is susceptible have been removed by the appropriate selection of task and procedural variables.

An important factor now arises in connection with the interpretation and use of the mean square tracking errors as estimates of pavement unserviceability. This involves the treatment of the sources of variation due to subjects and due to the pavement × subject interaction. A requirement of the formulation is that it is necessary to be able to express the individual response measures on a common scale of measurement.

Ghiselli (5) points out that under many circumstances measurements of human characteristics cannot utilize an absolute zero as a reference point and that equal differences in raw scores may not be indicative of equal differences in the trait being measured. Consequently the raw scores of individuals must be treated in some way so that the transformed scores can

TABLE 6

STANDARDIZED TRACKING ERRORS—REPLICATION NO. 1

Subject No.	Pavement Section									
	0	1	2	3	4	5	6	7	8	9
1	-0.27	1.10	-0.27	1.23	-0.55	-0.55	-0.96	1.51	0.68	-0.82
	-0.82	0.82	-0.27	1.37	-1.37	-0.27	-0.96	0.68	1.78	-1.10
2	-0.13	0	-0.79	0.26	-0.66	-1.18	-0.26	1.71	2.37	-0.66
	-0.66	-0.26	-0.53	0.66	-0.66	-1.05	-0.13	1.58	1.18	-0.66
4	-1.05	0.58	0.47	0.70	-0.58	-1.16	-0.81	2.21	0.81	-0.12
	-1.16	-0.23	0	0.70	-0.70	-1.28	-1.05	1.74	0.47	-0.70
5	-0.80	0.40	-0.40	1.60	-0.26	-0.93	-0.93	0.93	0.40	-1.07
	-1.20	1.20	-0.93	2.13	-0.13	-0.67	-0.93	0.53	0.80	-0.93
6	-0.99	0.56	0	-0.14	-0.99	-0.99	-0.56	0.99	0.85	-0.56
	-0.99	0.56	-0.14	1.27	-1.27	-0.14	-0.42	2.25	1.69	-0.85
7	-0.69	0.83	-0.42	0.42	-0.56	-1.39	-0.97	1.81	0.97	0
	-0.69	0.83	-0.56	1.25	-1.11	-0.28	-0.42	-0.28	2.08	-1.11
8	-0.61	0.20	-0.51	0.82	-0.92	-1.22	-1.22	1.94	1.73	-0.92
	-0.10	-0.31	-0.41	0.10	-0.61	-1.22	-0.41	1.84	0.71	-0.20
9	-1.31	0.30	-0.91	0.40	-1.01	-0.81	-0.91	0.91	2.32	-0.20
	-1.31	0.71	-0.10	1.01	-0.71	-0.61	-0.40	0.71	1.62	-0.20
	-12.78	7.29	-5.77	13.78	-12.09	-13.19	-11.34	21.06	20.46	-10.10
Mean	-0.80	0.41	-0.36	0.86	-0.75	-0.82	-0.70	1.32	1.28	-0.63

TABLE 7

STANDARDIZED TRACKING ERRORS—REPLICATION NO. 2

Subject No.	Pavement Section									
	0	1	2	3	4	5	6	7	8	9
1	-1.45	1.45	-0.72	1.33	0.48	-0.84	-0.72	1.57	1.08	-0.96
	-0.24	0.36	-0.72	0.36	0.36	-1.45	-0.72	1.33	0.36	-0.96
5	-1.17	1.83	-0.33	0.83	-0.17	-0.17	-0.67	1.17	0.17	-0.17
	-1.17	1.50	-0.17	1.33	-1.00	-1.00	-1.33	1.50	0.17	-0.67
6	-0.33	-0.11	-0.56	1.22	-0.67	-0.67	-0.56	1.11	1.11	-0.83
	-0.56	0.33	-1.22	0.89	-0.78	-1.00	-0.44	2.00	1.67	-1.11
7	-1.32	-0.22	-0.22	0.33	-0.55	-0.88	-0.77	1.10	1.54	-0.55
	-1.10	0.55	0.77	1.32	-0.88	-0.44	-0.99	1.76	1.43	-0.77
8	-0.38	0.85	-1.23	1.32	-0.75	-0.75	-0.57	1.60	0.38	-0.85
	-0.94	1.04	-0.57	1.23	-0.66	-0.85	-0.75	1.89	0.75	-0.57
	-8.66	7.58	-4.97	10.16	-4.62	-8.05	-7.52	15.03	8.66	-7.50
Mean	-0.87	0.76	-0.50	1.02	-0.46	-0.81	-0.75	1.50	0.87	-0.75
Grand Mean	-0.82	0.57	-0.41	0.92	-0.64	-0.82	-0.73	1.39	1.12	-0.68

be directly compared. Ghiselli points out that a convenient technique for observations of this type is to transform the raw observations into standardized variables. A standard score expresses an individual's score in units that are given as standard deviations of scores of his group. The mean square tracking errors contained in Tables 1 and 2 have been transformed into standard tracking errors with a zero mean value and unit standard deviation, and are given in Tables 6 and 7, respectively. The conversion of each individual's behavior to a common continuum assumes that the individual's units of measurement of behavior are made comparable by equating their variabilities.

The subjective pavement ratings of Table 3 could also be transformed into standard ratings. However Guilford (7) has suggested that linearity assumptions are not valid in connection with ratings, particularly in respect to the central tendency effect.

Ghiselli (5) points out that a useful numerical index of the reliability of an experimental technique is to compute the correlation coefficient obtained from separate applications of the test. Correlation coefficients have been computed for the five subjects for which replicated data were obtained and these are

Subject No.	1	5	6	7	8
r	0.80	0.85	0.97	0.89	0.86

The mean reliability index for the five subjects is 0.87 indicating that the test-retest reliability of the technique is quite good.

Sources of unreliability may arise because of several factors. A major source of unreliability is probably the instability of the test environment. Variations in the path and speed of the test vehicle, the influence of passing trucks and cars on the motion of the vehicle may all contribute to the random fluctuations in the test results. In addition, the performance of the individual being assessed will fluctuate as a function of the temporary variations in the state of the subject. Factors such as the individual's motivation, emotional state, and susceptibility to fatigue may have an important influence on the stability of a subject's performance.

It must be recognized that the tracking behavior reported in this paper is for a relatively homogeneous group of subjects and for one type of highway vehicle. Consequently any generalizations of the experimental observations to a larger population must be undertaken with extreme caution. The use of a wider range of test subjects could be handled through standardization of their observed responses providing the linearity assumptions are still valid. Nevertheless the experimental program reported in this paper has indicated that the measurement technique is a reliable procedure for field conditions.

COMPARISON OF SUBJECTIVE RATINGS AND TRACKING BEHAVIOR

Figure 11 shows the relationship between the mean present performance rating and the mean standard tracking error for each pavement section. The equation relating these two variables is

$$PPR = 6.307 - 1.352\,T \qquad (4)$$

where

PPR = mean present performance rating, and
T = mean standard tracking error.

It is interesting to note that the relationship is linear at least for the pavements examined in this investigation. It was previously mentioned that Coermann (4) observed an essentially linear relation between mechanical body response and reported subjective magnitudes in the low frequency range of vibration. In fact, Coermann suggests that relative displacements of the effective body mass can be calculated with sufficient accuracy from the mechanical impedance of the subject and then used to estimate subjective tolerance.

Figure 11 indicates that only two pavement sections, Nos. 5 and 3 differ greatly from the trend line. Test section 3 possessed a high degree of surface distortion although it

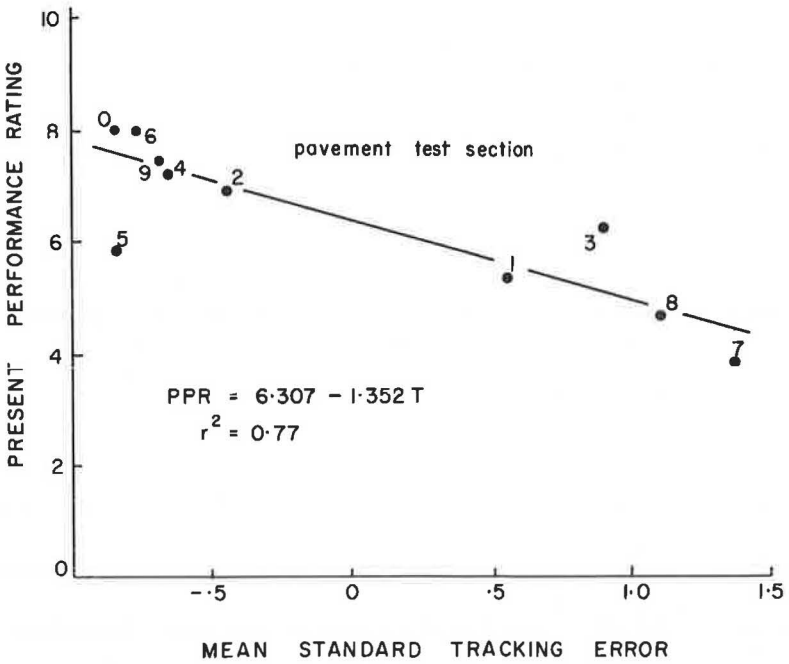

Figure 11. Present performance rating vs mean standard tracking error.

was located on a highway whose overall geometric properties were quite good. Section 5, on the other hand, was located on a highway whose overall geometric characteristics were of a lower standard, and whose surface contained areas of cracking that did not influence the motion of the vehicle. These observations suggest that raters are influenced by their overall impression of the highway section, rather than solely by the attributes of the pavement itself. Hutchinson (8) has pointed out that this type of systematic error, the halo effect, is a common source of distortion in subjective ratings. These observations on the presence of the halo effect are confirmed by the relations established in the next section between the human response measures and pavement roughness. Recent studies of pavement ratings reported by Yoder (16) have also indicated that significant systematic errors are present in pavement ratings that cannot be explained by the roughness characteristics of pavements.

The previously described requirements for a pavement unserviceability demand that the criterion measures be scaled on an interval scale. Only when such a scale status is achieved is the calculation of an average human response valid. Implicit in the use of the mean standard tracking error is that this measure achieves interval scale status. Measurements on interval scales should remain invariant under linear transformations of the scale. The question remains as to whether the mean standard tracking errors would remain invariant under changes in the task variables and the use of a more heterogeneous group of subjects. These questions can only be answered by further empirical investigation.

A most significant problem that remains unanswered is under what conditions are equal increments in the mean standard tracking error reflected as equal increments in the underlying pavement ratings. Unfortunately, this question cannot be answered at the present time until a more fundamental understanding of human response to motion is developed and the appropriate variables of the driver-vehicle system isolated.

The apparent linear relation between the mean standard tracking error and the mean present performance rating implies that either criterion is equally valid as an estimator of pavement unserviceability. The criterion that is least sensitive to extraneous

environmental influences yet sufficiently sensitive to the influence of motions induced by pavement roughness should be selected.

RELATION BETWEEN TRACKING ERROR AND PAVEMENT ROUGHNESS

The roughness content of each pavement section was sampled by recording the outer wheelpath surface elevation profile at 1-ft intervals. The spectral density characteristics of each profile were examined and they indicated that the total variance characteristics of roughness amplitudes were sufficient to define the roughness content of a profile. Quinn (13) has pointed out that the longest wavelengths of interest to vehicle performance are of the order of 100 feet.

The roughness content of each profile was expressed by sampling 100-ft long sections of the profile and fitting a straight line to the roughness amplitudes. The roughness content of the short length of profile was expressed by means of the residual sum of squares divided by the number of pieces of data. Table 8 contains the calculated variances and the average variance for each profile.

Figure 12 shows the relationship observed between the mean standard tracking error and the mean amplitude variance associated with 100-ft long segments of the profile; it indicates that a well defined linear relation exists between these two variables which may be defined by

$$T = 0.038\,R - 1.732 \qquad (5)$$

where

T = mean standard tracking error, and
R = roughness amplitude variance × 10^4.

TABLE 8

VARIANCE OF ROUGHNESS AMPLITUDES

Section No.	Variance Estimates × 10^4										Mean
0	24,	2,	68,	22,	31,	53,	33,	2,	33,	5,	27
1	34,	23,	36,	32,	147,	24,	94,	44,	55,	114,	56
	30,	41,	97,	41,	36,						
2	13,	18,	10,	40,	15,	112,	41,	105,	41,	14,	37
	21,	2,	47,	66,	28						
3	11,	73,	44,	19,	16,	28,	31,	65,	247,	16,	72
	56,	210,	207,	33,	35						
4	15,	54,	5,	11,	11,	66,	25,	59,	14,	47,	27
	18,	5,	36,	21,	16,						
5	52,	11,	4,	68,	16,	13,	68,	8,	10,	27,	31
	12,	4,	53,	97,	23						
6	17,	16,	36,	13,	14,	8,	27,	9,	29,	84,	23
	51,	10,	15,	24,	8						
7	77,	122,	66,	30,	38,	56,	41,	40,	134,	136,	83
	139,	60,	136,	95,	77						
8	46,	29,	15,	18,	113,	231,	43,	58,	164,	41,	73
	47,	64,	71,	71,	61						
9	3,	11,	18,	16,	63,	35,	67,	8,	3,	54,	24
	4,	24,	35,	14,	123						

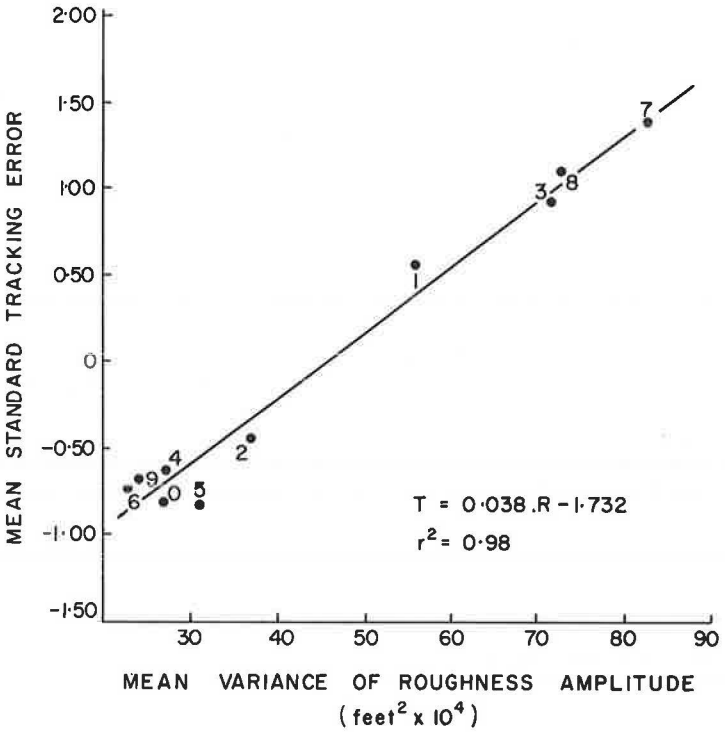

Figure 12. Mean standard tracking error vs roughness amplitude index.

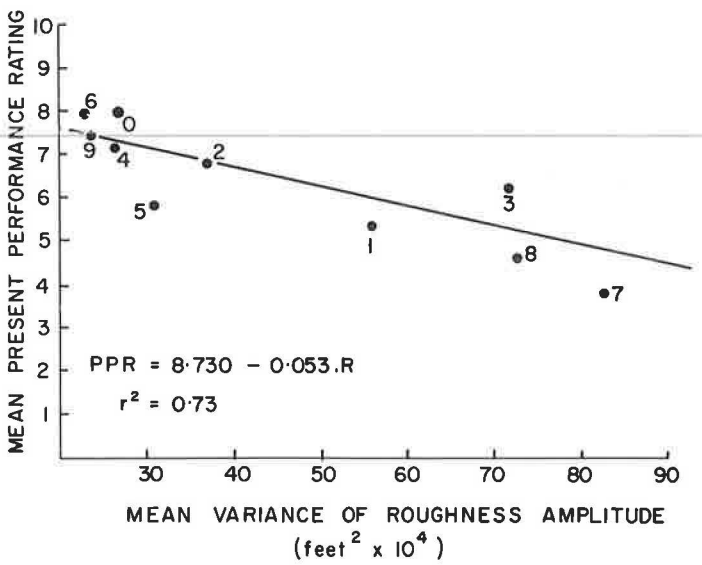

Figure 13. Present performance rating vs roughness amplitude index.

For ease of description, the term R might be called the roughness amplitude variance. Eq. 5 was fitted to the data according to the least squares criterion.

Figure 13 shows the relationship observed between the mean present performance rating and the roughness amplitude index. A linear relation has been fitted to the data and the equation of this line is

$$PPR = 8.730 - 0.053\ R \tag{6}$$

where

PPR = mean present performance rating, and
R = mean roughness amplitude index.

It has already been pointed out that the performance ratings associated with pavement sections 5 and 3 apparently contained halo effects. The presence of these systematic errors is confirmed by the relation shown in Figure 13.

SUMMARY AND CONCLUSIONS

1. The AASHO Road Test formulation of pavement unserviceability is based on the philosophy that the structural performance of a highway pavement can best be measured through a consensus of experts using a subjective rating scale as a basis for measurement. Several well-known systematic rating errors are known to distort ratings.
2. The structure of the pavement rating scale is such that failure levels of unserviceability cannot be established independently of the serviceability unit.
3. An examination of available knowledge on human response to motion suggests that a more rational and reliable approach to the measurement of pavement unserviceability is to measure decrements in human tracking behavior.
4. A portable tracking task has been designed which can be readily mounted in any highway vehicle. The task variables associated with the tracking technique were selected on the basis that differences in the ability of subjects to perform the task should be minimized by selecting a relatively simple task. The input function consists of a triangular wave form of 1.2-cm amplitude, and 30-cm wavelength. The speed of movement of the input function is 6 cm/sec. A subject is required to track the input function manually from a specified position in the test vehicle.
5. Subjects can be readily oriented and trained in the task, and the observations obtained in this investigation indicate that the major systematic errors are removed after about 6 trials.
6. A subject's performance can easily be measured by calculating the mean square error in position of his output and then transforming this to a standard tracking error.
7. The relation observed between the standard tracking error and the present performance rating confirms the existence of halo effects in the subjective pavement ratings.
8. A high degree of correlation was observed between the mean standard tracking error and parallel measures of pavement roughness.
9. In the absence of a more complete knowledge of driver behavior and human response to motion the validity of the mean standard tracking error as a criterion of pavement unserviceability can be established objectively. However, the relationship of the standard tracking error to the subjective ratings and the support of previous studies of mechanical body response would suggest that the validity of this criterion is quite high.
10. The reliability of this tracking technique, the ease with which the human response measures can be obtained for widely dispersed pavement sections, and the absence of any major systematic distortions would suggest that this procedure, or some modification of it, could easily be adopted as a standard technique assessing human response to vehicle motion.

ACKNOWLEDGMENTS

The work reported in this paper was financed at the University of Waterloo by the Ontario Highway Department under their Joint Highway Research Program. The assistance of M. D. Armstrong and G. Chong of the Ontario Highway Department

in establishing the field program is gratefully acknowledged. Dr. E. L. Thomas of the University of Toronto contributed to the initial development of the tracking device. Mrs. Douglas Mary Hutchinson created a number of the illustrations.

REFERENCES

1. Adams, J. A. Human Tracking Behavior. Psychological Bull., Vol. 58, pp. 55-79, 1961.
2. Canadian Good Roads Association. Manual on Pavement Investigations. Tech. Publ. No. 11, 1959.
3. Carey, W. N., Jr., and Irick, P. E. The Pavement Serviceability-Performance Concept. Highway Research Board Bull. 250, pp. 40-58, 1960.
4. Coermann, R. R. The Mechanical Impedance of the Human Body in Sitting and Standing Position at Low Frequencies. Human Factors, Vol. 4, pp. 227-254, 1962.
5. Ghiselli, E. E. Theory of Psychological Measurement. McGraw-Hill, 1964.
6. Goldman, D. E. Review of Subjective Responses to Vibratory Motion of the Human Body in the Frequency Range 1 to 70 cps. Naval Medical Res. Inst., Bethesda, Md., 1948.
7. Guilford, J. P. Psychometric Methods. McGraw-Hill, 1954.
8. Hutchinson, B. G. Principles of Subjective Rating Scale Construction. Highway Research Record 46, pp. 60-70, 1964.
9. Magid, E. B., and Coermann, R. R. Human Response to Motion. Chap. 5, Human Factors in Technology. E. Bennett, ed., McGraw-Hill, 1963.
10. Morgan, C. T., et al. Human Engineering Guide to Equipment Design. McGraw-Hill, 1963.
11. Parks, D. L. Defining Human Reaction to Whole Body Vibration. Human Factors, Vol. 4, pp. 305-314, 1962.
12. Poulton, E. C. On Simple Methods of Scoring Tracking Error. Psychological Bull., Vol. 59, pp. 320-328, 1962.
13. Quinn, B. E., and Zable, J. L. Evaluating Highway Elevation Power Spectra from Vehicle Performance. Highway Research Record 121, pp. 15-26, 1966.
14. Stevens, S. S. Cross Modality Validation of Subjective Scales for Loudness, Vibration, and Electric Shock. Jour. Exper. Psychology, Vol. 57, pp. 201-209, 1959.
15. Versace, J. Measurement of Ride Comfort. Preprint 638A, SAE, 1963.
16. Yoder, E. J., and Milhous, R. T. Comparison of Different Methods of Measuring Pavement Condition. Highway Research Board, January 1965.
17. Young, M. L. Psychological Studies of Tracking Behaviour. Report No. 3850, Naval Res. Lab., 1951.

Prediction of Skid-Resistance Gradient and Drainage Characteristics for Pavements

DESMOND F. MOORE, Research Mechanical Engineer, Transportation Research Department, Cornell Aeronautical Laboratory, Inc.

For slick pavements, the major factor influencing the onset of skidding or hydroplaning is surface texture. To evaluate the effectiveness of this parameter in specific instances, a simple instrument called an outflow meter has been designed, constructed, calibrated, and tested. The outflow meter not only compares the relative drainage abilities of surfaces by assigning a drainage number to each, but also serves to establish the slope of the wet sliding coefficient of friction vs speed characteristic for a particular texture. In this manner, periodic testing of pavement sections that have marginal slipperiness will indicate when resurfacing is necessary. Also, the extent of locked-wheel skid testing is drastically reduced by the instruments described herein.

•HIGH-SPEED skidding can cause serious accidents because of the loss of directional ground stability and braking traction. When this occurs, the vehicle, whether an automobile or aircraft, drifts in an uncontrolled manner with negligible restraint by the tires. Although skidding may occur on slippery surfaces at relatively low vehicle velocities, a different type of skid will occur at high speeds, even though the road or runway exhibits a high skid-resistance characteristic at low and normal speeds. This phenomenon, called hydroplaning, is caused when the tire rides on a thin film of water.

The hydroplaning phenomenon may occur whether the tire is initially either rolling or locked (as in braking). For every set of experimental conditions in wet weather, therefore, there exist two critical velocities, called the hydroplaning-limit-in-rolling and the hydroplaning-limit-in-sliding. In fact, the sliding hydroplaning limit corresponds to a much lower vehicle velocity than the rolling situation, and this factor alone promotes skidding hazards as seen by the following example. Assume that a vehicle starts from rest on a level, wet pavement and accelerates constantly until, at some instant, the vehicle velocity is equal to the hydroplaning-limit-in-sliding. Because the tires are rolling and the vehicle is accelerating, the driver is unaware that he is in the critical range between the two hydroplaning limits. If there is no occasion to apply the brakes, the vehicle will continue to accelerate until the higher or rolling pneumatic limit is approached, at which stage the vehicle will drift out of control.

Under certain conditions, the higher hydroplaning limit may be almost twice that of the lower (1). Assuming that the driver approaches the upper limit and then applies his brakes upon detecting the onset of hydroplaning, he finds that even when the vehicle speed decreases below the upper hydroplaning limit (because of wind resistance), control of the vehicle cannot be regained until the speed decreases to a value below the lower or sliding limit—if he maintains the locked-wheel condition. Thus, while the vehicle decelerates from perhaps 75 to 40 mph, it will be hydroplaning, and drift out of control. It may be argued that if the driver releases the brakes immediately after applying them in panic at the upper hydroplaning limit (or if he has the presence of mind

Paper sponsored by Committee on Surface Properties—Vehicle Interaction and presented at the 45th Annual Meeting.

never to apply the brakes under these conditions), then the wheel will begin to roll again below the upper limit. Unfortunately, there is evidence to suggest that once hydroplaning-in-rolling occurs, the forces and moments acting on the tire tend to keep it from rotating, whether or not the brakes are applied (2).

The greatest safety hazard occurs under the above conditions because the driver is unaware that his vehicle is operating between the two hydroplaning limits, and it takes only a light application of the brakes to trigger the locked-wheel hydroplaning condition at speeds that are far in excess of the lower hydroplaning limit. Of course, the situation is far less serious if the driver applies his brakes at a vehicle speed that only slightly exceeds the lower limit, because wind resistance in this instance only needs to slow the vehicle one or two miles per hour to regain control.

Therefore, it is imperative that the nature of tire-surface interaction for the case of rolling on a wet surface be fully understood, particularly between the hydroplaning limits in sliding and rolling. Recognizing this need, Cornell Aeronautical Laboratory, Inc., under contract to the Bureau of Public Roads (Contract number CPR 11-1058) has conducted a combined analytical and experimental study of the fundamental mechanism of rolling (3) during the past year.

THE MECHANISM OF ROLLING

Consider the case of a tire rolling on a wet surface at speeds below the hydroplaning-limit-in-rolling (Figs. 1A and 1B). A hydroplaning upward thrust exists in the wedge just ahead of the contact area of the tire; the magnitude of this thrust is determined by such factors as effective tread width, water layer depth, tire inflation pressure, and vehicle velocity. The contact area itself (4) comprises three zones (Fig. 1B) as follows:

1. Sinkage, or Squeeze-Film Zone: Under wet conditions, the forward part of what would normally be considered the contact area under dry conditions floats on a thin film of water, the thickness of which decreases progressively as individual tread elements traverse the contact area. Since the tire, water-film, and road surface have virtually no relative motion in the contact area, the tread elements in effect attempt to squeeze out the water between rubber and pavement.
2. Draping, or Transition Zone: The draping zone begins when the tire elements, having penetrated the squeeze film, commence to drape over the major asperities of the surface and to make contact with the lesser asperities.
3. Actual Contact, or Tractive Zone: This is the region where the tire elements, after draping, have attained an equilibrium position vertically on the surface. The length of this region depends on vehicle velocity; it occupies the rear portion of the overall contact area. Tractive effort is developed here.

The squeeze-film zone is of primary importance in the investigation of hydroplaning phenomena. It is apparent that when the time of squeezing action of a particular tread element entering the contact length exceeds the time of traversal of the element through the contact area, there are no draping or actual contact zones and hydroplaning occurs. The time of squeezing depends on inflation pressure, water viscosity, dimensions of a tread element, initial film thickness, and surface texture—but is independent of vehicle speed (4). The time of traversal, on the other hand, varies inversely with speed. By increasing vehicle velocity, therefore, it is possible to reduce the time of traversal to a value equal to or less than the time of squeezing. In this event, a rubber element entering the contact region sweeps through the contact length before all the water has been squeezed out, and the hydroplaning-in-rolling limit has been attained.

The objective is to minimize the times of squeezing and draping so that the time remaining to develop traction is maximized and, therefore, for a given set of conditions the hydroplaning limit is postponed to its maximum value. According to the results of previous investigators, the major factor influencing the time of squeezing is the nature of the surface roughness (5, 6), whereas both surface roughness and the dynamic properties of rubber determine the time of draping. To obtain experimental support for the theoretical concepts proposed in this study, a surface texture laboratory was built.

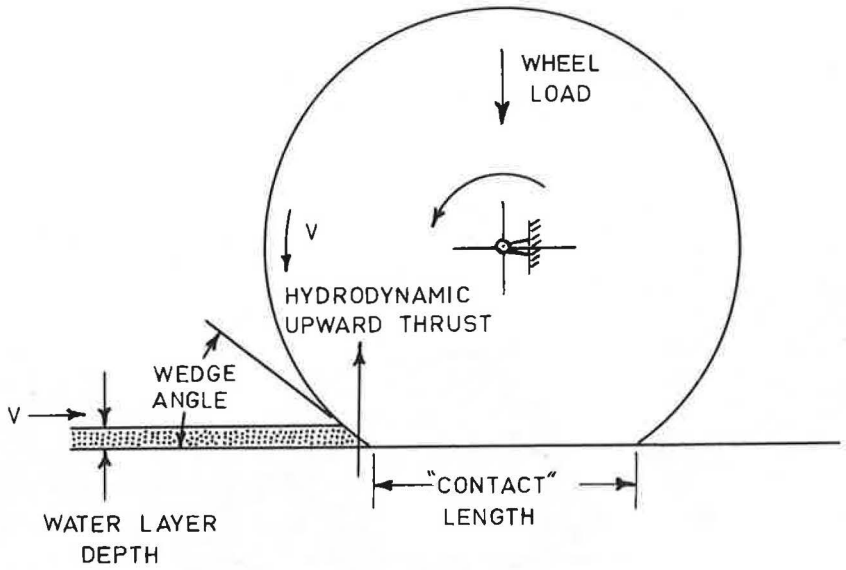

A — GENERAL

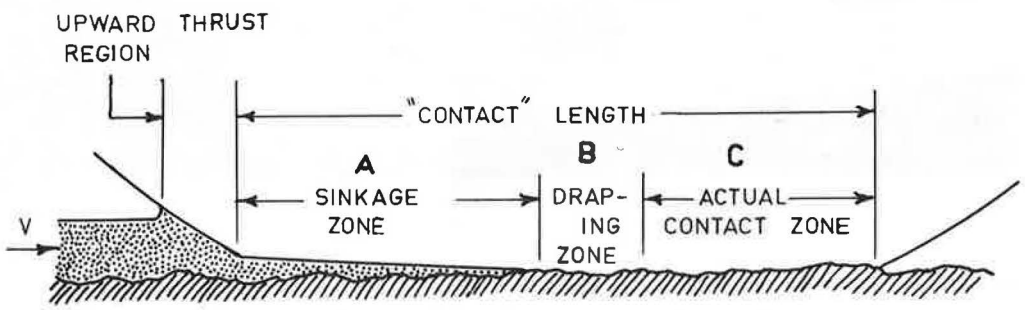

B — THREE ZONES IN THE CONTACT AREA (ROUGH SURFACE)

Figure 1. Wet rolling below the hydroplaning limit.

SURFACE TEXTURE LABORATORY

Figure 2 illustrates the general layout of the laboratory, including apparatus and equipment. The latter consists of an outflow meter (to assess the relative drainage abilities of selected pavements), a profile measuring device (to verify the predictions afforded by the outflow meter), a draping apparatus (to simulate the draping zone outlined in the previous section), a sinkage model (that duplicates the squeeze-film action in the sinkage zone), and a British portable skid-resistance tester for general laboratory use. The outflow meter and profile measuring device are discussed in this paper. It will be seen that this combination gives a valid prediction of both the drainage characteristics and skid-resistance gradient for selected pavements.

Valid experimental data to support the analytical concepts proposed in the next section may, in theory, be obtained from any of three sources:

1. An instrumented vehicle performing specified maneuvers;
2. A test wheel loaded against, and driven by, a steel drum; or
3. A laboratory, using simplified models to simulate the interaction between tire and pavement.

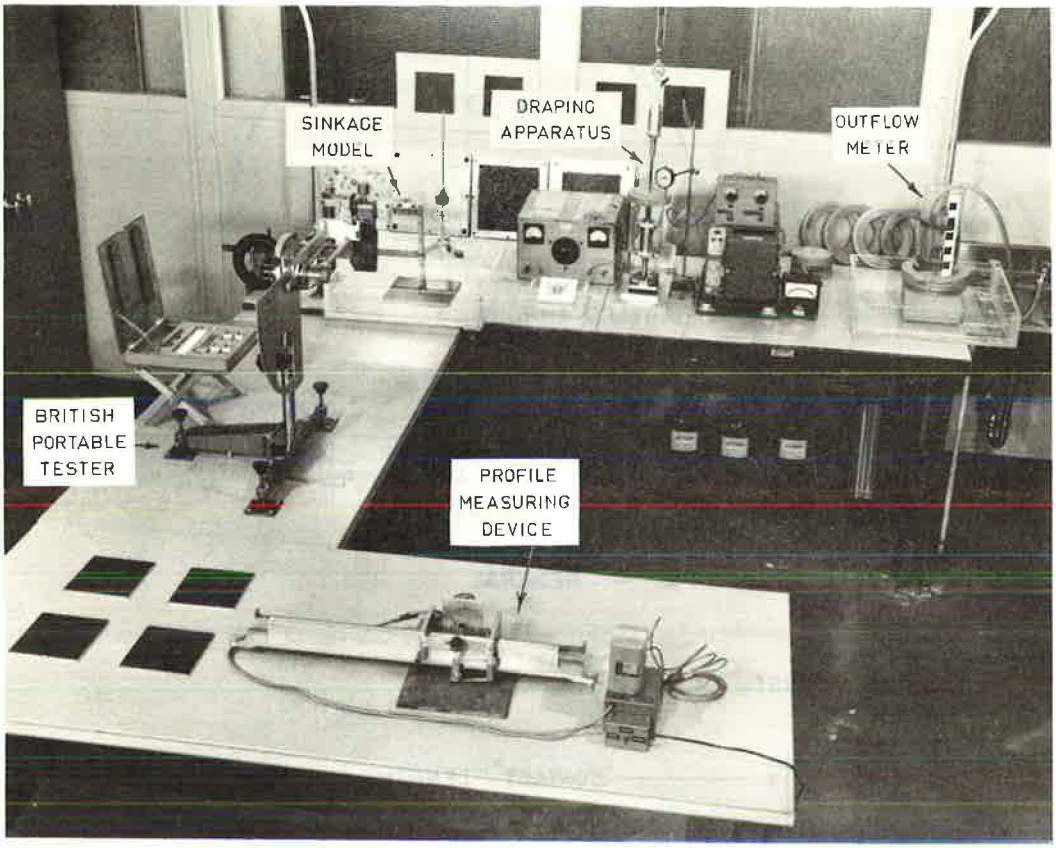

Figure 2. General view of surface texture laboratory.

However, the interpretation of such data is perhaps realistic only in the case of the third alternative. This is so because the rolling of a tire is sufficiently complex that, by changing one variable in a given test (e.g., inflation pressure) in 1 or 2 above, the resulting change in a dependent variable (such as perhaps temperature) is a function not only of the variable that is changed but also of several other variables, many of which are unknown. In the above example it is clear that an increased inflation pressure will cause a decrease in temperature—but what percent of the decrease accrues to volume changes, rubber properties (flexing), microslip changes in the contact area, etc.? Only the use of simplified laboratory models can separate these respective contributions and, for this reason, it is believed that the fundamentals of the rolling process can be properly understood only by using simple analysis supported by data from a surface texture laboratory.

Three types of surface roughness were used in this investigation, classified as follows:

1. Regularly rough surfaces (cubed or square-pyramid asperities or projections) for calibration of the outflow meter,
2. Random surfaces (waterproof sandpaper) for laboratory use, and
3. Random surfaces (actual roads) for field testing.

NOMENCLATURE

A = area of outflow channel, or apparent contact area, $in.^2$;
c = characteristic channel dimension, in.;
C_D = coefficient of discharge;

d = mean void width of surface asperities, in.;
D = inner diameter of outflow meter, in.;
D.N. = drainage number;
fs_V = wet sliding coefficient of friction;
g = acceleration due to gravity, ips;
Ip = polar moment of inertia of channel cross-sectional area, $in.^4$;
K_0, K_1, K_2, K_3 = constant coefficients;
ℓ = height of liquid level in outflow meter above asperities, in.;
MHR_E = mean hydraulic radius (experimental), in.;
MHR_T = mean hydraulic radius (theoretical), in.;
M, M' = instrument constants;
N = number of channels under rubber ring of outflow meter;
N' = number of asperities per unit area of surface;
p, p' = apparent pressure, psi;
p_i = inflation pressure, psi;
P = wetted perimeter of channel, in.;
Q = volume flow rate through one channel, $in.^3/sec$;
Q_{TOT} = total volume flow rate through channels, $in.^3/sec$;
S.N. = skid number;
t = efflux time for outflow meter, sec;
V = vehicle velocity, mph;
W = load on outflow meter, lb;
ϵ = average asperity height, in.;
Δ = thickness of rubber ring, in.;
ρ = density of water or glycerin, $slug/in.^3$;
η = draping factor; and
μ = absolute viscosity, lb $sec/in.^2$.

THE OUTFLOW METER

The outflow meter is designed to measure directly the mean hydraulic radius of the surface texture of a road or runway. This is an essential criterion for assessing drainage ability as shown elsewhere (7). Figure 3 shows two views of the meter, and Figure 4 shows the device in actual use. The meter consists of a transparent lucite open-end cylinder with a thin neoprene ring of square cross section cemented to one end. The unit is mounted vertically on the surface to be tested; the ring is compressed onto the surface texture by a predetermined circumferentially applied load. The vessel is filled with water, and the time of efflux of a certain quantity of water between the rubber and the surface voids is obtained by observing, with a stopwatch, the time for the level in the vessel to drop from the upper to the lower graduation mark.

Theory

Let ℓ_i, ℓ_f, and ℓ be the initial, final, and intermediate heights, respectively, of the water level in the cylinder above the center plane of the channels between rubber and surface (Fig. 3). Using the hydrodynamic analogy (7) between the uniform torsion of a prismatic bar flow through a cross section of the same shape under a steady pressure gradient, it is found that the total flow rate through the channels between rubber and surface is given by:

$$Q_{TOT} = NQ = \frac{NA^4}{160\,\mu\,Ip}\left(\frac{\rho g \ell}{\Delta}\right) \qquad (1)$$

where

Δ = thickness of rubber ring,
$(\rho g \ell/\Delta)$ = pressure gradient under ring, and
N = number of asperities or channels under ring.

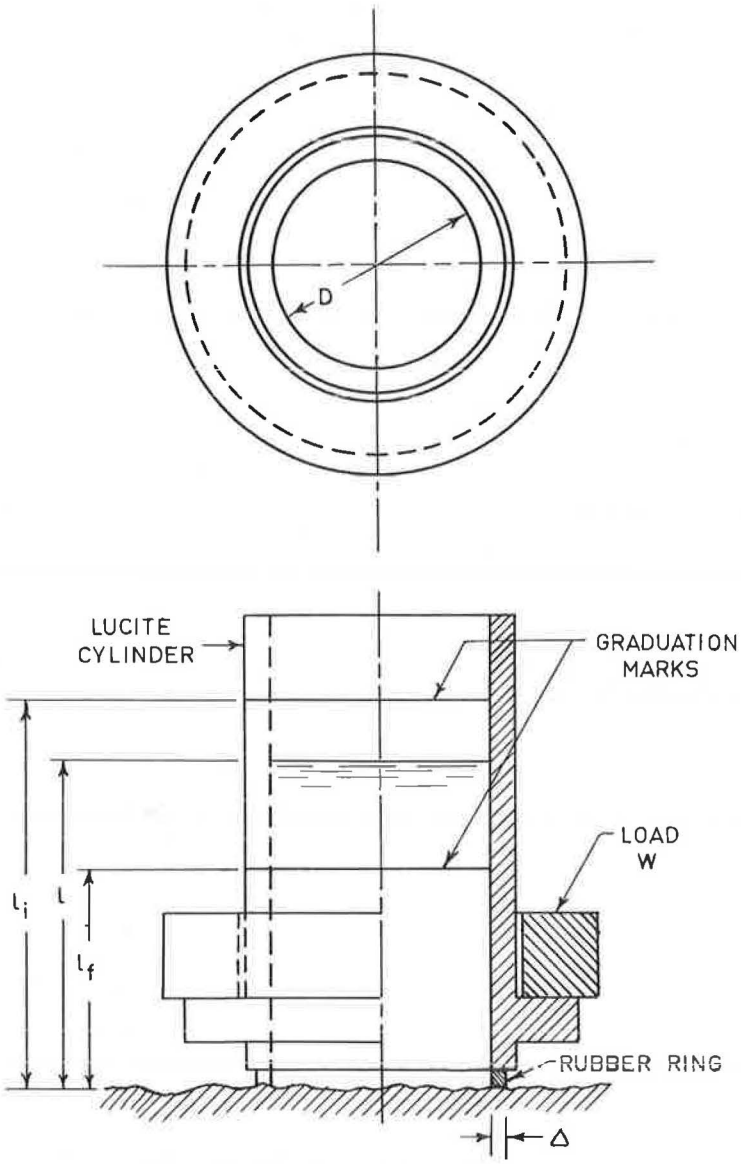

Figure 3. Two views of the outflow meter.

Substituting the characteristic channel dimension $c = A/\sqrt[4]{Ip}$ in this equation, and remembering that for the drop in level of the water in the vessel

$$Q_{TOT} = \frac{\pi D^2}{4} \cdot \frac{d\ell}{dt} \tag{2}$$

we obtain an expression for c:

$$c = M \sqrt[4]{\frac{\mu}{tN}} \tag{3}$$

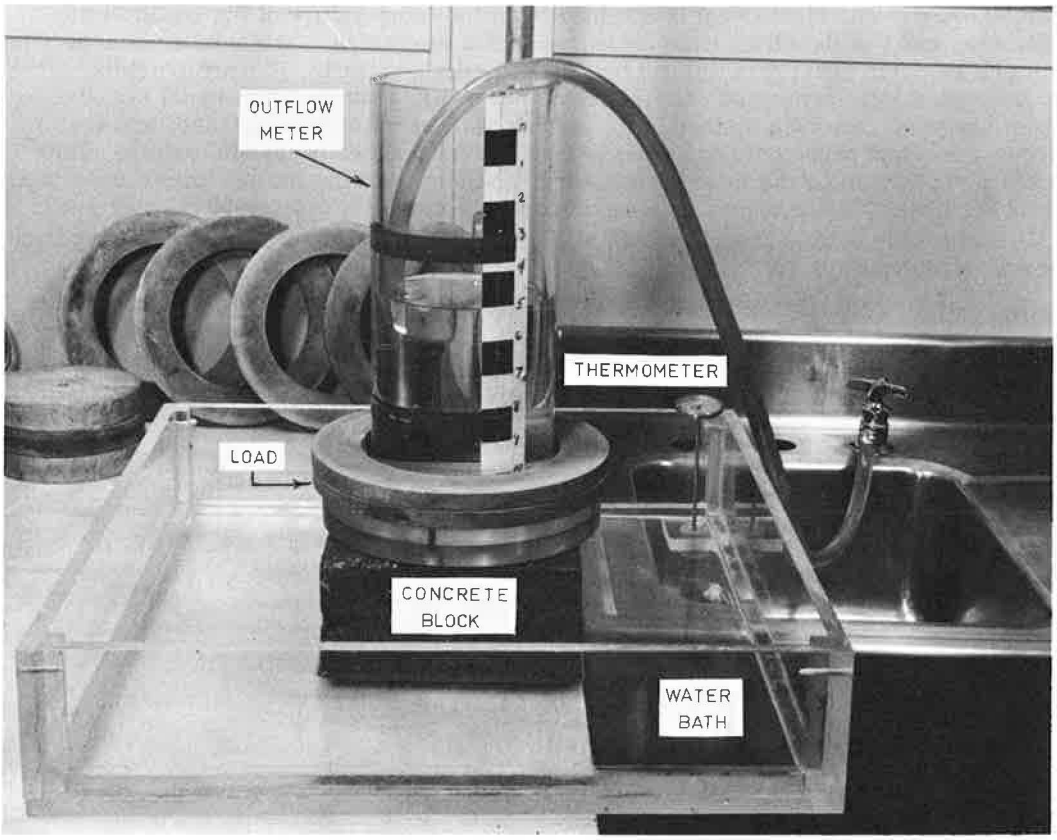

Figure 4. The outflow meter in use.

where

t = time for water level to fall through height ($\ell_i - \ell_f$), and

M = $\sqrt[4]{(40\pi D^2\Delta/\rho g)\ell n(\ell_i/\ell_f)}$ = instrument constant.

Now the ratio of the characteristic channel dimension to the mean hydraulic radius (MHR) is found to be approximately constant, e.g.,

$$(c/MHR) \doteq 6.67 \tag{4A}$$

with a maximum error of about 10 percent for all possible channel configurations and a maximum error of about 4 percent for all probable channel configurations. It can also be shown that, if the distribution of asperities in the surface is uniform in the sense that the linear density is the same in all directions, then

$$N = \pi D\sqrt{N'} \tag{4B}$$

where N' is the number of asperities per square inch of surface texture. Combining Eqs. 3, 4A, and 4B, the following important result is obtained:

$$MHR = M'\sqrt[4]{\mu/tN'^{1/2}} \tag{5}$$

where $M' = 0.1128\, M/\sqrt[4]{D}$ (also an instrument constant). From this equation, it can be seen that, if the three quantities μ, t, and N' are known, the mean hydraulic radius

can be found. The viscosity μ is obtained from the temperature of the liquid in the cylinder, and t is the efflux time measured with a stopwatch. The number of asperities per unit area (the areal density) can be obtained either visually, photographically, or by pressing a mastic compound onto the texture to obtain a three-dimensional negative for later analysis. Another method is to coat the surface with Prussian blue, and then press a sheet of paper onto the asperity tips to obtain asperity-density prints. This method appears to be the most satisfactory, and was used for the sandpaper and actual road surfaces. Little accuracy is required in estimating N′, since 50 percent error in $\sqrt{N'}$ means only a 10 percent error in MHR, and the latter is only just outside the limits of expected accuracy.

Calibration

The outflow meter is calibrated and checked by mounting it under different loads on surfaces having both cubed and square-pyramid asperities (Fig. 5). These surfaces

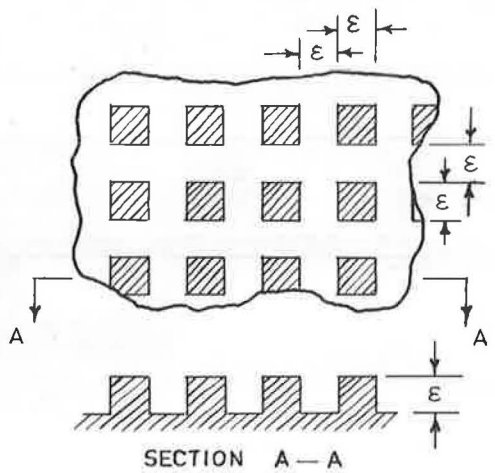

A — CUBED ASPERITY SURFACE

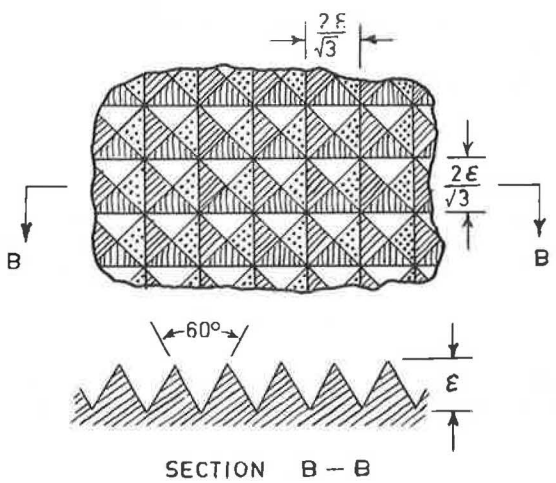

B — SQUARE PYRAMID ASPERITY SURFACE

Figure 5. Calibration surfaces for outflow meter.

were machined from aluminum plate stock, and it is possible to compute the area between the regular-type asperities and the neoprene ring of the outflow meter. Because the size of the cubed and square-pyramid projections is too large to permit a gradual drop in the level of water in the cylinder, a viscous glycerol solution is substituted for the water. This restores viscous flow beneath the rubber ring and makes the theory of the last section valid. A Cannon-Fenske viscometer is used to establish the exact viscosity of the glycerol, and it is found to be 98 percent pure. Thus the exact viscosity can be obtained from tables as a function of temperature, since this is necessary for calibration purposes.

Putting D = 4.75 in., $\Delta = \frac{1}{8}$ in., $\ell_i = 9.1$ in., $\ell_f = 4.1$ in., and ρg (for glycerol) = 78.1 lb/ft^3, it is found that M = 8.89 in.$^{3/2}$ lb$^{-1/4}$, and M′ = 0.678 in.$^{5/4}$ lb.$^{-1/4}$. Thus, Eq. 5 becomes:

$$MHR_E = 0.678 \sqrt[4]{\mu/tN'^{1/2}} \tag{5A}$$

where the subscript E denotes experimentally determined.

The mean hydraulic radius is also theoretically defined as

$$MHR_T = \eta C_D \left(\frac{A}{P}\right) \tag{6}$$

where

η = draping factor (because of the penetration of the neoprene ring by the surface projections),
C_D = coefficients of discharge,
A = equivalent outflow area between ring and asperities (defined in 7), and
P = perimeter per channel (7).

The values of A and P for each of the cubed and square-pyramid asperities surfaces (neglecting draping) are calculated according to a general method outlined in the Appendix of (7). By equating the right sides of Eqs. 5A and 6, it is found that:

$$\eta C_D = 0.678 \left(\frac{P}{A}\right) \sqrt[4]{\mu/tN'^{1/2}} \tag{7}$$

Now, the draping factor is defined as unity for zero load (i.e., when there is no draping). All the outflow meter tests, however, are conducted using loads ranging from 5 to 25 lb. By extrapolating to zero load, the value of the radical in Eq. 7 at zero load may be obtained on each calibrating surface from its values at finite loads. Thus, assuming C_D is constant on one surface for all loads,

$$C_D = 0.678 \left(\frac{P}{A}\right) \sqrt[4]{\mu/tN'^{1/2}} \Bigg|_{\substack{\text{zero} \\ \text{load}}} \tag{7A}$$

From Eqs. 7 and 7A:

$$\eta = \left[\left(\frac{t}{\mu}\right)_{\substack{\text{zero} \\ \text{load}}} \Big/ \left(\frac{t}{\mu}\right) \right]^{1/4} \tag{8}$$

TABLE 1

Type of Surface	ϵ (in.)	P/A	C_D
Cubed	3/32	42.7	0.76
Cubed	1/8	31.9	0.86
Square-pyramid	1/8	47.6	0.92
Square-pyramid	3/16	32.5	0.86

A sample data sheet for the outflow meter tests is shown in the Appendix of (3). Several tests for each set of conditions were made, and the mean value of MHR_E was obtained from Eq. 5A. Table 1 gives values of P/A for each surface and finally the values of C_D.

Considering that the flow is viscous, the values of the coefficient of discharge are reasonable and point to the fact that results obtained with the outflow meter closely predict the mean hydraulic radius of the texture. By substituting experimental data into the right side of Eq. 7, the product ηC_D may be computed at each load for each surface. Figure 6 shows plots of ηC_D for both the cubed and square-pyramid asperity surfaces. By extrapolating to zero load (whereupon $\eta \rightarrow$ unity), the

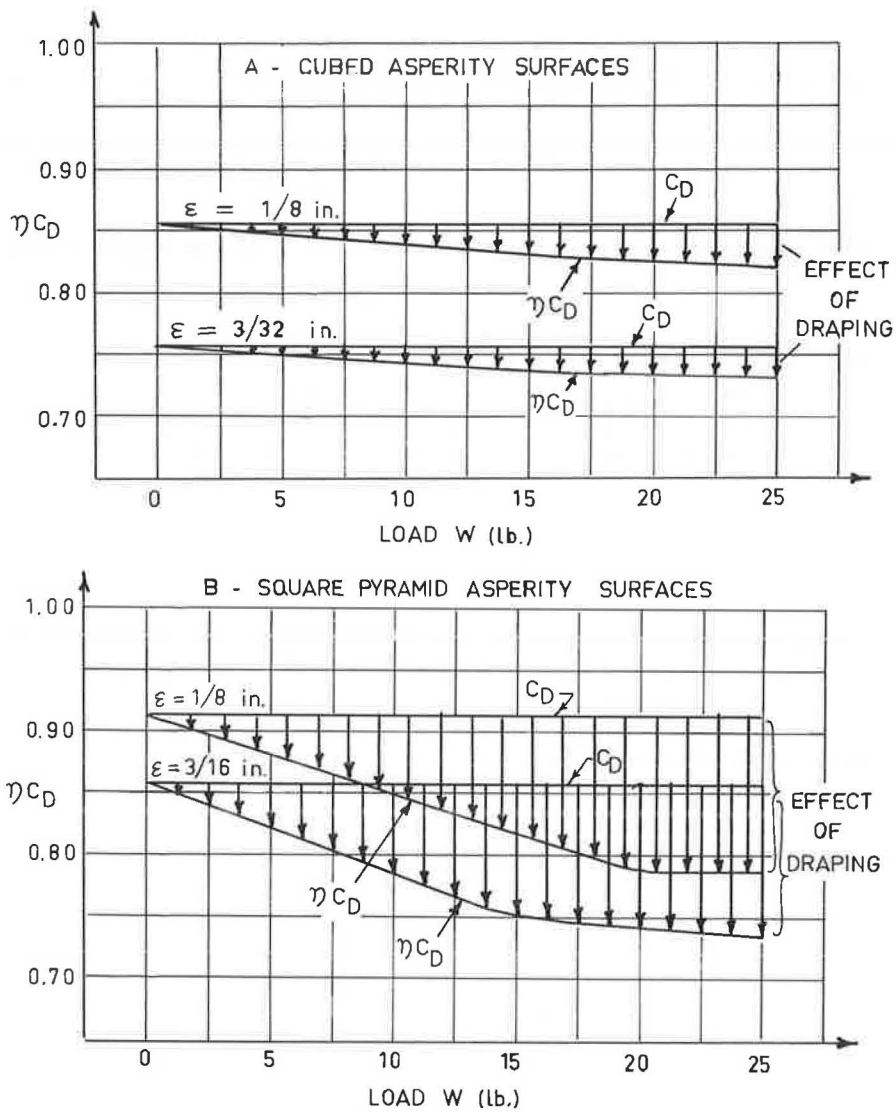

Figure 6. Calibration curves for outflow meter.

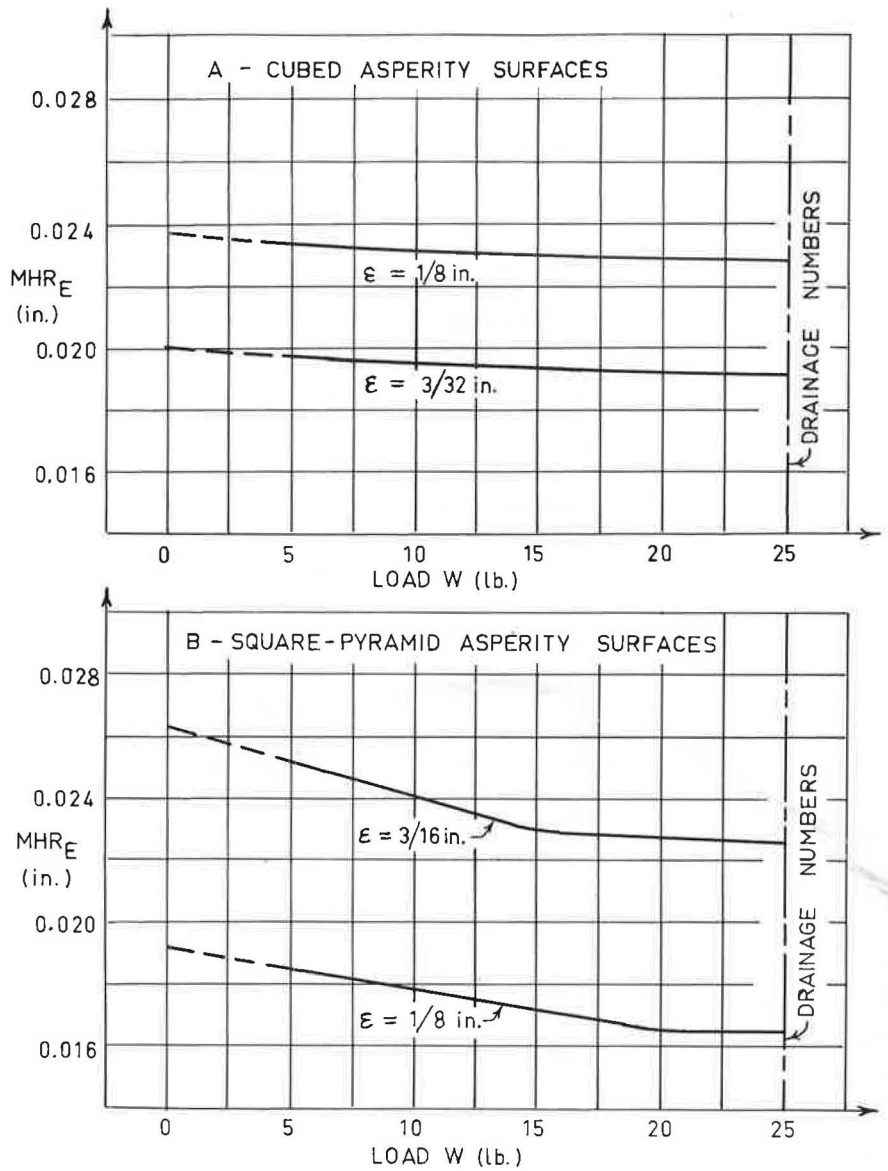

Figure 7. Mean hydraulic radii for calibration surfaces.

value of C_D in each case is obtained and, assuming C_D is independent of load, an indication of the draping effect on each surface is presented.

As might be expected, the draping effect on the square-pyramid surfaces is considerably greater than on the cubed surfaces. Other observations from Figure 6 are:

1. The maximum draping for a particular surface geometry appears constant and independent of asperity size.
2. The rate of increase of the draping effect with load is greater for the square-pyramid texture.
3. The draping effect on the square-pyramid texture becomes saturated (i.e., further increase of load does not affect the degree of draping) at loads which are smaller for larger sizes of asperity.

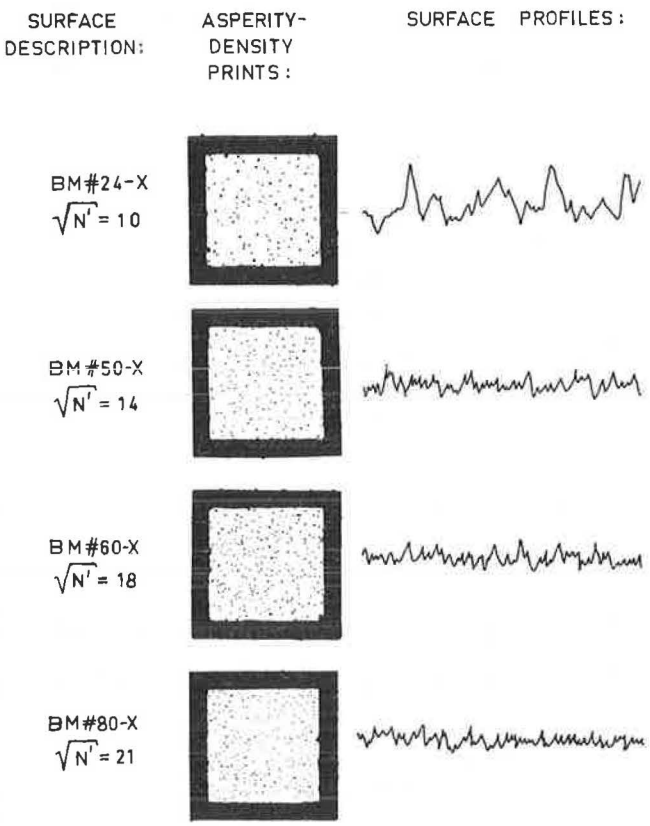

Figure 8. Asperity-density prints and profiles for sandpaper surfaces.

The draping factor η may be plotted against load from Eq. 7. An alternative is to divide the ηC_D values at each load in Figure 6 by the corresponding value at no load. These curves are not shown, however, since they are similar to those in Figure 6. Figure 7 gives the MHR_E for each surface as a function of load or draping. The mean hydraulic radius is a valid measure of drainage, and it is seen that the drainage ability is impaired when the degree of draping increases.

The calibration tests with the outflow meter show that the instruments can be used to predict the drainage ability of surfaces. It gives a measure of the size of texture insofar as coarser surfaces more readily permit surface water to flow in the voids between asperities. The outflow meter may now be used on randomly-rough surfaces (as opposed to the calibration surfaces that may be classified as regularly-rough).

Results on Sandpaper Surfaces

A convenient set of random surfaces for laboratory use was provided by the Behr-Manning Company, classified for reference purposes as follows:

B.M. #80-X	Fine
B.M. #60-X	Medium Fine
B.M. #50-X	Medium Coarse
B.M. #24-X	Coarse

These surfaces are waterproof, and were mounted on 6-in. square backing plates. The range of texture represented is considerably smaller than that for the calibration surfaces, and is comparable with that on road surfaces. The texture is sufficiently fine

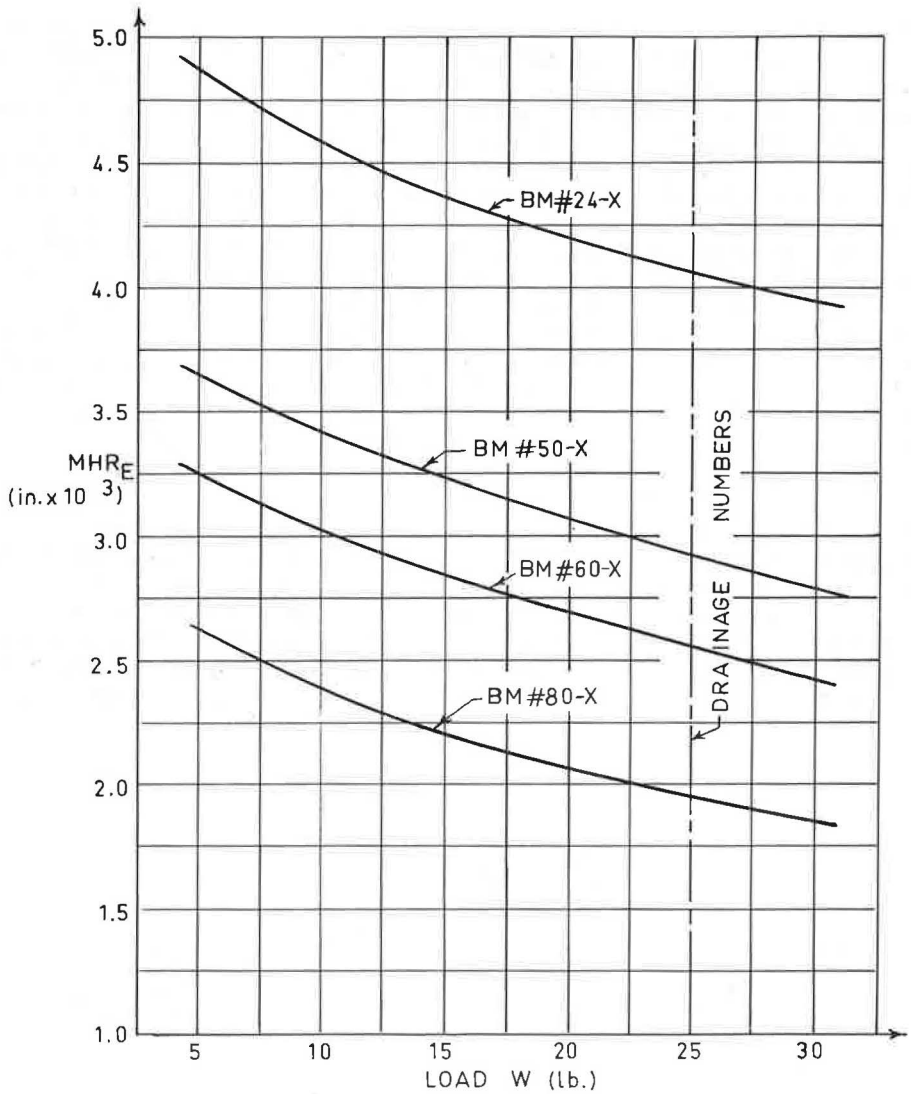

Figure 9. Mean hydraulic radii for sandpaper surfaces.

to permit the use of water (Fig. 4). Since the density of water is less than that of the calibrating liquid (i.e., glycerin), the constant M′in Eq. 5A is greater:

$$MHR_E = 0.716 \sqrt[4]{\mu/tN'^{1/2}} \qquad (5B)$$

To evaluate the areal density N′, asperity-density prints are obtained with Prussian blue dye (as described earlier). Figure 8 shows asperity-density prints for each of the sandpaper surfaces. The areal density N′is read by marking off a square inch on the prints and counting (by means of a movable slit) the number of points appearing. Also included in Figure 8 are the profiles of each surface (obtained with the profile measuring device).

The outflow meter is used on each surface for a range of loads. Figure 9 shows the mean hydraulic radii plotted as a function of load, and, as might be expected, it decreases with increasing pressure on the rubber ring. It should be noted that it is pos-

sible to obtain the curves in Figure 9 without calibrating or checking the instrument as described in the last section. The calibrating procedure, however, shows that the results obtained are valid and reliable. Apart from the obvious fact that the coarser sandpapers have larger MHR_E, it is seen that the rate of increase of draping with increasing load is constant for all sizes of texture (equal to about 30 micro in. per lb). This rate of increase approaches that for the square-pyramid surfaces, indicating at once that the sandpaper exhibits predominantly peaked or close-to-peaked asperities.

There is a source of error in reading N' from the asperity-density prints. Furthermore, the number of points obtained is a function of the pressure applied to the paper. Speculation suggests that N' should be made to increase with load for each texture, by applying a greater pressure to the paper (in producing the prints) to correspond to the higher loads. This would aggravate the slopes of the curves in Figure 9. However, as suggested earlier, relatively large discrepancies in N' can occur without sacrificing accuracy, since the one-eighth power of N' appears in Eqs. 5A and 5B. It is, therefore, convenient and simpler to assume one value of N' for each surface, provided the same firm pressure is exerted on the paper to obtain the prints in each case.

Results on Actual Road Surfaces

Both the outflow meter and profile measuring device were used on two selected asphalt road surfaces (one "bleeding" and aged, the other lightly trafficked and one year old), and on one disused but relatively rough concrete surface. One of the difficulties encountered in the field tests was a realistic interpretation of the number of asperities per square inch, N'. For the sandpaper surfaces, the asperities are pointed and relatively uniform in size and spacing, so that N' is read fairly accurately with the slit method. On actual surfaces, however, the situation is different and the asphalt surfaces

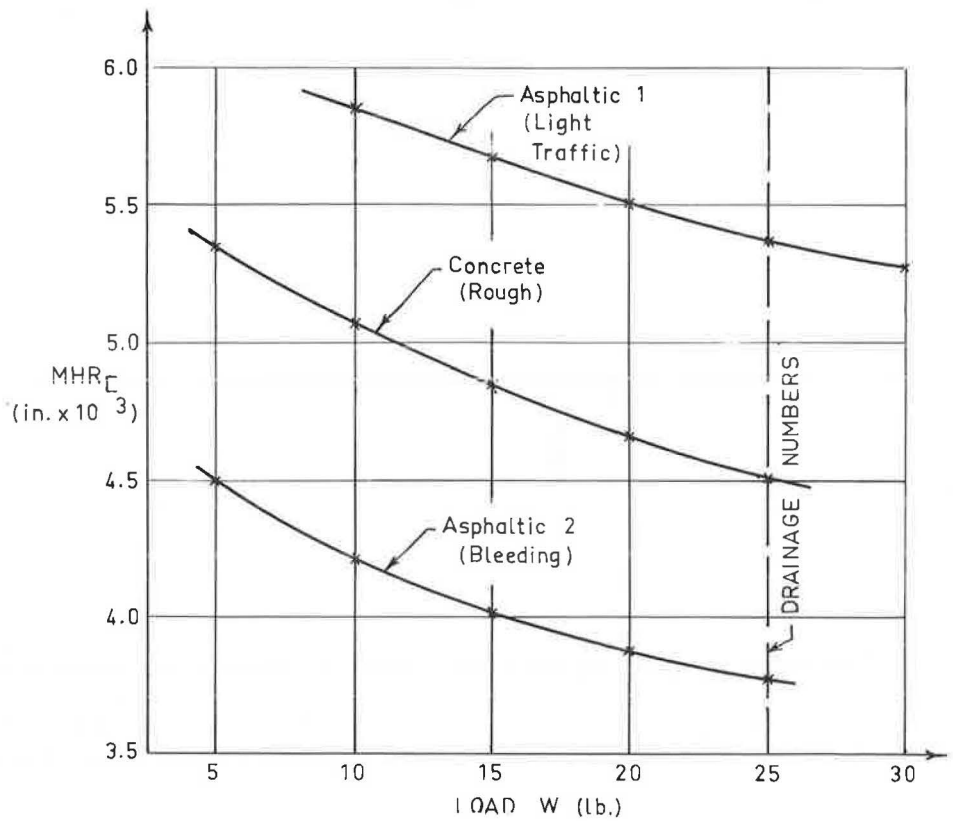

Figure 10. Mean hydraulic radii for road surfaces (obtained with outflow meter).

in particular show not only smaller asperities, but also, large flattened areas that cannot be classified as asperities. From replicas of the surfaces obtained by coating the area under inspection with dye, estimates of N' have been made but undoubtedly these estimates are more approximate than in the case of the sandpaper surfaces.

A value of $N' = 7$ was assigned to the lightly-trafficked asphalt surface, and a value of $N' = 8$ to the other two surfaces. These selected values will be discussed later, and it will be shown that they are not unreasonable. The "bleeding" asphalt surface presents an added problem, because it is virtually impossible to obtain an estimate of N' from direct observation—in this case, the amplified profile of the surface is helpful. Figure 10 shows the variation of MHR_E obtained with the outflow meter vs the load W applied. It is observed that the MHR_E for the concrete surface lies almost exactly between the corresponding values of MHR_E for the rough and bleeding asphalt surfaces at the same load W. The mean slope $\Delta MHR_E/\Delta W$ for the concrete surface appears to be slightly greater than for the other two surfaces, indicating perhaps a slightly less rounded texture.

PROFILE MEASURING DEVICE

Figures 11 and 12 show two views of a device designed to accurately record the local variations in surface geometry. It consists of a platform that moves horizontally on teflon runners relative to a base frame which is supported on the texture by three leveling screws. The platform is driven in either direction at $\frac{1}{5}$ ips by a reversing motor through a rack and pinion mechanism. An aluminum block mounted relative to the platform on twin cantilever springs (this arrangement provides frictionless vertical motion of the block, with a restoring force provided by the springs) has an inclined needle point at the lower end which follows the profile of the surface as the platform moves. The upper end of the block has a thin flexible extension that is connected to the core of a linear variable-differential transformer. A reversing switch for the motor and a Transpac 20-30 d.c. constant-voltage source for the transformer are grouped together in a single unit, as shown in Figure 11.

The output from the transformer caused by fluctuations in the position of the core is then fed into an oscillograph. Almost any vertical sensitivity or amplification of the texture may be achieved but, for the higher sensitivities, a filter network must be installed to eliminate low-frequency drift and to keep the oscillograph trace on the chart. Leveling of the base frame is attained by adjusting the leveling screws to center the circular bubble mounted on the platform. The optimum angle and sharpness of the needle

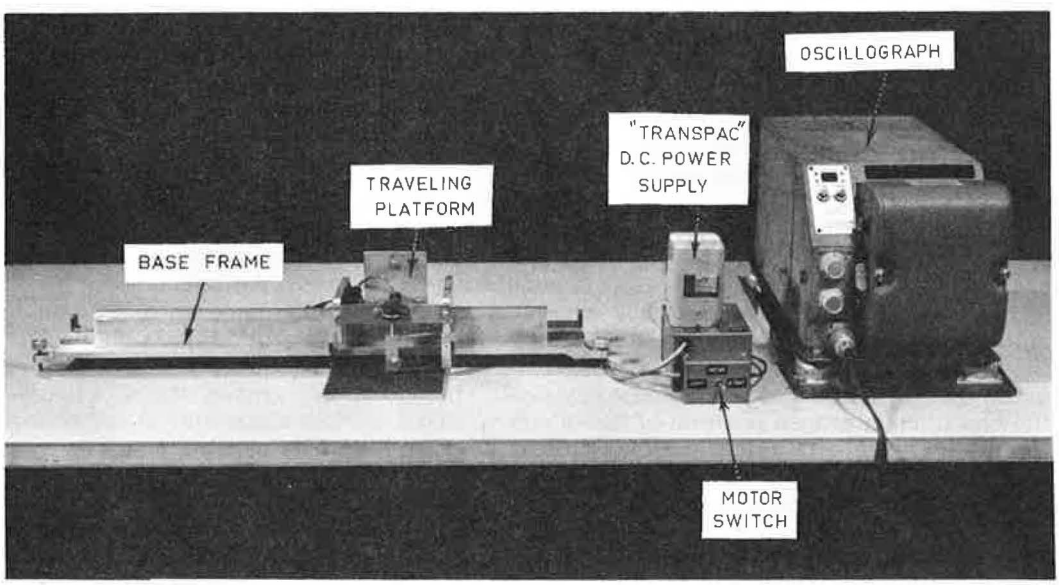

Figure 11. Front view of profile measuring device.

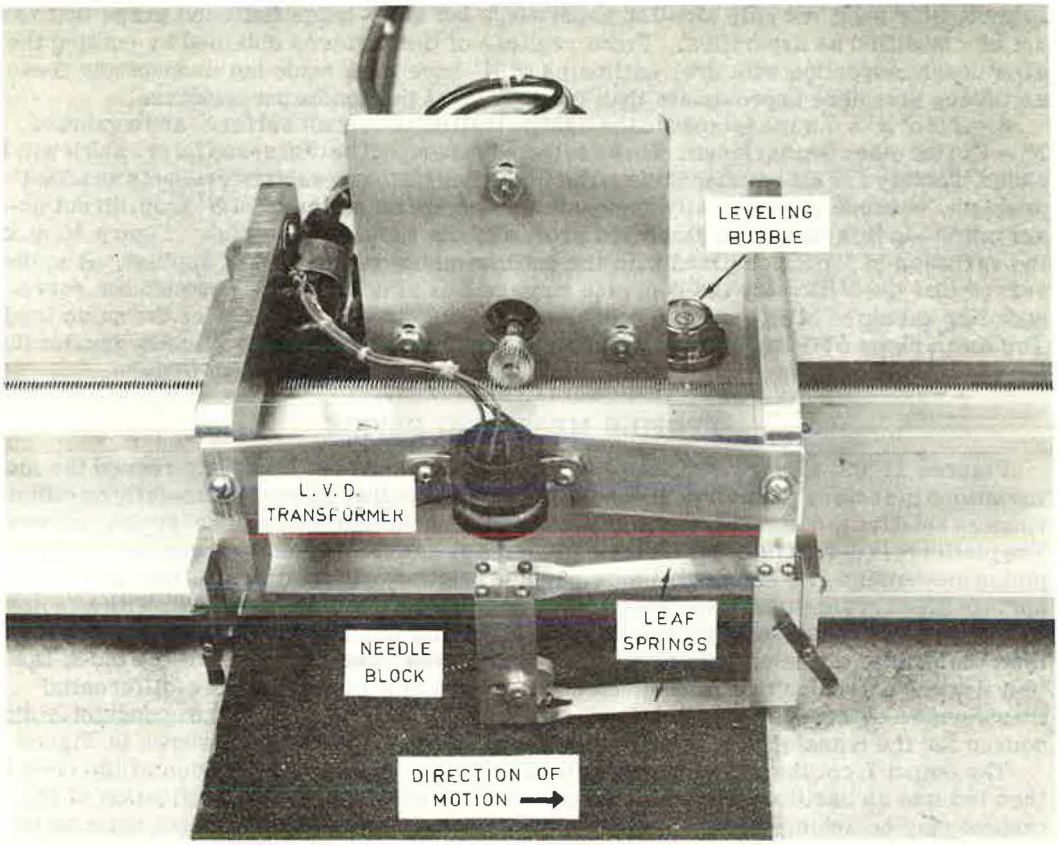

Figure 12. Details of traveling platform.

must be selected by trial and error to obtain a compromise between the conflicting requirements of not sticking and true reproduction of the surface profile.

Sample profiles for the sandpaper surfaces are shown beside the corresponding asperity-density prints in Figure 8. It is observed that the vertical scale in this figure is several times the horizontal scale for the profiles (the ratio is about 10:1), but, despite this distortion, they give an indication of the sharpness and size of the surface texture. If the horizontal scale factor is increased and made equal to the vertical scale factor (so that the profile is amplified without distortion), it is possible to obtain a theoretical value of the mean hydraulic radius for each surface. The method used is similar to that described by Meyer (8). The peaks of major asperities are connected by straight-line segments of approximately equal length, thereby creating channels or drainage areas between these segments and the actual surface. A planimeter is used to measure the drainage areas for a representative length along the texture, and an opisometer is used to obtain the length of the wetter perimeter for each channel. Thus, the mean hydraulic radius (area/perimeter) is obtained for each surface. It should be noted that the method of joining asperity peaks simulates, in terms of drainage area, the equilibrium draped position of tire elements about surface asperities at the rear of the contact area. An amplification factor of 20 in the horizontal and vertical directions was used for the sandpaper surfaces, and a factor of 40 for the actual road surfaces.

The profile measuring device permits the computation of MHR_T in accordance with Eq. 6 by using a simplifying assumption that $\eta C_D = 1$. The reason for making this assumption is that a surface profile is two-dimensional and gives no indication of the three-dimensional aspects of the flow. Previous work (7) shows, in fact, that the physical outflow area obtained from a surface profile is less than that obtained using an

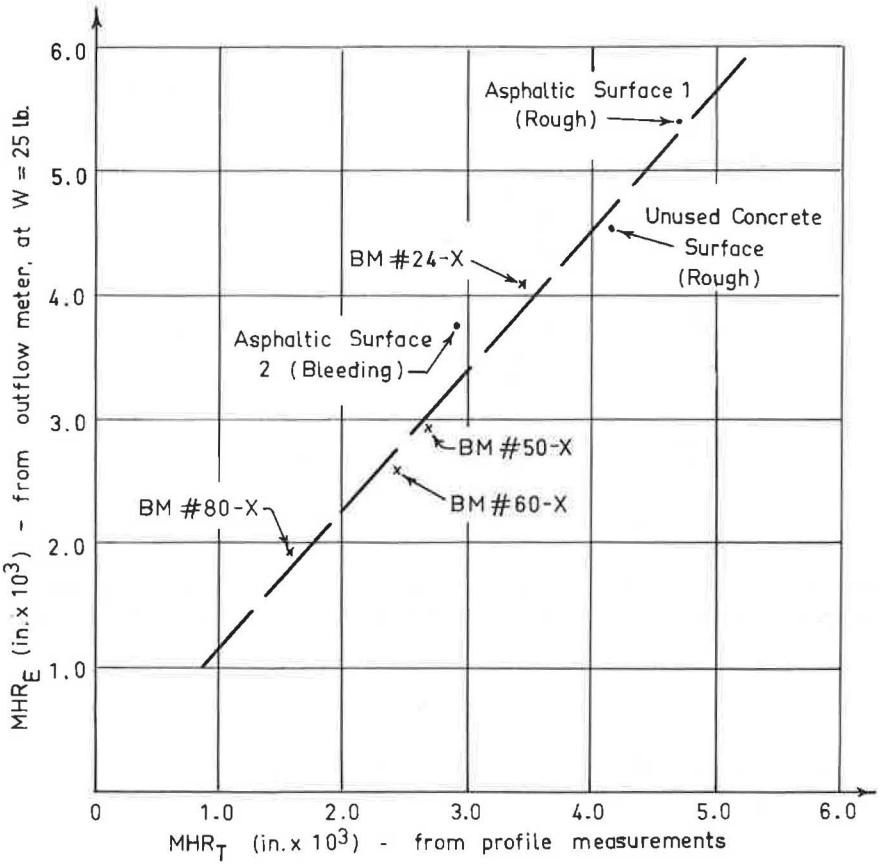

Figure 13. Comparison of MHR obtained from outflow meter and profile measuring device.

equivalent outflow area. (The method of obtaining the equivalent outflow area is described in the same reference, and it accounts for the third dimension of the texture.) This consideration would tend to reduce MHR_T, so that the assumption $\eta C_D = 1$ (which tends to increase MHR_T) provides a compensating effect.

Figure 13 shows a comparison between the MHR_E (at W = 25 lb) obtained from the outflow meter and the corresponding MHR_T (with $\eta C_D = 1$) computed from the profile data for each of the sandpapers and actual surfaces. It is seen that the relationship is remarkably linear, indicating that the outflow meter data have been verified by a profile analysis of the textures selected. Furthermore, the slope of the line is virtually 45 deg, which suggests that the MHR_T is only slightly less than the corresponding value of MHR_E. The greatest departure from the linear relation between MHR_T and MHR_E is in the case of the bleeding asphalt surface. This is to be expected, because the theoretical channelization concept (7) upon which the theory of the outflow meter is based requires well-defined channels, and this is obviously not entirely true for bleeding asphalt. The reason for choosing the value of MHR_E at W = 25 lb in the correlation plot of Figure 13 is given in the next section.

DRAINAGE NUMBERS FOR ALL SURFACES

Since the mean hydraulic radius is a function of draping or load (applied to the rubber ring in the case of the outflow meter, or to the tread elements in the contact area for a pneumatic tire), it is convenient to select one load value, and the $MHR_E \times 10^4$ obtained at this load will be called a drainage number. The load selected for the outflow meter should be the one that most nearly provides the same average pressure

TABLE 2

Surface Description		Drainage Number
Calibration Surfaces	Cubed, $\epsilon = 3/32$ in.	193
	Cubed, $\epsilon = 1/8$ in.	230
	Sq. Pyramid, $\epsilon = 1/8$ in.	166
	Sq. Pyramid, $\epsilon = 3/16$ in.	226
Sandpaper Surfaces	B.M. #24-X	40.7
	B.M. #50-X	29.2
	B.M. #60-X	25.8
	B.M. #80-X	19.3
Actual Road Surfaces	Asphaltic I (rough)	53.7
	Asphaltic II (bleeding)	37.7
	Concrete (rough)	45.2

under the rubber ring as under the rolling tire. Assume that the asperity-density for the sandpaper surfaces is the same as that for a typical roadway. For the pneumatic tire:

$$W = p_{act} A_{act} = pA \tag{9A}$$

where p and A are the apparent average pressure and apparent contact area, respectively. Similarly, for the rubber ring of the outflow meter:

$$W' = p'_{act} A'_{act} = p'A' \tag{9B}$$

so that from Eqs. 9A and 9B:

$$\frac{W}{W'} = \left(\frac{p_{act}}{p'_{act}}\right)\left(\frac{A_{act}}{A'_{act}}\right) = \left(\frac{p}{p'}\right)\left(\frac{A}{A'}\right) \tag{10}$$

Putting $p_{act} = p'_{act}$, it follows from the assumption of equal asperity density that $p = p'$ and, therefore, from Eq. 10:

$$W' = A'\left(\frac{W}{A}\right) = A'p_i \tag{11}$$

where p_i is the inflation pressure in the tire.

Now, for the rubber ring, the apparent area $A' = \pi D\Delta = 1.865$ in.^{2} Reducing this value to about 1.5 in.^{2} (the value of Δ is so small that there will be edge effects that reduce the effective value of Δ), and putting $p_i = 20$ psia, it is seen from Eq. 11 that $W' = 30$ lb. In fact, a load of 25 pounds was selected, because 30 pounds acting on the square-pyramid surfaces produce excessive penetration of the rubber ring.

The above reasoning is approximate, but it serves to indicate the value of the load recommended for the outflow meter at which to evaluate the drainage numbers. Table 2 shows the drainage numbers not only for the sandpaper and actual road surfaces, but also for the calibration surfaces.

USE OF OUTFLOW METER TO PREDICT WET SLIDING COEFFICIENT

The use of the outflow meter in obtaining drainage numbers for typical road and laboratory surfaces has been demonstrated, and as such it serves as a valuable instru-

ment to compare the relative drainage abilities of different pavements. It will now be shown that, in addition, a prediction of the slope of the friction-velocity curve is possible for the case of sliding on a wet surface.

It is generally agreed (4, 6) that the functional dependence of the wet sliding coefficient on velocity may be described as follows:

$$fs_V = K_0 + K_1V + K_2V^2 \tag{12}$$

where

fs_V = wet sliding coefficient of friction at velocity V,
V = vehicle velocity, ips, and
K_0, K_1, K_2 = constants which depend on the nature of the road surface.

Over a limited speed range, it is possible to make $K_2 = 0$ without sacrificing accuracy. Eq. 12 now reads:

$$fs_V = K_0 + K_1V \tag{12A}$$

where the constant K_1 is negative and is a function of pavement properties. Differentiating Eq. 12A with respect to V,

$$\frac{dfs}{dV} = K_1 \tag{13}$$

According to Meyer (8), a relationship exists between the skid-resistance gradient and the average asperity height ϵ. This relationship is approximately represented by the following equation:

$$\frac{d(S.N.)}{dV} = -(0.67 - 0.165 \log_{10} \epsilon') \tag{14}$$

where

$$\epsilon' = \epsilon \times 10^3 \text{ (in.)}$$

and

$$S.N. = \text{skid number} = 100\, fs_V \tag{15}$$

According to the results obtained with the outflow meter (3), it has been found that:

$$MHR_{\substack{\text{zero}\\\text{load}}} \doteq 0.2\, \epsilon_{max} \ (\pm 5\%) \tag{16}$$

where

$MHR_{\substack{\text{zero}\\\text{load}}}$ = mean hydraulic radius of the texture in the absence of draping.

Now (3),

$$\left.\begin{aligned} D.N. &\doteq 8\, MHR_{\substack{\text{zero}\\\text{load}}} \times 10^3 \\ \epsilon_{max} &\doteq 1.60\, \epsilon \end{aligned}\right\} (\pm 5\%) \tag{17}$$

and

TABLE 3

Surface Description		Gradient, df_{sV}/dV, or K_1
Sandpaper Surfaces	B.M. #24-X	-0.00471
	B.M. #50-X	-0.00495
	B.M. #60-X	-0.00504
	B.M. #80-X	-0.00525
Actual Road Surfaces	Asphaltic I (rough)	-0.00447
	Asphaltic II (bleeding)	-0.00477
	Concrete (rough)	-0.00464

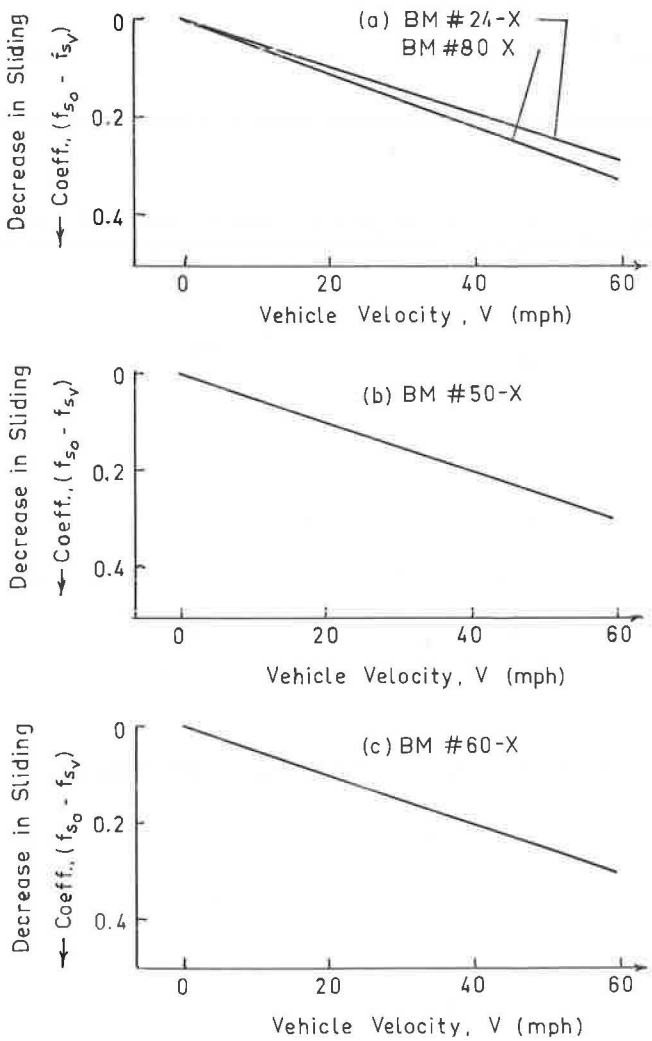

Figure 14. Predicted skid-resistance gradients for sandpaper textures.

where

D.N. = drainage number for surfaces = $MHR\big|_{25\ lb}$

and

ϵ_{max} = maximum asperity height.

Substituting from Eqs. 15, 16, and 17 into 14, the following result emerges:

$$\frac{dfs_V}{dV} = -(7.37 - 1.65 \log_{10} D.N.) \times 10^{-3} \tag{18}$$

By comparing Eqs. 13 and 18, it is seen that

$$K_1 = -(7.37 - 1.65 \log_{10} D.N.) \times 10^{-3} \tag{18A}$$

Substitution of the drainage numbers from Table 2 into Eq. 18A yields values of K_1 or dfs_V/dV for each of the sandpaper and actual surfaces. Table 3 shows these gradients. Note that when V = 0, $fs_V = fs_0$ and Eq. 18A then reads

$$fs_V = fs_0 - (7.37 - 1.65 \log_{10} D.N.) \times 10^{-3} V \tag{19}$$

The value of fs_0 still remains to be determined, and it is believed to be primarily a function of the sharpness of the texture (9). For purposes of plotting the last equation, assume that fs_0 is the same for all surfaces. (This assumption is far from true, but the object is to show the rate of decay of fs_V with increasing vehicle speed from an initial value fs_0, which is as yet undetermined for each texture.) Figure 14 shows that the coarser surfaces exhibit a greater drop in the sliding coefficient, and this is in accord with field observations and experience. The gradients for the actual surfaces have not been shown in Figure 14, since they are almost identical with those for the B.M. #24-X sandpaper surface.

A check on the accuracy of Eq. 19 may be obtained by considering the results obtained by Schulze and Beckmann (9). From the data of locked-wheel skid tests on 48 roads in West Germany under wet conditions, they obtained an empirical relation between the sliding coefficient fs_V and surface properties (the mean void width d between asperities):

$$d = 13.5 - 72.6 (fs_{12.5} - fs_{37.5}) + 103.6 (fs_{12.5} - fs_{37.5})^2 \tag{20}$$

with a correlation coefficient of 0.87.

Putting $d = 100/\sqrt{N'}$ (where N′ = number of asperities per square inch of texture, obtained visually by means of asperity-density prints as outlined earlier), this equation becomes:

$$\frac{1}{\sqrt{N'}} = 0.135 - 0.726 (fs_{12.5} - fs_{37.5}) + 1.036 (fs_{12.5} - fs_{37.5})^2 \tag{20A}$$

Substituting for the fs_V values from Eq. 19:

$$(fs_{12.5} - fs_{37.5}) = (0.1843 - 0.0412 \log_{10} D.N.)$$
$$= K_3 \text{ (e.g., constant for any one surface)} \tag{21}$$

Thus, from Eq. 20A:

$$\frac{1}{\sqrt{N'}} = 0.135 - 0.726 K_3 + 1.036 K_3^2 \tag{22}$$

TABLE 4

Surface Description		K_3	Computed $\sqrt{N'}$	Observed $\sqrt{N'}$
Sandpaper Surfaces	B.M. #24-X	0.1179	15.7	10
	B.M. #50-X	0.1239	16.4	14
	B.M. #60-X	0.1261	16.7	18
	B.M. #80-X	0.1313	17.4	21

where $K_3 = f(D.N.)$ from Eq. 21. Note that Eq. 22 is now a function of surface properties alone. The value of K_3 for each of the sandpaper and concrete block surfaces may now be calculated, and $\sqrt{N'}$ computed. A comparison between the computed and observed values of $\sqrt{N'}$ is then possible, as shown in Table 4 for sandpaper surfaces. It is noted that the mean value of the computed $\sqrt{N'}$ (e.g., 16.5) is comparable with the mean value of the observed $\sqrt{N'}$ (e.g., 16). Since the latter values are obtained on an approximate basis (asperity-density prints), the agreement is good. The spread in the computed values is considerably lower than those in the observed values, because the criterion upon which the former is based (see Eq. 20A and 9) is essentially an average computed for the 48 texture samples, thereby neglecting the spread indicated by the correlation coefficient.

As an example of the computation of $\sqrt{N'}$, consider that the rough asphalt surface for which $\sqrt{N'}$ (observed) is about 7. Hence, MHR_E is obtained from Eq. 5B. Thus,

$$D.N. = MHR_E \times 10^4 \text{ (at W = 25 lb)} = 53.7$$

$$K_1 = -(7.37 - 1.65 \log_{10} D.N.) \times 10^{-3} = 4.51 \times 10^{-3}$$

$$K_3 = (0.1843 - 0.0412 \log_{10} D.N.) = 0.113$$

and

$$\frac{1}{\sqrt{N'}} = 0.135 - 0.726 K_3 + 1.036 K_3^2 = 0.0588$$

so that

$$\sqrt{N'} \text{ (computed)} = 17.9$$

The equations for K_1, K_3, and $1/\sqrt{N'}$ are from previous pages. Since the computed and observed values of $\sqrt{N'}$ do not agree, it seems probable at first that the lesser asperities within the inspected area must effectively increase the observed value of $\sqrt{N'}$. However, the observed value of $\sqrt{N'}$ would have to be increased quite drastically (in this case, to a value probably in the neighborhood of 16) before agreement with the calculated value can be obtained in the manner outlined above. It is not necessary to attain such agreement; since the one-year old asphalt surface is a little rougher than the B.M. #24-X sandpaper surface (this is seen both from the profiles of each and from Fig. 13), it may logically fit on any extension to Table 4. In other words, the finer or coarser a surface is relative to the mean size of texture in Table 4, the greater can be the expected discrepancy between the observed and computed values of $\sqrt{N'}$.

The profile measurements confirm the validity of outflow meter data, and it can be concluded that not only does the outflow meter compare the relative drainage abilities of selected surfaces by assigning a specific drainage number to each, but also it serves to reasonably predict the slope of the wet sliding coefficient vs speed characteristic for each pavement. The correlation between the observed and calculated values of $\sqrt{N'}$ as seen from Table 4 shows that there is substantial agreement between the results of skid tests in the United States (8) and in West Germany (9). Furthermore, this agreement is obtained by using the outflow meter to measure K_1 or dfs_V/dV.

The magnitude of the coefficient of sliding friction under wet conditions and at any speed V remains to be determined. It is now widely accepted (9) that the sharpness of the surface texture determines the magnitude of fs_V, whereas the

mean or maximum asperity size decides the slope of the fs_V vs V characteristic for wet conditions. Assuming that a routine friction tester is used to measure the wet sliding coefficient at a particular speed V, then the outflow meter can be used to deduce the dfs_V/dV relationship, so that the sliding coefficient is known over a limited range of vehicle speeds. The extent of this range is determined by the upper and lower sliding velocities within which the dfs_V/dV ratio is constant in accordance with Eq. 13, and this in turn depends not only on surface texture, but also slightly on tread pattern. A range of 20-30 mph is not unreasonable (10).

CONCLUSIONS

As a result of this study, a simple outflow meter has been designed, developed, and calibrated to compare the relative drainage abilities of laboratory and actual road surfaces, and to predict in specific cases the gradient of the wet sliding coefficient of friction. The instrument is a valuable tool for highway departments, since it can serve for periodic testing of road surfaces so that a check on permissible surface wear is afforded, and thus an indication can be given in certain cases of the need for resurfacing.

ACKNOWLEDGMENTS

The author is indebted to the U.S. Department of Commerce and the Bureau of Public Roads for permission to publish this paper, and to the Cornell Aeronautical Laboratory for typing and editing services.

REFERENCES

1. Giles, C. G. Discussion at Symposium on Control of Vehicles During Braking and Cornering, I.M.E., London, June 1963.
2. Horne, W.B., and Dreher, R. C. Phenomena of Pneumatic Tire Hydroplaning. NASA TN D-2056, Nov. 1963.
3. Moore, D.F. A Study of Tire-Surfacing Interaction for the Case of Rolling on a Wet Surface. Cornel Aeronautical Laboratory Reports No. YD-1969-V-1 and YD-1969-V-2, Jan. and July 1965.
4. Moore, D.F. Drainage Criteria for Runway Surface Roughness. Jour. Royal Aeronautical Soc., Vol. 69, No. 653, pp. 337-342, May 1965.
5. Hughes, A.J. Tyre Design Considerations. Jour. Royal Aeronautical Soc., Vol. 67, p. 579, Sept. 1963.
6. Giles, C. G., and Lander, F. T. W. The Skid-Resisting Properties of Wet Surfaces at High Speeds: Exploratory Measurements with a Small Braking Force Trailer. Jour. Royal Aeronautical Soc., Vol. 60, pp. 83-94, Feb. 1956.
7. Moore, D. F. The Sinkage of Flat Plates on Smooth and Rough Surfaces. Ph.D. Dissertation, Pennsylvania State Univ., Dec. 1963.
8. Meyer, W. E. Some Results of Research on Skid Control. Paper No. B-5, 10th FISITA Congress, Tokyo, 1964.
9. Schulze, K.M., and Beckmann, L. Friction Properties of Pavements at Different Speeds. ASTM Spec. Tech. Publication No. 326, p. 44, June 1962.
10. Proc. First Internat. Skid Prevention Conf., Part 2. Virginia Council of Highway Investigation and Research, Aug. 1959.

Skid Resistance Guidelines for Surface Improvements on Texas Highways

B. F. McCULLOUGH, Supervising Design Research Engineer, and
K. D. HANKINS, Associate Design Engineer, Research Section, Highway Design Division, Texas Highway Department

This report pertains to the selection of a minimum skid resistance for use as another guideline for surface improvements by the Texas Highway Department. This problem was approached from an accident standpoint as well as from a design standpoint, since experience on several sections of roadway indicated a sharp reduction of accidents after surface improvements.

Skid resistance and accident data were collected on 517 rural sections that represented a random sample of Texas highways. The skid resistance values were obtained through the use of a towed trailer employing the locked-wheel principle on artifically wetted pavements. An analysis of this data showed that the possibility of a roadway section having a high accident rate increased as the coefficient of friction decreased.

On the basis of this study, composite skid resistances of 0.4 and 0.3 for testing velocities of 20 and 50 mph, respectively, were selected as guidelines for considering surface improvements. In addition, skid resistance values of 0.31 and 0.24 at 20 and 50 mph, respectively, were recommended as minimum values.

•EARLY IN 1963 the Texas Highway Department in cooperation with the Bureau of Public Roads initiated a research project to study skid characteristics of Texas highways. The first prerequisite for this project was to design and construct a device to measure skid resistance (1). After a detailed literature survey and considerable personal contact with other representatives working in this field, a two-wheel trailer was selected which obtained a locked-wheel skid resistance. It was felt that this type of test gave a closer simulation of a braking vehicle. The trailer was designed so that the skid resistance could be obtained with the pavement in a wet condition. The towing vehicle is a two-ton Dodge truck powered by a V-8 engine. The vehicle velocity and frictional force are produced as visual output on a strip chart recorder. Tests may be performed on either wheel individually or both wheels can be braked simultaneously.

After obtaining equipment to measure skid resistance, the question immediately arises—how can accidents be reduced with this device? It is realized that the causes for accidents are much more complex than the influence of the deceleration induced in the vehicle by the pavement surface after the brake application.

Skidding is defined by K. A. Stonex, Assistant Director, General Motors Proving Grounds, as the motion of a vehicle under conditions of partial or complete loss of control caused by the sliding of one or more wheels of a vehicle (2). How the vehicle reacts while skidding is a function of many variables of the vehicle itself, such as brake distributions, load distributions, and braking conditions. It has been found that if the front wheels are locked and the rear wheels roll freely the course of the car is straight. If the rear wheels are locked and the front wheels roll freely the car switches ends by

Paper sponsored by Committee on Surface Properties—Vehicle Interaction and presented at the 45th Annual Meeting.

TABLE 1

Section	Coefficient		Accidents[a]		Percent Reduction in Accidents
	Before	After	Before (1963)	After[b] (1964)	
1	.275	.462	974	560	42.5
2	.275	.359	1272	814	36.0
3	.275	.467	931	620	33.4
Sawed Concrete	.275		960	770	19.8

[a]Accidents are given per 100 million vehicle miles based on one year of observations.

[b]"After" accidents have been extrapolated to a yearly basis from seven months of information.

sliding sideways to a position approximately 180 deg to the position before brake application, much as a pendulum swings about its pivot (2). Many variations can be expected if variations are experienced in the number and extent to which wheels lock.

Since coefficient of friction is related to skidding, and studies have found that wet pavement coefficients are much lower than dry pavement coefficients, it seems obvious that skidding is related to weather conditions. It is common knowledge that the number as well as the severity of accidents increases on wet roadways. However, investigators both in this country and abroad have made detailed studies of accidents, skidding, and weather conditions. Giles and Sabey of the Road Research Laboratory, United Kingdom, report that 8 percent of the total number of accidents in dry conditions involved skidding, whereas 27 percent of the total number of accidents on wet roads involved skidding (3). Virginia investigators report 0.66 percent of the total number of accidents in dry conditions were skidding accidents and 14.65 percent of the total number of accidents on wet roads were skidding accidents (4). Virginia also reports that skidding of some nature occurred in 35 percent of 37,507 accidents during 1956 in Virginia. Dr. Bruno Werner reports that from 1953 to 1956 in open country one accident out of every 4 or 5 involved slippery road conditions as a cause in Germany (5). The Road Research Laboratory, United Kingdom, reports that urban areas, even though they have the majority of accidents, are by no means the chief areas, since over one-third of all skids on wet roads occur on rural roads (3).

The studies enumerated indicate that skidding accidents occur chiefly in wet weather, and coefficients are lower under wet conditions. Therefore, it follows that accidents are in some way related to skid resistance.

A few years ago a slick section of pavement in Texas was "deslicked" by sawing small, closely spaced longitudinal grooves in the concrete surface (6). This operation increased the coefficient of friction from 0.32 before sawing to 0.42 after sawing as measured by the stopping-distance method at 30 mph with wet pavement conditions. Immediately after the grooving work, the accident rate on the section decreased sharply, but within a year the grooves began to polish and the accident rate started to increase.

Recently sections of the sawed concrete were overlaid with asphaltic concrete containing two different types of aggregate. Coefficient of friction values were obtainted on the overlaid sections and also on the sawed section. Using the sawed section as a "before" coefficient and the coefficients obtained on the overlaid sections as "after" values, Table 1 compares the resultant accident rates. Even though there was a reduction in accidents on the sawed concrete from 1963 to 1964, the reduction of accidents on the overlaid sections was considerably greater.

These studies lead to the question, how can skid resistance measurements be used to decrease accidents? The most obvious answer is to establish a minimum coefficient of friction value. Technically, this minimum coefficient should vary as to location,

such as hills, intersections or curves, and probably between rural and urban areas. The AASHO Guide (7) refers to stopping sight distance and superelevation, both of which are minimum coefficient values described as "stopping distance" of a vehicle. Other agencies have set minimums, among them England (3), Michigan (8), and Virginia (9).

The objective of this report is to establish a guide for a minimum coefficient value to be used on Texas highways. This minimum coefficient value will be selected using minimum design requirements, accident information and economics. Although the value should vary with location, this report will only consider general guidelines for a statewide value. Future studies will encompass more specific applications.

METHOD OF ANALYSIS

During the initial background study and after a review of available information, it was found that considerable research would be necessary for a complete study of the influence of surface friction on accidents. In line with the objective of this study, it was felt that sufficient information could be accumulated to establish a guide for a needed minimum coefficient of friction value. This would be done quickly with the thought of a complete study shortly after.

Selection of Test Sections

The advisory committee for this project recommended that skid resistance tests be performed on 517 sections which were previously selected by the Texas Transportation Institute in connection with pavement structure research study (10). This decision was based on two considerations:

1. It was felt that existing data could be used for both projects and therefore no duplicate data gathering would be required.
2. The sections selected would provide a random sample and thereby assure a representative sample of Texas highways.

Since the 517 test sections are predominantly rural, additional sections were also selected in urban areas to provide a cross-check of any conclusions or observations. The urban sections were also used to develop study guidelines for the rural sections.

Urban. —The urban study was performed on Interstate Highway 35 in two cities, Austin and San Antonio. A preselected number of skids were performed on selected roadway sections in both cities. The roadway sections were selected on the basis of construction project boundaries. In general, when the sections are linked end to end they compose the entire distances between city limits. Information was collected within each section boundary on each of the several accident types. The accident information was obtained directly from the police department files for each of the two cities. In both cities, the skid resistance values were obtained on the outside lanes and these were used for comparison purposes.

Rural. —The rural tests were made on the 517 preselected sections. These sections are also being used as a part of an overall skid study of Texas materials which will be reported at a later date. Tests in rural sections consisted of respective averages of five skids made for each of the following conditions: at 20 mph in the inside wheelpath, 50 mph in the inside wheelpath, and at 20 mph with the left wheel or test wheel between the wheelpaths. Rural accident information was obtained from an annual report by the Texas Highway Department which compiles all accidents reported by the Texas Department of Public Safety (11).

Figures 1 and 2 show the inside wheelpath coefficient of friction frequency distributions for the 517 test sections for testing velocities of 20 mph and 50 mph, respectively. Note that the statewide average based on this sample is 0.506 at 20 mph and 0.391 at 50 mph.

Selection of Accident Type

It is difficult to define accidents caused by skidding, for in almost every accident the brakes will be applied. In an emergency situation, brake application may have various

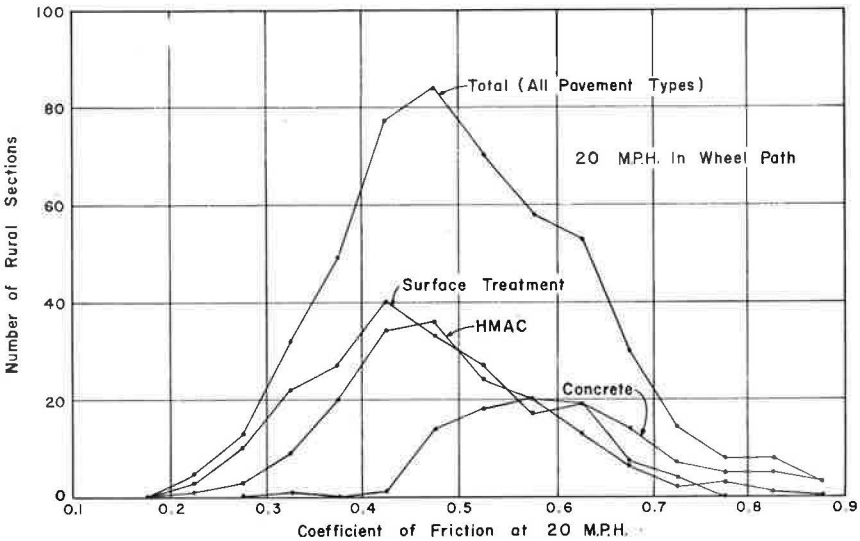

Figure 1. Number of rural sections compared with coefficient of friction at 20 mph.

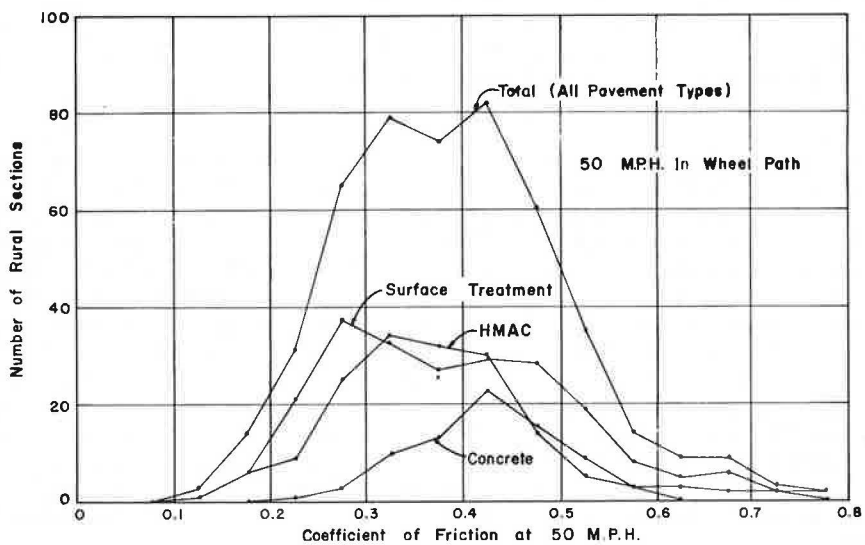

Figure 2. Number of rural sections compared with coefficient of friction at 50 mph.

results: (a) avoiding the accident, (b) speed reduction sufficient to cause only minor damage, or (c) complete loss of control thereby causing the accident. All skidding accidents may not be caused by brake applications, since it has been reported that 35 percent of skidding accidents occurred before brake application (4). There is then indecision as to which accident type to select for correlating with the coefficient of friction. Should the study be based on total accidents, assuming that the percent of skidding accidents occurring within the total number stays constant; or rain accidents, assuming that skidding occurs more frequently on the wet pavement; or skidding accidents, which in the present case are hand-selected, taking considerable time and expense?

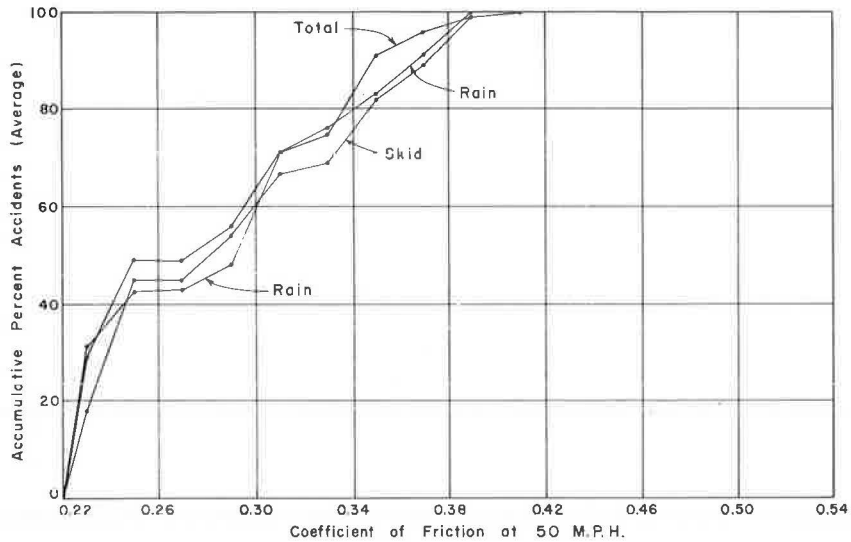

Figure 3. Study of average cumulative percent accidents and coefficient of friction for Austin and San Antonio on I-35.

The accidents selected in the urban areas were of three types: skid accidents, rain accidents, and total accidents. In an effort to "purify" the skid accidents selected, only those accidents caused by skidding were selected. Such accidents would be of the type in which the driver applied the brakes for speed reduction, lost control of the vehicle because of skidding, and the vehicle hit another object. The rain accidents actually occurred in a rain or a mist. The accidents are also a function of the vehicular density, especially those accidents on freeways with short gap or headways as compared with those accidents which occur in sparsely traveled sections. The section length also would influence the number of accidents. Therefore, in an effort to standardize the data, the accidents per length per average daily traffic were selected on a one-year basis. This standardization is called "Accidents Per 100,000,000 Vehicle Miles" (11).

Figure 3 shows the results of the urban study, which was used as a pilot study for the selection of accident type. The data indicate that the three accident types are closely associated. Skid accidents trailed total accidents in average cumulative percent, and the rain-accidents curve was the more variable of the three. This information led to the decision to select total accidents as a study tool for the rural investigation. One limiting feature is the possibility that all total accidents are not reported, depending upon the severity of the accident and the driver involved. However, accidents in which an injury or fatality occurs would in all probability be reported. Therefore, on the basis of this hypothesis, fatal and injury accidents were also included as a study tool.

PRESENTATION OF RESULTS

Although numerous reports have associated accidents with skid resistance, no studies have been reported in this country that attempt to arrive at a minimum skid resistance value through the use of accident data.

In this study, the accident data for the test sections described previously were used to investigate the effect of skid resistance on accidents. In order to develop future study guidelines, two different methods of analysis were used. One method was to directly compare accident data on a section of roadway with its coefficient of friction; the second method used a cumulative frequency distribution curve.

Direct Comparison

In this method, the accident rate per one hundred million vehicle miles for a given test section was plotted in terms of coefficient of friction for the test section. This

type of analysis was run using both total accidents for a section and the fatal and injury accidents for the section.

Total Accidents.—Figures 4 and 5 show the total accidents experienced on a section of roadway in terms of the coefficient of friction for that roadway at 20 mph and at 50 mph, respectively. Although there is a wide scatter of points, the data do indicate that accidents are, in general terms, inversely proportional to the coefficient of friction, or in other words, the accident rate tends to increase as the coefficient of friction decreases. The line to the right edge of the data can be designated as a line of maximum accidents. A section may have a low skid resistance and still have a low accident rate, but in no case will the accidents exceed that predicted by the line of maximum accidents. The change for a high accident rate increases as the skid resistance decreases. The line of maximum accidents clearly shows the inverse trend between these two parameters.

Using the line of maximum accidents as a guide, there is a very sharp increase in the number of accidents when the skid resistance drops below 0.45 for values obtained at 20 mph, whereas the rapid increase is noted near 0.35 for tests at 50 mph.

Fatal and Injury Accidents.—Figures 6 and 7 show the number of fatal and injury accidents experienced in a section of roadway instead of the total accidents used in the previous graphs. Figures 6 and 7 are for 20 mph and 50 mph, respectively. A line of maximum accidents has also been placed to the right of the data on both of these graphs. The trends and observations noted with total accidents are verified by these graphs. At 20 mph, a rapid increase in fatal and injury accidents is experienced when the coefficient of friction decreases below a value of 0.40. At 50 mph, the increase in fatal and injury accidents is experienced at 0.35 as was the case with total accidents.

Cumulative Comparison

Another method of comparison is to use the data and construct a cumulative frequency distribution curve. One complicating factor in making this type of analysis is that the data form a normal distribution pattern rather than a factorial type arrangement, as would be the case for a planned experiment (see Figs. 1 and 2). Therefore, a coefficient value near the mean skid resistance of all the test sections will show a much greater total number of accidents because of the greater number of test sections in this range. In order to offset this phenomenon, an average accident rate for each coefficient range was calculated on the basis of the number of sections in the particular range. The frequency curve was then compiled on the basis of these values. As a result, a coefficient range at the extremes of the distribution has the same influence as one near the mean.

Figures 8 and 9 show these cumulative percentages for 20 and 50 mph, respectively. Both total accidents and fatal and injury accidents are shown on these graphs. At 20 mph, the slope of the line starts decreasing between 0.45 and 0.50 for the total accidents, but in the case of fatal and injury accidents, there is no sharp break in the curve until a value between 0.5 and 0.6 is reached. At 50 mph, the slope begins to decrease at a coefficient value between 0.30 and 0.35 for both the total accidents and the fatal and injury accidents. The point of change is much more clear-cut at 50 mph than at 20 mph.

It is interesting to note that the two methods of analysis give critical values approximately equal although the values vary for speed as would be expected. For 20 mph, the data indicate that an increase of accidents is experienced when the coefficient of friction decreases below a value that is in a range of 0.4 to 0.5. At 50 mph, this value appears to be between 0.30 and 0.35. Purely from an accident standpoint, the previously enumerated values may be considered as minimum levels for roadways in the State.

DISCUSSION OF RESULTS

At this point, it is again emphasized that the accident data obtained in this report were in no way correlated to driver characteristics, vehicular characteristics, or geometric characteristics. The authors fully recognize that coefficient of friction is not the only cause of accidents, but the results of this study point out its importance.

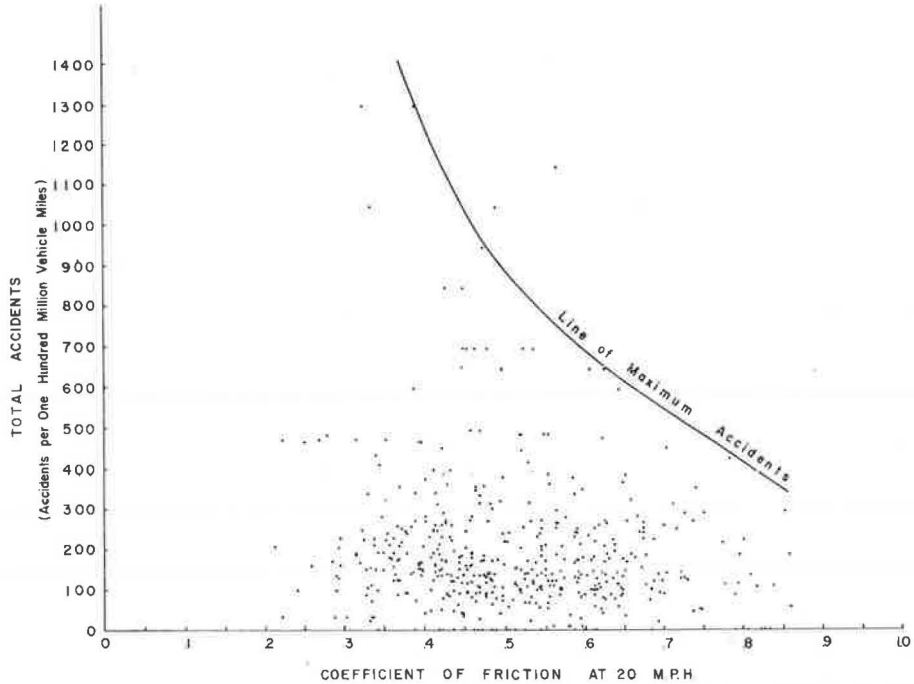

Figure 4. Comparison of total accidents and coefficient of friction at 20 mph.

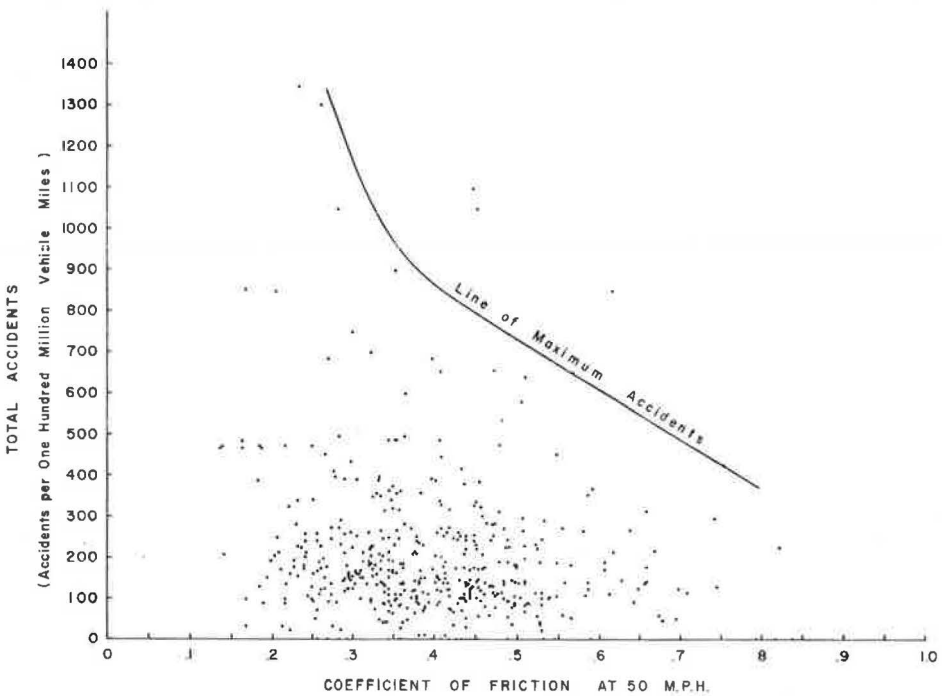

Figure 5. Comparison of total accidents and coefficient of friction at 50 mph.

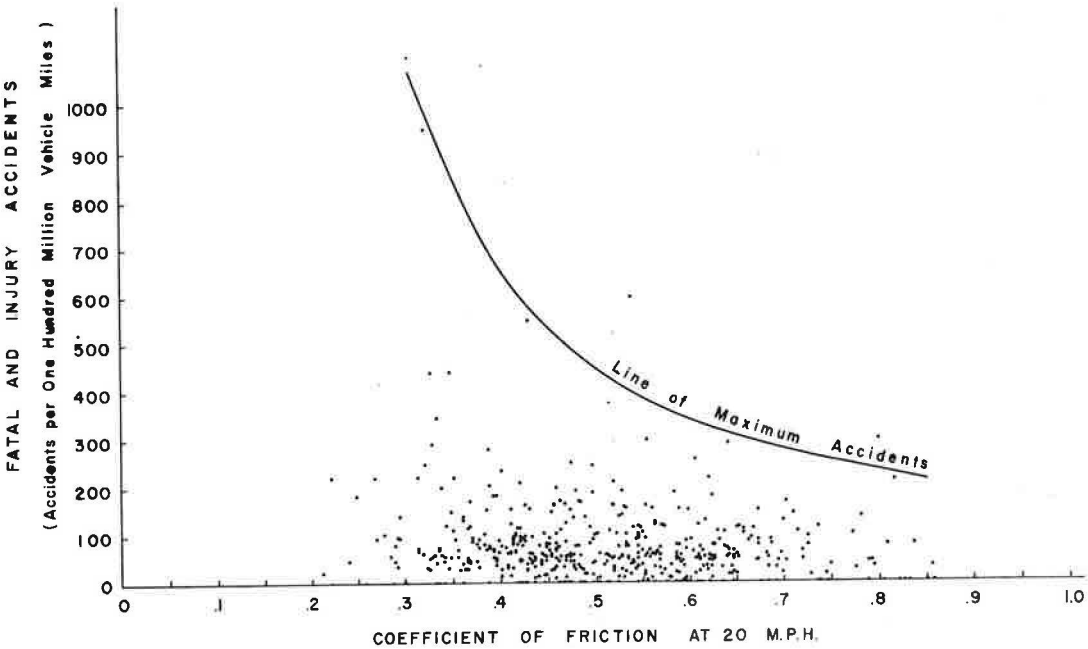

Figure 6. Comparison of fatal and injury accidents and coefficient of friction at 20 mph.

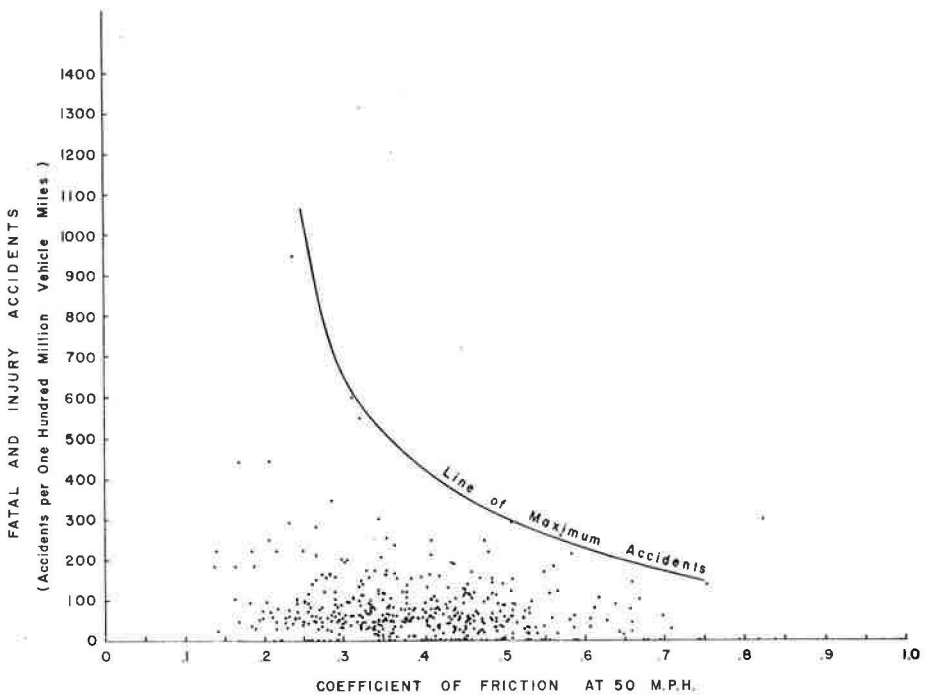

Figure 7. Comparison of fatal and injury accidents and coefficient of friction at 50 mph.

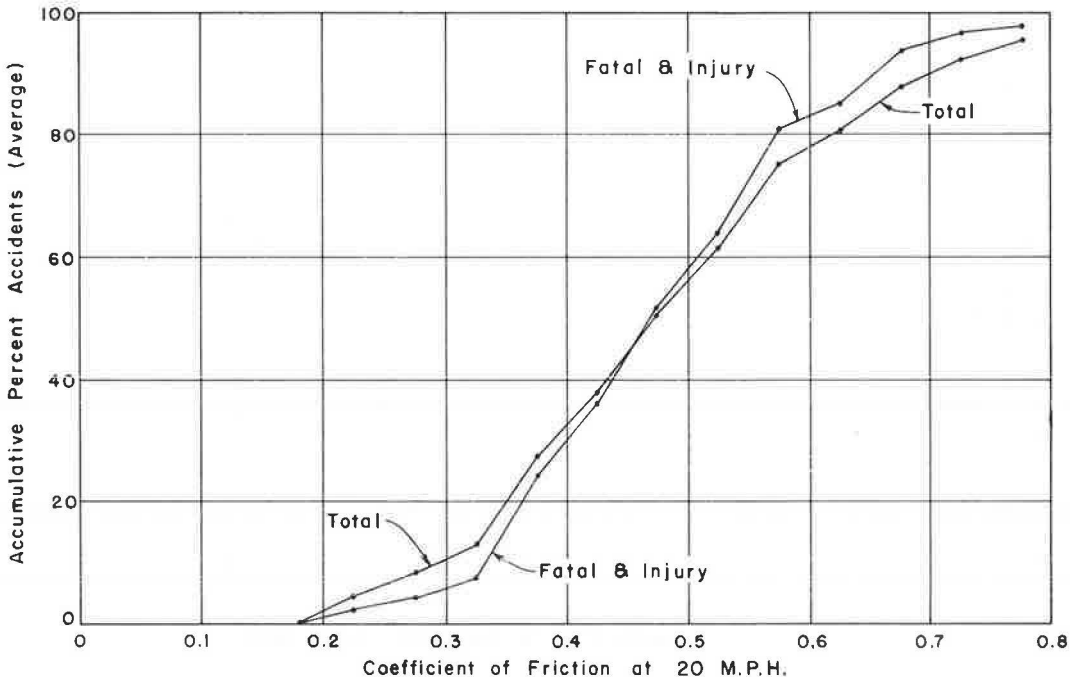

Figure 8. Study of average cumulative percent accidents and coefficient of friction at 20 mph.

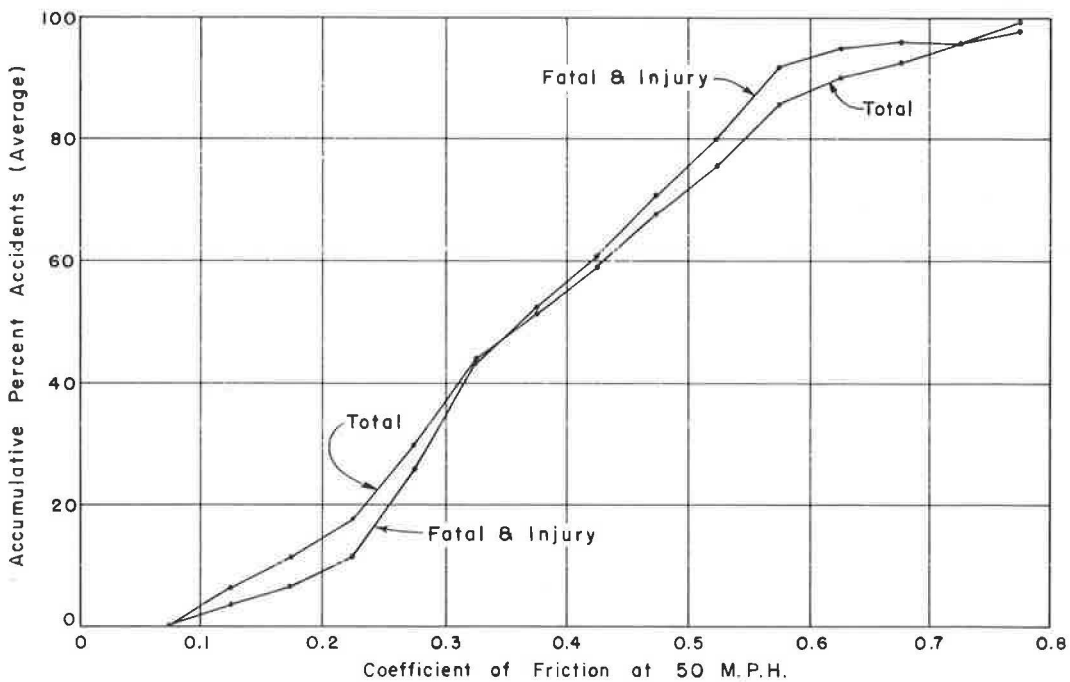

Figure 9. Study of average cumulative percent accidents and coefficient of friction at 50 mph.

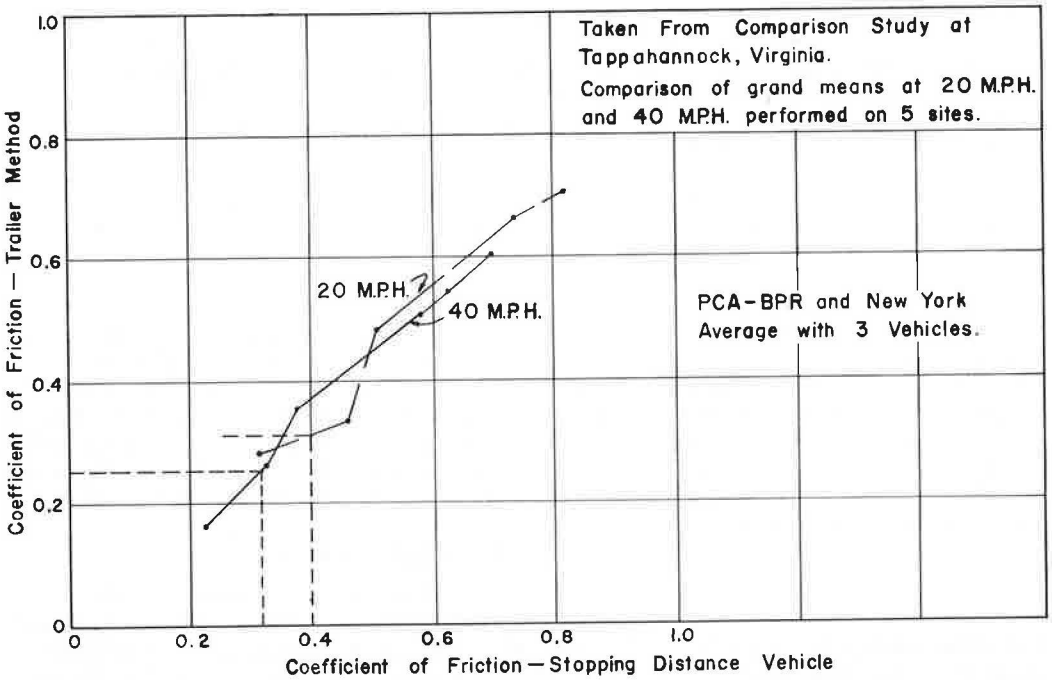

Figure 10. Comparison of stopping distance vehicle vs trailer results.

The size of sample used in this study, correlated with experience on specific locations, certainly lends credence to the approach used.

In this section, a composite minimum coefficient of friction to be used as another guide for skidproofing will be derived from both design and accident minimum coefficients of friction.

A design minimum coefficient of friction is stated in AASHO's policy on geometric design, which is the basis of design in most states. D. W. Loutzenheiser, Chief of Highway Design Division, Bureau of Public Roads, has a very good discussion of this topic in the report "Skid Resistance Values Used in Geometric Design" (12). This minimum coefficient is based on an assumed speed, an adequate perception, reaction time, and the assumption of good brakes or good vehicular characteristics. The minimum was established on the basis of data derived by the stopping distance vehicle method. The values obtained by this method are probably more closely associated with accidents, in that it parallels the "panic stop" situation. Since very little stopping distance data were available in Texas, and it is necessary to correlate the two methods, the work performed at Tappahannock, Virginia, was used as a basis (13). Figure 10 is a correlation of the two methods in which the three sedans were selected from the stopping distance information, and the New York, Portland Cement Association, and Bureau of Public Roads trailers were selected from the trailer information. These three trailers were chosen because their design is similar to the design of the Texas trailer.

Using the above relationship in connection with the curve showing the skid resistance in terms of velocity that was used as the criterion for stopping distance in the AASHO Guide, a minimum design coefficient as measured with the trailer method may be obtained. Table 2 was constructed using Figure 10 and a straight-line interpolation from 20 mph through 40 mph to obtain the minimum design coefficient value at 50 mph.

Accident Minimum

Strictly from an accident standpoint, the data discussed in the previous section indicate that accidents increase when the skid resistance decreases below the values in a

TABLE 2

Speed (mph)	Minimum Design Coefficient by Stopping Vehicle Method	Minimum Design Coefficient by the Trailer Method
20	0.4	0.31
40		0.25
50	0.3	0.24

TABLE 3

Speed (mph)	Recommended Composite Coefficient of Friction
20	0.40
50	0.30

range of 0.4 to 0.5 at testing speeds of 20 mph and 0.3 to 0.35 at 50 mph. Although it is not known to what extent all the accidents used in the analysis are related to skid resistance, the inner-relation between the two factors is evident, and it should be taken into consideration.

Composite Minimum

From a logical standpoint, the design coefficient for stopping distance as established by AASHO is an absolute minimum value that can be tolerated on the highway system. Consideration of the accident data brings forth the question, is this the minimum coefficient value to be maintained for safety? Loutzenheiser (12) refers to the AASHO design for Safe Stopping Distance and states:

> The friction factors used entail a substantial safety factor for good pavement, weather and tire conditions, but only a very low factor for the combination of pore conditions. Even in this case, there is a potential safety factor in the perception-reaction distance component and likely lower speed operations during adverse circumstances.

The accuracy of this statement is evident from the data reported. The statement, in conjunction with the data, indicates that the composite minimum should be greater than the design minimum from a standpoint of driver safety. Although this variation in design accident minimums may by hypothesized to be a result of vehicle characteristics or driver characteristics, the fact is that the variation exists and a composite minimum must be determined.

The selection of a composite minimum will not eliminate all accidents, but certainly the severity of the accident can be reduced. A reduction in impact velocity due to an improved skid resistance has a large effect on the force of impact, since the force is decreased by the square of the velocity. The number of vehicles is increasing on Texas highways and recently the speed limits were increased. Many roadways experience small headways and gaps and increasing the coefficient value cannot be expected to prevent all accidents, but it can be expected to reduce the severity and number of accidents.

Combining the design minimum of 0.31 at 20 mph with an accident minimum of 0.40-0.45 at 20 mph and the design minimum of 0.24 at 50 mph with the accident minimum of 0.30-0.35 at 50 mph, the composite figures in Table 3 are recommended for use by the Texas Highway Department. These composite minimums should be used as another guide for scheduling surface improvements on a section of highway.

Implications of Composite Minimum

After selection of a composite minimum, the immediate question arises, what percent of the highway system is below this minimum? Figures 11 and 12 indicate a cumulative frequency distribution of the coefficient of friction for the 517 preselected rural sections at testing velocities of 20 mph and 50 mph, respectively. If the selection

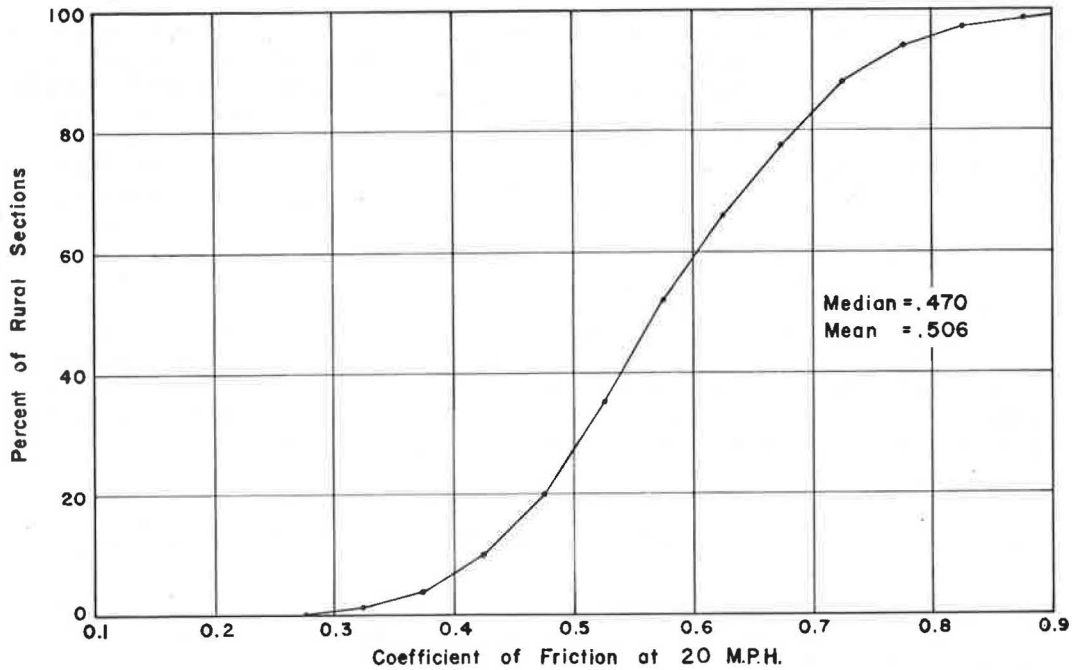

Figure 11. Cumulative percent of rural sections compared with coefficient of friction at 20 mph.

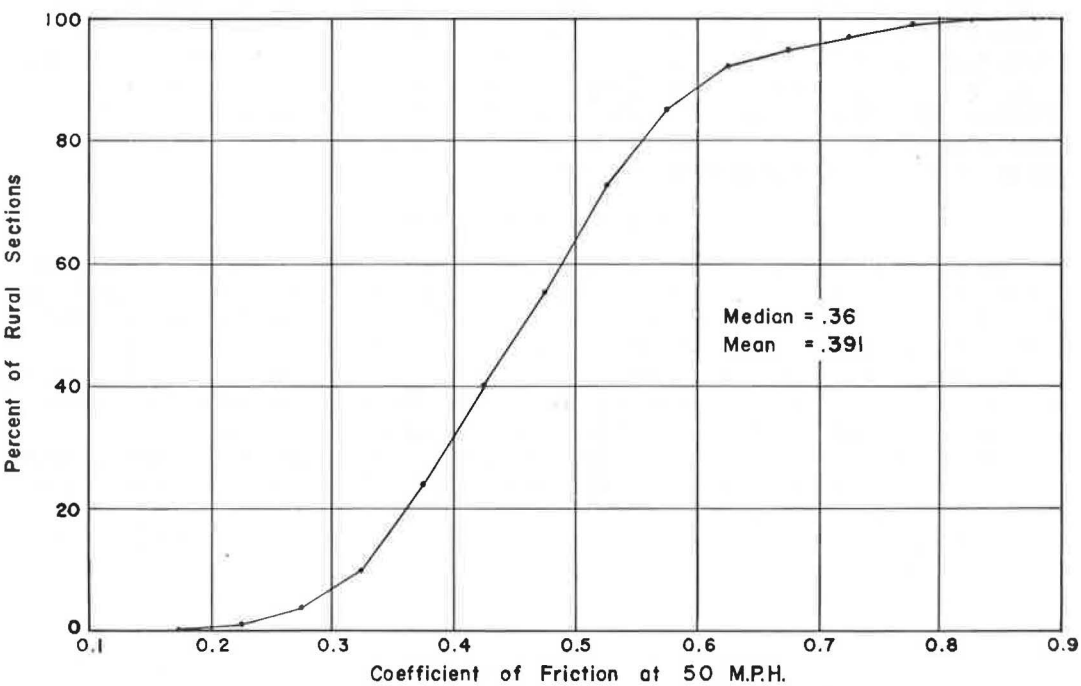

Figure 12. Cumulative percent of rural sections compared with coefficient of friction at 50 mph.

of these test sections represents a random sample from all Texas highways, then it may also be assumed that this selection represents all highways in the state. Entering Figure 11 with the composite minimum value of 0.40, it may be postulated that 27 percent of Texas highways do not meet this minimum value at the present time. Upon first consideration, this percentage seems large; however, if Figure 11 is entered with the absolute design minimum of 0.31, it is found that 8 percent of Texas highways do not comply with the design minimum at the present time. Investigating these percentages for a testing velocity of 50 mph, Figure 12 is entered with the composite minimum coefficient of 0.30. This analysis shows that 32 percent of Texas highways do not meet this value, and again using the absolute design minimum of 0.24, the data indicate 14 percent of Texas highways are deficient.

These composite minimums should be used as another guide for surface improvement. Economic considerations along with other overall project needs would preclude the use of these values as absolute minimums at the present time, but the composite minimums should be used as positive guides for surface improvement where feasible. The design minimums should be considered as absolute minimums.

CONCLUSIONS AND RECOMMENDATIONS

On the basis of this study the following conclusions and recommendations are warranted:

1. The number of accidents experienced on a highway is related to the magnitude of the surface's skid resistance. The smaller the skid resistance, the greater the chance of a high accident rate.
2. The composite minimum coefficients of 0.4 and 0.3 at testing velocities of 20 and 50 mph, respectively, should be used as another guide for programming pavement surface improvements. When the skid resistance decreases below this value, surface upgrading should be considered
3. The design coefficients of 0.31 and 0.24 at 20 mph and 50 mph should be considered as absolute minimum values. When the roadway skid resistance decreases below these values, an immediate surface improvement program should be undertaken.
4. It is recommended that the Maintenance Engineer in each district institute an inventory program to determine the level of skid resistance on each project in his area. This inventory should be kept current in order to provide another method of evaluating the program needs for seal coats, overlays, etc.

ACKNOWLEDGMENTS

Thanks are extended to the Police Department and to the City Traffic Engineering Section in Austin, Texas, for their assistance in providing access to the city accident files, especially to Messrs. W. H. Klapproth and W. T. Nuckols of the Traffic Engineering Sections and to Sergeants Cutler and Wilson of the Police Department.

The assistance of the San Antonio Police Department is gratefully acknowledged, and a special thanks to Mr. C. F. Braunig, District Traffic Engineer of the San Antonio District, who collected and compiled the accident data from that city.

The Skid Resistance Advisory Committee for this project has been especially helpful, and appreciation is expressed to Mr. R. O. Lytton of the San Antonio District and Mr. J. H. Aiken of the Waco District.

This project was conducted in cooperation with the Bureau of Public Roads, and the suggestions of Bureau personnel are acknowledged.

REFERENCES

1. McCullough, B. F., and Hankins, K. D. Texas Highway Department Skid Test Trailer Development. Research Report 45-1, April 1965.
2. Stonex, K. A. Elements of Skidding. Proc. First Internat. Skid Prevention Conf., Part I, Aug. 1959.
3. Giles, C. G., and Sabey, Barbara E. Skidding as a Factor in Accidents on the Roads of Great Britain. Proc. First Internat. Skid Prevention Conf., Part I, Aug. 1959.

4. Mills, J. P., Jr. Virginia Accident Information Relating to Skidding. Proc. First Internat. Skid Prevention Conf., Part I, Aug. 1959.
5. Werner, Bruno. Accidents Involving Slippery Road Conditions in Germany. Proc. First Internat. Skid Prevention Conf., Part I, Aug. 1959.
6. Hilgers, H. F., and McCullough, B. F. Slick When Wet. Texas Highways, Jan. 1963.
7. A Policy on Geometric Design of Rural Highways. AASHO, 1954.
8. Finney, E. A., and Brown, M. G. Relative Skid Resistance of Pavement Surfaces Based on Michigan's Experience. Report No. 295, Aug. 1958.
9. Dillard, J. H., and Alwood, R. L. Providing Skid-Resistant Roads in Virginia. July 1958.
10. Preliminary Listing of Data From Phases I and II for Application of AASHO Road Test Results to Texas Conditions. Dec. 1963.
11. Highway Traffic Accident Tabulation and Rates by Control and Section. 1962.
12. Loutzenheiser, D. W. Skid Resistance Values Used in Geometric Design. Proc. First Internat. Skid Prevention Conf., Part II, Aug. 1959.
13. Dillard, J. H., and Mahone, D. C. Comparison of Several Methods of Measuring Road Surface Slipperiness: Tappahannock, Virginia, 1962. May 1963.